

For Reference

NOT TO BE TAKEN FROM THIS ROOM

For Reference

NOT TO BE TAKEN FROM THIS ROOM

Ex LIBRIS
UNIVERSITATIS
ALBERTAENSIS



Thesis
1966
112

THE UNIVERSITY OF ALBERTA

A STUDY OF THE STRUCTURE OF THE NUCLEI P^{29} AND P^{31}

by

Walter Garfield Davies

A THESIS

SUBMITTED TO THE FACULTY OF GRADUATE STUDIES

IN PARTIAL FULFILLMENT OF THE REQUIREMENTS FOR THE DEGREE

OF DOCTOR OF PHILOSOPHY

DEPARTMENT OF PHYSICS

EDMONTON, ALBERTA

January, 1966

UNIVERSITY OF ALBERTA
FACULTY OF GRADUATE STUDIES

The undersigned certify that they have read, and recommend to the Faculty of Graduate Studies for acceptance, a thesis entitled A STUDY OF THE STRUCTURE OF THE NUCLEI p^{29} AND p^{31} , submitted by Walter Garfield Davies in partial fulfillment of the requirements for the degree of Doctor of Philosophy.

ABSTRACT

The structure of the nuclei P^{29} and P^{31} have been studied using the $Si^{28}(d,n)P^{29}$ and $Si^{30}(d,n)P^{31}$ reactions. Angular distributions of the neutrons leading to states in P^{29} up to an excitation of 4.5 MeV were obtained at deuteron bombarding energies of 4, 5 and 6 MeV. The angular distributions for the ground, first and second excited states of P^{29} were analysed using the distorted wave Born approximation. The experimental spectroscopic factors obtained in this analysis favour a Nilsson model description for the P^{29} nucleus.

Evidence for spin dependent structure was seen in the angular distribution of the neutrons leading to the 1.38 MeV ($J^\pi = 3/2^+$) and 1.96 MeV ($J^\pi = 5/2^+$) levels of P^{29} . The lifetime of the 4.34 MeV level was estimated to be about 0.9×10^{-20} seconds.

The angular distributions of the neutron groups leading to states in P^{31} up to 8.26 MeV of excitation were measured at deuteron bombarding energies of 3, 4 and 5 MeV. This work includes the identification of eleven previously unreported excited states in the region of excitation from 5 to 8 MeV and the assignment of spins and parities to the levels of P^{31} at 5.01, 5.25, 6.38, 6.48, 6.60, and 7.14 MeV. In addition the levels at 6.38 and 7.14 MeV have been identified as the first two $T = 3/2$ states of P^{31} corresponding to the ground and first excited states of Si^{31} .

The angular distributions corresponding to the ground state and the

excited states at 1.26, 2.23, 3.13, 5.01, 5.25, 6.38, 6.48, and 6.60 MeV in P^{31} were compared with the predictions of the distorted wave Born approximation. Spectroscopic factors have been deduced for these transitions and have been compared with the predictions of the strong coupling and weak coupling collective models as well as shell model calculations. The experimental spectroscopic factors favour a Nilsson model description of the P^{31} nucleus.

A high resolution neutron time-of-flight spectrometer was used in the present investigation. A description of the time-of-flight spectrometer with particular emphasis on the newly installed Mobley beam bunching system is given in chapter 2.

Appendix I gives a description of five programs used in the analysis of the data along with an outline of the theory of least squares.

ACKNOWLEDGMENTS

I would particularly like to thank my supervisor Dr. G. C. Neilson for suggesting this project and for his continued interest and participation in its execution. The excellent spectrometer used in these experiments is only part of his total contribution.

I would also like to thank Dr. W. K. Dawson for his help with the computer programming and Dr. J. T. Sample for many helpful discussions.

Particular thanks are due to Dr. K. Ramavataram who did the Nilsson model and vibrational model calculations discussed in this thesis and whose constant help and encouragement contributed significantly to the completion of this work.

I am also indebted to Mr. T. B. Grandy whose steadfast assistance in running all of the experiments and in analysing some of the data is greatly appreciated. I would like to thank Mr. A. A. Fife for his assistance in analysing the P^{30} data.

The assistance of Dr. K. L. Brown of Stanford University with the theory of the Mobley bunching system is also gratefully acknowledged.

I am also indebted to Mr. J. B. Elliott, Mr. L. Holm, Mr. E. Cairns, Mr. C. Green and Mr. R. Gordon for their work in constructing and maintaining much of the equipment used in this research.

I am very grateful to my wife Mary Anne for her help with many of the details of publishing this thesis and also for her encouragement during the past three years.

Thanks also to Miss G. Tratt for her careful typing of the manuscript.

Finally, I would like to thank the National Research Council and the University of Alberta for financial support during the course of this work.

TABLE OF CONTENTS

	Page
CHAPTER 1 INTRODUCTION	1
CHAPTER 2 EXPERIMENTAL APPARATUS AND ARRANGEMENT	11
2.1 Introduction	
2.2 The Accelerator and General Experimental Arrangement	12
2.3 The Target Assembly	14
2.4 The Beam Bunching System	16
(i) Introduction	16
(ii) The Operation of a Mobley Bunching Magnet	18
(iii) The Paraxial Ray Equations of a Uniform Field Sector Magnet	21
(iv) The Solution of the Ray Equations and the Matrix Method	28
(v) The Double Focussing Condition for a Sector Field Magnet	36
(vi) The Path Length Difference and the Bunching Condition	39
(vii) The R.F. Deflection Voltage	44
(viii) The Design of the Mobley Bunching System	46
(ix) Effects that Limit the Bunching	50
(a) The Nonlinearity of the Sweep Waveform	50
(b) The Geometrical Aberrations	51
(c) The Effect of Beam Emittance	53
(d) The Momentum Dispersion	70
(e) The Magnetic Field Homogeneity and Stability	72
(f) The Phase and Amplitude Stability of the R.F. Deflection System	73
(x) The Predicted Performance of the Bunching System	75
(xi) The Measured Performance of the Bunching System	76
(xii) The Radio Frequency Deflection System	77

CHAPTER 3	THE $\text{Si}^{28}(\text{d},\text{n})\text{P}^{29}$ REACTION	81
3.1	Introduction	81
3.2	Experimental Procedure	82
3.3	J-Dependence of the Angular Distributions of the 1.38 ($J = 3/2$) and 1.96 ($J = 5/2$) States of P^{29}	87
3.4	Analysis of the Angular Distributions	88
	(i) DWBA Analysis	88
	(ii) PWBA Analysis	92
3.5	Comparison with Theory	94
3.6	The $\text{Si}^{28}(\text{d},\text{n})\text{P}^{29}$ Reaction at $E_d = 6$ MeV	99
CHAPTER 4	The $\text{Si}^{30}(\text{d},\text{n})\text{P}^{31}$ REACTION	103
4.1	Introduction	103
4.2	Experimental Procedure	105
4.3	The Levels of P^{31}	111
4.4	The Analysis of the Angular Distributions	113
4.5	Negative Parity and Isobaric Analogue States in P^{31}	119
4.6	Interpretation and Discussion	121
	(i) The Strong Coupling or Nilsson Model	121
	(ii) The Weak Coupling or Vibrational Model	126
	(iii) Discussion	128
APPENDIX I	THE STATISTICAL ANALYSIS OF EXPERIMENTAL DATA	134
I.1	Introduction	134
I.2	The Statistics of Nuclear Events	134
I.3	The Likelihood Function and the Method of Maximum Likelihood	136
I.4	The Maximum Likelihood Method for the Poisson Distribution	139
I.5	Formulation of the Least Squares Problem	141
	(i) The Linear Case	141
	(ii) The Nonlinear Case	146
I.6	General Discussion of the Method of Least Squares	150

FIGURES

		Following page
2-1	Physical arrangement of the target room and beam transport system	13
2-2	(a) The target chamber (b) Shielding	13
2-3	The target holder assembly	14
2-4	The energy resolution of a neutron time-of-flight spectrometer as a function of neutron energy and flight path d	17
2-5	Schematic representation of the principles of operation of a Mobley beam bunching system	18
2-6	The relationship between the rectangular Cartesian coordinates and the curvilinear coordinates used in the derivation of the paraxial ray equations of a sector magnet	22
2-7	Schematic representation of a symmetric sector magnet	51
2-8	Arrival time versus initial or acceptance time for a proton beam of various energies	52
2-9	Arrival time versus acceptance time for a deuteron beam of various energies	52
2-10	Representation of an ion beam by means of the central trajectory and two extreme rays of the beam	54
2-11	Four possible optical coupling systems that link the accelerator to the beam bunching system	63
2-12	Typical beam pulse obtained at the target for 3 MeV protons	76
2-13	Block diagram of the radio frequency deflection system	78
3-1	Block diagram of the neutron time-of-flight spectrometer	82
3-2	Neutron time-of-flight spectrum from the reaction $\text{Si}^{28}(\text{d},\text{n})\text{P}^{31}$ taken at 15° to the incident 5.09 MeV deuteron beam	83
3-3	Comparison of the angular distributions for neutrons leading to the ground and first excited states of F^{17} obtained in the present experiment with those obtained by Yaramis.	86

Figures continued

3-4	Angular distributions from the $\text{Si}^{28}(\text{d},\text{p})\text{Si}^{29}$ and $\text{Si}^{28}(\text{d},\text{n})\text{P}^{29}$ reactions for various deuteron bombarding energies	87
3-5	Angular distributions of the neutrons leading to the 0, 1.38, and 1.96 MeV states of P^{29} for $E_d = 4$ MeV	90
3-6	Angular distributions of the neutrons leading to the 0, 1.38, and 1.96 MeV states of P^{29} for $E_d = 5$ MeV	90
3-7	Angular distributions of the neutrons leading to the 3.103 and 3.47 MeV states of P^{29} for $E_d = 5.09$ MeV	93
3-8	Angular distributions of the neutrons leading to the 1.38 ($J^\pi = 3/2^+$) and 1.96 ($J^\pi = 5/2^+$) MeV levels of P^{29} for a deuteron bombarding energy of 6 MeV	99
3-9	Angular distributions of the neutrons leading to the 0, 1.38, and 1.96 MeV states of P^{29} for $E_d = 6$ MeV	99
3-10	Angular distributions of the neutrons leading to the 3.103, 3.47 and 4.34 MeV states of P^{29} for $E_d = 6$ MeV	101
4-1	Block diagram of the neutron time-of-flight spectrometer	105
4-2	Neutron time-of-flight spectrum from the reaction $\text{Si}^{30}(\text{d},\text{n})\text{P}^{31}$ taken at 0° to the incident 5.00 MeV deuteron beam	107
4-3	The relative efficiency of the neutron detector	109
4-4	Comparison of the angular distributions for neutrons leading to the ground and first excited states of F^{17} obtained in the present experiment with those obtained by Yaramis	110
4-5	Neutron time-of-flight spectrum from the reaction $\text{Si}^{30}(\text{d},\text{n})\text{P}^{31}$ taken at 60° to the incident 3.0 MeV deuteron beam	111
4-6	Angular distributions of the neutrons leading to the ground state and excited states at 1.26, 2.23, and 3.13 MeV for $E_d = 5$ MeV	116
4-7	Angular distributions of the neutrons leading to the 5.01, 5.25, 6.38, and 6.60 MeV states of P^{31}	116
4-8	Angular distributions of the neutrons leading to the 5.01, 6.48, and 6.60 MeV states of P^{31} for $E_d = 5$ MeV	119
4-9	Angular distributions of the neutrons leading to the 6.38 and 7.14 MeV states of P^{31}	120
4-10	Energy level diagrams of P^{31} and P^{29} showing the similarities in the structure of the two nuclei and the comparison of P^{31} with the predictions of the Nilsson model	124

Figures continued

4-11	Single particle energy levels of the Nilsson model as a function of the deformation η	124
4-12	Energy levels of P^{31} compared with the predictions of (a) The Vibrational Model (b) The Shell Model	128

CHAPTER 1

INTRODUCTION

Although nuclear phenomena have been intensively studied for thirty years, the true nature of the nuclear forces has not yet been ascertained. Even if the nuclear forces were known in detail, it is unlikely that the nuclear problem could be solved with the present mathematical techniques at our disposal. Consequently many models of the nucleus have been proposed which take into account various aspects of the nuclear forces that have been established. Among the most important of these are the shell model and the various collective models. The interpretation of the experimentally determined nuclear phenomena in terms of these models has two very important consequences for the future development of nuclear theory. Firstly it allows the present concept of the nuclear interaction to be tested in a realistic, if not in a direct, manner. Secondly and perhaps equally as important it allows the sharpening of the mathematical tools used in the solution of the many body problem. Although none of the nuclear models currently available is able to explain all the experimentally measured properties, considerable progress has been made in an understanding of these phenomena in a qualitative, if not in a completely quantitative, fashion.

For example, many of the properties of nuclei in the $2s - 1d$ shell can be understood in terms of the collective model (Go 60). For odd A nuclei,

which are the subject of the present discussion, the most successful formulation of this model is the one due to Nilsson (Ni 55) in which rotational and vibrational states are built on the single particle states of the odd nucleon moving in a permanently deformed potential well. In the Nilsson model the properties of the ground state and the low lying excited states can be classified in terms of the particle number of the odd nucleon (Go 60). Considerable success has been achieved in the understanding of the nuclei in the region of $A = 25$ on this basis. The work of Litherland et al (Li 58) on Mg^{25} and Al^{25} is of particular interest in this regard. The nuclei in the vicinity of F^{19} also show collective properties that can be understood on the basis of the Nilsson model (Go 60, Pa 57, Pa 58). More recently the nuclei in the region of mass-28 have been studied in order to investigate the range of validity of the strong-coupling collective model in the 2s-1d shell (Br 57, Br 58, Ha 62, Ha 63, Ej 64, Bi 65).

The nuclides Si^{29} , P^{29} , P^{31} and S^{31} are of particular interest since they lie just above the "closed" Si^{28} core expected on the basis of the j-j coupling shell model. An investigation of Si^{29} by Bromley et al (Br 57, Br 57a) lead them to the conclusion that Si^{29} could most reasonably be described by the Nilsson model with a negative or oblate deformation $\eta = -3$. They find in fact that the predictions of the single particle shell model are not in agreement with:

- (1) The experimental gamma ray transition probabilities for the decay from the second excited state to the first excited state and the ground state of Si^{29} .

- (2) The measured magnetic moment (-0.56 n.m. as compared with -1.96 n.m. predicted by the shell model).
- (3) The experimental $\log ft$ value > 6.5 for the beta decay of Al^{29} to Si^{29} .

It therefore seems reasonable to conclude that the assumption of an inert spherically symmetric Si^{28} core is not very good. However the failure of the single particle shell model does not rule out the possibility that Si^{29} and its mirror P^{29} can be described in terms of the weak coupling collective model in which the odd nucleon is coupled to a closed Si^{28} core making quadrupole oscillations. Weak coupling or vibrational model calculations have been made for Si^{29} by Pandya (Pa 59) and for P^{29} by Ejiri (Ej 64). Reasonable agreement with the observed sequence of energy levels is obtained although the predicted magnetic moments do not compare favourably with the experimental values. The gamma ray transition probabilities obtained from the vibrational model calculations do not compare as favourably with the experimental values as do those predicted by the Nilsson model. However the agreement is such that it does not exclude the application of the vibrational model to these nuclei. The relative spectroscopic factors obtained from the work of Calvert et al (Ca 57) for P^{29} using the plane wave Born approximation are in rather poor agreement with both the vibrational and Nilsson models.

The properties of P^{31} have been studied by Broude Willmott and Green (Br 58) and by Harris and Seagondollar (Ha 62, Ha 63) using the $Si^{30}(p,\gamma)P^{31}$ reaction. (Very little experimental information is currently available on the mirror nucleus S^{31}). These studies have resulted in a fairly complete

understanding of the level structure of P^{31} up to 5 MeV of excitation. The spins and parities of most of these levels have been fairly well established as have the transition probabilities for the electromagnetic transitions between the various levels. Unfortunately an ambiguity in the theoretical expression for the angular correlation of the cascade gamma rays associated with the 3.133 MeV state (Ha 63, Ri 64) of P^{31} lead to an incorrect spin assignment of $\frac{3}{2}^{+}$ for this level. A recent gamma ray polarization experiment by Van Rinsvelt and Endt (Ri 64) has resolved this problem and the spin and parity of the 3.133 MeV level has been fixed at $\frac{1}{2}^{+}$. In another gamma ray polarization experiment done by Harris, Hennecke and Prosser (Ha 64) the level at 4.43 MeV excitation in P^{31} has been identified as a negative parity state with $J^{\pi} = \frac{7}{2}^{-}$. The existence of a $\frac{7}{2}^{-}$ level as the first negative parity state in P^{31} implies that only a negative deformation is possible for P^{31} if indeed a permanent deformation does exist for this nucleus (Br 57). A further discussion of this point in conjunction with three other negative parity states identified in the present experiment will be given in chapter 4.

Attempts to explain the observed level sequence and gamma ray transition probabilities and multipolarities have been made using the Nilsson model with varying degrees of success (Br 58, Bi 65, Ra 65). In the original calculation of Broude et al (Br 58) the 3.133 MeV level of P^{31} was identified with the second member of a rotational band based on Nilsson orbit 9 on the basis of the $\frac{3}{2}^{+}$ spin and parity assignment to this level. The recent spin and parity assignment of $\frac{1}{2}^{+}$ to this level makes their

identification with Nilsson orbit 9 invalid. On the basis of this new information Nilsson model calculations have been made recently by Ramavataram (Ra 65) and Bishop (Bi 65). Since there is evidence (Br 57, Ej 64) (see also chapter 4) that the deformation of P^{31} should be smaller than for P^{29} or Si^{29} weak-coupling collective model calculations have also been made for P^{31} by Thankappen and Pandya (Th 60, Th 62) and by Ramavataram (Ra 65). Good agreement with the observed energy level sequence and gamma ray transition probabilities for the low-lying levels is obtained. However the magnetic moment predicted by this model is approximately twice the observed value ($\mu = 1.13$ n.m.) as is also the case for P^{29} . This model also predicts a vanishing stripping reduced width for the second excited state at 2.232 MeV which is not entirely consistent with the results of the present investigation (see chapter 4). A similar result is also obtained for P^{29} .

A shell model calculation for nuclei in the region from $A = 28$ to $A = 40$ has been made by Glaudemans, Wiechers and Brussaard (Gl 64) assuming a closed Si^{28} core with a two-particle interaction of the outer nucleons in the $2s_{1/2} - 1d_{3/2}$ shells. A further discussion of the applicability of these models to P^{29} and P^{31} will be given in chapters 3 and 4.

Although considerable information was available concerning the structure of the nuclei P^{29} and P^{31} it seemed particularly interesting to investigate the properties of the excited states of P^{29} and P^{31} in a (d,n) reaction where a single proton is transferred to the core nucleus. Such an investigation has the important advantage that the nucleon reduced widths may be extracted from the experimental cross sections in a relatively straightforward

fashion (Ma 60). At the time when the present project was undertaken little information was available concerning the nucleon reduced widths of P^{29} and P^{31} . The measurement and analysis of the differential cross sections for the (d,n) reaction leading to levels in P^{29} and P^{31} constitutes the subject matter of this thesis.

The reduced width θ^2 for a stripping reaction $A(a,b)B$ can be written as the product (Ma 60)

$$\theta^2 = S\theta_0^2$$

where S is a quantity known as the spectroscopic factor and θ_0^2 is the "single particle reduced width." The spectroscopic factor S is essentially the overlap integral between the wave function representing the final state of B and the wave function representing the initial state of A ; the "single particle reduced width" θ_0^2 is the probability for the stripping process assuming that the structure of the target nucleus A can be ignored. Thus if the levels of B can be described in terms of the single particle shell model one obtains $S = 1$ and $\theta^2 = \theta_0^2$. The spectroscopic factor is seen to be a measure of the effective single particle strength in the wave function leading to the final state in B . That the spectroscopic factor is a parameter which is dependent upon the details of the nuclear wave functions involved in the transformation from A to B makes it a useful mode of comparison between experiment and the predictions of the current nuclear models (Ma 60). The spectroscopic factors are usually obtained by the comparison of the differential cross sections obtained experimentally with those predicted by the distorted wave

Born approximation (DWBA). Because of the importance of deuteron stripping and other direct interaction reactions in current nuclear spectroscopy and to form a basis for the discussions of chapters 3 and 4, a brief description of the theoretical DWBA cross section will be given.

The differential cross section for a direct reaction in the distorted wave Born approximation can be written as (Au 63, Au 64)

$$\frac{d\sigma}{d\Omega} = \frac{\mu_a \mu_b}{(2\pi\hbar^2)^2} \frac{(2J_B + 1)}{(2J_A + 1)} \frac{k_b}{k_a} \sum_{\ell s j} \frac{|A_{\ell s j}|^2}{2s_a + 1} \sum |\beta_{s j}^{\ell m}|^2 \quad (1-1)$$

where

μ_a and μ_b are the reduced masses of the pairs (a,A) and (b,B);

k_a and k_b are the wave vectors for particles a and b;

J_A , J_B , s_a and s_b are the spins of particles A, B, a and b respectively with corresponding z components M_A , M_B , m_a and m_b ;

$A_{\ell s j}$ is related to the spectroscopic factor $S_{\ell j}$,

$$\beta_{s j}^{\ell m} = \frac{1}{(2\ell+1)^{1/2}} i^{-\ell} \int dr_a \int dr_b \chi_b^{(-)*}(\underline{k}_b, \underline{r}_b) f_{\ell s j m}(\underline{r}_b, \underline{r}_a) \chi_a^{(+)}(\underline{k}_a, \underline{r}_a)$$

$\chi_b^{(-)}$ is the outgoing distorted elastic scattering wave,

$\chi_a^{(+)}$ is the incoming distorted elastic scattering wave,

$f_{\ell s j m}$ is proportional to the radial wave function of the bound nucleon in deuteron stripping reactions.

The elastic scattering waves and the bound nucleon wave function are solutions of the radial Schrödinger equation

$$\phi_{\ell}''(r) - \frac{2m}{\hbar^2} \left[E_{c.m.} + V(r) - \frac{\hbar^2}{2m} \frac{\ell(\ell+1)}{r^2} \right] \phi_{\ell} = 0 \quad (1-2)$$

where the potential $V(r)$ is a sum of the coulomb and optical model potentials as well as a spin orbit potential if the latter is included. Because of the complexity of the potential $V(r)$ equation (1-2) must be solved by numerical methods on a high speed digital computer. It is usual to treat the angular momentum part of the problem in such a way that each term in the equation (1-1) corresponds to the transfer to the target of a nucleon with definite angular momentum j , which in turn is the sum of an orbital part ℓ and a spin part s , according to the vector coupling

$$\underline{j} = \underline{J}_B - \underline{J}_A, \underline{s} = \underline{s}_a - \underline{s}_b, \underline{j} = \underline{\ell} + \underline{s}.$$

If spin orbit coupling is neglected between the distorted waves $\chi_b^{(-)}$ and $\chi_a^{(+)}$ then different values of ℓ , s and j contribute incoherently to the differential cross section. In this case only one set of values for ℓ , s and j is usually allowed or important. In the present experiments the $\text{Si}^{28}(d,n)\text{P}^{29}$ and $\text{Si}^{30}(d,n)\text{P}^{31}$ reactions are such that $J_A = 0$ and $s_a = 1$ (neglecting the deuteron d-wave component) so that

$$\underline{J}_B = \underline{j} = \underline{\ell} + \underline{s}$$

where $s = s_b$. Consequently the angular momentum J_B is uniquely determined by the angular momentum j of the transferred proton and therefore only one term in the sum over $\ell s j$ is possible in equation (1-1). Thus in the reactions used in the present experiment the orbital angular momentum of the transferred proton can in principle be uniquely determined from the character of the angular distributions of the neutrons leading to

states in the residual nucleus. Also in the case of deuteron stripping, the parity of the final state in B is given by

$$\Pi_B = (-1)^\ell \Pi_A$$

since the spin and parity of the deuteron is taken to be 1^+ . Recently systematic differences have been observed (Le 64, Al 64) between the angular distributions leading to states in the final nucleus B with $J_B = \ell + \frac{1}{2}$ and $J_B = \ell - \frac{1}{2}$ for $\ell = 1, 2$ and 3 and for $J_A = 0$. Under favourable conditions this spin dependent structure allows both the spin J_B and the orbital angular momentum ℓ to be obtained from the experimental differential cross section. For deuteron stripping in the zero range approximation the factor $A_{\ell sj}$ is related to the spectroscopic factor $S_{\ell j}$ by the relation (Sa 64)

$$|A_{\ell sj}|^2 = 1.48 \times 10^4 (2s_a + 1) S_{\ell j}$$

where the factor 1.48×10^4 is proportional to the radial wave function of the captured nucleon obtained by solving equation (1-2) using a real potential well of Saxon-Woods shape (Sa 64). Under these conditions the spectroscopic factor

$$S = \frac{\sigma_{\text{exp}}}{\sigma_{\text{DWBA}}}$$

is a measure of the coefficient of fractional parentage (cfp) relating the component wave function denoted by ℓsj to the total wave function representing the final state in B.

These properties of direct interactions make the (d,p) and (d,n)

reactions very powerful tools indeed for the study of the structure of nuclei.

The availability of an excellent neutron time-of-flight spectrometer made the investigation of P^{29} and P^{31} possible. A discussion of the time-of-flight spectrometer will be given in chapter 2 with special emphasis on the newly installed Mobley beam bunching system.

CHAPTER 2

EXPERIMENTAL APPARATUS AND ARRANGEMENT

2.1 Introduction

The nuclei P^{29} and P^{31} formed in a (d,n) reaction were studied using a high resolution neutron time-of-flight spectrometer. Neutron energy measurement by the time-of-flight technique involves the precise determination of a zero-time (start) signal which signifies the starting time of the neutron as it traverses an accurately determined flight path, and the determination of a stop signal which allows the elapsed time and hence the neutron velocity to be measured. Since the neutron flight times encountered are in the nanosecond time domain, fast timing techniques are required. Various methods for obtaining a precise zero-time signal have been used (Ne 60), (Ne 63). However, the most successful of these is the pulsed beam technique. In these experiments top terminal pulsing of the accelerator and a Mobley magnet compression system were used to obtain high intensity beam bursts of approximately 0.6 ns (FWHM) at a repetition rate of 1 MHz. The start signal was obtained from the pulsed beam as it passed through a cylindrical beam sensing capacitor near the target. The associated stop pulse was obtained by detecting the neutron in an organic scintillator viewed by a photomultiplier. The start-stop pulses obtained in this manner were

fed to a time-to-amplitude converter, the output of which was analysed by a multichannel pulse height analyser. The time-to-amplitude converter and associated circuitry involves the use of very high speed pulse circuits capable of operating in the sub-nanosecond time domain. A good discussion of the problems associated with the development of the electronic techniques required in the construction of a high resolution time-of-flight spectrometer can be found in references (Ne 59), (Ne 60), (Ne 63) and (Al 63).

During the period in which the experiments were performed two different neutron detection systems were employed since it became necessary to improve both the resolution and the time base of the spectrometer. For this reason a discussion of these systems will be given in conjunction with the experiments in which they were employed.

2.2 The Accelerator and General Experimental Arrangement

The pulsed deuteron beam employed in these experiments was obtained from the University of Alberta 5.5 MeV model CN Van de Graaff accelerator*. A high power radio frequency (R.F.) ion source was used to produce a 2 ma d.c. beam of ionized deuterium. A top terminal magnetic analyser and a three element Einzel electrostatic lens produces a well focussed beam which is pulsed by sweeping the beam across a small aperture. An elliptical sweep allows only one pulse per cycle of the deflection oscillator which improves the emittance properties of the ion beam. A pulse duration

*Model CN Van de Graaff, High Voltage Engineering Corporation, Burlington, Massachusetts, U.S.A.

ranging between 10 and 15 ns (FWHM) is obtained with this system.

Energy stabilization of the accelerator is accomplished by passing the beam through a 90° double focussing sector magnet with a 28.5 inch radius of curvature (ρ) and sensing the beam position with a pair of energy stabilizing slits 57 inches (2ρ) from the exit pole face of the analysing magnet. The momentum dispersion $\Delta p/p$ of the beam is approximately 3.5×10^{-3} for a 0.3 inch aperture defined by the energy slits and is limited by the necessity of maintaining maximum beam current on the target.

The physical arrangement of the beam transport system including the Mobley bunching magnet and neutron detectors is shown in figure (2-1). In order to minimize the background radiation in the target area the analysing magnet, energy slits, first carbon trap, switching magnet and quadrupole lenses are isolated from the target area by a two foot thick concrete wall. Additional background reduction is provided in the target room by an extensive system of concrete walls and water filled tanks as shown in figures (2-1) and (2-2). Further shielding is provided by a lead sheath and plug assembly partially shown in figure (2-2) which shields the detectors from radiation produced at the slits and beam sensing capacitor placed at the entrance to the target chamber. Considerable care was taken in the design and construction of all the beam sensing and defining devices to ensure that a minimum amount of radiation was produced by these devices.

The neutrons leading to states in the residual nucleus were detected in

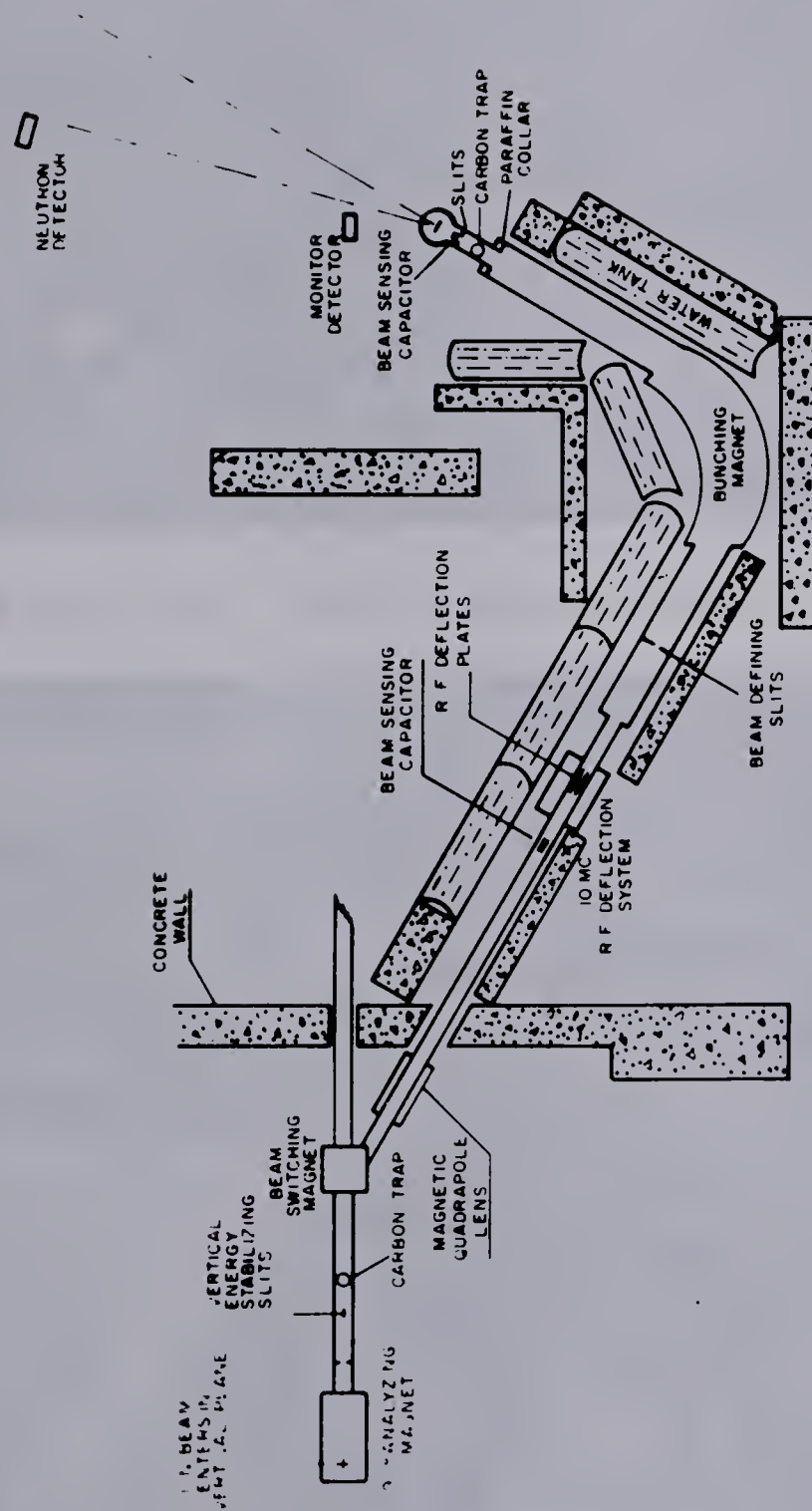


Figure 2-1. Physical arrangement of the target room and beam transport system.

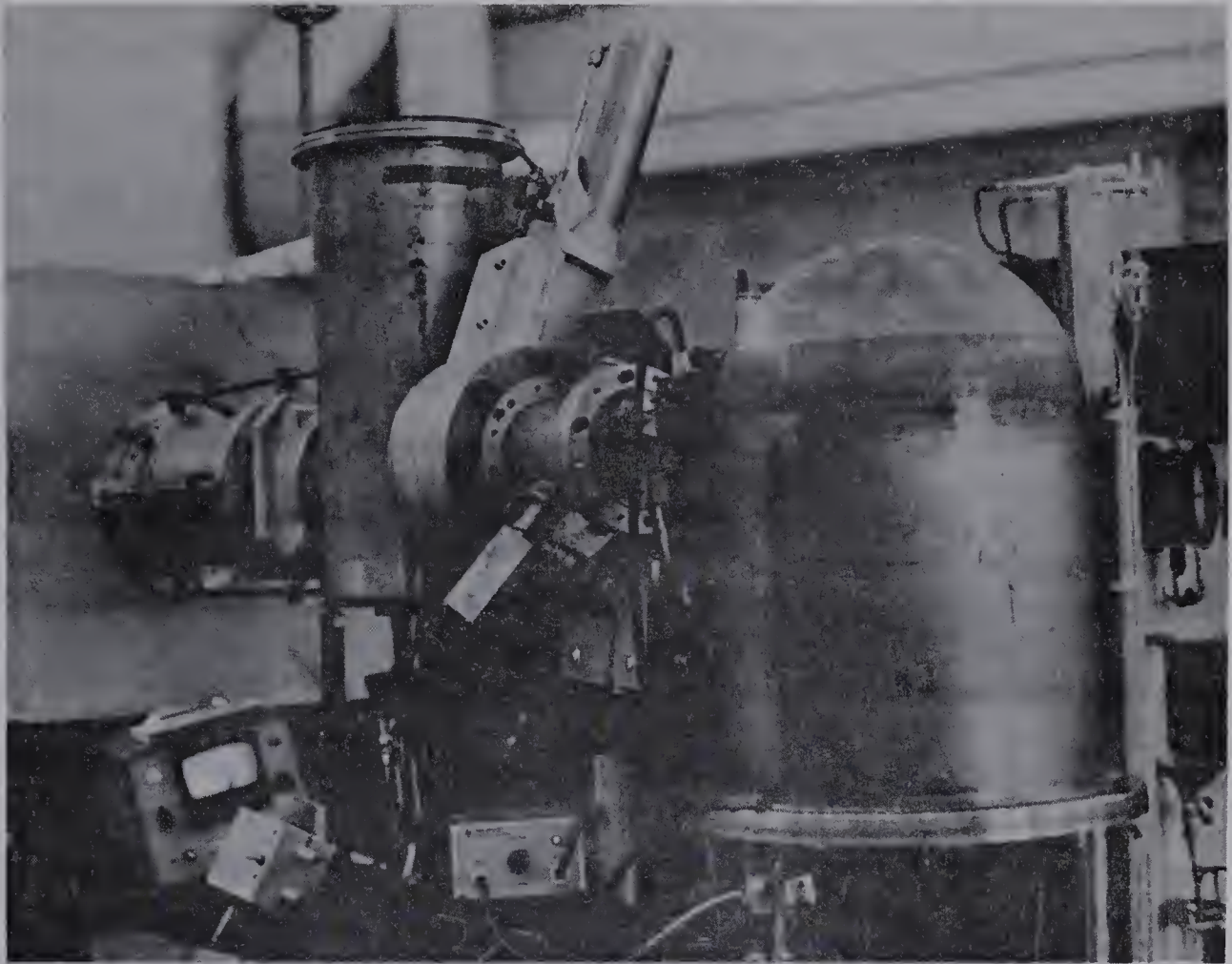
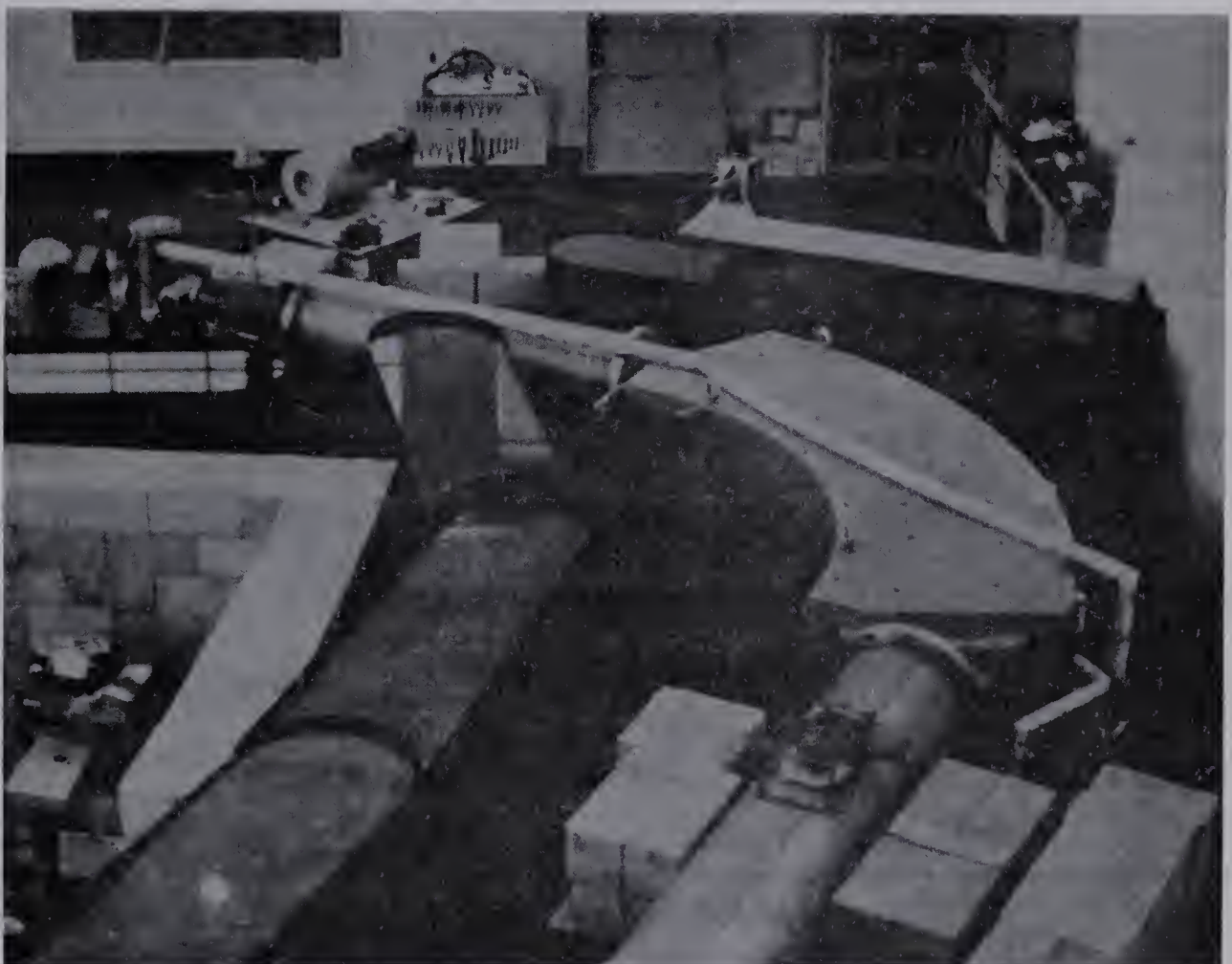


Figure 2-2. (a) The target chamber



(b) Shielding

NE 213 liquid scintillator* contained in a quartz cell and mounted on a Phillips XP 1040 photomultiplier.

The neutron detector carriage was mounted on a six meter boom which pivots about a point directly below the centre of the target chamber. Both the detector carriage and boom are motor driven and can be controlled remotely from the Van de Graaff console. The neutron flight path and the angular position of the detector are measured with gear driven precision potentiometers, the output of which is monitored by a four place digital voltmeter at the control console.

2.3 The Target Assembly

The targets were mounted in an insulated air cooled target holder denoted by A in figure (2-3), whose vertical, lateral and angular positions could all be independently adjusted from outside the vacuum chamber. Thermal and electrical contact with the target was made through a 1/32 inch gold plate, B, which was securely clamped to the target holder. The target was held in position on the gold backing by small gold mounting pins. The gold backing, as well as providing thermal and electrical contact, stopped the deuteron beam and thus provided a measurement of the total beam current on the target. Electrical contact with the target assembly was made with a short length of coaxial cable C which terminated in a BNC connector mounted in the base of the vacuum chamber. Cooling air was provided through two armoured tygon tubes denoted by D in the diagram. The target assembly was mounted in a 12 inch diameter

* Nuclear Enterprises Ltd., Winnipeg, Manitoba

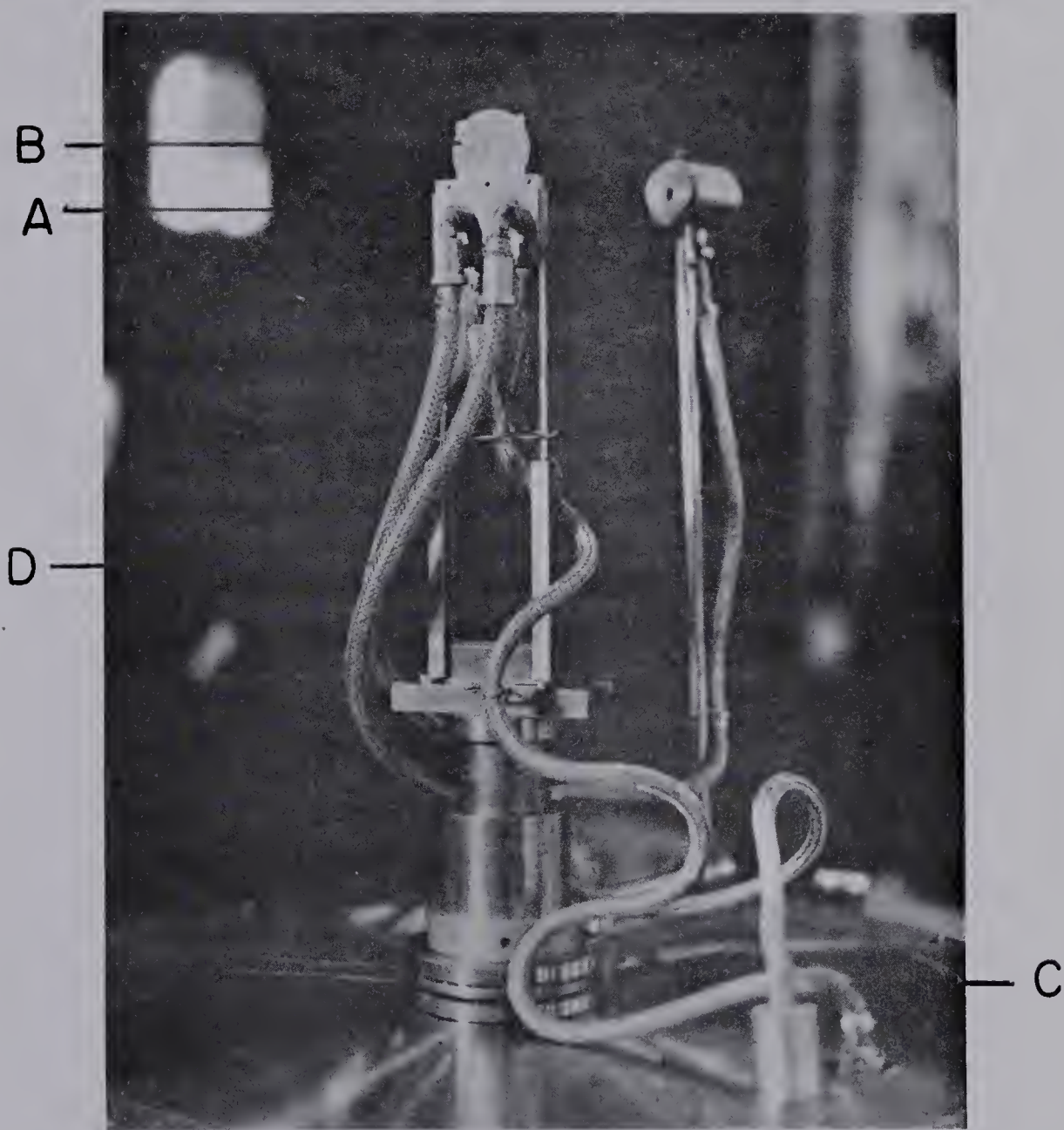


Figure 2-3. The Target holder assembly

vacuum chamber constructed from 1/32 inch stainless steel to minimize neutron absorption. Alignment of the target assembly was accomplished by viewing selected points on the target through a transit looking through an alignment port in the Mobley magnet vacuum chamber.

2.4 The Beam Bunching System

(i) Introduction

The time-of-flight technique has emerged as the most useful method available for neutron energy measurement when high efficiency of neutron detection over a broad spectrum of neutron energies is required. However, since the neutron flight times encountered are in the nano-second time domain, very short ion bursts of high intensity are required. Various methods for obtaining ultra-short bursts of ions have been investigated. However, the present discussion will be limited to the methods used in this laboratory.

The simplest technique from the point of view of the experimenter is to chop the beam using the differential impulse sweeping technique described by Fowler and Good (Fo 60). A spectrometer using this method was constructed by Neilson et al (Ne 59). This method is limited by the low beam current available at the target which in turn restricts the maximum flight path that can be employed and still maintain a reasonable counting rate. The intensity problem encountered with the use of this system can be illustrated by considering the duty cycle of an idealized chopper: viz. $I = I_0 f \Delta t$ where I is the beam current at the target, I_0 the beam entering the deflection system, f the frequency of the sweep oscillator and Δt the duration of the beam burst of the target. For the system described by Neilson (Ne 59) with $I_0 = 50 \mu\text{a}$, $f = 1.66 \text{ MHz}$ and $\Delta t = 2 \text{ ns}$, the average beam current is $0.166 \mu\text{a}$.

The factors that determine the timing resolution of a neutron spectrometer can be divided into two parts. Firstly there is the pulse width of the beam on the target, and secondly there is the electronic resolution of both the beam sensing and neutron detection circuitry.

These factors have been investigated by Neilson et al (Ne 63) and Alexander and Neilson (Al 63) and will not be discussed further at this time. Suffice it to say that the electronic resolution neglecting scintillator thickness can be reduced to the order of 0.1 ns. However, it is useful to investigate the relationship between energy resolution and timing resolution of a neutron spectrometer. The energy resolution ΔE is related to the timing resolution Δt by the expression $\Delta E/E = 2\Delta t/t$ where E and t are the energy and time-of-flight of the detected neutron respectively. Curves showing the energy resolution ΔE as a function of the timing resolution Δt for different flight paths are given in fig. (2-4) which gives a quantitative indication of the problems associated in constructing a high resolution time-of-flight spectrometer. From the above considerations it is seen that improvements in the beam pulsing methods are necessary if a substantial improvement in spectrometer resolution is to be realized. Two methods that have been successfully applied to this problem are the klystron buncher and the Mobley magnet buncher (Mo 52). Of these, the Mobley compression magnet has been most frequently employed and has also been the most successful of the two methods. A 75 inch Mobley compression magnet has been installed

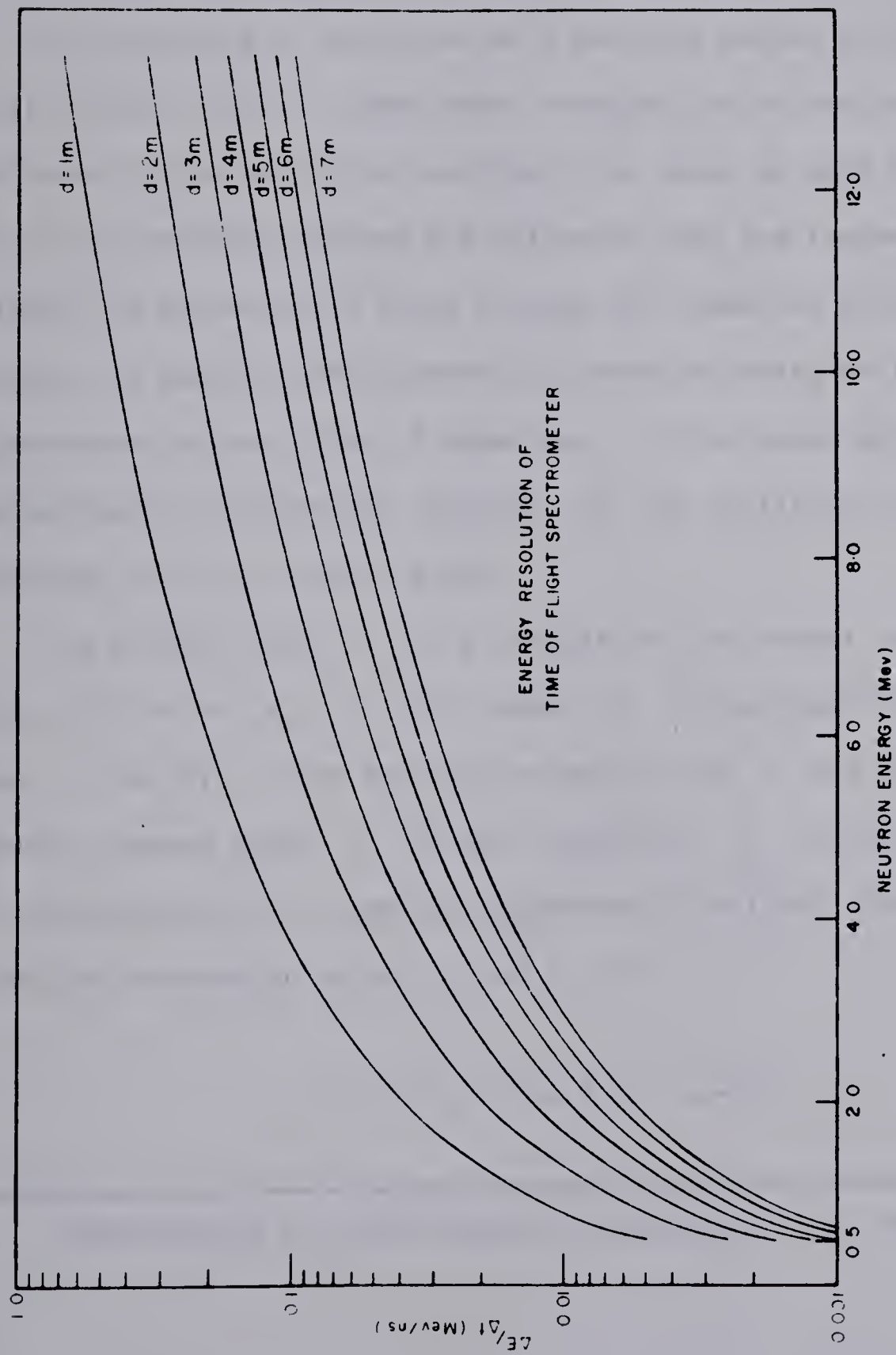


Figure 2-4 The energy resolution of a neutron time-of-flight spectrometer as a function of neutron energy and flight path d .

at the University of Alberta (UA) and will be discussed in detail in the following sections.*

(ii) The Operation of a Mobley Bunching Magnet

The principle of operation of a bunching magnet is shown schematically in fig. (2-5). A beam burst entering the deflection plates of the phase locked deflection oscillator is swept in such a manner that the first particles leaving the deflector take the longest paths through the magnet while those leaving last take the shortest paths through the magnet with intermediate particles being deflected to paths appropriate to their time of departure. If the phase and amplitude of the deflector are properly adjusted, all the particles will arrive at the image point in a short pulse.

The arrival time t_a of a particle at the target can be seen (fig. 2-5) to be $t_a = t + L/v$ where L is the length of the trajectory from A to B, v the particle velocity, and t the time at which the particle passed point A. If the trajectory L_0 is taken as the central or equilibrium orbit, then the difference in arrival times between particles traversing paths L and L_0 is

$$\Delta t_a = t_a - t_{a0} = t - \frac{L - L_0}{v} \quad (2-1)$$

*Manufactured by Spectromagnetic Industries Ltd., Hayward, California

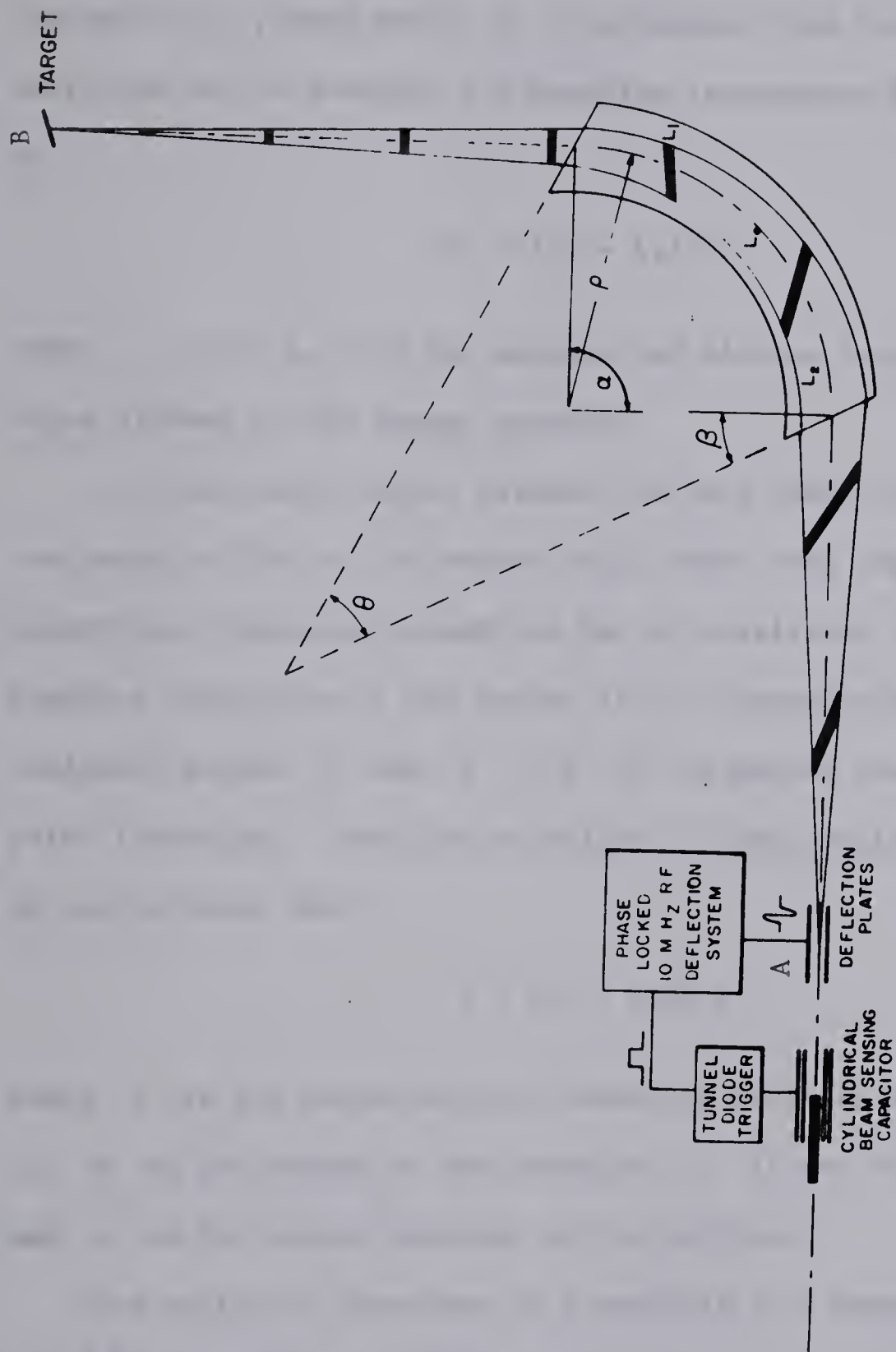


Figure 2-5 Schematic representation of the principles of operation of a Mobley beam bunching system.

where t is now measured from the point at which the particle traversing the path L_0 passes point A. The maximum time interval over which particles can be accepted for bunching (acceptance time) is also seen to be

$$\Delta t = (L_1 - L_2)/v \quad (2-2)$$

where L_1 and L_2 are the maximum and minimum lengths of the trajectories allowed by the magnet geometry.

A relationship exists between the path length difference and the magnetic flux of the magnet which shows that the design of the geometrical focussing properties can be considered independently of the bunching properties of the magnet if all trajectories pass through the conjugate points A and B (i.e. if the magnet possesses point to point focussing). From the principle of least action (St 55, p.29) it can be shown that

$$\Phi = (L_1 - L_2) \frac{c}{e} p \quad (2-3)$$

where Φ is the magnetic flux (Maxwells) enclosed between L_1 and L_2 , e is the charge of the particle, c is the velocity of light and p is the scalar momentum of the particle.

The radius of curvature of a particle in a magnetic field H is $\rho = \frac{c}{e} \frac{p}{H}$ so that eqn. 2-3 becomes

$$\Phi = (L_1 - L_2) H \rho \quad (2-4)$$

For the case of a uniform field magnet, $\Phi = AH$ and equation (2-4) reduces to

$$L_1 - L_2 = A/\rho \quad (2-5)$$

where A is the area bounded by the paths L_1 , L_2 , and the pole faces of the magnet. These relationships are quite general and are independent of the particular geometry of the magnetic field, subject to the condition that all trajectories passing through point A also pass through point B . Consequently the design of the focal properties of the magnet can be undertaken independently of the bunching properties of the magnet. If L_1 and L_2 are the maximum and minimum trajectories, the acceptance time for a uniform field magnet becomes

$$\Delta t = \frac{A}{\rho v} \quad (2-6)$$

The parameters that must be considered in the design of a bunching magnet are:

- (a) The time dispersion of the bunched beam (alternatively the bunching factor of the magnet).
- (b) The allowable angular divergence of the beam on the target.
- (c) The maximum velocity of the particles that are to be bunched.
- (d) The acceptance time of the magnet.
- (e) The beam spot size on the target.

All five parameters enter into the design of the bunching system determining first the geometrical design of the magnet which in turn sets limits on the frequency, peak voltage, and wave form that must be supplied by the deflection system. The successful operation of

such a system depends very heavily on the beam quality (i.e. emittance and momentum dispersion) entering the bunching system. As will be seen later, the beam quality is often the limiting factor for both the spot size on the target and the time spread of the bunched beam.

The simplest optical system from both a practical and a theoretical standpoint consists of a uniform field sector magnet in which the axial focussing is accomplished by the fringing field. A detailed analysis of the optical and time compression properties of a uniform field sector magnet such as the one in use at the University of Alberta will be given in the following sections.

(iii) The Paraxial Ray Equations of a Uniform Field Sector Magnet

In describing the optics of an ion moving in a magnetic field it is convenient to choose a coordinate system defined by the geometry of the magnet and the trajectory of a particle having the "design" momentum. All trajectories considered in the analysis are assumed to move in the vicinity of the central trajectory or ray axis which determines the focal and dispersive properties of the magnet. A suitable curvilinear coordinate system based on the central trajectory can be defined by the equation (Co 58)

$$\underline{r} = \underline{r}_0(s) \quad (2-7)$$

where s is the arc length measured along the ray axis from some fixed initial point. An instantaneous orthogonal coordinate system can be defined by unit vectors found by differentiating the reference vector

(eqn. 2-7). That is

$$\hat{\alpha}(s) = \frac{d\mathbf{r}_0(s)}{ds} \quad (2-8)$$

where $\hat{\alpha}(s)$ is the unit vector tangent to the curve at s , and

$$\frac{d\hat{\alpha}(s)}{ds} = \kappa(s)\hat{\beta}(s) \quad (2-9)$$

where $\kappa(s)$ is the curvature of the central trajectory and $\hat{\beta}(s)$ is the unit vector perpendicular to $\hat{\alpha}$ called the principal normal (See fig. 2-6).

A third unit vector $\hat{\gamma}(s)$ orthogonal to both $\hat{\alpha}$ and $\hat{\beta}$ can be defined as

$$\hat{\gamma}(s) = \hat{\alpha}(s) \times \hat{\beta}(s) \quad (2-10)$$

which completes the coordinate system. The plane defined by $\hat{\alpha}$ and $\hat{\beta}$ is called the osculating plane, while equation (2-9) is the first of three differential relations among $\hat{\alpha}$, $\hat{\beta}$, and $\hat{\gamma}$ which can be derived from the properties of the unit vectors (Sy 59). These relations, called the "Frenet-Serret formulas" are:

$$\frac{d\hat{\alpha}(s)}{ds} = \kappa\hat{\beta}(s); \quad \frac{d\hat{\beta}(s)}{ds} = \omega(s)\hat{\gamma} + \kappa(s)\hat{\alpha}(s) \quad (2-11)$$

$$\text{and} \quad \frac{d\hat{\gamma}(s)}{ds} = -\omega(s)\hat{\beta}(s)$$

where $\omega(s)$ is a scalar known as the torsion of the curve. For a plane curve $\omega(s)$ vanishes identically. The radius of curvature, ρ , and the radius of torsion, τ , are related to κ and ω by the equations

$$\rho = 1/\kappa \text{ and } \tau = 1/\omega.$$

$$P^2 = P_x^2 + P_y^2 + P_z^2 = P_\alpha^2 + P_\beta^2 + P_\gamma^2$$

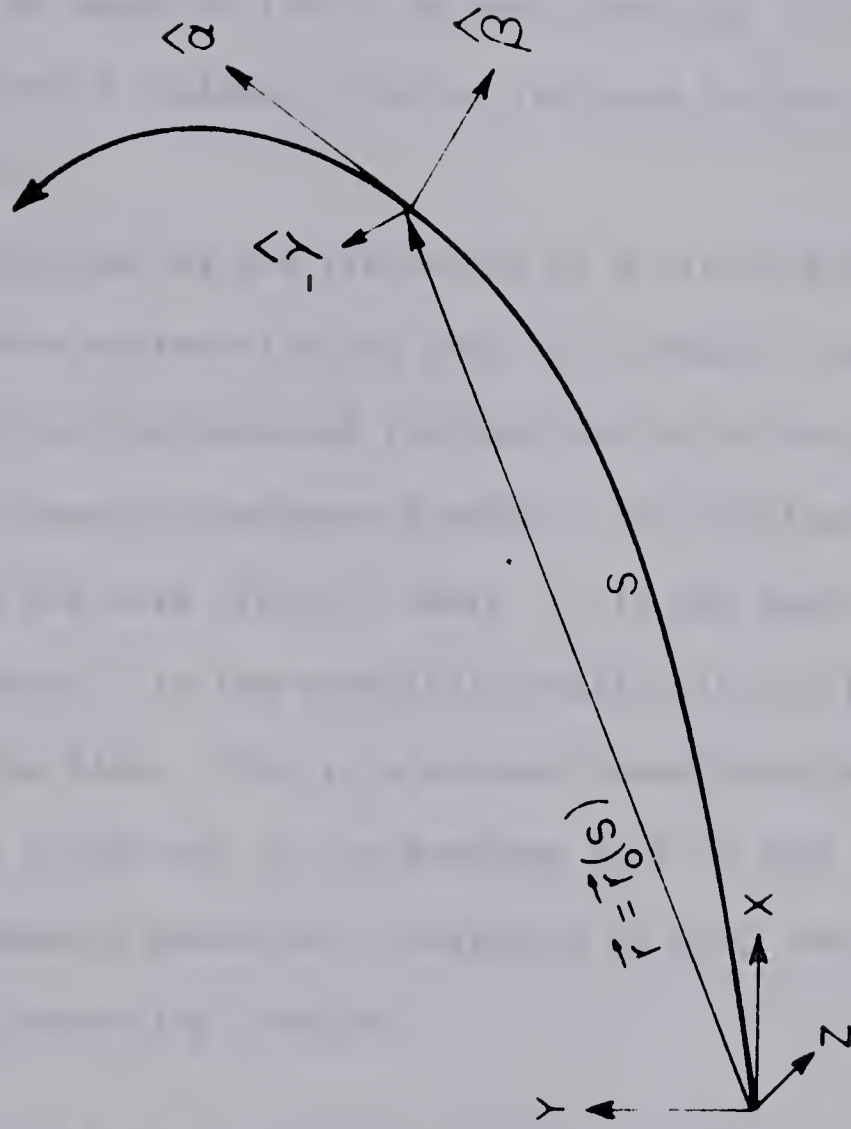


Figure 2-6. The relationship between the rectangular cartesian coordinates and the curvilinear coordinates used in the derivation of the paraxial ray equations of a sector magnet.

The position of any point in space, not too far from the central ray is given by

$$\underline{r}(s,x,z) = \underline{r}_0(s) + x\hat{\beta}(s) + z\hat{\gamma}(s) \quad (2-12)$$

The point defined by equation (2-12) is seen from fig. (2-6) to be unique for points whose distance from the ray axis is less than the radius of curvature ρ .

Hamilton's equation for the trajectory of a particle can be obtained in the new coordinate system with the help of a contact transformation relating the canonical variables and the Hamiltonian of the old (cartesian) and the new (curvilinear) coordinate systems. The required generating function must have the form $F(p,Q,t)$ where p is the canonical momentum in cartesian coordinates, Q is the canonical position in curvilinear coordinates and t is the time. This is a contact transformation of the third kind (Go 59, p.240) and in its simplest form is just $F_3(p,Q,t) = \sum_i p_i Q_i$. Thus the momenta canonically conjugate to s, x , and z can be obtained from the generating function

$$F_3(p_X, p_Y, p_Z; s, x, z) = \underline{p} \cdot [\underline{r}_0(s) + x\hat{\beta}(s) + z\hat{\gamma}(s)] \quad (2-13)$$

where p_X, p_Y , and p_Z are the components of the momentum \underline{p} in the cartesian coordinates (X,Y,Z) . The desired canonical momenta are:

$$p_s = \frac{\partial F_3}{\partial s} = \underline{p} \cdot \left[\frac{\partial \underline{r}_0(s)}{\partial s} + x \frac{\partial \hat{\beta}(s)}{\partial s} + z \frac{\partial \hat{\gamma}(s)}{\partial s} \right]$$

which by virtue of the Frenet-Serret formulae becomes

$$p_s = \underline{p} \cdot [(1 + \kappa x)\hat{\alpha} + \omega(x\hat{\gamma} - z\hat{\beta})] \quad (2-14a)$$

and

$$p_x = \frac{\partial F_3}{\partial x} = \underline{p} \cdot \hat{\beta} \quad (2-14b)$$

$$p_z = \frac{\partial F_3}{\partial z} = \underline{p} \cdot \hat{\gamma} \quad (2-14c)$$

The new Hamiltonian K is obtained from the relation (Go 59)

$$K = H + \frac{\partial F_3}{\partial t} = H$$

where H is the relativistic Hamiltonian

$$H = eV + c[m^2c^2 + (\underline{p} - e\underline{A})^2]^{1/2} \quad (2-15)$$

and the quantities V and A are the scalar and vector potentials of the electromagnetic field. In terms of the new variable, the Hamiltonian becomes*

$$H = eV + c \left\{ m^2c^2 + \frac{1}{(1+\kappa x)^2} [p_s - eA_s + \omega z(p_x - eA_x) - \omega x(p_z - eA_z)]^2 + (p_x - eA_x)^2 + (p_z - eA_z)^2 \right\}^{1/2} \quad (2-16)$$

where A_s , A_x , and A_z are obtained in an analogous manner to p_s , p_x , and p_z .

*Note that

$$p^2 = p_X^2 + p_Y^2 + p_Z^2 = p_\alpha^2 + p_\beta^2 + p_\gamma^2$$

and $(1 + \kappa x)p_\alpha = p_s + \omega_z p_\beta - \omega_x p_\gamma$

$$p_\beta = p_x \quad p_\gamma = p_z$$

The Hamiltonian equations of motion in the new coordinates are:

$$\begin{aligned}
 \dot{s} &= \frac{\partial H}{\partial p_s} , & \dot{p}_s &= - \frac{\partial H}{\partial s} , \\
 \dot{x} &= \frac{\partial H}{\partial p_x} , & \dot{p}_x &= - \frac{\partial H}{\partial x} , \\
 \dot{z} &= \frac{\partial H}{\partial p_z} , & \dot{p}_z &= - \frac{\partial H}{\partial z} .
 \end{aligned} \tag{2-17}$$

The first of these equations can be used to change the independent variable from t to s . The transformed equations become:

$$\begin{aligned}
 x' &= - \frac{\partial p_s}{\partial p_x} , & p'_x &= \frac{\partial p_s}{\partial x} , \\
 z' &= - \frac{\partial p_s}{\partial p_z} , & p'_z &= \frac{\partial p_s}{\partial z} \\
 t' &= \frac{\partial p_s}{\partial H} , & H' &= - \frac{\partial p_s}{\partial t}
 \end{aligned} \tag{2-18}$$

where the primes denote differentiation with respect to s , and where p_s obtained by solving equation (2-16) is now a function of x , p_x , z , p_z , H , t and s . Equations (2-18) are still in Hamiltonian form with the new Hamiltonian G given by $G = -p_s$ (2-19)

with pairs of canonically conjugate variables x , p_x ; z , p_z ; t , $-H$.

If the discussion is specialized to the case of a uniform field sector magnet with mirror symmetry, considerable simplification can be

obtained in Hamilton's equations. In particular $V = 0$ and \underline{A} is independent of time. Also the torsion, ω , is zero since the central trajectory lies in a plane with z always perpendicular to the median plane of the magnet and in the direction of the magnetic field. This leads to a simplified form of the Hamiltonian G which is independent of time. Hence the number of degrees of freedom has been reduced from three to two.

The components of the vector potential can now be obtained up to second order with the help of the relations

$$\begin{aligned}\nabla \underline{X} \underline{A} &= B_z \\ (\nabla \underline{X} \nabla \underline{X} \underline{A})_s &= (\nabla \underline{X} B)_s = 0 \\ \rho &= 1/\kappa = \frac{p}{eB_z},\end{aligned}\tag{2-20}$$

giving

$$\begin{aligned}A_s &= -\frac{p\kappa x}{e} \left(1 + \frac{1}{2}\kappa x\right) \\ A_x &= 0 \\ A_z &= 0\end{aligned}\tag{2-21}$$

for the components of the vector potential in the new coordinates. Solving equation (2-16) for p_s and substituting for \underline{A} one obtains the Hamiltonian

$$G = -p_s = p\kappa x \left(1 + \frac{1}{2}\kappa x\right) - (1 + \kappa x) \left[\frac{H^2}{c^2} - m^2 c^2 - p_x^2 - p_y^2 \right]^{1/2}.\tag{2-22}$$

Since

$$\frac{H^2}{c^2} - m^2 c^2 = p^2$$

the Hamiltonian G reduces to

$$G = p\kappa x(1 + \frac{1}{2}\kappa x) - (1 + \kappa x)[p^2 - p_x^2 - p_z^2]^{1/2}. \quad (2-23)$$

The paraxial ray equations for a uniform field sector magnet are obtained by expanding the Hamiltonian G in a power series in x , p_x , z and p_z and retaining only terms up to second order. Carrying out the expansion indicated above yields the result

$$G = \frac{1}{2} \left[\frac{p_x^2}{p} + \frac{p_z^2}{p} - 2p(1 - \frac{1}{2}\kappa^2 x^2) \right]. \quad (2-24)$$

Therefore the equations of motion are

$$\begin{aligned} x' &= \frac{p_x}{p}, & p_x' &= -p\kappa^2 x \\ z' &= \frac{p_z}{p}, & p_z' &= 0. \end{aligned} \quad (2-25)$$

Elimination of p_x and p_z in the equations for x' and z' yields the paraxial ray equations for the trajectories given below:

$$\frac{d^2 x}{ds^2} + \kappa^2 x = 0 \quad (2-26a)$$

$$\frac{d^2 z}{ds^2} = 0. \quad (2-26b)$$

(iv) The Solution of the Ray Equations and the Matrix Method

The solution of any linear second order differential equation of the form of equations (2-26) is uniquely determined by the initial values of x and its derivative x' . If $f(s)$ and $g(s)$ are linearly independent solutions of equation (2-26a) or (2-26b) satisfying the boundary conditions (Ha 6 a), (St 55)

$$\begin{aligned} f(s_0) &= 1 & f'(s_0) &= 0 \\ g(s_0) &= 0 & g'(s_0) &= 1 \end{aligned} \quad (2-27)$$

then the general solution can be written as

$$\begin{aligned} x(s) &= f(s)x_0 + g(s)x_0' \\ x'(s) &= f'(s)x_0 + g'(s)x_0' \end{aligned} \quad (2-28)$$

where x_0 and x_0' are the boundary values at s_0 , and as before the prime denotes the derivative with respect to s .

The general solution given by equations (2-28) has the form of a linear transformation and can be represented by the matrix equation

$$\begin{aligned} X(s) &= M(s|s_0)X_0 \\ \text{or} \quad \begin{pmatrix} x(s) \\ x'(s) \end{pmatrix} &= \begin{pmatrix} f(s) & g(s) \\ f'(s) & g'(s) \end{pmatrix} \begin{pmatrix} x_0 \\ x_0' \end{pmatrix} = \begin{pmatrix} m_{11} & m_{12} \\ m_{21} & m_{22} \end{pmatrix} \begin{pmatrix} x_0 \\ x_0' \end{pmatrix}. \end{aligned} \quad (2-30)$$

Since κ is a constant for a uniform field magnet, the solutions of

equation (2-26a) are

$$f(s) = \cos[\kappa(s-s_0)]$$

and $g(s) = \sin[\kappa(s-s_0)]/\kappa$

and the solutions of (2-26b) are

$$f(s) = 1, \quad g(s) = (s-s_0) .$$

The corresponding transformation matrices are

$$M_x(s|s_0) = \begin{pmatrix} \cos[\kappa(s-s_0)] & \sin[\kappa(s-s_0)]/\kappa \\ -\kappa \sin[\kappa(s-s_0)] & \cos[\kappa(s-s_0)] \end{pmatrix} \quad (2-31)$$

and

$$M_z(s|s_0) = \begin{pmatrix} 1 & (s-s_0) \\ 0 & 1 \end{pmatrix} . \quad (2-32)$$

The matrix M_z represents the transformation of a particle through a field free region, a result that can also be seen directly from equation (2-26b). The transformation matrices M_x and M_z contain all the paraxial focussing properties of the optical system in the region defined by s_0 and s for a monochromatic (i.e. $p = \text{constant}$) beam of particles. The theory of linear transformations allows the properties of successive piecewise constant regions to be obtained by the multiplication of their respective transformation matrices, that is

$$M(s_n|s_0) = M(s_n|s_{n-1}) \dots M(s_2|s_1)M(s_1|s_0) . \quad (2-33)$$

In fact, the usefulness of the matrix formulation arises mainly from the two features given above, namely: The formulation clearly separates the properties of the general solution, which depends only on κ , in region between s_0 and s , from the particular solutions which depend upon an appropriate choice of x_0 and x'_0 . Secondly, the transformation of an interval s_0 to s_n can be obtained by matrix multiplication of the respective sub-matrices. These properties of a linear transformation lead to a systematic interpretation of the matrix elements of an optical transformation from which follow the usefulness of the concepts of nodal points and principal planes.

Inspection of the matrices (2-31) and (2-32) shows that the determinant of M is unity. This property will be shown in section (ix) to be the result of the invariance of a quantity known as the bilinear covariant. However from the point of view of the theory of differential equations it expresses the fact that equations (2-26) do not contain terms in the first derivative (i.e. no energy is gained or lost by the particles as they traverse the region from s_0 to s).

The matrix representation of the paraxial optical equations has been used by several authors. A good discussion of the matrix method applied to magnetic beam transport systems can be found in an article by Penner (Pe 61). Additional information on the matrix method can be found in the following references: (Co 58), (St 55), (Ha 63a), (Ha 63b), (Br 64) and (Br 65).

The significance of the matrix elements and the location of nodal points and principal planes are discussed by Penner (Pe 61), Sturrock (St 55), and Haddock (Ha 63a), but because of their importance in understanding the properties of the system being analyzed, a short discussion of these properties will be given here. Before embarking on the discussion of the significance of the matrix elements, it is useful to make the following change of variables. From equation (2-25) it is seen that $x' = p_x/p = \tan \phi = \phi$ in the paraxial approximation. Thus the angle ϕ can be used in place of x' in the discussion of the optical properties of a system.

Consider the general optical transformation

$$\begin{pmatrix} x_1 \\ \phi_1 \end{pmatrix} = M(s|s_0) \begin{pmatrix} x_0 \\ \phi_0 \end{pmatrix} \quad (2-34)$$

where

$$M(s|s_0) = \begin{pmatrix} m_{11} & m_{12} \\ m_{21} & m_{22} \end{pmatrix}.$$

If $m_{12} = 0$, the x component of the general ray (x_0, ϕ_0) is transformed into $x_1 = m_{11} \cdot x_0$ so that m_{11} represents the transverse linear magnification. Similarly if $m_{21} = 0$ the ϕ component of the ray (x_0, ϕ_0) is transformed into $\phi_1 = m_{22} \cdot \phi_0$ and m_{22} represents the angular magnification of the system. If $m_{11} = 0$ a ray $(x_0, 0)$ parallel to the optic axis is focussed to a point on the optic axis at the exit

reference plane of the system, that is

$$\begin{pmatrix} 0 \\ \phi_1 \end{pmatrix} = M \begin{pmatrix} x_0 \\ 0 \end{pmatrix} \text{ and } \phi_1 = m_{21}x_0.$$

The matrix element m_{21} has the dimensions of $1/L$ and is defined as $1/f_1$ where f_1 is a focal length of the system. The exit boundary contains a focal point of the system and thus represents a focal plane. Finally, if $m_{22} = 0$ a ray $(0, \phi_0)$ passing through the optic axis at the entrance reference plane is transformed into a ray travelling parallel to the optic axis at the exit reference plane, that is

$$\begin{pmatrix} x_1 \\ 0 \end{pmatrix} = M \begin{pmatrix} 0 \\ \phi_0 \end{pmatrix} \text{ and } x_1 = m_{12} \phi_0.$$

Thus m_{12} , which has the dimensions of L , is also a focal length, f_2 , of the system and the input reference plane contains a focal point of the system.*

It is of interest to consider an optical system in which both reference planes contain focal points of the system. Under these

*Note that it is necessary that m_{11} (m_{22}) be zero for the exit (entrance) reference plane to be a focal plane, but it is not necessary that m_{11} and/or m_{22} be zero for m_{21} and/or m_{12} to be interpreted as focal lengths of the system.

conditions,

$$M = \begin{pmatrix} 0 & \pm f_2 \\ \mp 1/f_1 & 0 \end{pmatrix} \quad (2-35)$$

where the signs of m_{12} and m_{21} must be chosen such that $\det|M| = +1$. The condition that $\det|M| = +1$ also requires that $f_1 = f_2$. It is easily seen that if m_{21} is negative the optical transformation is "convergent" and if m_{21} is positive the optical transformation is "divergent."

The principal planes of an optical system are defined as the pair of planes that have an image-object relationship with a magnification of +1 (Ha 63b). These planes can be found by transforming the optical system M into a new system M_1 in which both the transverse and angular magnifications are unity. The required transformation is

$$M_1 = \begin{pmatrix} 1 & t_e \\ 0 & 1 \end{pmatrix} \begin{pmatrix} m_{11} & m_{12} \\ m_{21} & m_{22} \end{pmatrix} \begin{pmatrix} 1 & t_i \\ 0 & 1 \end{pmatrix} \quad (2-36)$$

$$= \begin{pmatrix} m_{11} + t_e m_{21} & m_{12} + m_{11} t_1 + (m_{22} + m_{21} t_1) t_2 \\ m_{21} & m_{22} + t_i m_{21} \end{pmatrix}$$

Now since m_{21} can be set equal to $-1/f$ with loss of generality, the principal planes must lie at distances

$$t_i = f(1 - m_{22}) \quad (2-37a)$$

and

$$t_e = f(1 - m_{11}) \quad (2-37b)$$

from the entrance and exit boundaries respectively of the system described by M . Since the matrix elements m_{11} and m_{22} in the matrix M_1 are equal to unity and since $m_{21} = -1/f \neq 0$, the matrix element m_{12} in M_1 must be zero if the determinantal condition is to be satisfied. Thus the matrix M_1 has the form

$$M_1 = \begin{pmatrix} 1 & 0 \\ -1/f & 1 \end{pmatrix} \quad (2-38)$$

and the original optical system described by M is obtained from M_1 by the transformation

$$M = \begin{pmatrix} 1 & t_2 \\ 0 & 1 \end{pmatrix} \begin{pmatrix} 1 & 0 \\ -1/f & 1 \end{pmatrix} \begin{pmatrix} 1 & t_1 \\ 0 & 1 \end{pmatrix} \quad (2-39)$$

where t_1 and t_2 are drift distances measured from the principal planes to the entrance and exit reference planes of the system described by M . The transformation (2-39) can be written as

$$M = \begin{pmatrix} 1 - \frac{t_2}{f} & t_1 + t_2 - \frac{t_1 t_2}{f} \\ -\frac{1}{f} & 1 - \frac{t_1}{f} \end{pmatrix} \quad (2-40)$$

and leads to the following useful properties. If the reference planes of the transformation M are focal planes, then $m_{11} = m_{22} = 0$ which

requires that $t_1 = t_2 = f$ which is just the usual condition relating the focal points to the centre of a thin lens. Thus M_1 , equation (2-38), is equivalent to a thin lens and shows that any optical transformation can be reduced to an equivalent thin lens and two drift spaces. If the reference planes are not focal planes the matrix elements m_{11} and m_{22} are not zero and represent the linear and angular magnifications respectively of the optical system. If the entrance reference plane represents an "object" plane, the image plane can be defined by the equation

$$\begin{pmatrix} 0 \\ \phi_1 \end{pmatrix} = M \begin{pmatrix} 0 \\ \phi_0 \end{pmatrix} \quad (2-41)$$

which requires that $m_{12} = 0$ or that

$$t_1 + t_2 - \frac{t_1 t_2}{f} = 0 .$$

This equation reduces to the well known imaging formula

$$\frac{1}{t_1} + \frac{1}{t_2} = \frac{1}{f} \quad (2-42)$$

where t_1 and t_2 are measured from the principal planes defined by equations (2-37a) and (2-37b).

The above discussion has been quite general and the transformation M can represent any optical transformation no matter how complex. That such a uniformity of interpretation is possible is the result of the

properties of a linear transformation discussed above and makes the matrix method the powerful method that it is.

(v) The Double Focussing Condition for a Sector Field Magnet

The solution of the ray equation for z was seen in section (iv) to represent a transformation through a field free region. Consequently the solution for normal entry and exit produces no focussing in the z (axial) direction. If, however, the pole faces are rotated there will be a component of the magnetic field in the x direction which will cause an angular deflection of the trajectories in the axial direction. The first order effect of these field components has been calculated by Camac (Ca 51) in the impulse approximation. The deflections are

$$\Delta\phi_0 = - \frac{z_0}{\rho} \tan \beta_1$$

where β_1 is the angle of rotation of the entrance pole face, and

$$\Delta\phi = \frac{z}{\rho} \tan \beta_2$$

where β_2 is the angle of rotation of the exit pole face. The effect of the rotation is to produce a thin "convex" lens at each pole face represented by the transformation matrix

$$M_z(\beta) = \begin{pmatrix} 1 & 0 \\ -\frac{\tan \beta}{\rho} & 1 \end{pmatrix}. \quad (2-43a)$$

The rotation of the pole face has the opposite effect on the radial trajectories in the magnet producing a thin "concave" lens at each pole face with transformation matrix (Pe 61)

$$M_x(\beta) = \begin{pmatrix} 1 & 0 \\ \frac{\tan \beta}{\rho} & 1 \end{pmatrix} . \quad (2-43b)$$

Referring to fig. (2-5) it is seen that $(s - s_0) = \rho\alpha$ inside the magnet so that the transformation matrices for the radial and axial directions of the bunching system can be written as

$$M_x = \begin{pmatrix} 1 & t_2 \\ 0 & 1 \end{pmatrix} \begin{pmatrix} 1 & 0 \\ \frac{\tan \beta_2}{\rho} & 1 \end{pmatrix} \begin{pmatrix} \cos \alpha & \rho \sin \alpha \\ -\frac{\sin \alpha}{\rho} & \cos \alpha \end{pmatrix} \begin{pmatrix} 1 & 0 \\ \frac{\tan \beta_1}{\rho} & 1 \end{pmatrix} \begin{pmatrix} 1 & t_1 \\ 0 & 1 \end{pmatrix} \quad (2-44a)$$

$$M_z = \begin{pmatrix} 1 & t_2 \\ 0 & 1 \end{pmatrix} \begin{pmatrix} 1 & 0 \\ \frac{\tan \beta_2}{\rho} & 1 \end{pmatrix} \begin{pmatrix} 1 & \rho\alpha \\ 0 & 1 \end{pmatrix} \begin{pmatrix} 1 & 0 \\ -\frac{\tan \beta_1}{\rho} & 1 \end{pmatrix} \begin{pmatrix} 1 & t_1 \\ 0 & 1 \end{pmatrix} \quad (2-44b)$$

where t_1 and t_2 are the distances from the entrance and exit reference planes (centre of the R.F. deflection plates and target) to the entrance and exit pole faces of the magnet. Since the actual system is symmetrical about the centre of the magnet, $\beta_1 = \beta_2 = \beta$ and $t_1 = t_2 = t$. Consequently the double focussing condition (i.e. the radial and axial focal points coincide) can be obtained by considering

only half of the system. Define

$$M_x\left(\frac{1}{2}\right) = \begin{pmatrix} c & \rho s \\ -\frac{s}{\rho} & c \end{pmatrix} \begin{pmatrix} 1 & 0 \\ \frac{\beta}{\rho} & 1 \end{pmatrix} \begin{pmatrix} 1 & t \\ 0 & 1 \end{pmatrix} = \begin{pmatrix} c+\beta s & t(c+\beta s)+\rho s \\ \frac{1}{\rho}(c\beta-s) & c + \frac{t}{\rho}(c\beta-s) \end{pmatrix} \quad (2-45a)$$

and

$$M_z\left(\frac{1}{2}\right) = \begin{pmatrix} 1 & \rho \frac{\alpha}{2} \\ 0 & 1 \end{pmatrix} \begin{pmatrix} 1 & 0 \\ -\frac{\beta}{\rho} & 1 \end{pmatrix} \begin{pmatrix} 1 & t \\ 0 & 1 \end{pmatrix} = \begin{pmatrix} 1 - \frac{\alpha}{2}\beta & t(1 - \frac{\alpha}{2}\beta) + \rho \frac{\alpha}{2} \\ -\frac{\beta}{\rho} & 1 - \frac{t}{\rho}\beta \end{pmatrix} \quad (2-45b)$$

where $\beta = \tan \beta$, $c = \cos(\alpha/2)$ and $s = \sin(\alpha/2)$. The condition that the first reference plane be a focal plane for both the radial and axial directions requires that the matrix element $m_{22} = 0$ for both transformations. Therefore

$$\tan \beta = \rho/t \quad \text{from equation (2-45b)} \quad (2-46a)$$

$$\text{and} \quad \cos \frac{\alpha}{2} = \frac{t}{\rho} \left(\sin \frac{\alpha}{2} - \cos \frac{\alpha}{2} \tan \beta \right) \quad (2-46b)$$

from equation (2-45a) .

Solving these equations for $\tan \beta$ gives the double focussing condition

$$\tan \beta = \frac{1}{2} \tan \frac{\alpha}{2} \quad (2-47)$$

for a symmetric sector magnet.

(vi) The Path Length Difference and the Bunching Condition

The elemental path length dS along the curve $\underline{r} = \underline{r}(s, x, z)$ (2-12) is given by

$$dS^2 = \left(\frac{\partial \underline{r}}{\partial s} \right)^2 ds^2 + \left(\frac{\partial \underline{r}}{\partial x} \right)^2 dx^2 + \left(\frac{\partial \underline{r}}{\partial z} \right)^2 dz^2 \quad (2-48a)$$

which reduces to

$$dS^2 = (1 + \kappa x)^2 ds^2 + dx^2 + dz^2 \quad (2-48b)$$

using equations (2-11) and (2-12) and the fact that the torsion of the curve is zero.

The determination of the path lengths of rays passing through the bunching system can be divided into three regions consisting of the two drift spaces between the deflector and the magnet, the magnet and the target and the magnet itself. In the drift spaces the curvature vanishes giving $dS^2 = dx^2 + dz^2 + ds^2$ so that the path length S can be determined by integrating the curve

$$\left(\frac{dS}{ds} \right)^2 = 1 + \left(\frac{dx}{ds} \right)^2 + \left(\frac{dz}{ds} \right)^2 \quad (2-49)$$

with respect to s .

Now the transformation through either drift space is

$$\begin{pmatrix} x, z \\ \phi \end{pmatrix} = \begin{pmatrix} 1 & t \\ 0 & 1 \end{pmatrix} \begin{pmatrix} x_0, z_0 \\ \phi_0 \end{pmatrix} \quad (2-50)$$

giving $\phi_x = dx/ds$ and $\phi_z = dz/ds$.

Hence

$$\frac{dS}{ds} = [1 + \phi_x^2 + \phi_z^2]^{1/2} \approx 1 + \frac{1}{2} \phi_x^2 + \frac{1}{2} \phi_z^2. \quad (2-51)$$

Thus in the paraxial approximation where $(\phi_x, \phi_z) \ll 1$ the path length becomes

$$S = \int_{s_0}^s ds = t \quad (2-52)$$

which is just the length of the central trajectory. Consequently the path length difference between off-axis rays and the central trajectory is zero to first order. Substituting $ds = \rho d\alpha$ in equation (2-48b) gives

$$dS^2 = dx^2 + dz^2 + (1 + \kappa x) \rho^2 d\alpha^2 \quad (2-52)$$

for the element of length of a trajectory inside the magnet. Expressing S as a function of α yields

$$\left(\frac{dS}{d\alpha}\right)^2 = \rho^2 (1 + \kappa x)^2 + \left(\frac{dx}{d\alpha}\right)^2 + \left(\frac{dz}{d\alpha}\right)^2$$

and

$$\frac{dS}{d\alpha} = \rho (1 + \kappa x) \left[1 + \frac{1}{\rho^2 (1 + \kappa x)^2} \left[\left(\frac{dx}{d\alpha}\right)^2 + \left(\frac{dz}{d\alpha}\right)^2 \right] \right]^{1/2} \quad (2-53)$$

for the path length of a trajectory through the magnet. The expansion of the square root in equation (2-53) results in the expression

$$\frac{dS}{d\alpha} = \rho(1 + \kappa x) + \frac{1}{\rho(1 + \kappa x)} \left[\frac{1}{2} \left(\frac{dx}{d\alpha} \right)^2 + \frac{1}{2} \left(\frac{dz}{d\alpha} \right)^2 \right] + \dots \quad (2-54)$$

in which the second term is seen to be much less than one. Neglecting the second term in equation (2-54) gives the following expression for the path length difference, ℓ , of a ray through the magnet:

$$\ell = \int_0^\infty \frac{dS}{d\alpha} d\alpha - \rho\alpha = \int_0^\infty x d\alpha \quad (2-55)$$

The transformation matrix through the magnet can be seen from equations (2-31), (2-43b) to be

$$M(\alpha) = \begin{pmatrix} 1 & 0 \\ \beta/\rho & 1 \end{pmatrix} \begin{pmatrix} c & \rho s \\ -s/\rho & c \end{pmatrix} \begin{pmatrix} 1 & 0 \\ \beta/\rho & 1 \end{pmatrix} = \begin{pmatrix} c+s\beta & \rho s \\ -\frac{1}{\rho}[s-2c\beta-s\beta^2] & c+s\beta \end{pmatrix} \quad (2-56)$$

where $\beta = \tan \beta$, $c = \cos \alpha$ and $s = \sin \alpha$. The path length difference is then

$$\begin{aligned} \ell &= x_1 \int_0^\alpha (\cos \alpha + \tan \beta \sin \alpha) d\alpha + \rho \phi_1 \int_0^\alpha \sin \alpha d\alpha \\ &= x_1 [\sin \alpha + (1-\cos \alpha)\tan \beta] + \rho \phi_1 [1 - \cos \alpha] \end{aligned} \quad (2-57)$$

where x_1 and ϕ_1 are the boundary values at the entrance to the magnet. The values of x_1 and ϕ_1 can be found in terms of x_0 and ϕ_0 ,

the boundary values at the deflection plates, by using the transformation matrix (2-50). The result is

$$\begin{aligned} x_1 &= x_0 + t\phi_0 \\ \phi_1 &= \phi_0 \end{aligned} \quad (2-58)$$

giving

$$\ell = [\sin \alpha + (1 - \cos \alpha) \tan \beta] + \rho [2(1 - \cos \alpha) + \sin \alpha / \tan \beta] \quad (2-59)$$

as the expression for ℓ in terms of x_0 and ϕ_0 where equation (2-46a) has been used to determine t . Substituting for $\tan \beta$ in the second term of equation (2-59) and using the identity

$$\tan \beta = \frac{1}{2} \tan \frac{\alpha}{2} = \frac{1}{2} \frac{\sin \alpha}{1 + \cos \alpha}$$

leads to the following simplification in the expression for the path length difference

$$\ell = [\sin \alpha + (1 - \cos \alpha) \tan \beta] x_0 + 4\rho\phi_0 \quad (2-60)$$

For an idealized beam in which $x_0 = 0$ and $\phi_0 = 0$ for all rays the difference in arrival times is (eqn. 2-1)

$$\Delta t_a = t + \frac{4\rho\phi}{v} \quad (2-61)$$

where ϕ , the deflection supplied by the deflection system, must be an appropriate function of time. Perfect bunching is obtained by making

$\Delta t_a = 0$ which requires that

$$\phi(t) = \frac{vt}{4\rho} \quad (2-62)$$

The maximum deflection angle (half angle) required is

$$\phi_m = \frac{v\Delta t}{8\rho} \quad (2-63)$$

where Δt is the acceptance time. Since a linear sweep with the required repetition rate and peak voltage is very difficult to obtain the linear sweep is usually approximated by a sine wave giving

$$\phi(t) = -\phi_0 \sin \omega t \quad (2-64)$$

where ω is the angular frequency of the oscillation and where the negative phase has been chosen for convenience. Equation (2-61) can now be written as

$$\Delta t_a = t - \frac{4\rho}{v} \phi_0 \sin \omega t \quad (2-65)$$

which if expanded in a power series in t becomes

$$\Delta t_a = t - \frac{4\rho\phi_0}{v} \left[\omega t - \frac{(\omega t)^3}{3!} + \frac{(\omega t)^5}{5!} - \dots \right] \quad (2-66)$$

The first order truncation of equation (2-66) is

$$\Delta t_a = \left(1 - \frac{4\rho}{v} \phi_0 \omega\right) t \quad (2-67)$$

which if equated to zero results in the relation

$$\phi_0 = \frac{v}{4\rho\omega} \quad (2-68)$$

between the particle velocity, the radius of curvature, the angular frequency and the deflection angle. The phase angle γ through which the sine wave passes in deflecting the beam is

$$\gamma = \frac{\omega\Delta t}{2} \quad (2-69)$$

Consequently the maximum sweep angle ϕ_0 and thus the peak voltage V_0 required of the deflection oscillator can be reduced by increasing the frequency ω , but only at the expense of increasing γ which will make the higher order terms in equation (2-66) larger and therefore increase the time dispersion of the bunched beam on the target.

(vii) The R.F. Deflection Voltage

The equation of motion for a charged particle passing through a pair of deflection plates of length L_d and separation d is (Ne 60)

$$\frac{d^2x}{dt^2} = \frac{eV_0}{md} \sin \omega t \quad (2-70)$$

where t is measured from the centre of the deflection system, V_0 is the peak voltage and m is the particle mass.

The transverse velocity of the particle at the exit end of the deflection plates is

$$v_x = \frac{2eV_0}{m\omega d} \sin \frac{\delta}{2} \sin \omega t \quad (2-71)$$

where $\delta = \omega \frac{L_d}{v}$ is the transit phase angle in radians of a particle with velocity v passing through the deflection plates. The deflection angle $\phi = v_x/v$ is then

$$\phi = \frac{2eV_0}{m\omega d v} \sin \frac{\delta}{2} \sin \omega t \quad (2-72)$$

in the paraxial approximation. On substituting the deflection angle ϕ_0 from equation (2-68) into equation (2-72) the deflection voltage V_0 required for optimum bunching is easily found to be

$$V_0 = \frac{E d}{4\rho \sin \delta / 2} \quad (2-73)$$

where E , the energy of the beam, and V_0 are both measured in MeV and where use has been made of the relation

$$v = (2E/m)^{1/2}.$$

The displacement of the beam as it leaves the deflection plates is (Ne 60)

$$x = x_0 \sin(\omega t - \delta/2) \quad (2-74)$$

where

$$x_0 \approx \frac{1}{4} \frac{eV_0}{E} \frac{L_d^2}{d}.$$

Substitution for eV_0 from equation (2-73) results in the expression

$$x = \frac{L_d^2}{16\rho \sin \delta / 2} \sin(\omega t - \delta/2)$$

for the displacement of the beam at the exit end of the deflection plates.

Thus the displacement at the centre of the plates is

$$x = \frac{L_d^2}{16\rho\sin\delta/2} \sin(\omega t - \delta/2) - \frac{L_d}{2} \phi_0 \sin \omega t . \quad (2-75)$$

(viii) The Design of the Mobley Bunching System

The design equations for a Mobley bunching system are summarized in table (2-1). These equations can be used to specify the magnet and deflector parameters once the criteria given in section (ii) have been specified. The design specifications are as follows:

- (a) The time dispersion Δt_a of the bunched beam must be less than 1 ns.
- (b) The angular divergence of the beam on the target must be less than 3° .
- (c) The system must bunch a 6 MeV proton beam.
- (d) The magnet acceptance time must be 10 ns.
- (e) The beam spot size must not be greater than 2 cm.

The two magnet parameters that can be adjusted to meet the design specifications are the radius of curvature ρ and the bending angle α . Holland (Ho 61) has investigated the dependence on α of the spread in arrival times due to the geometrical aberrations of the magnet. Using an "exact" calculation he finds that the optimum deflection angle lies between 60° and 90° . The deflection angle α was chosen to be 90° in the University of Alberta system which limits the bending radius to about 75 inches. Table (2-2) gives a summary of the design parameters of the University of Alberta Mobley bunching system along with some important properties of the ion beam. The table lists the extreme values of these parameters where this is applicable.

TABLE (2-1)

The Design Equations of a Mobley Bunching System

Equation	Eqn. No.	Definition
$\Delta t = \frac{L_2 - L_1}{v} = A/\rho v$	(2-2)	Relation between acceptance time, path length difference, pole face area and deflection angle.
$= 8\rho \phi/v$	(2-6)	
$\phi_m = \frac{v\Delta t}{8\rho}$	(2-63)	Maximum beam deflection angle into the magnet required for optimum bunching as a function of particle velocity, acceptance time and radius of curvature.
$\tan \beta = \frac{1}{2} \tan \frac{1}{2} \alpha$	(2-47)	The double focussing condition for a uniform field sector magnet.
$L = \rho/\tan \beta$	(2-46a)	Distance from the magnet pole faces to the focal points of the magnet.
$x_{app} = 2\rho\phi_m/\sin \frac{\alpha}{2}$	*	The aperture required to bunch a beam requiring deflection ϕ_m .
$B = p/e\rho$	(2-20)	The magnetic field required to bunch a beam with momentum p for a radius of curvature ρ .
$\phi_0 = \frac{v}{4\rho\omega}$	(2-68)	The maximum "deflection" angle for a sinusoidal sweep to produce optimum bunching.
$V_0 = \frac{E d}{4\rho \sin \delta/2}$	(2-73)	The peak voltage required to produce the deflection ϕ_0 required for optimum bunching.
$\delta = \frac{\omega L d}{v}$		
$\ell = 4\rho\phi$	(2-60)	The path length difference for a "pencil beam" deflected through an angle ϕ at a focal point.

*Not calculated in the text.

TABLE (2-2)

Design Parameters for a Bunching System that Will Accept a 6 MeV Proton Beam for 10 ns.

	Parameter	Symbol	Value
Ion Beam	Energy	E	6 MeV
	Emittance	Ω	3×10^{-3} rad-cm
	Momentum dispersion	$\Delta p/p$	0.35×10^{-2}
	Maximum velocity	v	3.4×10^9 cm/sec = 0.113 c
	Repetition rate		1 MHz
Bunching Requirements	Acceptance time	Δt	10 ns
	Time dispersion (FWHM) maximum	Δt_a	1 ns
	Minimum bunching factor	$\Delta t/\Delta t_a$	10
	Angular divergence	$2\phi_m$	3°
Magnet	Deflection of median ray	α	90°
	Radius of curvature	ρ	75 inches 190.5 cm
	Rotation of pole face	β	$26^\circ 34'$; $\tan \beta = \frac{1}{2}$
	Distance from pole face to focal points	$L=2\rho$	150 in. 381 cm.
	Maximum deflection angle (half angle)	ϕ_m	1.25° ; 0.0218 rad
	Maximum aperture	$2x_{app}$	11.06 in. 28 cm.
	Magnetic field	B	3735 gauss
	Useful pole face area	A	1000 in ² 6480 cm ²
	Gap		3 inches
	Path length difference	ℓ	$\frac{3}{2}x + 4\rho\phi$
	Angular frequency	ω	(10 MHz) 6.28×10^7 rad/sec.

Table (2-2)

Parameter		Symbol	Value
Deflector	Bunching phase angle	γ	18° 0.628 rad
	Maximum R.F. deflection voltage peak*	V_0	58434 volts
	Deflection plate length	L_d	37 cm
	Maximum separation	d	2.54 cm

* Calculated using 37 cm plates with 2.5 cm separation.

The beam emittance shown in table (2-2) is the maximum value specified by High Voltage Engineering Corporation for the accelerator while the momentum dispersion was calculated assuming a 0.3 inch aperture at the focal point of the analyzing magnet.

The maximum angular divergence of the beam on the target is seen to be only 2.5° which can be neglected in most experiments.

At this point it is not possible to predict the time dispersion or the beam spot size on the target since these quantities result from second order aberrations, the beam quality and other limitations such as the magnetic field homogeneity and R.F. deflector stability, effects that have been completely ignored in this discussion. A reasonably comprehensive discussion of the factors that limit the bunching will be given in the following section.

(ix) Effects that Limit the Bunching

(a) The Nonlinearity of the Sweep Waveform

The effect of the nonlinear sweep on the bunching can be estimated by considering the second term in the expansion of the sine function in equation (2-66). This term leads to the expression

$$\Delta t_a = \frac{(\omega t)^2}{6} t = \frac{(\gamma)^2}{6} t \quad (2-76)$$

for the contribution of the nonlinear sweep to the time dispersion.

Using the value for γ from table (2-2) results in a total time dispersion of 0.6 ns due to the nonlinearity of the sweep. This

estimate will be seen to be too large when the geometrical aberrations of the magnet are included since there is a cancellation between these two effects.

(b) The Geometrical Aberrations

The effect on the bunching of the geometrical aberrations neglected in the paraxial approximation was estimated using an "exact" geometrical calculation for the path length differences through the magnet. The geometrical construction, used by Holland (Ho 61), is given here both for completeness and because the notation used by Holland differs from that used in the present discussion. Figure (2-7) defined the variables and shows the relationships among the various quantities. In particular the path length of the central ray is seen to be

$$L_0 = 2y \sec \beta + \rho \alpha \quad (2-77)$$

and the path length of an off-axis ray is

$$L = y \sec (\beta + \phi_1) + \rho(\alpha + \phi_1 + \phi_2) + y \sec(\beta + \phi_2)$$

so that the path length difference becomes

$$\ell = \rho(\phi_1 + \phi_2) + y[\sec(\beta + \phi_1) + \sec(\beta + \phi_2) - 2 \sec \beta] \quad (2-79)$$

The value of y given by

$$y = \ell_1 \cos \beta$$

can be expressed as

$$y = 2\rho \cot\left(\frac{1}{2} \alpha\right) \cos \beta$$

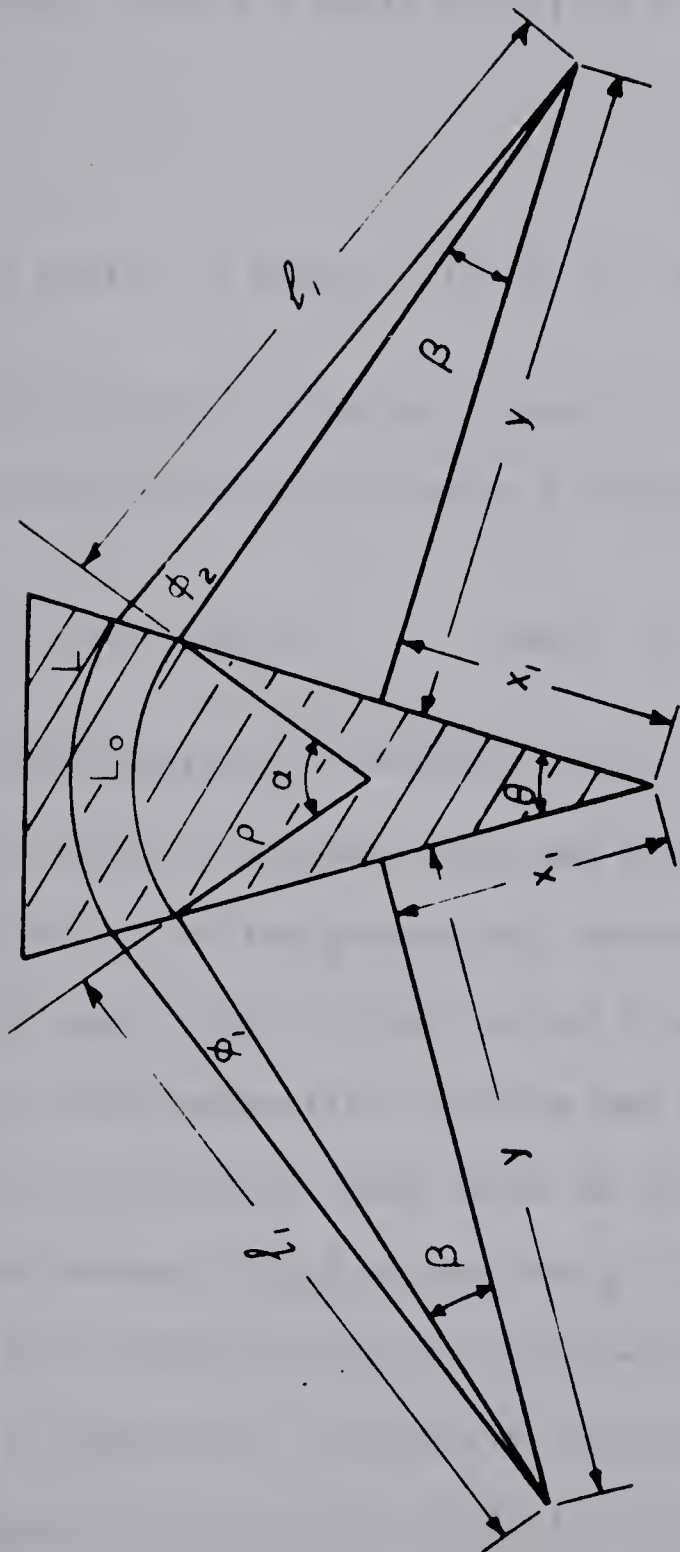


Figure 2-7. Schematic representation of a symmetric sector magnet. The diagram defines the notation used in the text.

where use has been made of equations (2-46a) and (2-47). The value of ϕ_2 which is equal to ϕ_1 in the paraxial approximation can be found by rearranging an expression given by Geerk and Heinz (Ge 52). The result is

$$\phi_2 = \sin^{-1} \{ [x_1 + y \tan(\beta + \phi_1)] \sin \theta / \rho - \sin(\theta + \beta + \phi_1) \} - \beta \quad (2-80)$$

where

$$x_1 = \rho [\sin \beta + \sin(\theta + \beta)] / \sin \theta - y \tan \beta.$$

The equation for the path length difference (2-79) was programmed for a computer calculation using a sinusoidal deflection

$$\phi_1 = -\phi_0 \sin \omega t \quad \text{where} \quad \phi_0 = \frac{v}{4\rho\omega}$$

as given in equations (2-64) and (2-68). The results of these calculations are shown in figures (2-8) and (2-9). In all cases it is seen that the effect of the geometrical aberrations on the bunching is small giving an upper limit of 0.24 ns for 6 MeV protons. A more realistic estimate of the geometrical effects can be obtained by forming the RMS average of the arrival times shown in the figures. For a 6 MeV proton beam this average is 0.1 ns and for a 6 MeV deuteron beam the average is 0.06 ns. The figures (2-8) and (2-9) show that the arrival times are not a symmetrical function of the input time t and that an improvement in the bunching could be obtained by a phase shift toward more negative times. Such a phase shift would, of course, require a

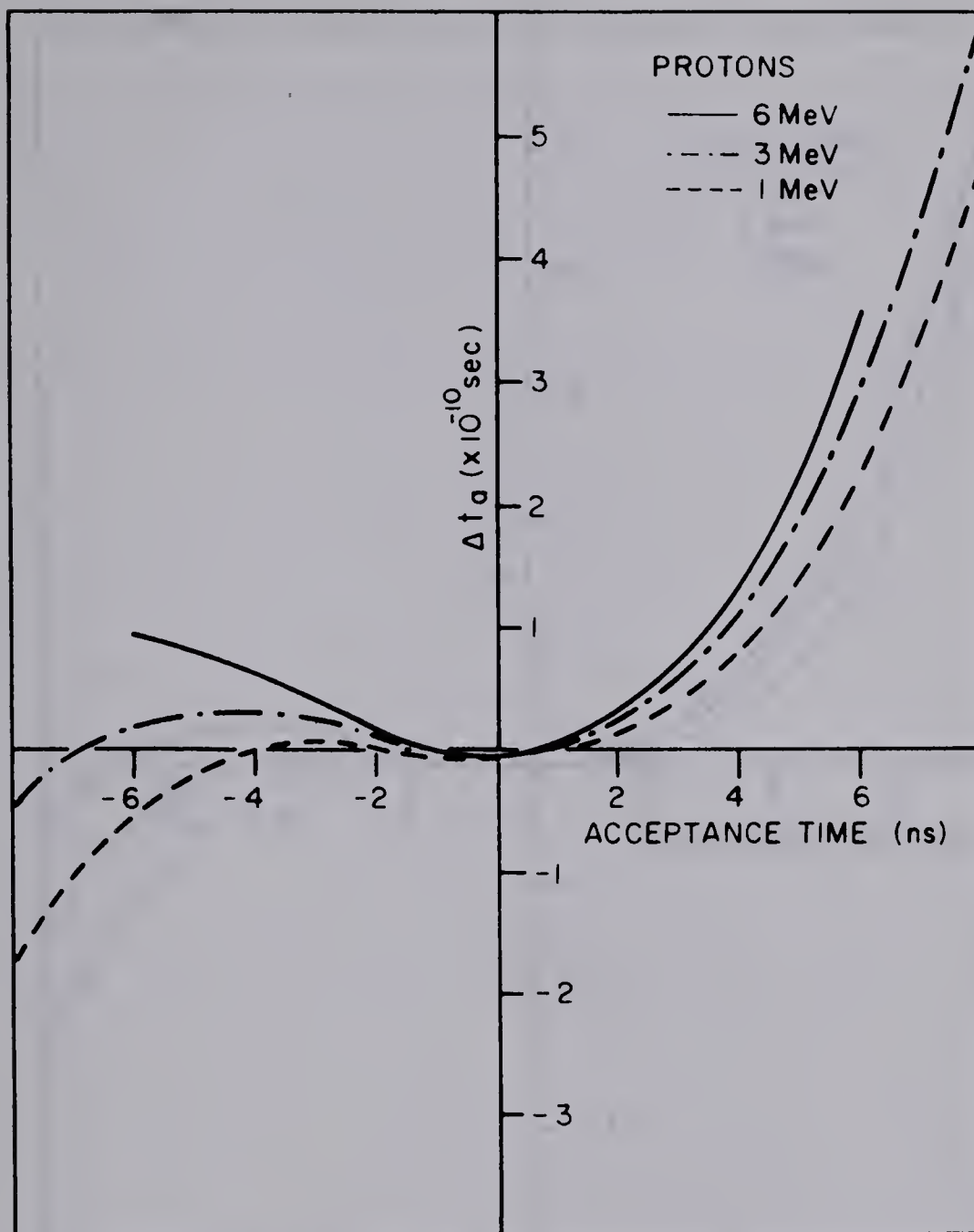


Figure 2-8. Arrival time versus acceptance time for a proton beam of various energies. The results shown include only the geometrical effects of the magnet and the effect of the sinusoidal sweep waveform of the deflector.

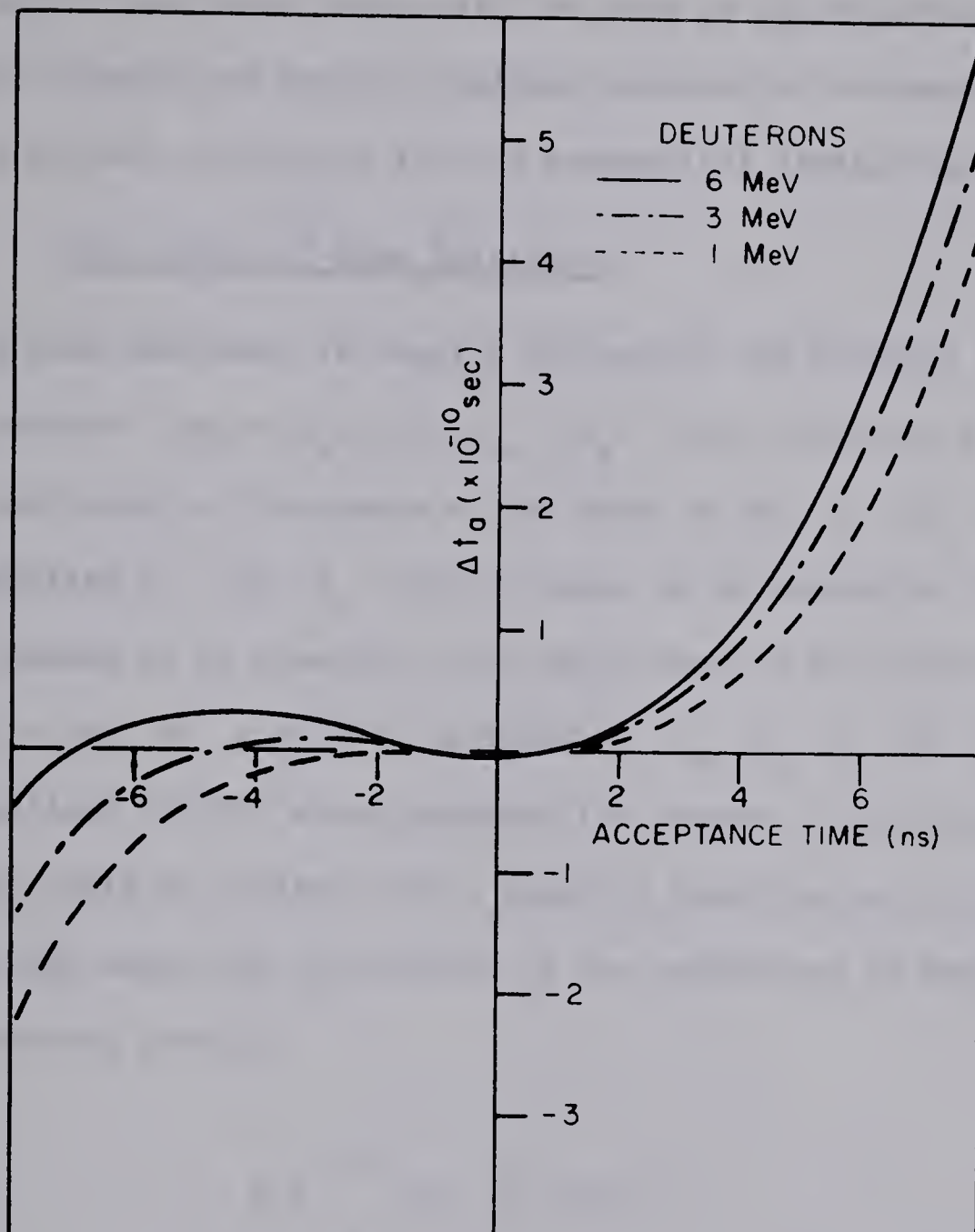


Figure 2-9. Arrival time versus acceptance time for a deuteron beam of various energies. The results shown include only the geometrical effects of the magnet and the effect of the sinusoidal sweep waveform of the deflector.

larger magnet aperture and as will be seen in later sections the geometric effects are not the limiting factors in the bunching. This makes an attempt to correct for the geometrical limitations unnecessary.

The Effect of Beam Emittance

The beam emittance is usually defined in the paraxial approximation as the products $x\phi_x = \Omega_x$ and $z\phi_z = \Omega_z$ which represent the maximum extent and angle of divergence of the beam in the x and z directions. The quantities Ω_x and Ω_z will be shown to be constants of the motion in the absence of an electric field which move in the "phase-space" defined by the $2n$ canonical coordinates p_x, p_z, H and x, z, t (see equations (2-18)) which describe the system. The invariance of Ω can most easily be derived from a quantity known as the bilinear covariant (Fo 60) which can be obtained by two variations of Hamilton's characteristic function

$$W = \int_{t_a}^{t_b} (\underline{p} \cdot \dot{\underline{q}} - H) dt \quad . \quad (2-81)$$

The first variation leads to

$$\delta W = \int_{t_a}^{t_b} (\delta \underline{p} \cdot \dot{\underline{q}} + \underline{p} \delta \dot{\underline{q}} - \delta H)$$

which if integrated by parts yields

$$\delta W = \underline{p} \cdot \delta \underline{q} \Big|_{t_a}^{t_b} + \int_{t_a}^{t_b} \left(\delta \underline{p} \cdot \left(\dot{\underline{q}} - \frac{\partial H}{\partial \underline{p}} \right) - \delta \underline{q} \cdot \left(\dot{\underline{p}} + \frac{\partial H}{\partial \underline{q}} \right) \right) dt \quad (2-82)$$

where the first term vanishes at the end points by definition of the variation (Go 59 p. 225) and where the second term vanishes identically if

$$\dot{\underline{q}} = \frac{\partial H}{\partial \underline{p}} \quad \text{and} \quad \dot{\underline{p}} = - \frac{\partial H}{\partial \underline{q}} \quad . \quad (2-83)$$

A second variation Δ of equation (2-82) gives the result

$$\Delta \delta W = (\Delta \underline{p} \cdot \delta \underline{q} + \underline{p} \Delta \cdot \delta \underline{q}) \Big|_{t_a}^{t_b} \quad . \quad (2-84)$$

If the variations δ and Δ are carried out in reverse order, the result is

$$\delta \Delta W = (\delta \underline{p} \cdot \Delta \underline{q} + \underline{p} \cdot \delta \Delta \underline{q}) \Big|_{t_a}^{t_b} \quad . \quad (2-85)$$

Now since δ and Δ are independent variations the dual variation $\Delta \delta$ must be equal to the variation $\delta \Delta$ so that on equating equations (2-84) and (2-85) one is left with

$$(\Delta \underline{p} \cdot \delta \underline{q} - \delta \underline{p} \cdot \Delta \underline{q}) \Big|_{t_a}^{t_b} = 0 \quad . \quad (2-86)$$

The quantity in parentheses in equation (2-86) is known as the bilinear covariant (sometimes called the Lagrange relation) and clearly has the same value at any two times along the path. The meaning of the bilinear covariant can be illustrated with the help of figure (2-10). In the figure, which represents a special case of the bilinear covariant, the ray denoted 1 is formed by the variation δx at s_a on the

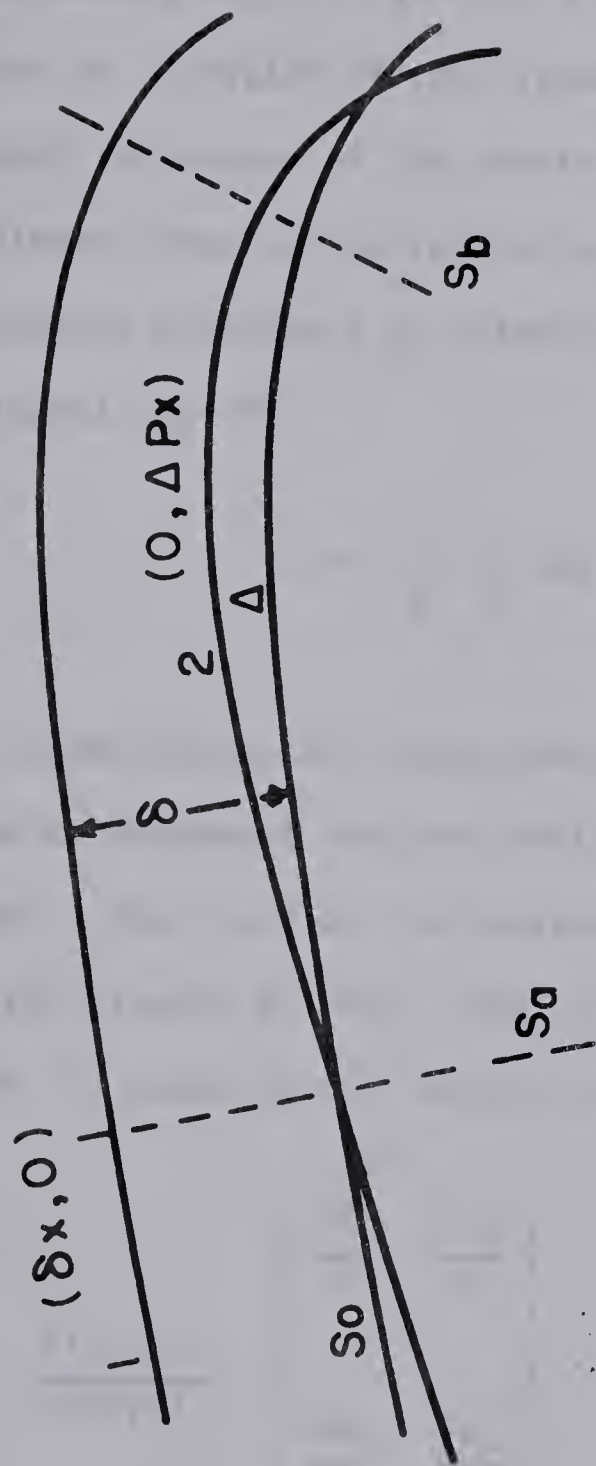


Figure 2-10. Representation of an ion beam by means of the central trajectory and two extreme rays of the beam.

central trajectory s and the ray denoted 2 is formed by the variation $\Delta\phi$ at s_a . Thus the bilinear covariant expresses a particular relationship, a relationship which is in fact a constant of the motion, among the components of a triplet of rays formed by the central ray itself and two independent variations of the central ray.

The bilinear covariant is related to, and in fact can be derived from, the integral invariants of Poincaré. Poincaré's theorem states that the integral (Go 59)

$$J_1 = \int_S \sum_i dq_i dp_i \quad (2-87)$$

is invariant under canonical transformation where S indicates that the integrals can be evaluated over any arbitrary two-dimensional surface in phase space. The proof of the invariance of J_1 is effected by noting that the element of area $dqdp$ in phase space transforms to the element $dudv$ by means of the Jacobian determinant

$$\frac{\partial(q_i, p_i)}{\partial(u, v)} = \begin{vmatrix} \frac{\partial q_i}{\partial u} & \frac{\partial p_i}{\partial u} \\ \frac{\partial q_i}{\partial v} & \frac{\partial p_i}{\partial v} \end{vmatrix} \quad (2-88)$$

according to the relation

$$dq_i dp_i = \frac{\partial(q_i, p_i)}{\partial(u, v)} dudv \quad (2-89)$$

Thus the statement that J_1 is a constant under contact transformation viz.

$$\int_S \int \sum_i dq_i dp_i = \int_S \int \sum_k dQ_k dP_k$$

can also be written as

$$\int_S \int \sum_i \frac{\partial(q_i, p_i)}{\partial(u, v)} dudv = \int_S \int \sum_k \frac{\partial(Q_k, P_k)}{\partial(u, v)} dudv \quad (2-90)$$

Since the regions of integration are arbitrary, the integrals can be equal only if the integrands are identical. Hence

$$\sum_i \frac{\partial(q_i, p_i)}{\partial(u, v)} = \sum_k \frac{\partial(P_k, Q_k)}{\partial(u, v)} \quad (2-91)$$

The proof of the invariance of J_1 , which will not be given here, has now been reduced to showing that the sum of the Jacobians is invariant. A proof of Poincaré's theorem is given by Goldstein (Go 59) who also indicates how to extend the proof to

$$J_2 = \int_S \int \int \sum_{i,k} dq_i dp_i dq_k dp_k \quad (2-92)$$

and eventually to

$$J_n = \int \dots \int dq_1, \dots dq_n dp_1 \dots dp_n \quad (2-93)$$

The integral J_n is equivalent to saying that the volume of phase space is invariant under contact transformation.

The condition for the invariance of the sum of the Jacobians can also be written as

$$\sum_i \left(\frac{\partial q_i}{\partial u} \frac{\partial p_i}{\partial v} - \frac{\partial p_i}{\partial u} \frac{\partial q_i}{\partial v} \right) = \sum_k \left(\frac{\partial Q_k}{\partial u} \frac{\partial P_k}{\partial v} - \frac{\partial P_k}{\partial u} \frac{\partial Q_k}{\partial v} \right) \quad (2-94)$$

where each side of this equation has the form of a Lagrange bracket of u and v , defined as

$$\{u, v\} = \sum_i \left(\frac{\partial q_i}{\partial u} \frac{\partial p_i}{\partial v} - \frac{\partial p_i}{\partial u} \frac{\partial q_i}{\partial v} \right). \quad (2-95)$$

The properties of the Lagrange bracket which are discussed in Goldstein (Go 59) and Sturrock (St 55) make it a very useful tool in both ordinary and ion optics. The Lagrange bracket is closely allied with the bilinear covariant derived earlier as will now be shown. Consider a ray with coordinates p, q where $p = p(u, v)$ and $q = q(u, v)$ where u, v are parameters that specify the ray. If two adjacent rays denoted as $(u + \delta u, v)$ and $(u, v + \Delta v)$ are formed by the small perturbations δu and Δv of the ray (u, v) as shown in figure (2-10) then

$$\delta p = \frac{\partial p}{\partial u} \delta u, \quad \Delta p = \frac{\partial p}{\partial v} \Delta v \quad (2-96)$$

$$\delta q = \frac{\partial q}{\partial u} \delta u, \quad \Delta q = \frac{\partial q}{\partial v} \Delta v.$$

The bilinear covariant is obtained from the Lagrange bracket by forming

the quantity $\{u,v\}\delta u\Delta v$ which by way of equations (2-96) becomes

$$\delta \underline{q} \cdot \Delta \underline{p} - \delta \underline{p} \cdot \Delta \underline{q} = \left[\frac{\partial \underline{q}}{\partial u} \cdot \frac{\partial \underline{p}}{\partial v} - \frac{\partial \underline{p}}{\partial u} \cdot \frac{\partial \underline{q}}{\partial v} \right] \delta u \Delta v \quad (2-97)$$

where the vector notation indicates a summation of components. Consequently both the Lagrange bracket and the bilinear covariant are constants of the motion.

The bilinear covariant, equation (2-97), can now be used to show that the determinant of any optical transformation matrix is unity. This can most easily be done by considering the triplet of rays shown in figure (2-10). As was indicated earlier ray 1 was formed by the variation δx at s_a and ray 2 was formed by the variation $\Delta \phi$ (or equivalently Δp_x) so that the bilinear covariant has the form

$$\delta x \Delta \phi = \text{constant}$$

at the point s_a . The two rays 1 and 2 are represented by the orthogonal vectors

$$\begin{pmatrix} \delta x \\ 0 \end{pmatrix} \text{ and } \begin{pmatrix} 0 \\ \Delta \phi \end{pmatrix} \quad (2-98)$$

at s_a and can be transformed to the point s_b by the transformation matrix $M(s_b|s_a)$ given in equation (2-30). The bilinear covariant for the transformation s_a to s_b is

$$\delta x_b \Delta \phi_b - \Delta x_b \delta \phi_b = \delta x_a \Delta \phi_a \quad (2-99a)$$

which by virtue of the transformation matrix M becomes

$$m_{11}\delta x_a - m_{12}\Delta\phi_a = m_{21}\delta x_a - m_{22}\Delta\phi_a \quad (2-99b)$$

or

$$(m_{11}m_{22} - m_{12}m_{21})\delta x_a \Delta\phi_a = \delta x_a \Delta\phi_a \quad (2-99c)$$

Thus the quantity in parentheses in equation (2-99c), which is the determinant of M , is equal to unity (+1). Conversely the condition that an arbitrary 2x2 matrix M be an optical transformation is that the $\det|M| = +1$.

In the derivation given above it has been implicitly assumed that the bilinear form $(\delta\mathbf{q} \cdot \Delta\mathbf{p} - \mathbf{p} \cdot \Delta\mathbf{q})$ is independently a constant of the motion for each of its pairs of canonically conjugate coordinates. That this separation is possible in the case discussed above can be seen by considering the equations of motion (2-25) and (2-26). In these equations the x and z directions are not coupled and it is implicit in the equations that H and t are constants; therefore the bilinear covariant can be broken into the two independently invariant quantities

$$(\delta x \Delta\phi_x - \delta\phi_x \Delta x) = \Omega_x \quad (2-100)$$

and $(\delta z \Delta\phi_z - \delta\phi_z \Delta z) = \Omega_z$

where Ω_x and Ω_z are constants.

Since in the paraxial approximation $\delta x = x_a$ and $\delta\phi = \phi$ etc.

equation (2-100) can be written as

$$\begin{aligned} (x_a \phi_{xb} - \phi_{xa} x_b) &= \Omega_x \\ (z_a \phi_{zb} - \phi_{za} z_b) &= \Omega_z . \end{aligned} \tag{2-101}$$

If at some point s_a the rays x_a and ϕ_a are chosen as the extreme rays of the system then the bilinear covariant is just

$$\begin{aligned} x_a \phi_{xb} &= \Omega_x \\ z_a \phi_{za} &= \Omega_z \end{aligned} \tag{2-102}$$

which is seen to be the definition of the emittance of the beam. In a general optical system, for instance one which contains a deflection system, the components of the bilinear covariant are not necessarily independent and the bilinear covariant must be written as

$$\begin{aligned} (\delta \underline{q} \cdot \Delta \underline{p} - \delta \underline{p} \cdot \Delta \underline{q}) \\ &= (\delta x \Delta \phi_x - \delta \phi_x \Delta x + \delta z \Delta \phi_z - \delta \phi_z \Delta z + \delta t \Delta H - \delta H \Delta t) \\ &= \text{constant} \end{aligned} \tag{2-103}$$

where the transformation used in equation (2-18) has been used to change the independent variable from t to s . If it is assumed that any device that couples pairs of canonical coordinates is only effective between t and x , as is the case in the present discussion then the bilinear covariant can be broken into the two independently invariant

quantities*

$$(\delta z \Delta \phi_z - \delta \phi_z \Delta z) = \Omega_z \quad (2-104a)$$

and $(\delta x \Delta \phi_x - \delta \phi_x \Delta x + \delta t \Delta H - \delta H \Delta t) = \Omega_x \quad (2-104b)$

The general beam bunching operation can be investigated with the help of the bilinear covariant given in equation (2-104b). A detailed analysis of the beam pulsing technique used in the top terminal pulsing (see section 2-2) has been made by Fowler and Good (Fo 60). Their analysis shows that the pulsing operation necessarily introduces an energy spread in the beam. However this spread is small compared with the inherent energy dispersion introduced by the accelerator, an effect which will be discussed in detail in the next section. The bunching effect of the magnet can be treated by a similar technique to the one used by Fowler and Good above. In this case let δx represent the maximum extent of the beam (see figure 2-10), $\Delta \phi_x$ the maximum angular divergence, δt the time difference between the leading and trailing edge of the beam and ΔE the energy dispersion of the beam so that equation (2-104b) becomes

$$(\delta x \Delta \phi_x + \delta t \Delta E) \Big|_{s_a} = (\delta x \Delta \phi_x - \delta E \Delta t - \delta \phi_x \Delta x + \delta t \Delta E) \Big|_{s_b} \quad (2-105)$$

where s_a and s_b represent the deflection plates and target of the bunching system and where H has been replaced by E . The criterion

*Note that in this coordinate system the units of H are those of velocity, i.e. E/P .

for bunching is that $\delta t = 0$ at s_b so that $\delta\phi_x$ or Δx or both must increase to compensate for the disappearance of the term $\delta t \Delta E$. In a Mobley bunching system $\delta\phi_x$ is increased by the deflection system so that δt may be reduced to zero. The remaining time spread Δt depends both on the energy spread induced in the beam due to sweeping and on $\delta x \Delta\phi_x$ which is taken as the emittance of the beam leaving the accelerator.

The effect of the term $\delta x \Delta\phi_x$ on the bunching will now be investigated by considering the path length differences between the two extreme rays δx and $\Delta\phi_x$ as they pass through the magnet. For the purposes of this discussion it will be assumed that the deflection system has been turned off so that the quantities $\delta x \Delta\phi$ and $\delta E \Delta t$ will individually be constants of the motion. In the paraxial approximation used in the present discussion the extreme rays of the system will be represented by the orthogonal vectors

$$\begin{pmatrix} x_a \\ 0 \end{pmatrix} \text{ and } \begin{pmatrix} 0 \\ \phi_b \end{pmatrix} \quad (2-106)$$

where the subscripts "a" and "b" will be used to emphasize the fact that two independent rays are being utilized. The value of the bilinear covariant for these rays is $x_a \phi_b = \Omega$ at the origin where Ω is the emittance of the beam in the x direction and is a constant in the system being discussed. The path length difference for an off-axis ray passing through the University of Alberta bunching system is

$$\ell = \frac{3}{2} x + 4\rho\phi \quad (2-107)$$

where $\rho = 190.5$ cm.

The effect of the emittance Ω and the optical system coupling the source to the bunching system can be studied using the four optical systems shown in figure (2-11). The transformation matrices for the systems, which can be written down by inspection, are shown in the figure and will not be referred to explicitly in the discussion. As a reference for comparison the path length difference

$$\ell = \ell_a + \ell_b = \frac{3}{2} x_a + 4\rho\phi_b \quad (2-108)$$

will be used which corresponds to a system with the source at the entrance to the bunching system or alternatively to system B in figure (2-11) with $f = F^*$

Figure (2-11A) shows a simple lens connecting the source to the reference plane of the bunching system. The path length difference for the two rays is easily seen to be

$$\ell = \frac{3}{2} F\phi_b - 4 \frac{x_a}{F} .$$

Clearly $\ell = 0$ if

$$F^2 = \frac{8}{3} \rho \frac{x_a}{\phi_b} .$$

*The path length differences for the two rays have been added since there is always a ray combination that will produce the sum, that is

$$\ell = \ell_a - \ell_b = \frac{3}{2} x_a - 4\rho(-\phi_b) = \frac{3}{2} x_a + 4\rho\phi_b$$

if ϕ_b is negative.

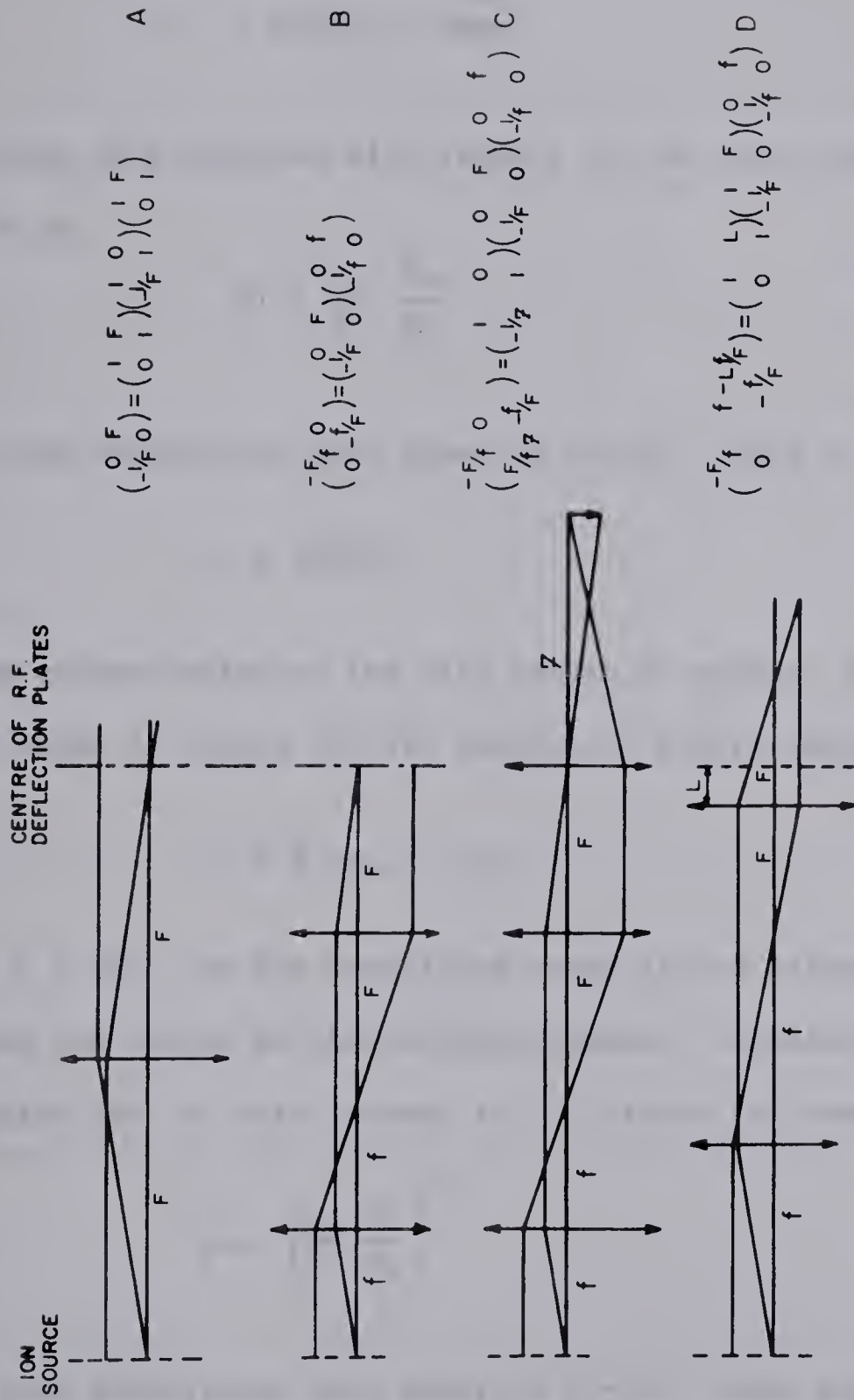


Figure 2-11. Four possible optical coupling systems that link the accelerator to the beam bunching system.

However for the rays $-x_a$ and ϕ_b , ℓ will not be zero since

$$\ell = \frac{3}{2}F\phi_b + 4\rho\frac{x_a}{F} \quad (2-109)$$

Minimizing this function with respect to the focal length F again results in

$$F^2 = \frac{8\rho}{3} \frac{x_a}{\phi_b} \quad (2-110)$$

which when substituted into equation (2-109) leads to

$$\ell = 2\sqrt{6\rho\Omega} \quad (2-111)$$

for the minimum value of the path length in system A. Similarly the system shown in figure (2-11B) results in a path length difference

$$\ell = \frac{3}{2} p x_a + 4\rho\phi_b \quad (2-112)$$

where $p = -F/f$ is the magnifying power of the telescopic system coupling the source to the bunching system. Minimization of this expression for ℓ with respect to p yields the result

$$p = \left(\frac{8\rho}{3} \frac{\phi_b}{x_a} \right)^{1/2} \quad (2-113)$$

which when substituted into equation (2-112) again gives

$$\ell = 2\sqrt{6\rho\Omega} \quad (2-114)$$

for the minimum value of the path length difference.

One might now ask if a more complicated optical coupling arrangement allowing more freedom in the determination of the transformed rays might result in an even greater reduction in the path length differences, since in both coupling systems discussed above the optical system has allowed only a change in the ratio of x and ϕ in the resultant rays while preserving their orthogonal character. Two optical systems which do allow this extra freedom are shown in figures (2-11C) and (2-11D). The system shown in figure (2-11C) consists of a telescope, as in B, feeding into a simple lens placed coincident with the R.F. deflection plates. Setting $p = -F/f$ as before the path length difference can be written as

$$\ell = \frac{3}{2} p x_a - 4\rho \frac{p}{f} x_a + 4\rho \frac{\phi_b}{p} \quad . \quad (2-115)$$

Minimizing this expression as a function of p gives

$$p = \left(\frac{4\rho\phi_b}{(3/2 - 4\rho/f)x_a} \right)^{1/2} \quad (2-116)$$

which when substituted into equation (2-115) yields

$$\ell = \frac{3}{2} \left(\frac{4\rho f \Omega}{(3/2 f - 4\rho)} \right)^{1/2} - 4\rho \left(\frac{4\rho \Omega}{f(3/2 - 4\rho)} \right)^{1/2} + \left(\frac{4\rho(3/2 - 4\rho)\Omega}{f} \right)^{1/2} \quad (2-117)$$

for the path length difference. Equations (2-116) and (2-117) are parametric functions of the focal length f . A simpler expression which is somewhat more illuminating can be obtained by adjusting f so the

term in x_a vanishes identically. The required expression for \mathcal{F} is

$$\mathcal{F} = \frac{8\rho}{3} \quad (2-118)$$

which when substituted into equation (2-115) gives

$$\ell = 4\rho \frac{\phi_b}{p} \quad (2-119)$$

Thus the path length difference ℓ can be made arbitrarily small by making p arbitrarily large, a result which can also be seen from equation (2-117) in the limit as \mathcal{F} approaches $8\rho/3$. In the limit as $\mathcal{F} \rightarrow \infty$ equation (2-115) reduces to equation (2-112) with the result that

$$\ell = 2 \sqrt{6\rho\Omega}$$

as one would expect.

An analogous result to the one given above can be obtained using the optical system shown in figure (2-11D). In this system the coupling is a simple telescope but the final drift distance is not required to be equal to the focal length of the lens. The path length difference for this system is

$$\ell = -\frac{3}{2} p x_a + \frac{3}{2} \left(f - \frac{L}{p}\right) \phi_b - 4\rho \frac{\phi_b}{p} \quad (2-120)$$

where p is now taken as $p = +F/f$. Minimization of equation (2-120) with respect to p gives the following result for the value of p :

$$p = \left(\left(\frac{8\rho}{3} + L \right) \frac{\phi_b}{x_a} \right)^{1/2}. \quad (2-121)$$

On substituting this value of p in the equation for the path length difference one obtains

$$\ell = -\frac{3}{2} \left(\left(\frac{8\rho}{3} + L \right) \Omega \right)^{1/2} + \frac{3}{2} f \phi_a - (4\rho + L) \left(\frac{\Omega}{\left(\frac{8}{3} \rho + L \right)} \right)^{1/2}. \quad (2-122)$$

Again a simpler expression can be obtained by setting, in this case, the term in ϕ_b equal to zero. This results in the following relations among F , f , p and L :

$$p = \left(\frac{8\rho}{3} + L \right) / f, \quad f = \left(\frac{8\rho}{3} + L \right) / p \quad (2-123)$$

$$F = \frac{8\rho}{3} + L \quad \text{and} \quad L = F - \frac{8\rho}{3}.$$

The path length difference for this system is

$$\ell = -\frac{3}{2} p x_a. \quad (2-124)$$

If $L = F$ then equation (2-120) reduces to

$$\ell = 2\sqrt{6\rho\Omega}$$

and it is, of course, not possible to produce the cancellation resulting in equation (2-124).

The four optical systems discussed above show that it is possible by correctly adjusting the parameters of the system to reduce the effect of the beam emittance on the time dispersion of the bunched beam. In particular it is seen in systems C and D that the effect can be made arbitrarily small by appropriate adjustment of the power of the coupling telescopes. However the reduction in time dispersion indicated above can only be achieved at the expense of beam intensity since when p becomes arbitrarily large, as in C, the beam width also becomes large and because of the finite aperture of the magnet beam will be lost. A similar result is obtained if p approaches zero in system D. Since the beam spot size and angular divergence on the target are affected by the methods used to reduce the time dispersion, the criteria regarding these quantities will limit the extent to which the time dispersion resulting from the beam emittance can be diminished. Table (2-3) shows the resultant time dispersion and beam spot size for the four optical systems described above where realistic values for the parameters have been employed. The beam emittance was taken to be 1×10^{-3} rad. cm. where it was assumed that $x_a = 0.2$ cm. and $\phi_b = 5 \times 10^{-3}$ radians.

For all cases given in the table the angular divergence on the target due to the beam emittance is much less than the divergence introduced by the R.F. deflection and can therefore be neglected.

The beam emittance can be obtained by measuring the beam spot size at the focal point and at the exit principal plane of any lens since

at the focal point the spot size is $x_f = f\phi_b$ and at the exit principal plane the spot size is $x_{te} = x_a$ where x_a and ϕ_b represent the extreme rays of the system. However to obtain the bunching time for the optical systems shown in figure (2-11C,D) it is only necessary to measure the spot size at the focal point of the final lens since in these systems the contribution to the time dispersion from one of the extreme rays can always be eliminated.

TABLE (2-3)

The Effect of Beam Emittance on Bunching and Beam Spot Size for the Optical Systems Shown in Figure (2-11)

Optical System	Expression for the path length ℓ	Path length difference cm*	Δt for 6 MeV protons	Power of telescope or focal length	Beam spot size
Reference (B)	$\ell = \frac{3}{2} x_a + 4\phi_b$	4.10 cm	1.2 ns	1	0.2 cm
A	$\ell = 2\sqrt{6\rho\Omega}$	2.14 cm	0.64 ns	142.5 cm	0.7 cm
B	$\ell = 2\sqrt{6\rho\Omega}$	2.14 cm	0.64 ns	3.56	0.7 cm
C	$\ell = 4\rho \frac{\phi_0}{p}$	1.27 cm	0.373 ns	3.0	0.6 cm
D	$\ell = \frac{3}{2} x_0 p$	0.3 cm	0.088 ns	1	2.54 cm
		0.9 cm	0.306 ns	3	0.85 cm

* $\Omega = 10^{-3}$

$x_a = 0.2$ cm

$\phi_b = 5 \times 10^{-3}$ cm

The optical system (2-11D) is closest to the one in actual use at the University of Alberta. However at this time no exact ray trace of the system has been carried out to determine just how far from the optimum system it is.

(d) The Momentum Dispersion

The effect of momentum dispersion on the trajectories can be found by solving the inhomogenous differential equations (Ha 63a)

$$\frac{dx^2}{ds^2} + \kappa x = \frac{\kappa \Delta p}{p_0} \quad (2-125)$$

where p_0 is the design momentum and Δp is the momentum dispersion.

The particular solution of equation (2-125a) is (Ha 63a)(Pe 61)

$$h(s) = \rho(1 - \cos(\kappa(s-s_0))) \quad (2-126)$$

and the general solutions are the same as those given in equations (2-31) and (2-32). Therefore the optical transformation can be written as

$$x(s) = f(s)x_0 + g(s)x'_0 + h(s)\Delta p/p_0 \quad (2-127)$$

$$x'(s) = f'(s)x_0 + g'(s)x'_0 + h'(s)\Delta p/p_0$$

which if put in matrix form becomes

$$H = \begin{pmatrix} \cos \alpha + \sin \alpha \tan \beta & \rho \sin \alpha & \rho(1 - \cos \alpha) \\ -\frac{1}{\rho}(\sin \alpha - 2 \cos \alpha \tan \beta - \sin \alpha \tan^2 \beta) & \cos \alpha + \sin \alpha \tan \beta & \sin \alpha \\ 0 & 0 & 1 \end{pmatrix} \quad (2-128)$$

The ray vector is now the transpose of the vector $(x, \phi, \Delta p/p)$. It should be pointed out that the determinant of the matrix (2-128) is unity.

The path length difference resulting from the momentum dispersion is obtained by integrating the x component of the momentum dispersion solution. The result is

$$\int_0^\alpha \rho(1 - \cos \alpha) d\alpha = \rho(\alpha - \sin \alpha) \Big|_0^\alpha$$

$$= \rho(\alpha - \sin \alpha) \quad .$$
(2-129)

The total path length difference becomes (see equation (2-60))

$$\ell = [\sin \alpha + (1 - \cos \alpha) \tan \beta] x_0 + 4\rho\phi_0 + \rho(\alpha - \sin \alpha) \frac{\Delta p}{p_0}$$
(2-130)

which for the University of Alberta Mobley bunching system reduces to

$$\ell = \frac{3}{2} x_0 + 4 \rho\phi_0 + \rho\left(\frac{\pi}{2} - 1\right) \frac{\Delta p}{p_0} \quad .$$
(2-131)

Using the value $\Delta p/p_0 = 0.35 \times 10^{-2}$ from table (2-2) one obtains

$$\ell_1 = \rho\left(\frac{\pi}{2} - 1\right) \frac{\Delta p}{p_0} = 0.382 \text{ cm}$$

which is equivalent to a time dispersion of 0.11 ns for a 6 MeV proton beam. This value for $\Delta p/p_0$ produces a beam spot size on the target given by

$$x_p = 3\rho \frac{\Delta p}{p_0} \quad ,$$
(2-132)

of 2 cm which is somewhat larger than is observed in practice. If a one cm. spot size is assumed to be solely the result of the momentum dispersion then one finds from equation (2-132) that $\Delta p/p_0$ is 0.175×10^{-2} which gives a path length difference of only 0.19 cm corresponding to a time dispersion of only .06 ns.

Another source of momentum dispersion that was not considered in the discussion given above is the so-called klystron effect produced by the R.F. field of the deflection system. This effect is very difficult to estimate quantitatively, but that it is very small is born out by the fact that the beam spot size at the target is completely accounted for by the momentum dispersion resulting from the accelerator.

(e) The Magnetic Field Homogeneity and Stability

Since a change in momentum of the particle is indistinguishable from a change in the magnetic field the term $\kappa \Delta p/p$ can be replaced by $\kappa \Delta B/B$ in equation (2-125). Thus the solution of equation (2-125) for $\Delta B/B$, which is identical to that given in equation (2-126), leads to the expression

$$\ell' = \rho \left(\frac{\pi}{2} - 1 \right) \frac{\Delta B}{B} \quad (2-133)$$

for the path length difference resulting from the magnetic field inhomogeneity in the (UA) bunching system. The design specification for the upper limit on $\Delta B/B$ is 1/200 resulting in a path length difference of 0.55 cm which corresponds to a time spread of approximately 0.16 ns. Measurements of the magnetic field of the magnet over an area

of a few square feet indicated that the magnetic field was probably homogeneous to at least one part in 500. This value yields a path length difference of 0.22 cm with a corresponding time dispersion of 0.064 ns for a 6 MeV proton beam.

(f) The Phase and Amplitude Stability of the R.F. Deflection System

The calculations on the performance of the bunching system made in the previous sections have assumed an R.F. deflection system that is perfectly locked in phase with the incoming beam pulses and has exactly the amplitude required for optimum bunching. Unfortunately it is impossible to produce these optimum conditions.

The problem of phase stability is a most difficult one since it is usual to have the deflection oscillator frequency ranging from ten to twenty times higher than the beam pulse frequency. The effect of the phase instability ξ is to cause a deflection of the centre of the beam pulse to the left or to the right depending upon the sign of ξ viz.

$$\phi = -\phi_0 \sin(\omega t + \xi) \quad .$$

Such a deflection causes no first order change in the bunching but produces second and higher effects. Alternatively the phase shift ξ is equivalent to lengthening the beam pulse on one side of $t = 0$ and shortening it on the other side and as a consequence of this interpretation the geometrical effects of the phase shift can be estimated by referring to figures (2-8) and (2-9). However the usual mode of

operation is to employ beam defining slits that limit the maximum angular deflection of the beam. With these slits in place (see figure (2-1)) the phase instability will not affect the bunching of the beam but will result in a loss of beam current with a resultant modulation of the beam amplitude.

The time dispersion resulting from the amplitude instability $\Delta\phi_0$ of the R.F. deflection system can be calculated using equations (2-67) and (2-68). Equation (2-67) leads to

$$\Delta t_a = - \frac{4\rho}{v} \omega \Delta\phi_0 t$$

which reduces to

$$\Delta t_a = - \frac{\Delta\phi_0}{\phi_0} t$$

on substituting for v from equation (2-68). Thus the maximum time dispersion for a given acceptance time Δt is

$$\Delta t_a = - \frac{\Delta\phi_0}{\phi_0} \Delta t = \frac{\Delta V_0}{V_0} \Delta t$$

The R.F. deflection system has a short term amplitude stability of the order of 1 part in 200 which corresponds to a time dispersion of 0.05 ns. Added to this dispersion is the effect of an error in the adjustment of the R.F. amplitude. If the largest error in V_0 resulting from the latter effect is 0.01 then the total time dispersion is 0.11 ns.

Finally there is a slight time dispersion resulting from the displacement of the beam produced by the sweeping operation. The result

of this displacement given by equation (2-75) is a nearly constant shift in the central ray of about 0.45 cm. However because of the nonlinearity of the sweep wave form the displacement is not quite constant and introduces a path length difference of about 0.02 cm.

(x) The Predicted Performance of the Bunching System

The factors that limit the bunching of the (UA) Mobley bunching system are summarized in table (2-4). The table shows that the most important factor limiting the bunching is the emittance of the ion beam. By careful adjustment of the optical coupling system between the accelerator and the bunching system it was seen that the effect of the beam emittance can be reduced to approximately 0.35 ns which gives a lower limit of about 0.42 ns for the time dispersion of the system. The time dispersions shown in the table were calculated for a 6 MeV proton beam which is the most favourable energy since the geometrical aberrations are negligible. At lower beam energies the effects of the amplitude instability, the beam emittance and the momentum dispersion all increase which tends to worsen the bunching. However since the geometrical aberrations are negligible there should be little difference in the bunching factors for protons, deuterons or alpha particles.

In the calculations given above a beam with a uniform particle density profile has been employed. In fact the measurements of the beam profile show a nearly Gaussian charge distribution in both the radial and axial planes. If this were taken into account the effective beam emittance, momentum dispersion and spot size would be reduced.

TABLE (2-4)

The Effects that Limit Bunching

Effect	Symbol	Value	Time dispersion* ns
Geometrical aberration	--	RMS av.	0.1
Beam emittance	Ω	1×10^{-3}	Lens B 0.64 Lens C 0.37
Momentum dispersion	$\Delta p/p$	0.35×10^{-2}	0.11
Magnetic field	$\Delta B/B$	0.5×10^{-2}	0.16
Homogeneity		0.2×10^{-2}	0.064
Sweep amplitude stability	$\Delta V/V$		0.10
RMS dispersion	using maximum values		0.68
	using minimum values		0.42
Bunching factor	$\Delta t/\Delta t_a$	15 - 24	

*Calculated for a 6 MeV Proton Beam

(xi) The Measured Performance of the Bunching System

The time dispersion of the bunched beam was initially measured by collecting the beam in a specially designed Faraday cup, the output pulse of which was displayed on a Tektronix 661 sampling oscilloscope.* The target assembly manufactured by High Voltage Engineering Corporation had a grounded grid in front of the Faraday cup which prevented an image of the approaching beam pulse from broadening the output pulse.

*Tektronix Incorporated, Portland, Oregon.

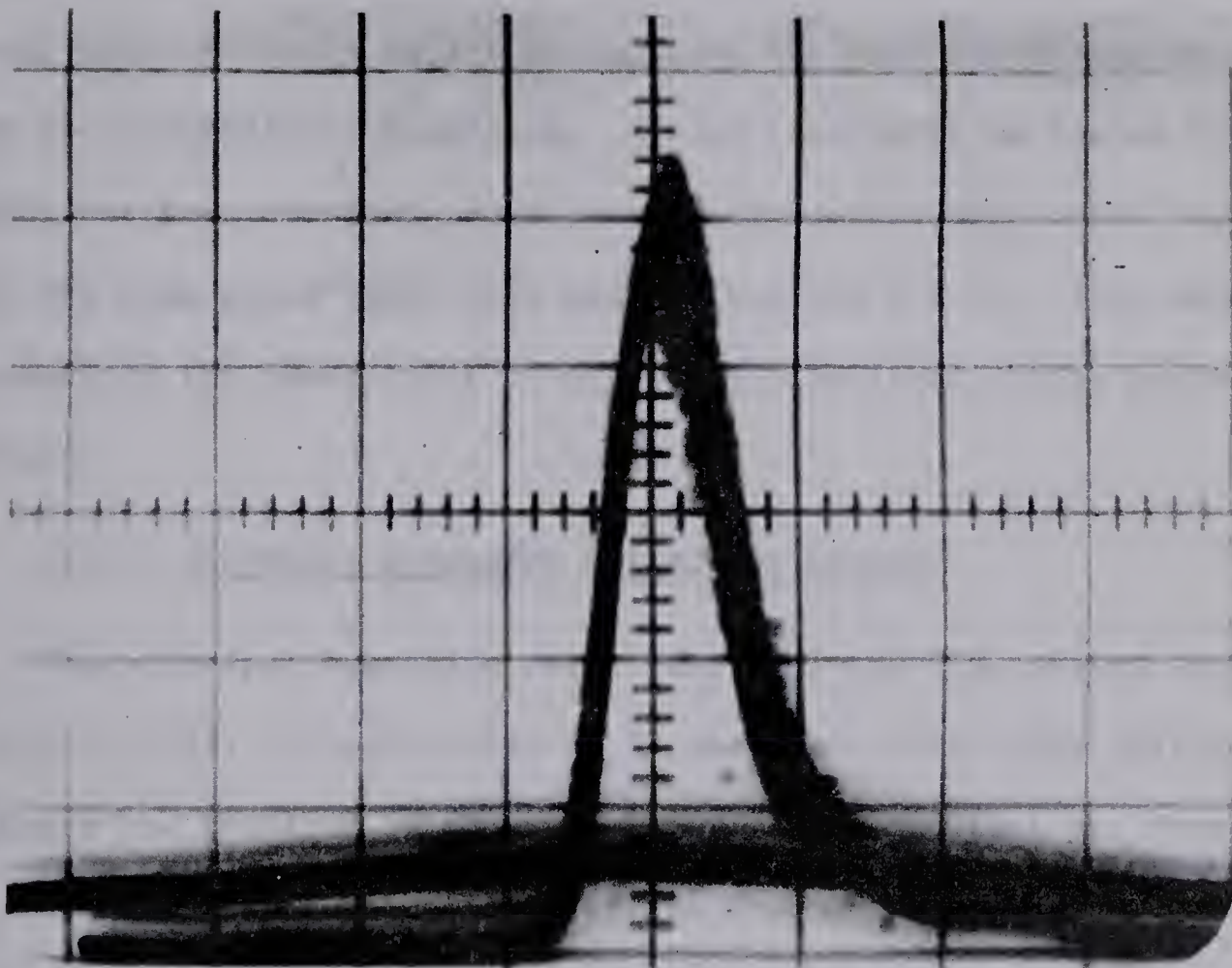


Figure 2-12. Typical beam pulse obtained at the target for a 3 MeV proton beam. Upper trace is the bunched beam; lower trace is the unbunched 10 ns beam pulse from the accelerator. The horizontal scale is 1 ns per division.

Figure (2-12) shows a typical output pulse obtained with the measuring apparatus described above. The pulse width is seen to be 0.8 ns (FWHM) which is well within the specified value of 1 ns. Recent resolution measurements of the total time-of-flight spectrometer have been made using the $D(t,n)He^4$ reaction which produces very high energy neutrons (~ 14 MeV) thus reducing the time dispersion resulting from the scintillator thickness. A time resolution as low as 0.7 ns (FWHM) has been obtained under these conditions, which would indicate that the beam pulse width lies between 0.5 and 0.6 ns. This value is approaching the lower limit of operation calculated in the preceding section.

(xii) The Radio Frequency Deflection System

The principal operating requirements of the R.F. system were given in table (2-2). In particular it is seen that very large peak to peak voltages are required on the deflection plates and that the frequency of operation is a factor of ten larger than the beam repetition rate, both of which make the problems of amplitude and phase stability more critical. The necessity of such large output voltages makes the use of a very high Q deflection tank circuit mandatory. This in turn requires excellent mechanical and frequency stability if reasonable amplitude and phase stability are to be achieved.

Since the beam chopping circuitry (see section (ii)) is located in the high voltage terminal of the accelerator it is impossible to obtain the phase information from the 1 MHz sweep oscillator itself.

The phase information must then be obtained from the ion beam which is more difficult than might appear at first sight, since at best ion sources are rather unstable devices. Consequently the 10 MHz R.F. deflection oscillator must maintain excellent phase and amplitude stability under conditions of fluctuating control information. The failure on the part of the manufacturer to realize the fluctuating and intermittent character of the pulsed beam resulted in the inability of the system to operate except under ideal conditions. To overcome this difficulty, the beam sensing, phase detection and phase controlled oscillator circuitry was completely redesigned and rebuilt by Dr. G. C. Neilson, Mr. E. B. Cairns and Mr. L. Holm of this laboratory.

A block diagram of the redesigned deflection system is shown in figure (2-13). The phase information is obtained from the beam as it passes through a cylindrical beam sensing capacitor, the induced charge producing a voltage which is then differentiated and fed to the tunnel diode cross-over-pickoff circuit. The output of the cross-over-pickoff is a constant amplitude pulse with its width controlled to 50 ns. This pulse passes through a 0 - 250 ns electronic variable delay which allows the phase shift resulting from the separation of the beam sensing capacitor and the deflection plates to be corrected. This phase shift is, of course, a function of the particle velocity and hence must be adjusted as the beam energy and/or the particle type is varied. The delayed signal is then fed into the 10 MHz crystal oscillator gate integrator, the limiter shaper and the frequency stabilizing integrator

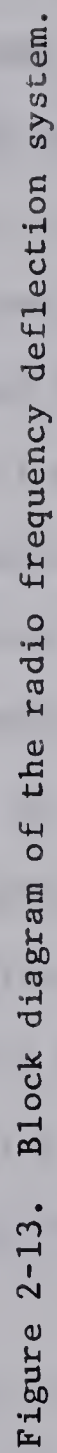


Figure 2-13. Block diagram of the radio frequency deflection system.

all of which have control over the operation of the 10 MHz phase controlled oscillator, the heart of the system. Under normal operating conditions the crystal oscillator gate inhibits the operation of the crystal controlled oscillator. However in the event that no phase information is obtained for a period of 20 μ s the crystal controlled oscillator is activated and takes over control of the main oscillator. This prevents a serious frequency drift from occurring which would cause overloading and the automatic shut-down of the system. In the normal operating condition the bias on the frequency control varicaps in the phase controlled oscillator is adjusted by the opposing d.c. signals from the frequency stabilizing integrator and the 1 MHz phase detector, the time constants of which have been adjusted so as to produce a minimum of frequency variation between the 1 MHz control pulses or when control information is lost. In addition to the frequency and phase control provided by the 1 MHz phase detector circuitry the oscillator is directly excited by the doubly differentiated signal from the limiter shaper. This signal not only improves the phase stability of the oscillator but greatly facilitates the recovery of the system after an interruption in control information has occurred.

Phase and amplitude stabilization of the deflection tank circuit is achieved by two feedback loops including the phase and automatic gain control (A.G.C.) sensor and the gain and phase controlled amplifier. Phase control is accomplished by an R-C phase shift network employing varicaps whose bias is adjusted by the output signal from the 10 MHz

phase detector. Gain stabilization is achieved using a conventional circuit employing remote cutoff pentodes. The R.F. amplitude on the deflection plates is controlled by adjustment of the A.G.C. bias.

The peak voltages and the maximum deflection angles (half angles) required for optimum bunching of 10 ns beam pulses are shown in table (2-5) at various energies and for the four projectiles in use at this laboratory. The table illustrates the large dynamic range required of the system in order to cover the various operating conditions.

TABLE (2-5)

Peak voltages and maximum deflection angles required for optimum bunching.

ENERGY (MEV)		PROTONS	DEUTERONS	HELIUM 3(1)	HELIUM 4(1)
1.000	RF VOLTS	4399.	3534.	3302.	3299.
	RADIANS	.00893	.00631	.00516	.00448
1.500	RF VOLTS	7758.	5960.	5303.	5022.
	RADIANS	.01093	.00773	.00632	.00548
2.000	RF VOLTS	11705.	8802.	7656.	7079.
	RADIANS	.01263	.00893	.00730	.00633
2.500	RF VOLTS	16162.	12001.	10303.	9398.
	RADIANS	.01412	.00998	.00816	.00708
3.000	RF VOLTS	21076.	15521.	13211.	11946.
	RADIANS	.01546	.01094	.00894	.00776
3.500	RF VOLTS	26408.	19334.	16357.	14700.
	RADIANS	.01670	.01181	.00965	.00838
4.000	RF VOLTS	32127.	23418.	19724.	17646.
	RADIANS	.01786	.01263	.01032	.00896
4.500	RF VOLTS	38209.	27757.	23298.	20771.
	RADIANS	.01894	.01340	.01095	.00950
5.000	RF VOLTS	44632.	32336.	27067.	24064.
	RADIANS	.01997	.01412	.01154	.01002
5.500	RF VOLTS	51381.	37143.	31022.	27518.
	RADIANS	.02094	.01481	.01210	.01051
6.000	RF VOLTS	58438.	42168.	35154.	31126.
	RADIANS	.02187	.01547	.01264	.01097

CHAPTER 3

THE $\text{Si}^{28}(\text{d},\text{n})\text{P}^{29}$ REACTION1. Introduction

Information on the low lying excited states of P^{29} has been obtained employing the $\text{Si}^{28}(\text{d},\text{n})\text{P}^{29}$ reaction as part of a programme aimed at investigating the properties of nuclei around mass 28. A preliminary report of the results obtained in regard to P^{31} using this reaction appeared earlier¹⁾.

Nilsson model and weak-coupling collective model calculations²⁾ have been made for P^{29} . The Nilsson model calculations included both rotation-particle coupling and rotation-vibration interactions. In the weak-coupling model a Si^{28} core, including excitations of up to 3 phonons, was coupled to the odd proton in the $2s_{1/2}$ or $1d_{3/2}$ shells.

In the present experiment angular distributions of the neutron groups leading to the low lying excited states of P^{29} have been measured at deuteron bombarding energies of 4 and 5 MeV. These distributions have been compared with the predictions of the distorted wave Born approximation (DWBA). Spectroscopic factors have been deduced for the transitions to the different levels of P^{29} and are compared with the results of the strong coupling and weak coupling collective model calculations²⁾ as well as shell model calculations³⁾.

2. Experimental

The experiment was performed with the University of Alberta 5.5 MeV Van de Graaff accelerator and the associated high resolution neutron time-of-flight spectrometer. Top terminal pulsing and a Mobley magnet compression system deliver beam bursts of approximately 0.8 ns (FWHM) with a repetition rate of 1 MHz and an average beam current of about 2 μ A. The block diagram of the time-of-flight spectrometer electronics is shown in fig. 1. Fast signals from the neutron detector and from the beam pick-off circuit are fed into a conventional pulse overlap time converter⁴⁾. The output of the time converter is fed into the first half of a 1024 channel pulse height analyzer which is gated by signals from (1) a gamma ray eliminator, (2) a neutron threshold discriminator, and (3) a negative time eliminator, as shown in fig. 1. A parallel time-of-flight system is used as a monitor, the spectrum of which is recorded in the second half of the pulse height analyzer.

With a flight path of 6.4 m, the overall energy resolution was about 150 KeV for 6 MeV neutrons, corresponding to an overall time resolution of less than 2 ns for the system. Spectra were obtained by bombarding an enriched Si²⁸ target* with deuterons of 4 and 5 MeV.

*The target, 190 μ g/cm² thick, enriched to approximately 99% Si²⁸ was supplied in the form of SiO₂ deposited on gold by A.E.R.E., Harwell, U.K.

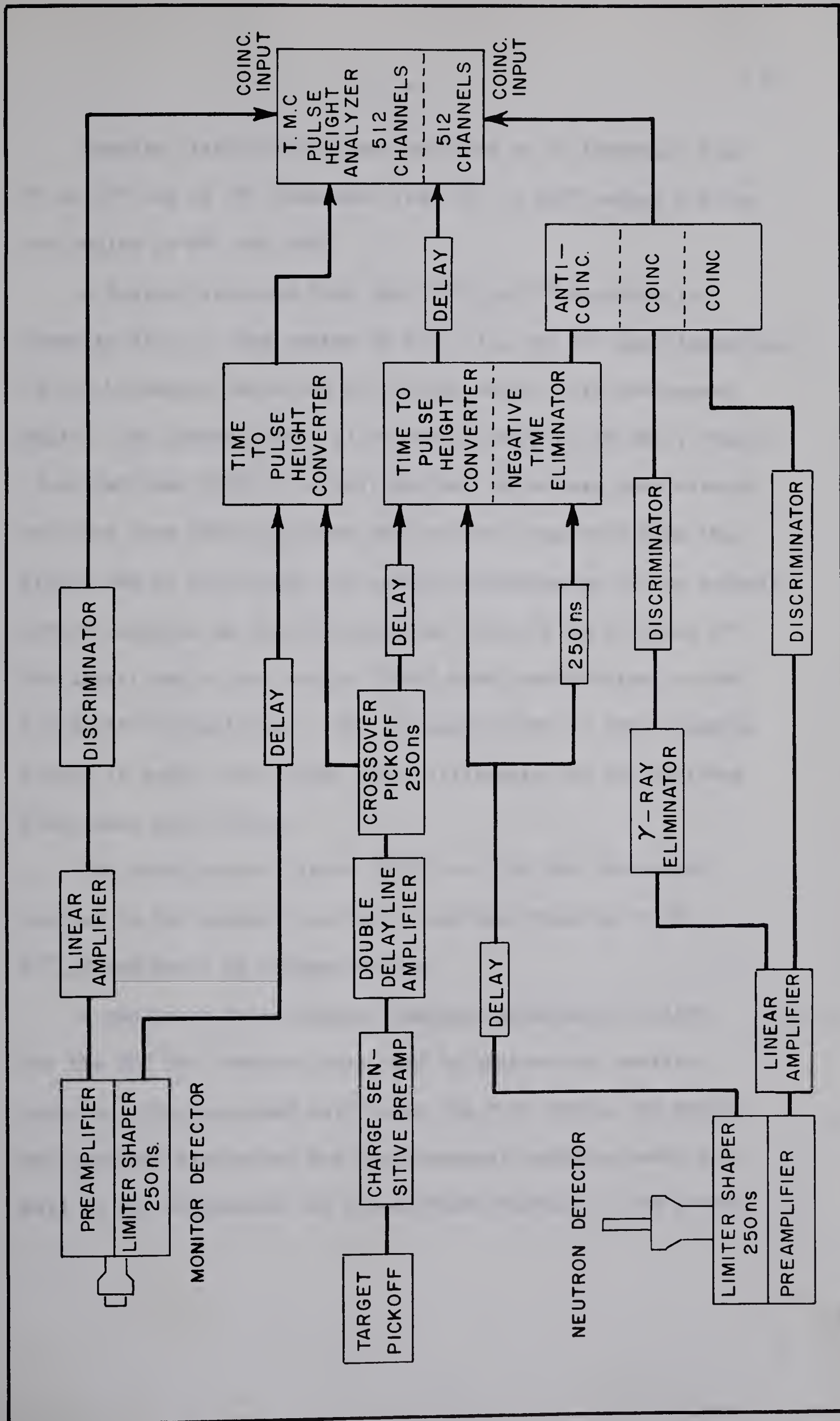


Fig. 1. Block diagram of the neutron time-of-flight spectrometer.

Angular distributions were measured at 5° intervals from 0° to 45° and at 15° intervals from 45° to 150° except for the two angles at 90° and 105° .

A typical spectrum from the $\text{Si}^{28}(\text{d},\text{n})\text{P}^{29}$ reaction is shown in fig. 2. The states of P^{29} , F^{17} , and N^{13} were identified by the kinematic variation of neutron energy with laboratory angle. The ground, first (1.36 MeV), second (1.98 MeV), fourth (3.01 MeV) and fifth (3.4 MeV) excited states are seen clearly resolved from the background and are well separated from the groups due to the oxygen and carbon contamination of the target. Carbon deposits on the beam defining slits 30 cm in front of the target and on the target itself make contributions to the $\text{C}^{12}(\text{d},\text{n})\text{N}^{13}$ transitions. The increased width of these neutron groups is due to the flight time differences for the neutrons from these two sources.

The third excited state of P^{29} at 2.40 MeV was weakly excited in the present experiment and was obscured by the F^{17} ground state at forward angles.

A nonlinear least squares computer programme, written for the SDS 920 computer, was used to analyse the neutron spectra. The programme calculated the peak areas, the means and standard deviations for the (assumed) Gaussian peaks as well as the parameters for a background function. The errors

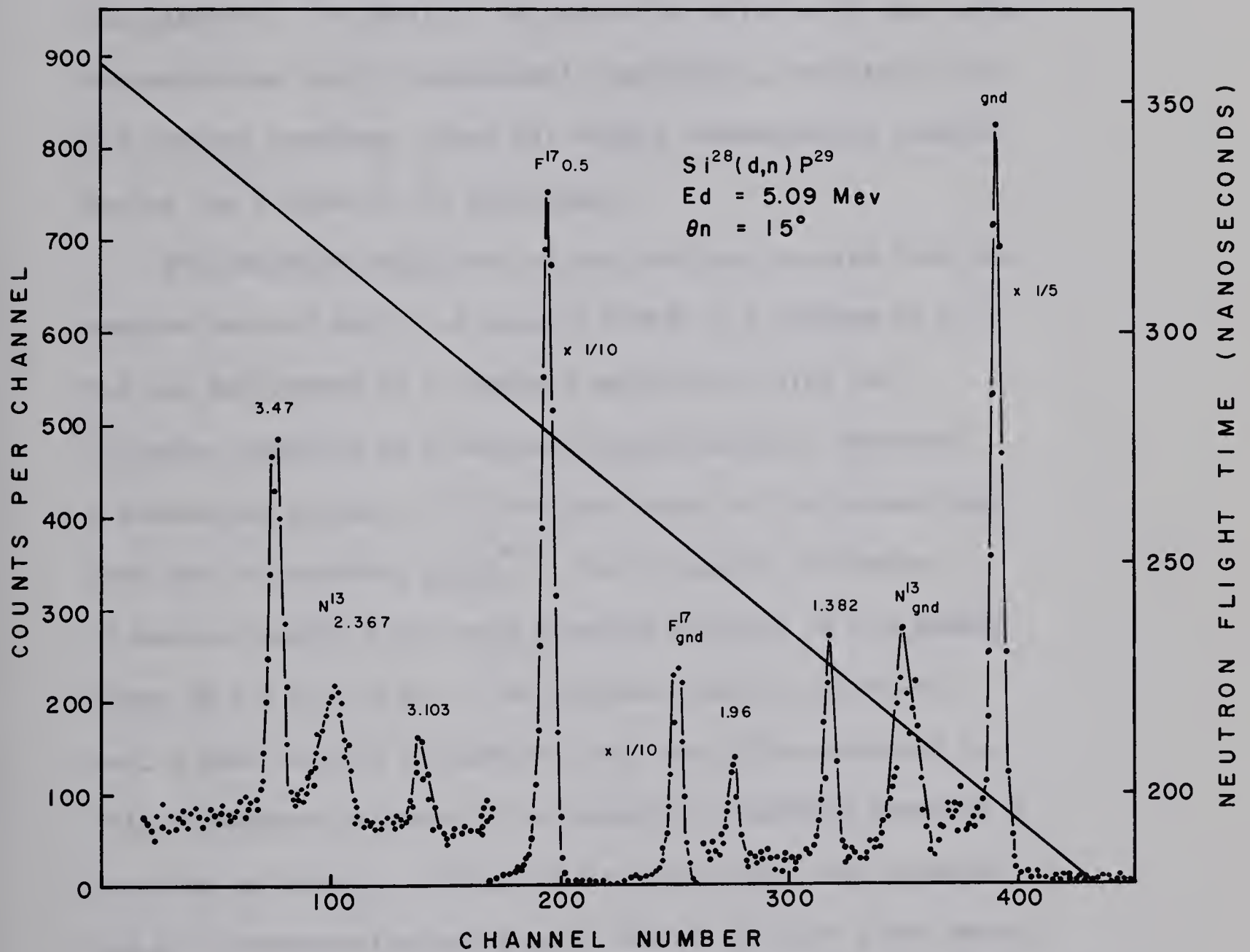


Fig. 2. Neutron time-of-flight spectrum from the reaction $\text{Si}^{28}(\text{d}, \text{n})\text{P}^{29}$ taken at 15° to the incident 5.09 MeV deuteron beam. Neutron flight path $S_n = 6.42 \text{ m}$. The number above each peak is the P^{29} excitation energy in MeV. Neutron flight times are indicated by a time calibration line.

assigned by this programme to the above quantities include both the statistical errors and the χ -squared fitting error⁵⁾. All peaks in the main spectrum as well as in the monitor spectrum were fitted using this programme which allows one to remove, in a systematic and objective manner, the background under the spectrum. The ability to remove the effects of the carbon contamination was of considerable importance, especially for the monitor spectrum, since the carbon contamination doubled during the course of the experiment.

The relative efficiency of the neutron detector from the neutron cut-off energy of about 0.9 MeV to a maximum of 2.5 MeV was determined by a separate experiment using the $T(p,n)He^3$ reaction as a source of mono-energetic neutrons. A bombarding energy of 3.4 MeV was chosen to correspond with that used by Goldberg et al⁶⁾. The kinematic variation of neutron energy with angle provided neutrons in the energy range of 0.5 to 2.6 MeV. The absolute cross-sections of ref. 6 were used in conjunction with the yields obtained in this experiment to construct a relative efficiency curve as a function of energy. This curve was then normalized to match the n-p cross-section curve at an energy of about 5 MeV where, to a good approximation, the efficiency for neutron detection is determined by the n-p scattering cross-section.

Absolute differential cross-sections (mb/sr) for $\text{Si}^{28}(\text{d}, \text{n})\text{P}^{29}$ at $E_D = 5.09$ MeV

Level	Exn. (MeV)	Lab. Angle	0	5	10	15	25	30	35	45	60	75	100	120	135	150
0	Gnd.	C. of M. Angle $d\sigma/d\Omega$	0.0 67.4	5.2 54.1	10.5 42.9	15.7 27.3	26.2 6.77	31.4 2.0	36.6 1.99	46.9 4.10	62.4 5.17	77.6 2.94	102.7 0.84	122.4 .95	136.9 1.60	151.4 2.62
1	1.38	C. of M. Angle $d\sigma/d\Omega$	0.0 2.26	5.3 1.89	10.6 2.71	15.8 3.68	26.3 5.85	31.5 7.81	36.8 6.99	47.2 6.27	62.8 3.71	78.1 2.27	103.1 2.66	122.8 2.09	137.2 1.81	151.6 1.77
2	1.96	C. of M. Angle $d\sigma/d\Omega$	0.0 0.44	5.3 0.56	10.6 0.67	15.9 1.45	26.4 2.80	31.7 3.21	37.0 3.26	47.4 3.06	63.0 1.68	78.3 0.90	103.4 1.11	123.0 1.04	137.4 0.97	151.7 0.88
4	3.10	C. of M. Angle $d\sigma/d\Omega$	0.0 1.78	5.4 1.37	10.7 1.58	16.1 1.94	26.8 2.54	32.1 2.26	37.4 2.56	48.0 1.75	63.7 0.81	79.1 0.82	104.2 1.43	123.7 2.39		
5	3.47	C. of M. Angle $d\sigma/d\Omega$	0.0 11.4	5.4 11.3	10.8 10.8	16.2 10.3	27.0 9.40	32.3 8.80	37.7 8.23		64.0 7.06	79.5 3.75				

The neutron groups corresponding to the ground and first excited states of F^{17} were observed over the entire angular range and these angular distributions were compared with those of Yaramis⁷⁾ (fig. 3). The excellent agreement obtained between these two sets of data provides a good check on our relative efficiency curve. Additionally, the earlier measurements⁷⁾ give the absolute cross-sections for the transitions to the ground and first excited states of F^{17} for a deuteron energy of 5 MeV. This enables one to convert the relative cross-section data for the transitions to the different levels of P^{29} at an $E_d = 5$ MeV to absolute cross-sections. These are given in table 1. Such a conversion is based on the assumption that the target used in the present experiment is mainly SiO_2 , as specified by the suppliers. On the basis of this assumption, it is believed that the errors in absolute cross-sections are not larger than 25%. The errors arise from three main sources:

1. The combination of the statistical errors in the previous⁷⁾ and present experiments.
2. The normalization error in combining the results of the two experiments.
3. A systematic error, estimated to be $< 10\%$, from uncertainties in the amount of oxygen adsorbed on the surface of the target.

The errors in the relative cross-sections are estimated to be less than 10%.

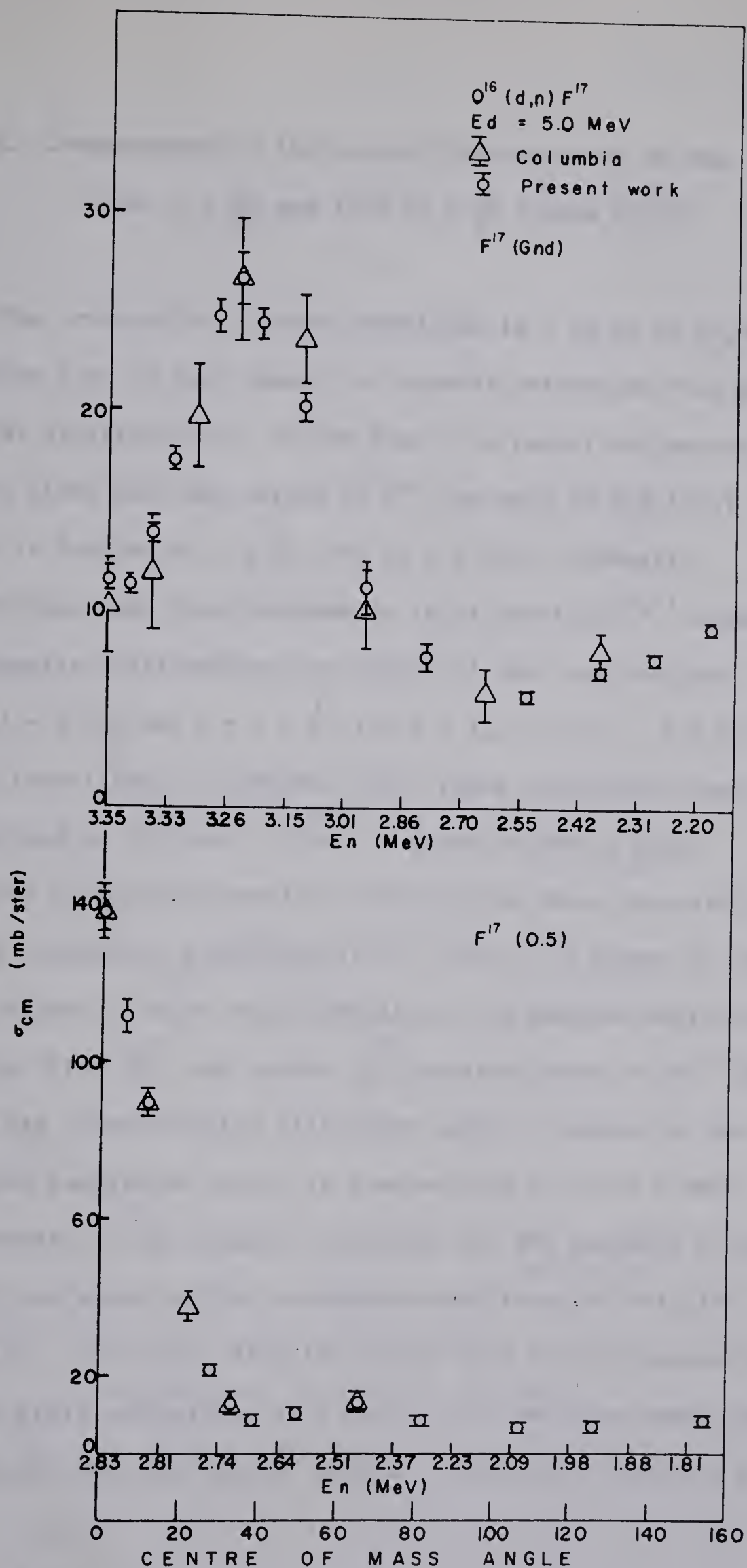


Fig. 3. Comparison of the angular distributions for neutrons leading to the ground and first excited states of F^{17} obtained in the present experiment with those obtained by Yaramis⁷⁾.

3. J-Dependence of the Angular Distributions of the

1.38 ($J = \frac{3}{2}$) and 1.96 ($J = \frac{5}{2}$) States of P^{29}

The ℓ -value for a given transition in a (d,p) or (d,n) reaction can, in most cases, be uniquely determined from the angular distributions. In the case of a target nucleus with a ground state spin and parity of 0^+ , the spin of the final state is limited to $\ell \pm \frac{1}{2}$. For $E_d > 6$ MeV, systematic differences have been observed in (d,p) reactions^{8,9)} between the angular distributions for states of the final nucleus with $J = \ell + \frac{1}{2}$ and $J = \ell - \frac{1}{2}$ for $\ell = 1, 2$, and 3. For the $\ell = 2$ transitions of interest here, these differences can be summarized as follows⁸⁾: The $J = \frac{3}{2}$ states show a sharp drop-off in the differential cross-section after the main peak with a minimum at approximately 55° ; the $J = \frac{5}{2}$ states do not show either of these characteristics. The angular distributions¹⁰⁾ for the first ($\frac{3^+}{2}$) and second ($\frac{5^+}{2}$) excited states of Si^{29} show that this characteristic difference tends to weaken as the deuteron bombarding energy is lowered from 9.0 to 6.0 MeV. The results of the present experiment for the analogue states of P^{29} are shown in fig. 4 together with those of ref. 10 for Si^{29} . It is seen from the figure that the J-dependent structure is still perceptible at 5 MeV. For a deuteron bombarding energy of 4 MeV the spin $\frac{3^+}{2}$ angular distribution does not fall

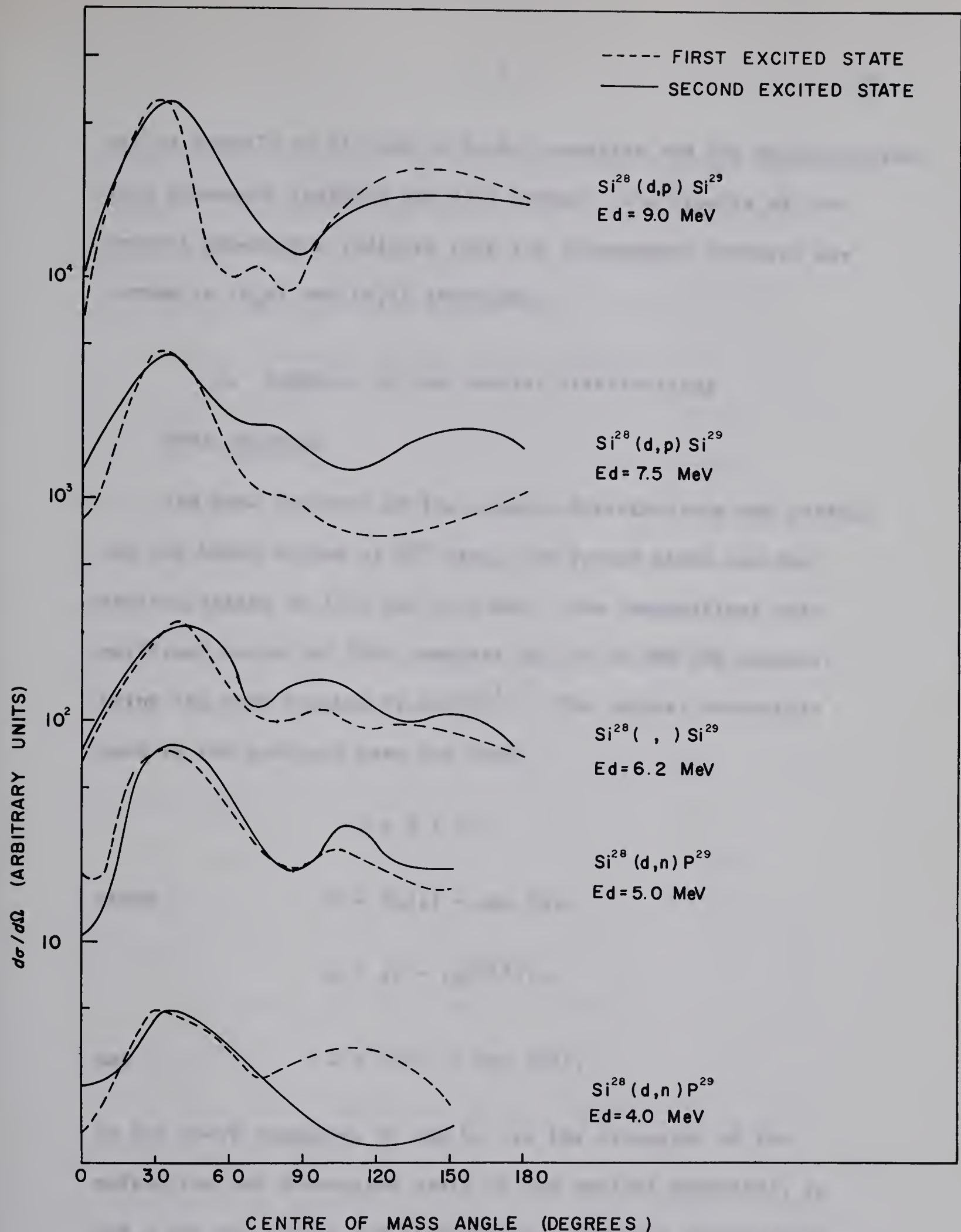


Fig. 4. Angular distributions from the $\text{Si}^{28}(\text{d},\text{p})\text{Si}^{29}$ and $\text{Si}^{28}(\text{d},\text{n})\text{P}^{29}$ reactions for various deuteron bombarding energies. These are plotted so as to show the structural differences apparent between the $J^\pi = \frac{3}{2}^+$ and $J^\pi = \frac{5}{2}^+$ states. The angular distributions are normalized such that the corresponding peak cross sections coincide. The $\text{Si}^{28}(\text{d},\text{p})\text{Si}^{29}$ results are taken from ref.10.

--- FIRST EXCITED STATE
 --- SECOND EXCITED STATE

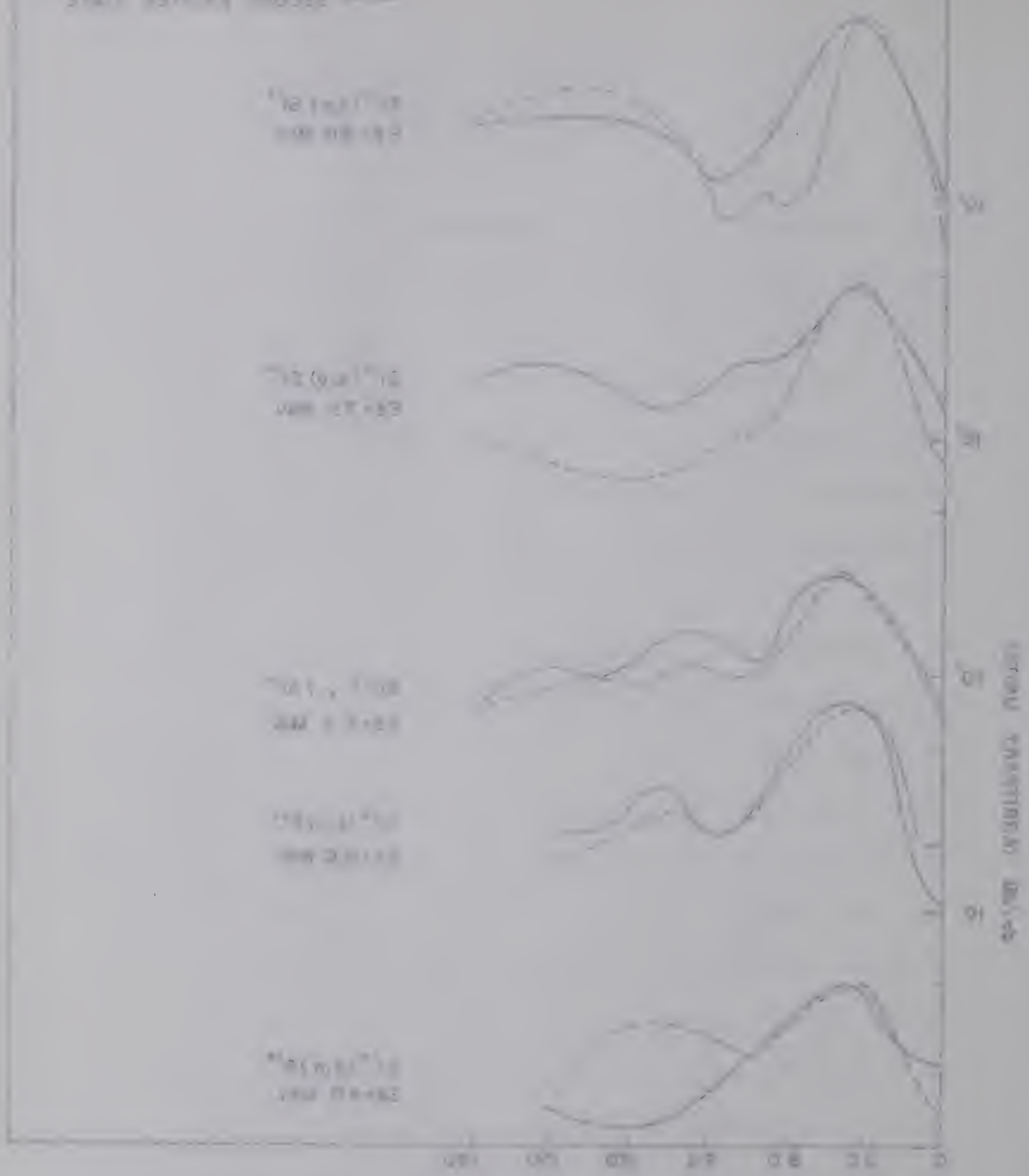


Fig. 4. Radial probability distribution $P(r)$ versus distance r for the first and second excited states of the hydrogen atom. The curves are calculated for the states $2s$, $3s$, $3p$, $3d$, and $4s$. The radial probability distribution is defined as $P(r) = 4\pi r^2 |\psi(r)|^2$, where $\psi(r)$ is the wave function. The curves show that the probability of finding the electron at a certain distance r from the nucleus is maximum for the first excited state and minimum for the second excited state.

off as sharply as it does at higher energies and the characteristic spin dependent features are less marked. The results of the present experiment indicate that the J-dependent features are common to (d,p) and (d,n) reactions.

4. Analysis of the Angular Distributions

DWBA Analysis

The DWBA analysis of the angular distributions was carried out for bound states of P^{29} viz., the ground state and the excited states at 1.38 and 1.96 MeV. The computations were performed on an IBM 7040 computer and on an SDS 920 computer using the code written by Smith¹¹⁾. The optical potentials used in the analysis have the form

$$U = V + iW$$

where

$$V = V_0 / (1 + \exp(x))$$

$$x = (r - r_0 A^{1/3}) / a$$

and

$$W = W_0 / (1 + \exp(x)).$$

In the above formulae, V_0 and W_0 are the strengths of the refractive and absorptive parts of the optical potential; r_0 and a are the radius and diffuseness parameters respectively for the Saxon-Woods form factor; r is the separation of the

reacting nuclei. It should be noted that only a volume absorption potential was included in the calculations. The zero range approximation¹²⁾ is made for the n-p interaction.

Deuteron and neutron scattering data are not available for Si^{28} and P^{29} in the energy range of interest here. From the available scattering data for nuclei in this region of mass number^{13,14)} and for $E_d \approx 5$ MeV, it was decided to confine the search for "best fit" potentials to 40 - 60 MeV for V_n , 45 - 100 MeV for V_d , 3 - 8 MeV for W_n , and 6 - 12 MeV for W_d . For V_n and V_d the range of potentials of 40 - 60 MeV was covered in 2 MeV steps, while the range of 60 - 100 MeV for V_d was covered in 5 MeV steps. This search ranged over sets of values for V_n , V_d , W_n , and W_d which were generally consistent with those found in the literature^{11,13,14,15)}.

The choice of values for the radius parameters used in the calculations was made on the basis of the work of Smith and Ivash¹³⁾, viz., $r_{0n} = 1.25$ fm, $r_{0d} = 1.4$ fm, $a_n = 0.5$ fm, and $a_d = 0.7$ fm and were held constant throughout the present calculations.

Two sets of well-depth and shape parameters ($V_p = 49$ MeV, $r_{0p} = 1.25$ fm, $a_p = 0.5$ fm, and $V_p = 31$ MeV, $r_{0p} = 1.4$ fm, $a_p = 0.7$ fm) were used in the calculation of the bound proton wave function.

This analysis was carried out for the results obtained at $E_d = 4$ MeV and at $E_d = 5$ MeV. However, the present discussion will be limited to the 5 MeV data since it was found that, in general, the same set of parameters gave the "best-fits" in both cases. The criterion for choosing the final set of parameters was that an overall "best-fit" be obtained for the three lowest states of P^{29} . However, little significance was attached to the theoretical "fits" near the minima in the cross-section in view of the approximations inherent in the DWBA theory and those involved in the numerical integration. Apart from this limitation, several sets of parameters were found which satisfied the above criterion, some of which are listed in table 2.

The "best-fits" to the experimental data for each set of parameters used for the bound proton states are shown in figs. 5 and 6 for deuteron bombarding energies of 4 and 5 MeV respectively. These are designated a and b in figs. 5 and 6 as well as in tables 2 and 4.

It is seen that the spectroscopic factors for either the first or the second excited states relative to that of the ground state show a maximum variation of 15% for a given r_{0p} and a_p . Conversely, for the two sets of r_{0p} and a_p used in the present calculations, holding all other parameters constant, the variation in the relative spectroscopic factors is of the order of 25%.

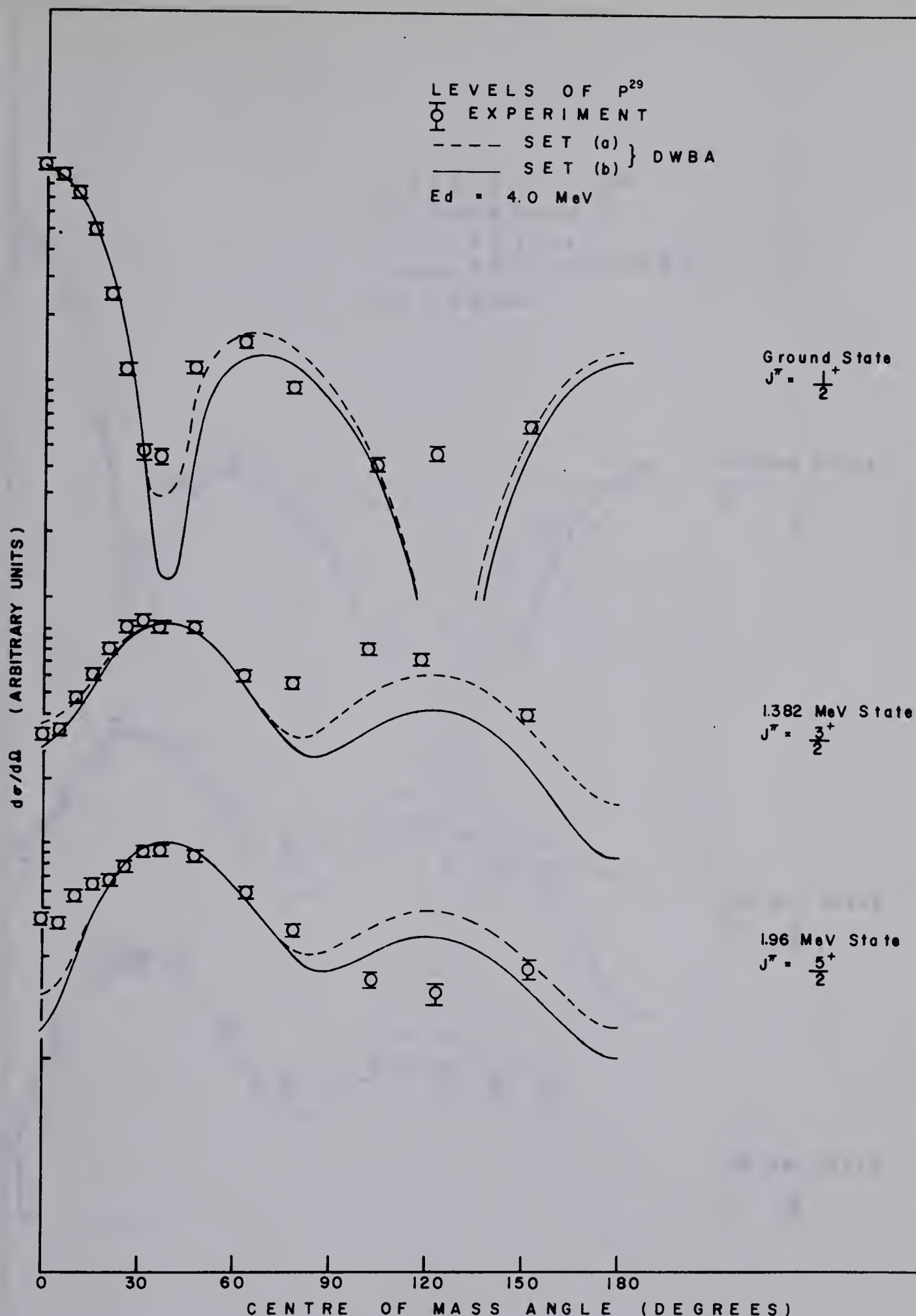


Fig. 5. Angular distributions of the neutrons leading to the 0, 1.38, 1.96 MeV states of P^{29} for $E_d = 4 \text{ MeV}$. The lines marked a and b in the figure were calculated using the DWB approximation¹¹⁾.

The parameters denoted by set a are: $V_n = 50 \text{ MeV}$, $V_p = 49 \text{ MeV}$, $V_d = 52 \text{ MeV}$, $W_n = 6 \text{ MeV}$, $W_d = 12 \text{ MeV}$, $r_{op} = 1.25 \text{ fm}$. Set b is the same as set a except that $V_p = 31 \text{ MeV}$, $r_{op} = 1.4 \text{ fm}$, and $a_p = 0.7 \text{ fm}$. (See table 2)

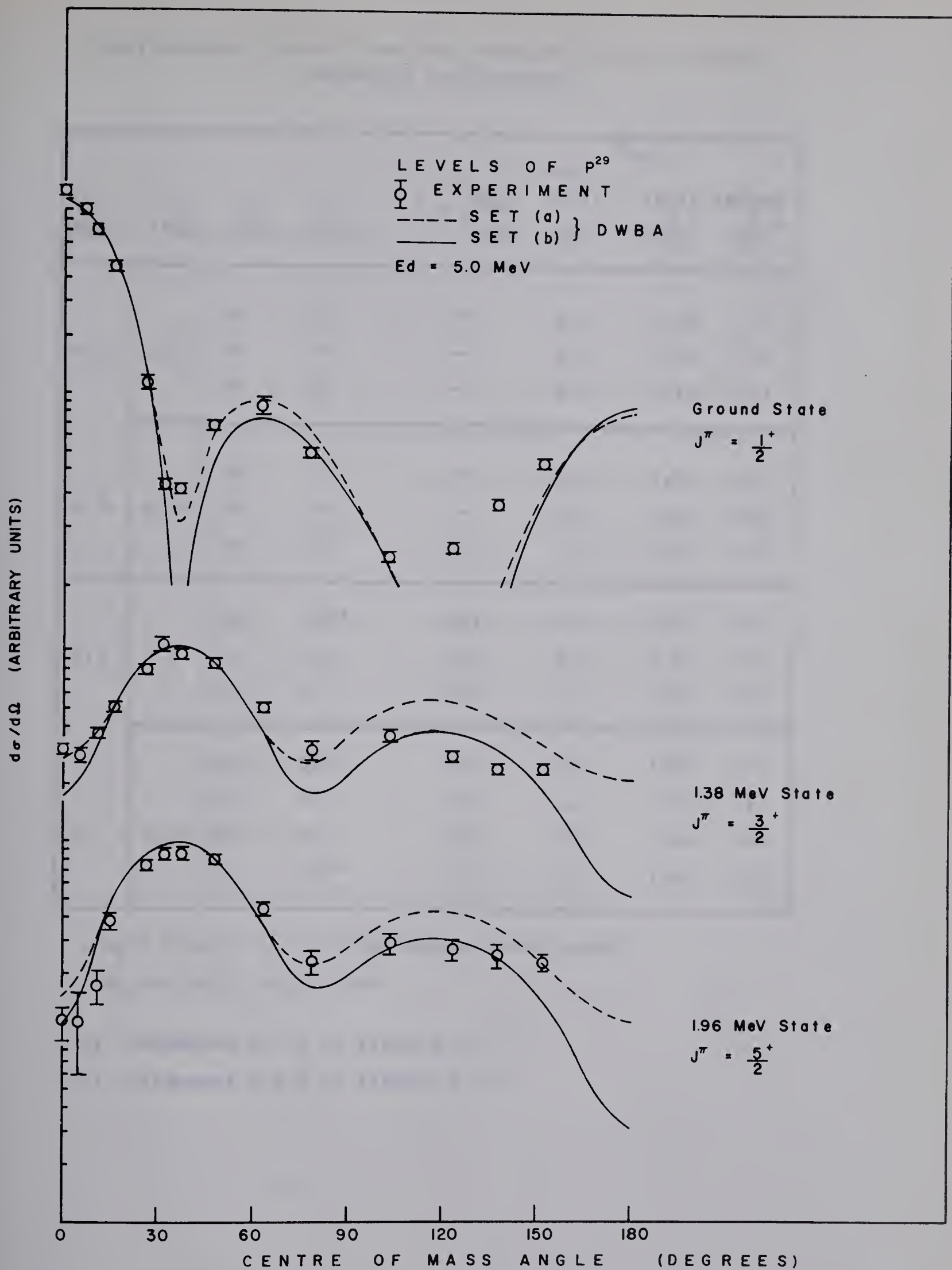


Fig. 6. Same as for fig. 5 for $E_d \approx 5 \text{ MeV}$.

Spectroscopic factors from DWBA calculations for selected parameter combinations

E_d (MeV)	r_p (fm)	V_n (MeV)	V_d (MeV)	$S = \frac{\sigma_{\text{exp}}}{\sigma_{\text{DWBA}}}$	S_{rel}		
					Gnd. state $(\frac{1}{2})^+$	first $(\frac{3}{2})^+$	second $(\frac{5}{2})^+$
4.0	3.8	50	52^+	--	1.0	2.49	.71
		50	54	--	1.0	2.26	.66
		46	60	--	1.0	2.12	.63
4.0	4.26	50	52	--	1.0	2.05	.62
		50	54	--	1.0	1.93	.59
		46	60	--	1.0	1.96	.60
5.1	3.8	50	$52^a)$.83	1.0	2.23	.41
		50	54	.86	1.0	2.11	.37
		46	60	.98	1.0	1.90	.34
5.1	4.26	50	$52^b)$.45	1.0	1.80	.34
		50	54	.46	1.0	1.73	.33
		46	60	.51	1.0	1.64	.30
		50	52^{++}	.41	1.0	1.80	.34

$^+W_n = 6$ MeV $W_d = 12$ MeV except where noted.

$^{++}W_n = 6$ MeV $W_d = 8$ MeV

a) Parameter set a of figures 6, 5

b) Parameter set b of figures 6, 5

For a given set of parameters, the relative spectroscopic factor obtained for the first excited state at an E_d of 4 MeV is about 15% larger than that obtained at 5 MeV. For the second excited state, which is comparatively weakly excited, the relative spectroscopic factor is larger by almost a factor of 2. Contributions to the second excited state from compound nucleus formation are expected to be significantly smaller at 5 MeV. Hence the spectroscopic factor for this state obtained at 5 MeV should be the more reliable of the two.

Absolute spectroscopic factors were calculated for the first three states of P^{29} using the absolute cross-sections given in table 1. In accord with earlier results^{16,17)} the variation in the absolute spectroscopic factors is seen from table 2 to be much larger than the variation in the relative spectroscopic factors.

PWBA Analysis

The excited states of P^{29} at 3.103 and 3.470 MeV, seen in the present experiment, are unbound and could not be analysed by the DWBA programme. It was found using Butler theory¹⁷⁾ that a qualitative fit could be obtained only for the three bound states and for the unbound state at 3.47 MeV. In this analysis the ℓ -values were restricted to those consistent with the established spins and parities of these or their analogue

Table 3

Spectroscopic factors from PWBA analysis						
Level	Exn. (MeV)	ℓ_p	$E_d = 4 \text{ MeV}$		$E_d = 5.1 \text{ MeV}$	
			r_p	S_{rel}	r_p	S_{rel}
0	0	0	5.5	1	5.5	1
1	1.38	2	5.5	1.33	4.0	0.99
2	1.96	2	4.25	0.55	4.5	0.18
5	3.47	3			6.0	0.70

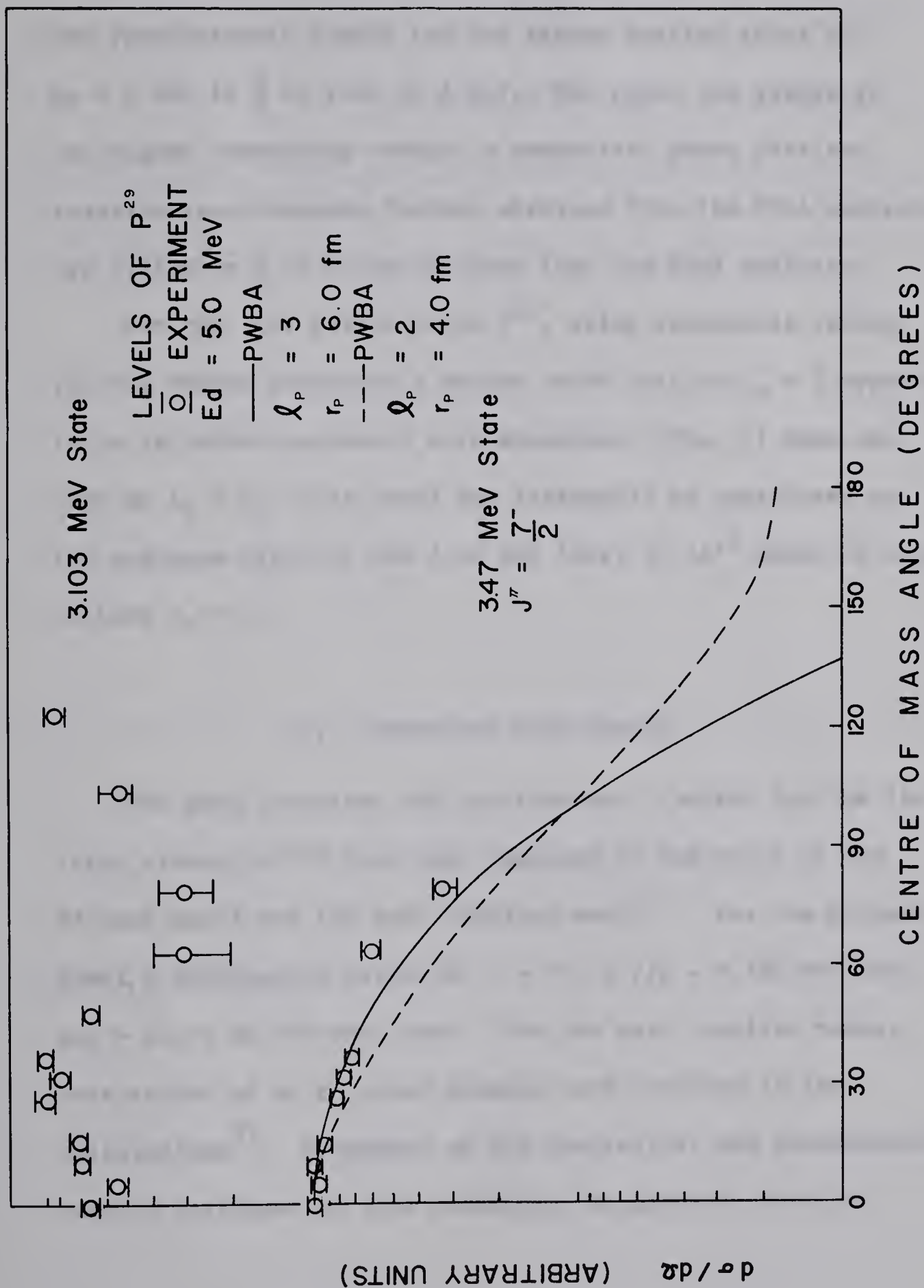


Fig. 7. Angular distributions of the neutrons leading to the 3.103 and 3.47 MeV states of P^{29} for $E_d = 5.09$ MeV. The smooth curves were calculated using the PWB approximation with parameters as indicated.

levels¹⁸⁾ in Si^{29} . The relative spectroscopic factor obtained by this analysis for the first excited state at $E_d = 5$ MeV is seen (table 3) to be about 30% smaller than that at 4 MeV. The spectroscopic factor for the second excited state at $E_d = 5$ MeV is $\frac{1}{3}$ of that at 4 MeV. For these two states at the higher bombarding energy, a comparison shows that the relative spectroscopic factors obtained from the PWBA analysis are typically $\frac{1}{2}$ of those obtained from the DWBA analysis.

For the 3.47 MeV state of P^{29} , using reasonable values for the radius parameter a Butler curve with an $\ell_p = 3$ appears to be in better agreement with experiment (fig. 7) than one with an $\ell_p = 2$. This level may reasonably be considered as the analogue state of the 3.62 MeV level of Si^{29} which is known¹⁸⁾ to have $\ell_n = 3$.

5. Comparison with Theory

The wave functions and spectroscopic factors for the low lying states of P^{29} have been computed on the basis of the Nilsson model and the weak coupling model²⁾. For the Nilsson model, a deformation parameter $\eta = -3$, $h^2/2g = 0.450$ MeV and $h\omega_\beta = h\omega_\gamma = 20$ MeV were used. For the weak coupling model, core states of up to three phonons were included in the calculations²⁾. A summary of the theoretical and experimental results pertinent to this discussion is given in table 4.

Spectroscopic factors obtained from theory and experiment for the levels of p^{29}

				Relative Spectroscopic Factor					
(1)	(2)	(3)	(4)	Experiment			Theory		
				(5)	(6)		(7)	(8)	(9)
Level	Excitation Energy	J^π	ℓ_p	PWBA	DWBA (a)	DWBA (b)	Nilsson Model	Vibrational Model	Shell Model
0	0	$\frac{1}{2}^+$	0	1.0	1.0	1.0	1.0	1.0	1.0
1	1.382	$\frac{3}{2}^+$	2	.99	2.2	1.80	2.11	.68	1.0
2	1.955	$\frac{5}{2}^+$	2	.18	.41	.34	.45	0	0
3	2.40	$(\frac{3}{2}^+)$	--	--	--	--	.02	.28	0
4	3.103	$\frac{5}{2}^+$	--	--	--	--	.01	0	0
5	3.47	$(\frac{5}{2}, \frac{7}{2})^-$	3	.7	--	--	.60	1.0	--

The information in columns (1) to (9) is derived from the following sources:

- (1), (2), and (3) from reference (2) and (13)
- (4), (5), and (6) from the present work for $E_d = 5$ MeV
- (7), (8), and (9) from references (2) and (3).

Sub-columns (a) and (b) of column (6) refer to parameter sets (a) and (b) in table 2 and figs. 6 and 5.

The spectroscopic factor for the first excited state relative to the ground state obtained from the DWBA analysis indicates that the ground state does not carry the full single particle strength for the $2 s_{1/2}$ transition. This result is in disagreement with the predictions of the weak coupling model (table 4). For nuclei in the region of mass 28 this shows that the approximation of a tightly bound Si^{28} core is not good. This is further confirmed by the fact that the relative spectroscopic factor for the transition to the $\frac{5}{2}^+$ state at 1.96 MeV is about $\frac{1}{5}$ of that obtained for the $\frac{3}{2}^+$ first excited state of p^{29} .

The DWBA results are in good agreement with the predictions of the Nilsson model. This result is not altogether unexpected since in the Nilsson model the deformed potential causes the mixing of the $1 d_{5/2}$, $2 s_{1/2}$, and $1 d_{3/2}$ orbitals. The weak-coupling model as applied to this nucleus does not appear to have "core" states which properly take into account the excitations of the $d_{5/2}$ nucleons into the $s_{1/2}$ and $d_{3/2}$ orbitals. It is clear that in shell model calculations for nuclei around mass 28, one would have to include configurations in which the nucleons in the $(d_{5/2})$ orbits are allowed to be excited into $s_{1/2}$ and $d_{3/2}$ orbits.

Acknowledgements

The authors wish to thank T. B. Grandy for his help in running the experiment and in its analysis. We are also

indebted to J. B. Elliott and L. Holm and C. Green for their work in constructing and maintaining much of the equipment used in this research.

One of the authors (W.G.D.) would like to thank the National Research Council for financial assistance during the period in which the work was done.

References

- 1) B. Cujec, W. G. Davies, W. K. Dawson, T. B. Grandy, G. C. Neilson and K. Ramavataram, *Physics Letters* 15 (1965) 266
- 2) H. Ejiri, *Nucl. Phys.* 52 (1964) 578
- 3) P. W. M. Glaudemans, G. Wiechers and P. J. Brussaard, *Nucl. Phys.* 56 (1964) 529, 548
- 4) G. C. Neilson, W. K. Dawson and F. A. Johnson, *Rev. Sci. Instr.* 30 (1959) 963
- 5) M. E. Rose, *Phys. Rev.* 91 (1953) 610
- 6) M. D. Goldberg, J. D. Anderson, J. P. Stoering and C. Wong, *Phys. Rev.* 122 (1961) 1510
- 7) B. Yaramis, *Phys. Rev.* 124 (1961) 836
- 8) L. L. Lee and J. P. Schiffer, *Phys. Rev.* 136 (1964) B405
- 9) J. L. Alty, L. L. Green, G. C. Jones and J. F. Sharpey-Schafer, *Physics Letters* 13 (1964) 55
- 10) J. A. Kuehner, E. Almqvist and D. A. Bromley, *Nucl. Phys.* 21 (1960) 555
- 11) W. R. Smith and E. V. Ivash, *Phys. Rev.* 128 (1962) 1175
- 12) N. Austern, *Selected Topics in Nuclear Theory*, edited by F. Janouch (International Atomic Energy Agency, 1963) p. 17
- 13) W. R. Smith and E. V. Ivash, *Phys. Rev.* 131 (1963) 304
- 14) R. N. Maddison, *Proc. Phys. Soc.* 79 (1962) 264
- 15) B. H. Wildenthal, R. W. Krone and F. W. Prosser Jr., *Phys. Rev.* 135 (1964) B680
- 16) W. R. Smith, *Phys. Rev.* 137 (1965) B913
- 17) M. H. McFarlane, *Direct Interactions and Nuclear Reaction Mechanisms*, edited by C. Vili (Gordon and Breach, New York, U.S.A., 1963) p. 3
- 18) P. M. Endt and C. Van der Leun, *Nucl. Phys.* 34 (1962) 1

6. The $\text{Si}^{28}(\text{d},\text{n})\text{P}^{29}$ Reaction at $E_d = 6$ MeV

Following the completion of the experimental work at $E_d = 4$ and $E_d = 5$ MeV which has just been discussed, substantial improvements were made in the time-of-flight spectrometer which made it possible to do an experiment on P^{29} at $E_d = 6$ MeV. The purpose of this experiment was to investigate the effect of the increased bombarding energy on the J-dependent structure of the neutron angular distributions and the spectroscopic factors as well as to provide information about excited states in P^{29} not reached in the work done at the 4 and 5 MeV bombarding energies. As a result of the increased background counting rate at the higher bombarding energy these objectives were only partially realized.

The angular distributions of the neutron groups leading to the 1.38 and 1.96 MeV states of P^{29} are shown in figure 8 for a deuteron bombarding energy of 6 MeV. It is seen from the figure that the J-dependent structure is considerably enhanced over that seen at the 4 and 5 MeV bombarding energies. (See section 3 of this chapter). This result lends substantial support to the conclusion that the J-dependent features are common to both (d,n) and (d,p) reactions.

The angular distributions of the neutrons leading to the ground state and the excited states at 1.38 and 1.96 MeV of P^{29} and their associated DWBA fits are shown in figure 9. The optical model parameters shown in the insert in the figure were obtained by the fitting procedures outlined in section 4 of this chapter and of section (4.4) in chapter 4.

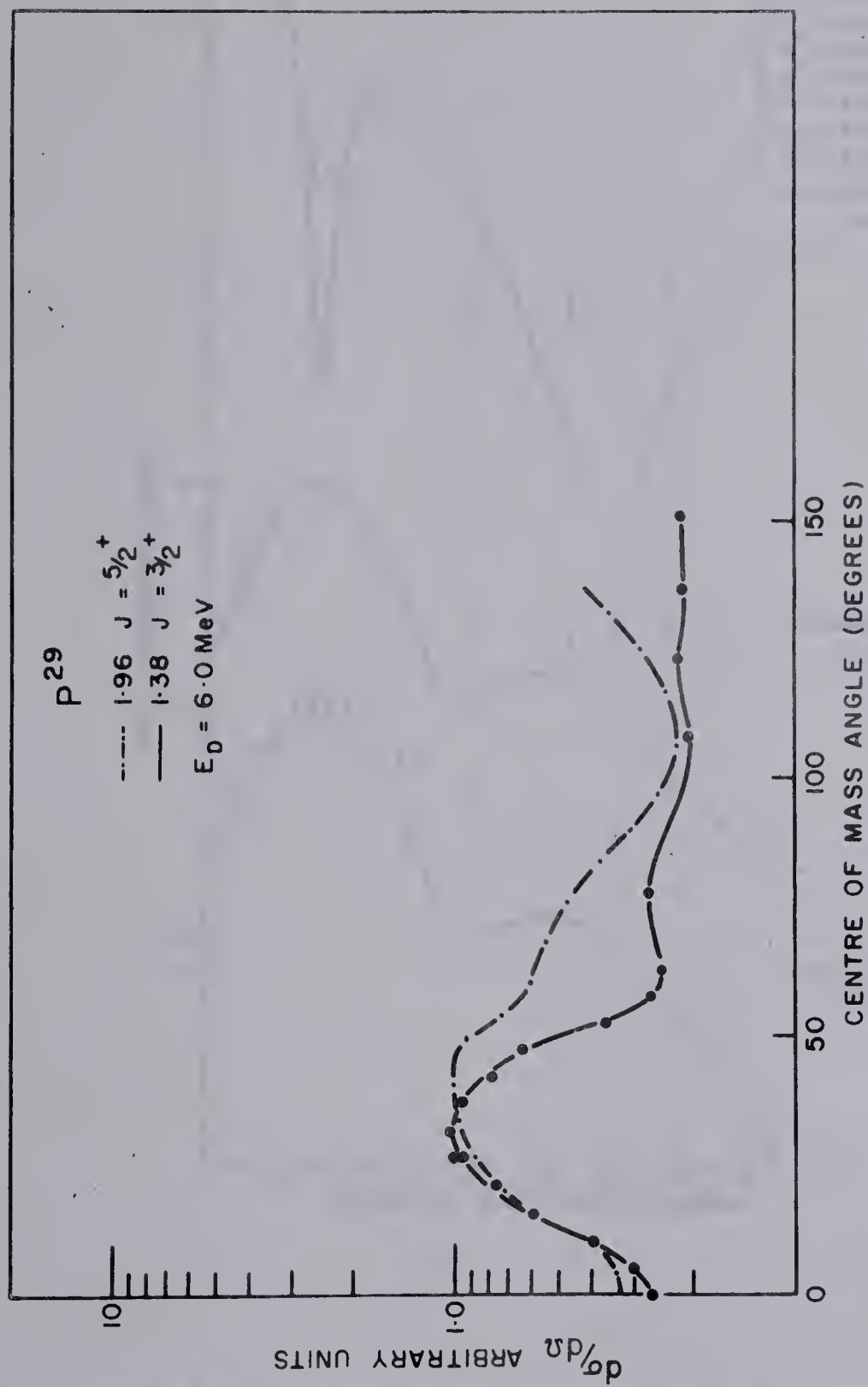


Fig. 8 Angular distributions of the neutrons leading to the 1.38 and 1.96 MeV levels of P^{29} for a deuteron bombarding energy of 6 MeV. The angular distributions are plotted so as to show the structural differences apparent between the $J = \frac{3}{2}^+$ and the $J = \frac{5}{2}^+$ states.

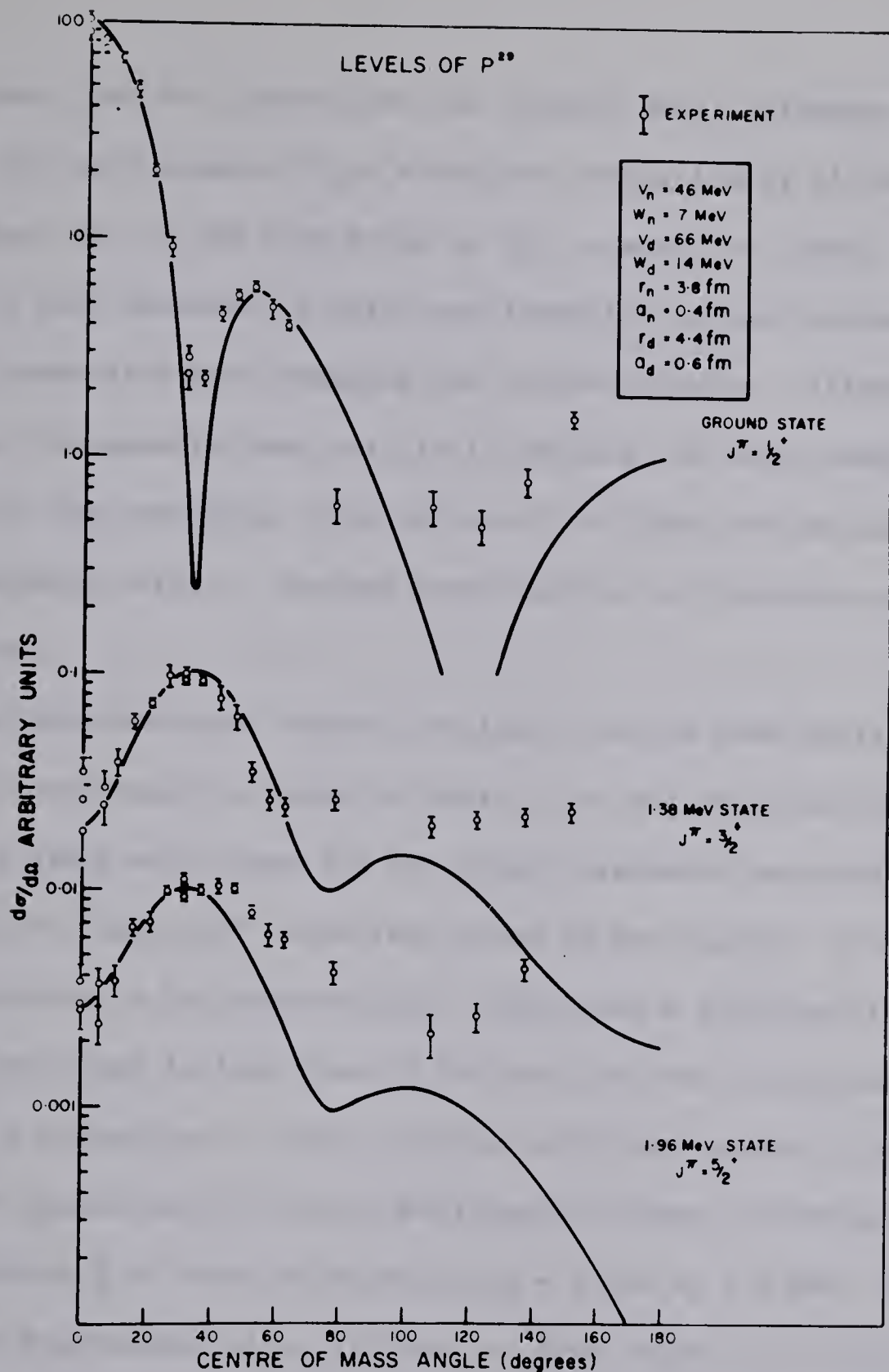


Fig. 9. Angular distributions of the neutrons leading to the 0, 1.38 and 1.96 MeV states of P^{29} for $E_d = 6 \text{ MeV}$. The smooth curves were calculated using the DWB approximation with parameters as indicated.

It is seen from the figure that the optical model parameters required to fit the data taken at $E_d = 6$ MeV are substantially different from those used to fit the data taken at $E_d = 4$ and $E_d = 5$ MeV. This anomaly has also been observed by Smith and Ivash (Sm 63) and appears to be an effect associated with crossing the coulomb barrier. Attempts to explain this anomaly have had little success and could possibly be the result of the particular formulation of the DWBA problem instead of a real physical effect. Further investigation of this point appears warranted.

The spectroscopic factors obtained from the DWBA analysis in the present experiment are shown in table 5 for the potentials given in figure 9 along with those for two other reasonable potential sets which bracket the "best-fit" potentials shown in the figure. It is seen that the variation of the spectroscopic factors as a function of the potential variations shown is less than 5% for both excited states analysed. However a comparison of these results with those given in table 3 shows that the spectroscopic factors obtained for these two states at $E_d = 6$ MeV are about $\frac{1}{2}$ of those obtained at $E_d = 4$ and $E_d = 5$ MeV. This result does not appreciably alter although it does weaken the conclusions drawn in section 5. However it does indicate the need for further experimental work at higher bombarding energies.

The levels of P^{29} with excitation energies of 3.103 MeV and higher are unbound and the neutron angular distributions leading to these levels could not be analysed with the DWBA program. As in the previous section

Butler theory (PWBA) was used in an attempt to fit these angular distributions, the results of which are shown in figure 10. Once again no reasonable fit could be obtained to the angular distribution leading to the 3.103 MeV level, but reasonable fits were obtained for the angular distributions corresponding to the 3.47 and 4.34 MeV levels. The excited state reported by Ejiri (Ej 64) at 4.08 MeV was not observed in the present experiment. However since this state is reported to have spin and parity $7/2^+$ it would be formed by the capture of an $\ell = 4$ proton making it difficult to see in the present experiment. It is seen from figure 10 that the $\ell = 3$ curve is still favoured over an $\ell = 2$ curve for the angular distribution corresponding to the 3.47 MeV state which supports the conclusion that this state is the analogue state of the 3.621 MeV state in Si^{29} that has recently been shown to have spin and parity $7/2^-$ (Mc 65). The angular distribution leading to the 4.34 MeV level of P^{29} can be fitted by an $\ell = 1$ or an $\ell = 2$ Butler stripping curve although the $\ell = 2$ curve is slightly favoured. However the work of Ejiri (Ej 64), Vorona (Vo 59) and Belote (Be 61) indicates that this level has spin and parity $3/2^-$ which would therefore be formed by the capture of an $\ell = 1$ proton.

The relative spectroscopic factors obtained from this analysis are shown in table 6. A comparison of these results with those given in table 3 show that the spectroscopic factors obtained at $E_d = 6$ MeV are about $\frac{1}{2}$ of those obtained at $E_d = 5$ MeV, while the spectroscopic factors obtained in the DWBA analysis are approximately twice as large as those obtained from the PWBA analysis at $E_d = 6$ MeV.

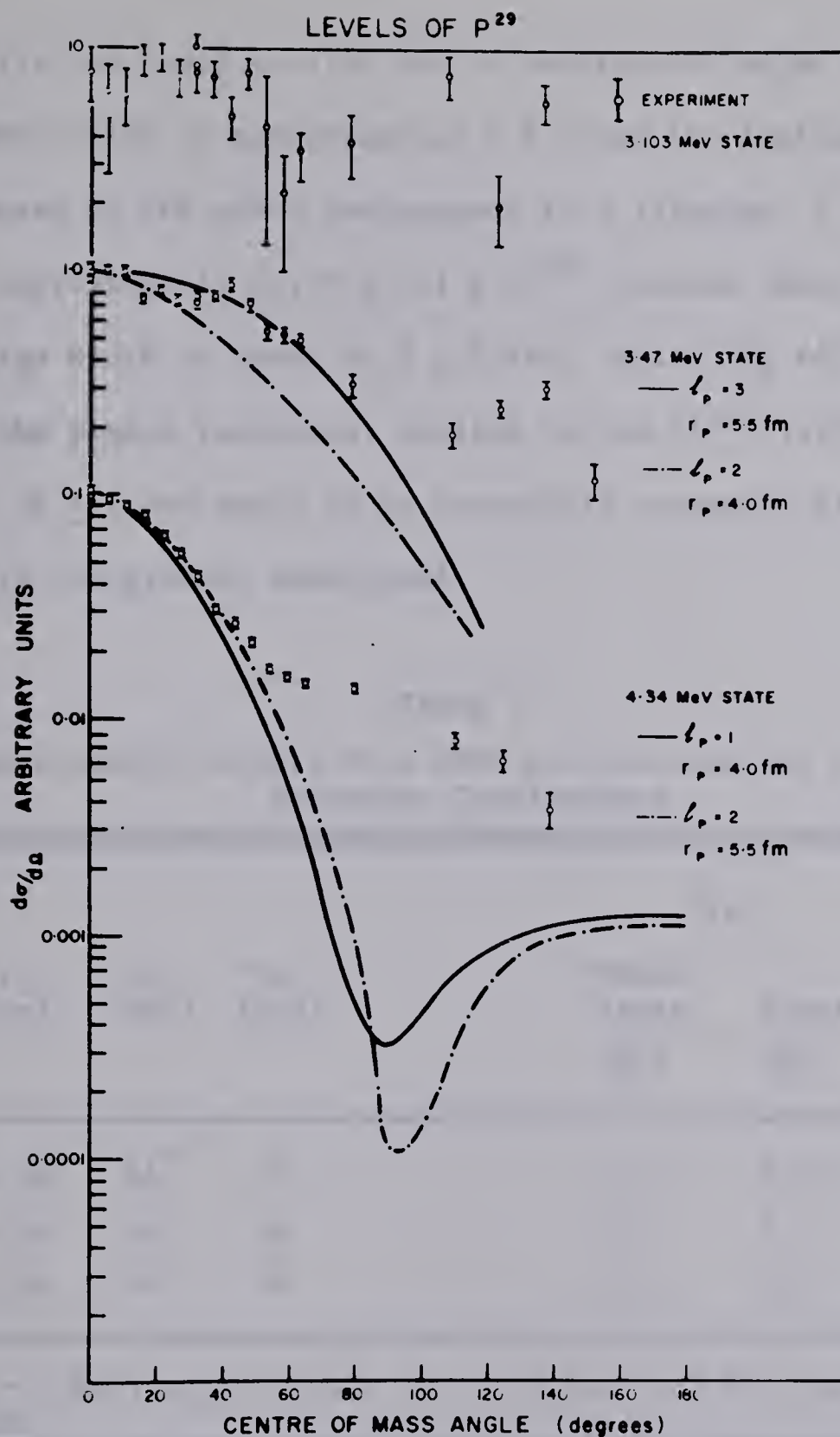


Fig. 10. Angular distributions of the neutrons leading to the 3.103, 3.47, and 4.34 MeV states of P^{29} for $E_d = 6$ MeV. The smooth curves were calculated using the PWB approximation with parameters as indicated.



Fig. 1. Dependence of the rate constant k on the concentration C of the reactant. The solid line corresponds to the experimental data, the dashed line to the calculated data. The rate constant k is in min^{-1} .

Finally the level at 4.34 MeV of excitation has an experimental width (FWHM) which is approximately 3.8 times the instrumental width. This increase in the width corresponds to a lifetime τ for this state of approximately $(0.95 \pm .3) \times 10^{-20}$ seconds which is equivalent to an energy width of about 69.5 ± 8 keV. Ejiri (Ej 64) found that the width of the proton resonance, excited in the $\text{Si}^{28}(\text{p}, \gamma)\text{P}^{29}$ reaction, was about 56 ± 6 keV which is in reasonable agreement with the result obtained in the present experiment.

TABLE 5
Spectroscopic Factors from DWBA Calculations for Selected
Parameter Combinations

E_d (MeV)	r_p (fm)	V_n (MeV)	V_d (MeV)	S_{rel}		
				Ground State $(\frac{1}{2}^+)$	First $(\frac{3}{2}^+)$	Second $(\frac{5}{2}^+)$
6.0	4.26	44^+	70	1.0	0.97	.14
	4.26	46	66	1.0	1.0	.15
	4.26	50	58	1.0	1.0	.16

$^+ \omega_n = 7$ MeV, $\omega_d = 14$ MeV, $r_n = 3.8$ fm, $a_n = 0.4$ fm, $r_d = 4.4$ fm, $a_d = 0.6$ fm.

TABLE 6
Spectroscopic Factors from PWBA Analysis

Level	E_{xn} (MeV)	ℓ_p	$E_d = 6$ MeV	
			r_p (fm)	S_{rel}
0	0	0	5.0	1.0
1	1.38	2	4.0	0.52
2	1.96	2	4.0	0.10
5	3.47	3	5.5	0.38
7	4.34	1	4.0	0.96

CHAPTER 4

THE $\text{Si}^{30}(\text{d},\text{n})\text{P}^{31}$ REACTION4.1 Introduction

The properties of the excited states of P^{31} have been studied using the $\text{Si}^{30}(\text{d},\text{n})\text{P}^{31}$ reaction in an attempt to clarify the position of the various nuclear models used to describe the odd mass nuclei in this region of the periodic table.

Experimental information has been obtained for P^{31} by several authors, particularly by Broude, Green and Willmott (Br 58) and by Harris and Seagondollar (Ha 62) and (Ha 63). In these experiments the γ -rays emitted from the resonances in the $\text{Si}^{30}(\text{p},\gamma)\text{P}^{31}$ reaction were studied providing information on the spins and parities of the levels of P^{31} as well as providing information on the branching ratios and multipolarities of the electromagnetic radiation.

Attempts were made to describe the observed properties of the level structure and electromagnetic transitions using the Nilsson model (Br 58) and the weak coupling model in which a single particle in the $2s_{1/2} - 1d_{3/2}$ orbits is coupled to the Si^{30} core making quadrupole oscillations (Th 60), (Th 62). More recently shell model calculations have been made for nuclei in this region by Glaudemans, Wiechers and Brussaard (Gl 64). In their calculations an inert Si^{28} core is assumed with a two particle interaction of the extra core nucleons in the $2s_{1/2} - 1d_{3/2}$ orbits.

In many of these calculations account was taken of the experimental spin and parity assignment $3/2^+$ to the third excited state of P^{31} at 3.133 MeV of excitation. This led Broude et al to identify the 3.133 MeV level with the second member of a rotational band based on the Nilsson orbit 9, while the other levels were obtained with the coupling of two rotational bands based on orbits 8 and 11. A recent experiment by Van Rinsveld and Endt (Ri 64) and the results of the present experiment (Cu 65) lead to a spin and parity assignment of $1/2^+$ for the 3.133 MeV state of P^{31} . This permits the identification of the 3.133 MeV state with the lowest member of the rotational band based on the Nilsson orbit 11.

On the basis of this information Nilsson model and weak coupling collective model calculations were made by Dr. K. Ramavataram (Ra 65) for P^{31} . The Nilsson model calculations included both rotation-particle coupling and rotation-vibration interactions. In the weak-coupling model a Si^{30} core, including excitations of up to 3 phonons, was coupled to the odd proton in the $2s_{1/2}$ or $1d_{3/2}$ sub-shells. More recently a Nilsson model calculation has been made by Bishop et al (Bi 65) which differs from the one made above in that the Nilsson single particle energies were not treated as parameters. Also at this time a project was undertaken to develop a 3 particle Nilsson model in which the 3 particles outside the Si^{28} core were allowed to occupy Nilsson orbits 8, 9 and 11.

In the present experiment, angular distributions of the neutron

groups leading to states in P^{31} up to 8.26 MeV of excitation have been measured at deuteron bombarding energies of 3, 4 and 5 MeV. This work includes the identification of 11 previously unreported excited states in the region of excitation from 5 to 8 MeV (Cu 65) and the assignment of spins and parities to 6 levels of P^{31} (Cu 65) (Da 65) exclusive of the spin and parity assignment $1/2^+$ made to the 3.133 MeV state in support of the measurement of Van Rinsvelt and Endt (Ri 64). In addition the levels at 6.38 and 7.14 MeV have been identified as the first two $T = 3/2$ states of P^{31} corresponding to the ground and first excited states of Si^{31} .

The angular distributions corresponding to eight of the levels observed in the present experiment have been compared with the predictions of the distorted wave Born approximation (DWBA). Spectroscopic factors have been deduced for these transitions and are compared with the predictions of the strong coupling and weak coupling collective models as well as the shell model calculations (Gl 64).

4.2 Experimental Procedure

The experiments were performed with the University of Alberta 5.5 MeV Van de Graaff accelerator and associated Mobley beam bunching system which has been described in chapters 2 and 3.

The block diagram of the spectrometer electronics, which differs from that used in the P^{29} experiments at the 4 and 5 MeV bombarding energies, is shown in figure (4-1). In order to improve the resolution

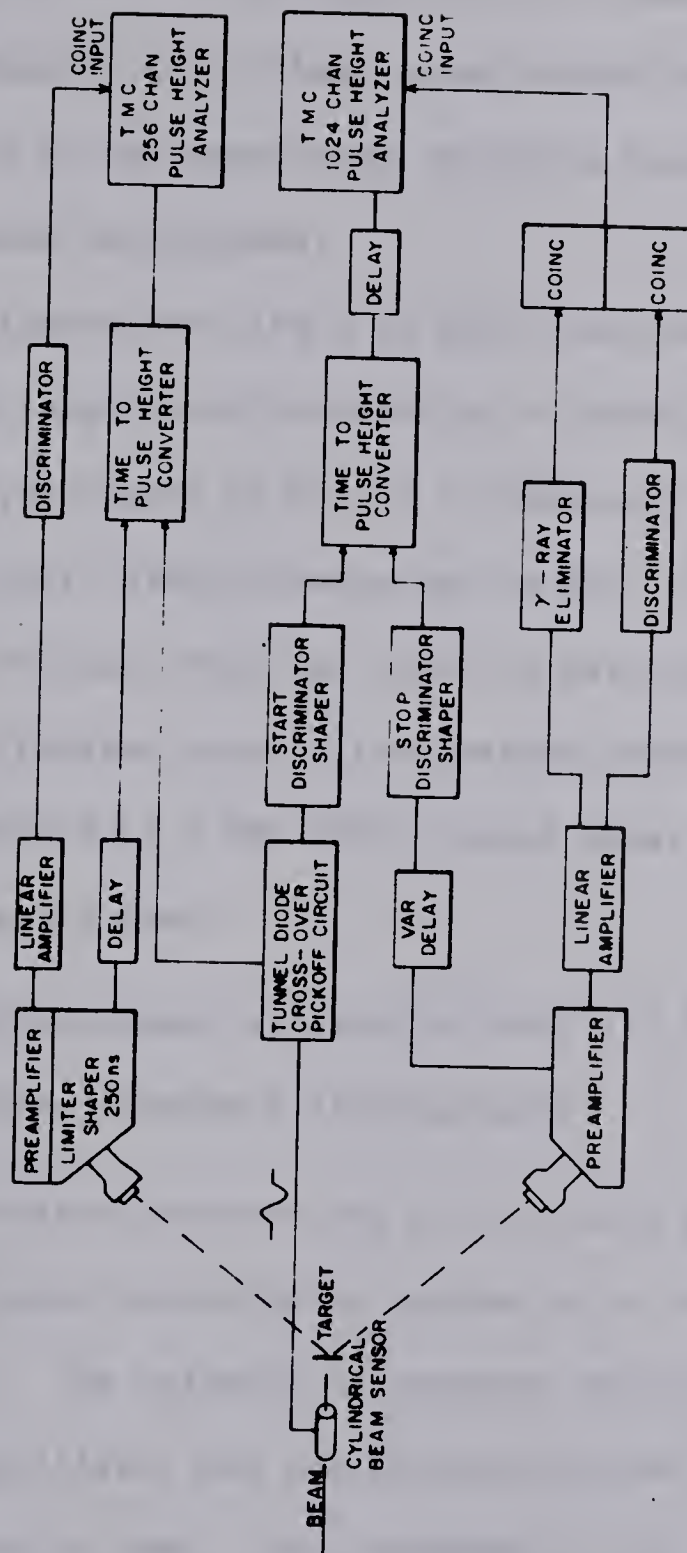


Figure 4-1. Block diagram of the neutron time-of-flight spectrometer.

and the time base of the spectrometer a completely new time to amplitude converter (TAC), based on a design by D. L. Wieber (Wi 63), was employed which makes extensive use of high speed tunnel diode switching circuits. Since the TAC is of the start-stop variety a broad time base, in this case 500 ns, could be obtained.

The fast signals from the 3 cm long beam sensing capacitor 30 cm in front of the target were detected by a tunnel diode cross-over-pickoff circuit, designed by Dr. G. C. Neilson, the output of which was fed to the start discriminator in the TAC. The corresponding stop pulses for the TAC were obtained from the 14th dynode of the Phillips XP 1040 photomultiplier used in the neutron detector. The output of the TAC was analysed by a TMC 1024 channel pulse height analyser which was gated by signals from

- (1) a neutron-gamma ray discriminator (Al 61)
- (2) a neutron threshold discriminator.

The principal neutron detector was a 3-1/2 inch diameter by 3/4 inch thick $\text{Ne } 213^*$ liquid scintillator mounted on a Phillips XP 1040 photomultiplier. The cylindrical geometry maximizes the optical coupling between the scintillator and the photomultiplier as well as minimizing the light collection time. The thickness of the scintillator introduces an uncertainty in the flight time of about 0.6 ns for 6 MeV neutrons. An overall time resolution of 1.25 ns was obtained with this system which corresponds to an energy resolution of about 80 keV for 6 MeV neutrons traversing a 6.3 m flight path.

*Nuclear Enterprises, Ltd., Winnipeg, Manitoba

Spectra were obtained by bombarding an enriched Si^{30} target* with deuterons of 3, 4 and 5 MeV. At the 4 and 5 MeV bombarding energies angular distribution measurements were made at 5° intervals from 0° to 45° and at 15° intervals from 45° to 150° except for the angle at 90° . At the 3 MeV bombarding energy angular distributions were measured at 15° intervals from 0° to 75° and at 120° to 150° .

A typical spectrum from the $\text{Si}^{30}(\text{d},\text{n})\text{P}^{31}$ reaction is shown in figure (4-2). The levels of P^{31} , P^{29} , F^{17} and N^{13} were identified by the kinematic variation of neutron energy with laboratory angle. Levels which could not be identified by comparison with the kinematics of known levels were identified by a least squares computer program described in Appendix I which fitted these data for the best mass and Q-value. Since any Si^{29} contamination on the target is very difficult to identify from the kinematic variation alone, a separate experiment was done using an enriched Si^{29} target and a deuteron bombarding energy of 5 MeV. The results of this experiment showed that there was negligible contamination of the P^{31} spectra arising from the $\text{Si}^{29}(\text{d},\text{n})\text{P}^{30}$ reaction. However they did show that there was a hitherto unsuspected O^{18} contamination affecting the region of the 3.292, 3.414, and 3.505 MeV state of P^{31} which arises from the 4.04 MeV level of F^{19} . The intensity of the 4.04 MeV level of F^{19} which has an angular distribution

*The $210 \mu\text{g}/\text{cm}^2$ thick target, enriched to approximately 90% Si^{30} was supplied by A.E.R.E., Harwell, U.K., in the form of SiO_2 deposited on gold.

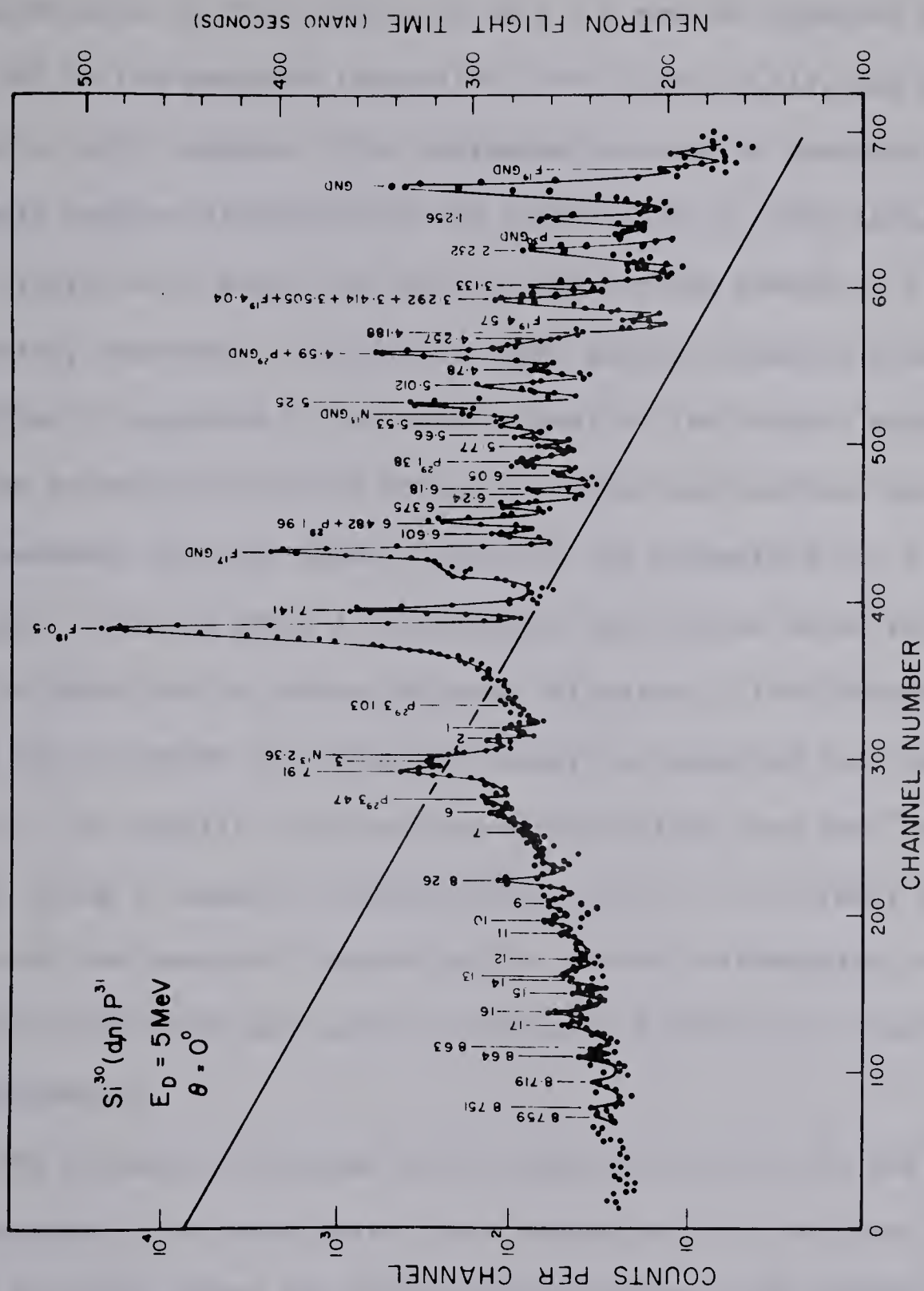


Figure 4-2. Neutron time-of-flight spectrum from the reaction $\text{Si}^{30}(\text{d}, \text{n})\text{P}^{31}$ taken at 0° to the incident 5.0 MeV deuteron beam. Neutron flight path $S_n \approx 6.31 \text{ m}$. The number above each peak is the p^{31} excitation energy in MeV. Neutron flight times are indicated by a time calibration line. The numbers 1 - 17 represent peaks that could not be identified with certainty.

characteristic of the transfer of an $\ell = 0$ proton accounted for more than 50% of the measured intensity of the 3.292, 3.414, and 3.505 MeV levels at zero degrees. This contamination made it impossible to obtain reliable angular distributions for transitions to these levels in P^{31} .

Figure (4-2) shows that many of the excited states of P^{31} are not completely resolved. A nonlinear least squares computer program, described in Appendix I, was used to analyse the neutron spectra. The program calculated the peak areas, the means and standard deviation for the (assumed) Gaussian peaks as well as the parameters for a background function. All the peaks in the spectra were fitted using this program which allowed one to obtain unbiased estimates of the intensities of the peaks and to remove the background under the spectrum in a systematic manner. The angular distributions were obtained from the "raw" intensities using a computer program written by Mr. T. B. Grandy which corrected the measured intensities for neutron attenuation and the detector efficiency and made the necessary laboratory to centre-of-mass transformation.

The relative efficiency of the neutron detector and the energy calibration of the accelerator were determined by a separate experiment using the $Li^7(p,n)Be^7$ and $C^{13}(\alpha,n)O^{16}$ reactions. The energy calibration of the accelerator was checked using the $Li^7(p,n)Be^7$ threshold which occurs at a proton bombarding energy of 1.881 MeV (Be 61). The relative efficiency measurements were made using the $Li^7(p,n)Be^7$ reaction which yields neutrons with energies up to 3.33 MeV and the $C^{13}(\alpha,n)O^{16}$ reaction

which provided a monoenergetic neutron group at 5.50 MeV (Wa 57). The neutrons were detected by the principal neutron detector and by a McKibben long counter with paraffin moderator (Al 60). The integrated counting rate, corrected for counting efficiency, measured by the McKibben long counter provided the normalization required to construct a relative efficiency curve as a function of neutron energy. Since the McKibben long counter detected neutrons leading to both the ground and the first excited states of Be^7 in the $\text{Li}^7(\text{p},\text{n})\text{Be}^7$ reaction a correction was applied to the raw McKibben counts using the results of Bevington et al (Be 61). The resulting relative efficiency curve is shown in figure (4-3) along with a least squares fit to the curve using the semi-empirical n-p cross section formula of Bame (Ba 57) and a cutoff given by

$$A \left[\frac{E_n - E_0}{E_n} \right]^n$$

where A , E_0 and n were parameters of the fit and where E_n is the neutron energy. The curve so obtained was used in the program referred to earlier as one of the corrections applied to the raw angular distribution data.

As in chapter 3 the neutron angular distributions corresponding to the ground and first excited states of F^{17} were normalized to the results of Yaramis (Ya 61) which allowed the relative cross sections corresponding to the various levels in P^{31} obtained at $E_d = 5$ MeV to be converted to absolute cross sections. A comparison of the angular distributions of the neutrons leading to the ground and first excited

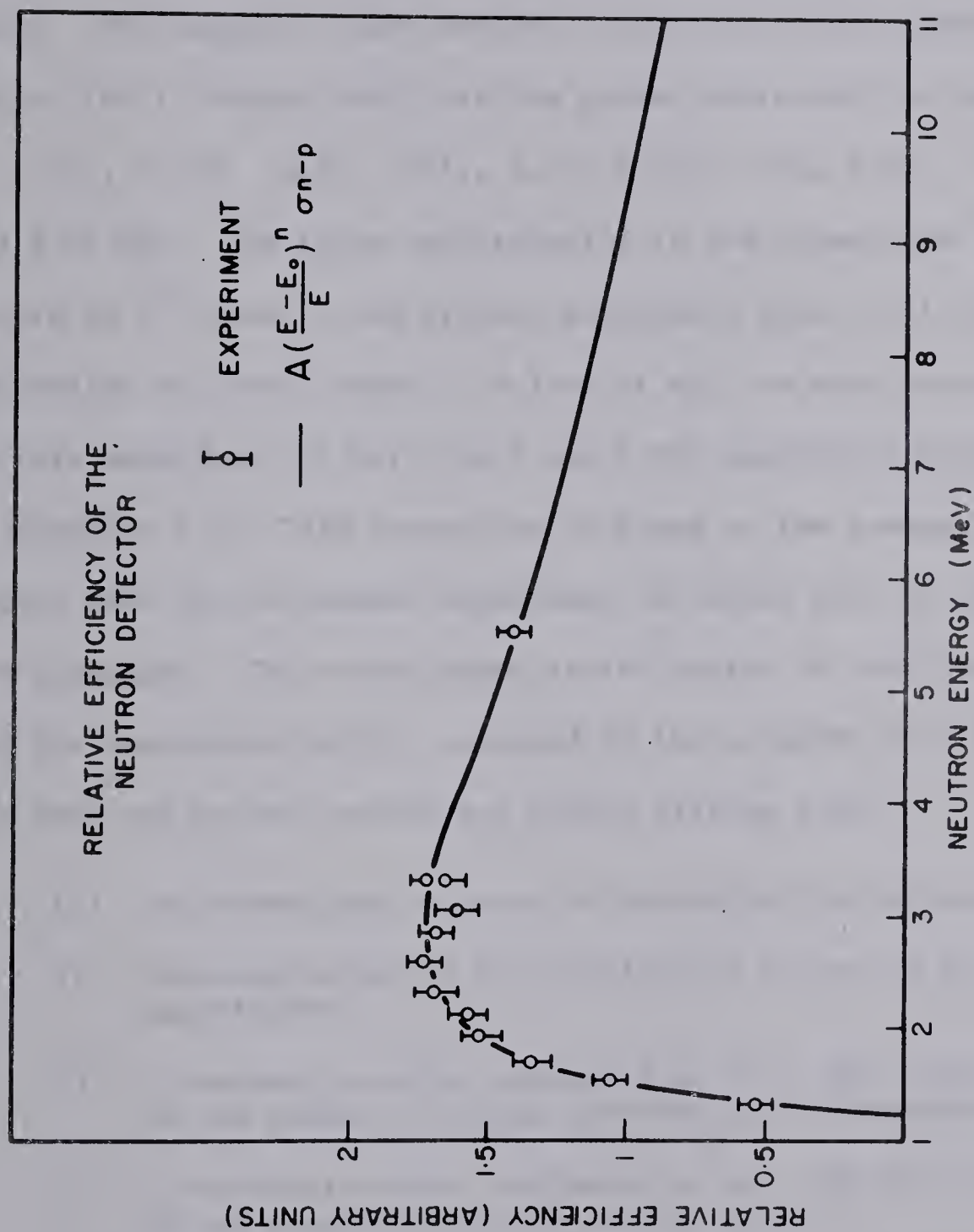


Figure 4-3. The relative efficiency of the neutron detector. The smooth curve was calculated using the semiempirical n-p cross section formula of Bame et al (Ba 57) with a cut-off as shown in the figure.

states of F^{17} obtained in the present experiment with those of Yaramis are shown in figure (4-4). The excellent agreement obtained between these two sets of data provides a good check on the relative efficiency curve. The absolute cross sections obtained in this manner are shown in tables (4-1) through (4-6) for the ground state and the excited states at 1.265, 2.232, 3.133, 5.012, 5.25, 6.382, 6.46, 6.601, 7.141, 7.91 and 8.26 MeV. The large uncertainties in the intensities of the other levels of P^{31} seen in the present experiment makes their inclusion in the tables of little value. (A list of all the experimental data obtained in this experiment at both the 4 and 5 MeV bombarding energies is given in Appendix II.) This conversion is based on the assumption that the target used in the present experiment is mainly SiO_2 as specified by the suppliers. The errors shown in the tables of absolute cross sections are the statistical errors assigned by the computer in the analysis of the data and do not include any errors arising from:

- (1) The normalization error in combining the two experiments.
- (2) The combination of the statistical errors in the two experiments.
- (3) A systematic error, estimated to be $< 10\%$, from uncertainties in the amount of oxygen adsorbed on the surface of the target.
- (4) A systematic error, estimated to be $< 5\%$ from the uncertainty of the abundance of Si^{30} on the target.

The errors associated with the conversion to absolute cross sections are believed to be less than 20%.

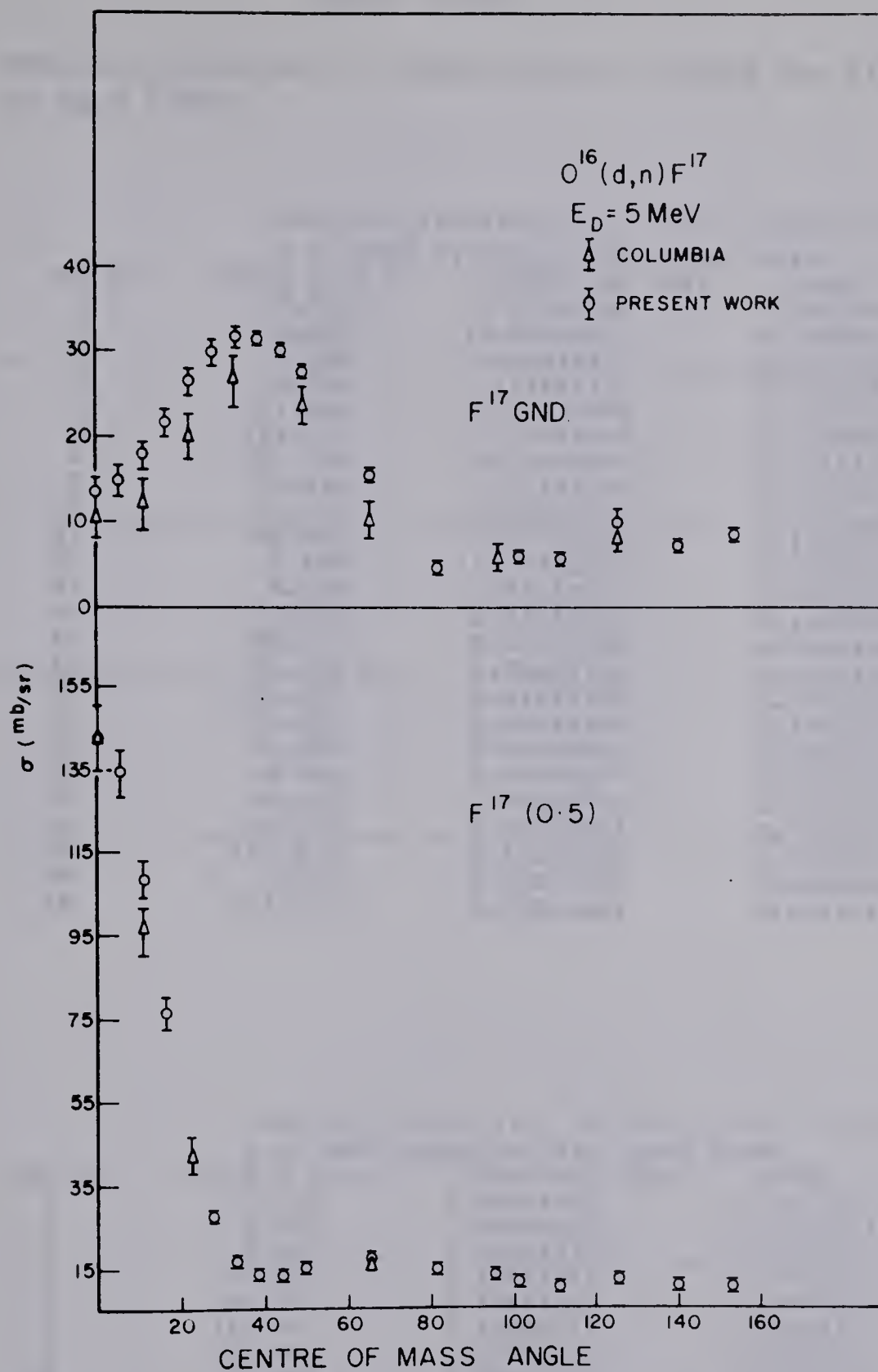


Figure 4-4. Comparison of the angular distributions for neutrons leading to the ground and first excited state of F^{17} obtained in the present experiment with those obtained by Yaramis (Ya 61).

TABLE (4-1)

Absolute differential cross sections (mb/sr) for $\text{Si}^{30}(\text{d},\text{n})\text{P}^{31}$ at $E_d = 5$ MeV.

ANGULAR DISTRIBUTION OF THE 0.0000 STATE OF P 31 FROM $\text{Si}^{30}(\text{D},\text{N})\text{P}^{31}$ JUNE 30/65			
RLN NC	ANGLE C OF M	CORRECTED AREA	ERROR
2	30.939	0.49766391	0.08207419
3	0.000	10.80136327	0.41010021
4	15.486	4.90478377	0.22445750
5	46.328	1.11856121	0.11003203
6	61.626	0.72522352	0.08944369
7	121.626	0.21552935	0.05208049
8	150.938	0.53238550	0.08161339
9	76.814	0.31197308	0.06440901
10	30.939	0.58429717	0.09246733
11	20.642	2.52937888	0.13202278
12	5.164	10.00750369	0.40765179
13	0.000	10.58105264	0.41038024
14	25.794	1.22355697	0.11255792
15	36.077	0.40675992	0.06824073
16	96.870	0.22681793	0.05364241
17	136.327	0.41887399	0.07515032
18	76.814	0.36643810	0.12863321
19	41.207	0.53792416	0.08058302
20	5.164	9.72084629	0.44218483
21	10.326	7.84625940	0.37613191
22	61.626	0.75541592	0.10104224
23	106.813	0.60278626	0.04665885
24	0.000	9.98625408	0.46080886
25	121.626	0.23869601	0.03417164

ANGULAR DISTRIBUTION OF THE 1.26500 STATE OF P 31 FROM $\text{Si}^{30}(\text{D},\text{N})\text{P}^{31}$ JUNE 30/65			
RLN NC	ANGLE C OF M	CORRECTED AREA	ERROR
2	31.005	1.90042360	0.13215674
3	0.000	0.90563426	0.13077351
4	15.520	1.05208779	0.10964973
5	46.422	1.10367963	0.09952241
6	61.741	0.56395892	0.07507385
7	121.741	0.41868619	0.06207195
8	151.005	0.61582531	0.08007312
9	76.942	0.53616214	0.07015254
10	31.005	1.92142978	0.14576338
11	20.688	1.37159939	0.09550466
12	5.175	1.00951232	0.14459968
13	0.000	1.10728483	0.14170949
14	25.850	1.60914040	0.12448564
15	36.153	1.75006542	0.10778449
16	97.003	0.65540826	0.06813534
17	136.421	0.60848723	0.07985538
18	76.942	0.45431106	0.12240422
19	41.292	1.46336895	0.10720573
20	5.175	0.95306053	0.14993777
21	10.349	1.11223911	0.14694506
22	61.741	0.60362528	0.08564776
23	106.942	0.62356371	0.07397105
24	0.000	0.89321597	0.15757268
25	121.741	0.51787324	0.04230537

TABLE (4-2)

ANGULAR DISTRIBUTION OF THE 2.23200 STATE OF P 31 FROM SI30(D,N) P31 JUNE 30/65				
RLN NC	ANGLE C OF M	CORRECTED AREA	ERROR	
2	31.067	1.55035995	0.11922182	
3	0.000	1.08892019	0.13538621	
4	15.552	1.33341891	0.11620457	
5	46.509	1.05894906	0.09696668	
6	61.848	0.46673824	0.06913691	
7	121.847	0.50913558	0.06276986	
8	151.066	0.30156590	0.06355664	
9	77.061	0.32271721	0.05388373	
10	31.067	1.36922579	0.11832803	
11	20.730	1.24649245	0.08776555	
12	5.186	1.09139977	0.14323138	
13	0.000	1.16871364	0.14075264	
14	25.902	1.44404333	0.11440894	
15	36.224	1.43549551	0.09375274	
16	97.125	0.43856544	0.05759847	
17	136.508	0.42702492	0.06866411	
18	77.061	0.29565413	0.10755156	
19	41.372	1.24926958	0.09849637	
20	5.186	1.03423189	0.15320394	
21	10.371	1.10751558	0.14511059	
22	61.848	0.59307459	0.08418878	
23	107.061	0.56098559	0.06838609	
24	0.000	0.96071509	0.16041897	
25	121.847	0.48161351	0.03915990	

ANGULAR DISTRIBUTION OF THE 3.13300 STATE OF P 31 FROM SI30(D,N) P31 JUNE 30/65				
RLN NC	ANGLE C OF M	CORRECTED AREA	ERROR	
2	31.136	0.00000000	0.00000000	
3	0.000	1.14032488	0.10187756	
4	15.588	0.47538056	0.06481073	
5	46.607	0.28601827	0.04940799	
6	61.968	0.18116840	0.03921844	
7	121.967	0.28553014	0.04848449	
8	151.135	0.25610438	0.05915030	
9	77.195	0.23374463	0.05475317	
10	31.136	0.13648971	0.03109222	
11	20.777	0.20698317	0.05648682	
12	5.198	1.22534136	0.10399147	
13	0.000	1.09496047	0.11526738	
14	25.960	0.10924799	0.04751137	
15	36.303	0.17067777	0.06165652	
16	97.263	0.13540791	0.03871002	
17	136.606	0.30885612	0.05890245	
18	77.195	0.00000000	0.00000000	
19	41.460	0.16111544	0.04741328	
20	5.198	1.11620855	0.10376523	
21	10.395	0.67972366	0.08751734	
22	61.968	0.21319331	0.05333908	
23	107.194	0.23334784	0.05352248	
24	0.000	1.27900227	0.10064720	
25	121.967	0.20174265	0.03429800	

TABLE (4-3)

ANGULAR DISTRIBUTION OF THE 5.01200 STATE OF P 31 FROM SI30(D,N) P31 JUNE 30/65			
RLN NC	ANGLE C CF M	CORRECTED AREA	ERROR
2	31.339	6.15352428	C.18965801
3	0.000	1.63831981	0.20301484
4	15.693	7.93235947	0.23514136
5	46.894	1.59002841	0.14908604
6	62.320	1.29385917	C.16066549
7	122.319	0.87080703	C.12051431
8	151.339	0.44269207	C.13200385
9	77.587	1.24568555	0.15136295
10	31.339	6.28627458	0.32990618
11	20.916	8.74623099	0.35267473
12	5.233	3.01043955	0.22384716
13	0.000	1.66792577	0.26648233
14	26.132	8.13350870	C.31644417
15	36.536	4.33082501	C.22839373
16	97.668	1.00954837	0.09480490
17	136.893	0.53185134	0.10139620
18	77.587	1.69345427	C.22681505
19	41.722	2.60150899	0.15976008
20	5.233	3.02291639	0.16191471
21	10.465	6.34913476	0.31777677
22	62.320	1.26815170	C.16295091
23	107.587	1.09368386	C.17423212
24	0.000	1.61907647	0.22948601
25	122.319	0.86920408	0.10289767

ANGULAR DISTRIBUTION OF THE 5.25000 STATE OF P 31 FROM SI30(D,N) P31 JUNE 30/65			
RLN NC	ANGLE C CF M	CORRECTED AREA	ERROR
2	31.373	0.39336210	C.20233404
3	0.000	4.81207638	C.46441693
4	15.711	1.89462140	0.27391530
5	46.942	C.45885133	C.10876206
6	62.379	0.50210407	0.11256870
7	122.379	0.03665335	0.05701725
8	151.373	0.22614797	0.06284321
9	77.654	0.13138527	C.09854494
10	31.373	0.18982540	0.15309358
11	20.939	0.75227757	0.25211451
12	5.239	4.15629392	0.42398804
13	0.000	4.18228622	C.40086663
14	26.161	0.47462987	C.18526616
15	36.576	0.26244020	0.11966279
16	97.737	0.00000000	0.00000000
17	136.942	0.12449029	C.07055121
18	77.654	0.21337840	0.11490959
19	41.766	0.32443583	0.10431933
20	5.239	3.65391806	0.35499535
21	10.477	3.12473097	C.32882908
22	62.379	0.39748788	0.10340077
23	107.653	0.03413943	C.05689971
24	0.000	4.07787633	0.34099969
25	122.379	0.00000000	C.00000000

TABLE (4-4)

ANGULAR DISTRIBUTION OF THE 6.3750 STATE OF P 31 FROM SI30(D,N) P31 JUNE 30/65			
RUN NC	ANGLE C OF M	CORRECTED AREA	ERROR
2	31.582	1.46176086	0.13860298
3	0.000	0.59436302	0.12030721
4	15.819	0.94675882	0.13451560
5	47.238	1.24663342	0.11313612
6	62.741	0.72237826	0.09503628
7	122.741	0.61505640	0.08417331
8	151.582	0.64893396	0.10756980
9	78.058	0.51444465	0.09769453
10	31.582	1.37630922	0.14141587
11	21.082	1.21293481	0.14759293
12	5.276	0.72632751	0.13309353
13	0.000	0.86460384	0.13209812
14	26.337	1.24410088	0.14236708
15	36.815	1.45222741	0.15668439
16	98.153	0.62542933	0.08200716
17	137.237	0.51372768	0.07849963
18	78.058	0.93447529	0.15025093
19	42.034	1.33009366	0.15697059
20	5.276	0.63701007	0.12612370
21	10.550	0.89784904	0.11366589
22	62.741	0.72927446	0.09760975
23	108.057	0.52175881	0.09836208
24	0.000	0.66984700	0.11404732
25	122.741	0.54536543	0.07215096

ANGULAR DISTRIBUTION OF THE 6.482 STATE OF P 31 FROM SI30(D,N)P31 JUNE 30/65			
RUN NO	ANGLE (C OF M)	CORRECTED AREA	ERROR
2	31.608	2.73	0.172
3	0.000	2.98	0.190
4	15.832	3.75	0.215
5	47.274	1.05	0.116
6	62.785	0.995	0.113
7	122.785	0.296	0.076
8	151.607	0.533	0.108
9	78.107	0.840	0.120
10	31.608	2.42	0.185
11	21.100	3.41	0.219
12	5.280	3.00	0.207
13	0.000	3.12	0.201
14	26.359	3.17	0.208
15	36.844	1.55	0.180
16	98.204	0.421	0.085
17	137.273	0.315	0.074
18	78.107	0.900	0.160
19	42.067	1.16	0.166
20	5.280	3.12	0.200
21	10.558	3.49	0.180
22	62.785	1.03	0.115
23	108.106	0.274	0.094
24	0.000	3.04	0.179
25	122.785	0.221	0.067

The 6.482 MeV state of P³¹ has been corrected for the contamination from the 1.96 MeV state of P²⁹.

TABLE (4-5)

ANGULAR DISTRIBUTION OF THE 6.6C1C0 STATE OF P 31 FROM SI30(D,N) P31 JUNE 30/65			
RLN NC	ANGLE C CF M	CORRECTED AREA	ERROR
2	31.637	1.04532675	0.17221C29
3	0.000	0.84843459	0.07237921
4	15.847	1.25194271	0.17489188
5	47.316	0.52545596	0.05734500
6	62.837	0.76929717	0.09365719
7	122.836	0.45278578	0.09137956
8	151.637	0.44613493	0.07971555
9	78.164	0.45607544	0.09274546
10	31.637	0.99353173	0.10497902
11	21.120	1.19053993	0.05775332
12	5.285	0.74603354	0.10717770
13	0.000	0.80392705	0.09554463
14	26.384	0.99010980	0.08533248
15	36.878	0.75099039	0.10253515
16	98.263	0.36167542	0.08860366
17	137.315	0.25060873	0.07833081
18	78.164	0.29275819	0.22235610
19	42.105	0.89333175	0.06871998
20	5.285	0.79205190	0.15048860
21	10.569	0.91041154	0.14750008
22	62.837	0.49446473	0.07477540
23	108.164	0.42058511	0.09767207
24	0.000	0.90103643	0.09843184
25	122.836	0.39504053	0.05389143

ANGULAR DISTRIBUTION OF THE 7.141C0 STATE OF P 31 FROM SI30(D,N) P31 JUNE 30/65			
RLN NC	ANGLE C CF M	CORRECTED AREA	ERROR
2	31.796	0.53610655	0.16376823
3	0.000	9.10074121	0.29271825
4	15.930	5.27590689	0.17955252
5	47.540	0.44266798	0.10810430
6	63.111	0.68052606	0.08482879
7	123.111	1.66220871	0.48177741
8	151.795	0.37228335	0.16962385
9	78.471	0.56833167	0.14304603
10	31.796	0.77355564	0.18371387
11	21.228	3.12963262	0.15107137
12	5.313	8.83271229	0.38880640
13	0.000	9.10152312	0.29539229
14	26.518	1.61599456	0.10273644
15	37.060	0.42793498	0.13271994
16	98.579	0.75900082	0.21850479
17	137.540	0.22192470	0.12913167
18	78.471	0.79520715	0.14667057
19	42.309	0.51638713	0.11664791
20	5.313	8.60066908	0.24503227
21	10.624	6.98650112	0.35418535
22	63.111	0.74014817	0.11530667
23	108.470	1.74500479	0.24309185
24	0.000	8.78194855	0.33528877
25	123.111	1.45860290	0.04054310

TABLE(4-6)

ANGULAR DISTRIBUTION OF THE 7.91CCO STATE OF P 31 FROM S130(D,N) P31 JUNE 30/65			
RLN NC	ANGLE C OF M	CORRECTED AREA	ERROR
2	32.131	1.58766657	0.37287878
3	0.000	2.92401953	0.34082571
4	16.103	3.03378596	0.28166671
5	48.015	0.94644422	0.11292799
6	63.693	0.69084135	0.11687154
7	123.692	0.20767185	0.08625724
8	152.131	0.27780576	0.10080491
9	79.119	0.12061244	0.39927343
10	32.131	0.00000000	0.00000000
11	21.458	0.00000000	0.00000000
12	5.371	3.05494601	0.33138506
13	0.000	3.40703363	0.26964212
14	26.801	0.00000000	0.00000000
15	37.445	0.89305537	0.10601176
16	99.249	0.32074498	0.08931097
17	138.014	0.16578343	0.12717844
18	79.119	0.00000000	0.00000000
19	42.740	0.64642937	0.11747498
20	5.371	2.98793575	0.26749522
21	10.740	2.85971622	0.34116029
22	63.693	0.73739420	0.08131568
23	109.119	0.22602612	0.08019421
24	0.000	3.06444567	0.22717998
25	123.692	0.00000000	0.00000000

ANGULAR DISTRIBUTION OF THE 8.26CCO STATE OF P 31 FROM S130(D,N) P31 JUNE 30/65			
RLN NC	ANGLE C OF M	CORRECTED AREA	ERROR
2	32.362	0.43993564	0.06877814
3	0.000	1.16928607	0.10226933
4	16.223	0.85090231	0.09095583
5	48.342	0.36820160	0.07335297
6	64.094	0.00000000	0.00000000
7	124.093	0.24696864	0.09880533
8	152.362	0.00000000	0.00000000
9	79.567	0.00000000	0.00000000
10	32.362	0.47394056	0.09056014
11	21.616	0.68821882	0.08102820
12	5.412	1.02798174	0.09983614
13	0.000	1.08126236	0.12885958
14	26.997	0.75595194	0.09105175
15	37.710	0.43963197	0.07609664
16	99.710	0.37392167	0.08927962
17	138.341	0.00000000	0.00000000
18	79.567	0.00000000	0.00000000
19	43.038	0.00000000	0.00000000
20	5.412	0.94523447	0.10316724
21	10.820	0.94834777	0.10902802
22	64.094	0.25324169	0.07340948
23	109.567	0.10935503	0.09378734
24	0.000	0.95704154	0.12770116
25	124.093	0.23698647	0.06993788

4.3 The Levels of P^{31}

Table (4-7) gives a list of the levels of P^{31} seen in the present experiment as well as a list of the previously determined levels with their spins and parities where these are known. The table includes 11 previously unreported excited states in the region of excitation from 5 to 8 MeV. All the levels with the exception of the two at 7.91 and 8.26 were identified at the three bombarding energies. However, the Q-values shown were originally calculated from the spectra taken at the 3 MeV bombarding energy since at the lower bombarding energy the levels are more easily resolved. (See figure (4-5)). Each of the levels given in table (4-7) was observed at a minimum of 5 different angles of neutron emission and was identified by the least squares program (Least Squares Mass and Q Identification) given in Appendix I. The Q values shown in the table for the levels at 6.38, 6.48, 6.60, 7.14, 7.91 and 8.26 MeV were calculated from the data taken at the 5 MeV bombarding energy and the small errors associated with these levels is due to the large number of angles (~ 17) at which the excitation energy was determined. A ground state Q value of 5.062 MeV (En 62) for the $Si^{30}(d,n)P^{31}$ reaction was used as a reference in the calculation of the excitation energies of the states shown in the table.

There is evidence to indicate that the state at 6.18 MeV excitation is a combination of two unresolved levels with different values of ℓ_p . There is also evidence for the existence of states in the region of excitation between 6.60 and 7.14, and 7.14 and 7.91 MeV but these states

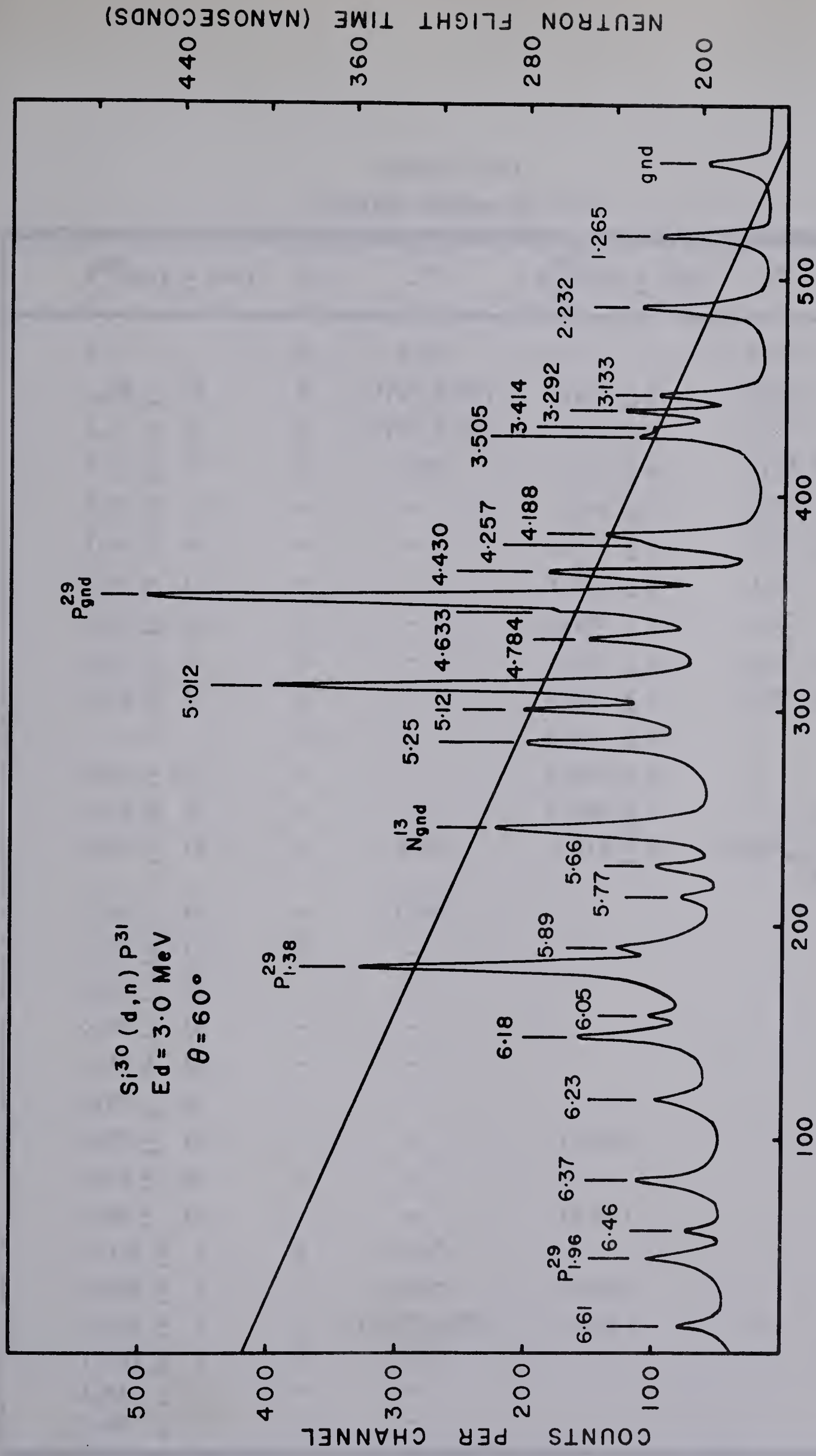


Figure 4-5. Neutron time-of-flight spectrum from the reaction $\text{Si}^{30}(\text{d}, \text{n})\text{P}^{31}$ taken at 60° to the incident 3.0 MeV deuteron beam. Neutron flight path $S_n = 6.41 \text{ m}$. The number above each peak is the P^{31} excitation energy in MeV and the neutron flight times are indicated by a time calibration line.

TABLE (4-7)
Excited States of P^{31}

$E_x^{(a)}$ (MeV \pm keV)	l_p	J^π	$E_x^{(b)}$ (MeV \pm keV)	J^π
0	0	$1/2^+$	0	$1/2^+$
1.28 \pm 14	2	$(3/2^+, 5/2^+)$	1.265 \pm 3	$3/2^+$
2.23 \pm 10	2	$(3/2^+, 5/2^+)$	2.232 \pm 4	$5/2^+$
3.10 \pm 12	0	$1/2^+$	3.133 \pm 4	$1/2^+$ (En 64)
3.28 \pm 12	-	-	3.292 \pm 4	$5/2^+$
3.41 \pm 20	-	-	3.414 \pm 5	$7/2^+$ (Ha 63)
3.49 \pm 13	-	-	3.505 \pm 5	$3/2^+$
4.17 \pm 12	-	-	4.188 \pm 5	$5/2^+$
4.24 \pm 12	-	-	4.257 \pm 5	$3/2^+$ (Ha 63)
4.43 \pm 10	-	-	4.430 \pm 5	$7/2^-$ (Ha 64)
*	-	-	4.59 \pm 5	-
4.61 \pm 15	-	-	4.633 \pm 5	-
4.78 \pm 10	-	-	4.784 \pm 5	-
5.01 \pm 10	1	$3/2^-$	5.012 \pm 5	$(1/2^+, 3/2^+)$ (Ha 63)
5.12 \pm 10	-	$1/2^+$		
5.25 \pm 10	0	-		
5.53 \pm 10	-	-		
5.66 \pm 10	-	-		
5.77 \pm 10	-	-		
5.89 \pm 10	-	-		
6.05 \pm 10	-	-	(6.05)	-
6.18 \pm 23	-	-		
6.24 \pm 10	-	-	(6.25)	-
6.375 \pm 4	2	$3/2^+$		
6.482 \pm 5	1	$1/2^-$	6.43	-
6.601 \pm 4	1	$(1/2^-, 3/2^-)$	6.55	-
7.141 \pm 3	0	$1/2^+$		
7.91 \pm 7	-	-		
8.26 \pm 6	-	-		

(a) Present experiment (b) Reference (En 62) except where otherwise indicated.

*The 4.59 MeV state of P^{31} is obscured by the ground state of P^{29} .

are too weakly excited to be analysed quantitatively from the present experimental data. Also the level at 4.59 MeV excitation (En 62) is completely obscured at all angles by the ground state of P^{29} .

A careful search was made for a new first excited state of P^{31} at 450 keV reported by Colli, Forti, and Gadioli (Co 64). Within the limits of statistical error, which in this case is equal to 1/50 of the ground state intensity, the presence of such a state could not be detected.

4.4 The Analysis of the Angular Distributions

The DWBA analysis of the angular distributions was carried out only for the intensely populated bound states listed in tables (4-1) through (4-5); viz. the ground state, and the excited states at 1.26, 2.23, 3.13, 5.01, 5.25, 6.38, 6.48, and 6.60 MeV. As in chapter 3 the computations were performed on the University of Alberta IBM 7040 computer and the SDS 920 computer using the code written by Smith (Sm 62). The optical potentials used in the analysis have the form

$$U = V + iW$$

where

$$V = V_0 / (1 + \exp(x))$$

$$W = W_0 / (1 + \exp(x))$$

$$x = (r - r_0 A^{1/3}) / a \quad .$$

In the above formulae, V_0 and W_0 are the strengths of the refractive and absorptive parts of the optical potential; r_0 and a are the radius and diffuseness parameters respectively for the Saxon-Woods form factor; r

is the separation of the reacting nuclei. Again only a volume absorption potential was included in the calculations and the zero range approximation (Au 63) was made for the n-p interaction.

Deuteron and neutron elastic scattering data are not available for Si^{30} and P^{31} in the energy range of interest here. From the available scattering data for nuclei in this region of mass number (Sm 63) (Ma 62) and for $E_d = 5$ MeV, it was decided to confine the search for "best-fit" potentials to 40 - 50 MeV for V_n , 45 - 100 MeV for V_d , 3 - 8 MeV for W_n and 6 - 12 MeV for W_d . For V_n the range of potentials from 40 - 50 MeV was covered in 1 MeV steps and for V_d the region from 45 - 70 MeV was covered in 2 MeV steps while the region from 70 - 100 MeV for V_d was covered in 5 MeV steps. This search ranged over sets of values which were generally consistent with those found in the literature (Sm 62), (Sm 63), (Ma 62) and (Wi 64).

Since it was found that a more extensive parameter search was necessary than that required to find reasonable fits to the experimental data for P^{29} at $E_d = 4$ and 5 MeV, the following parameter search procedure was employed in the analysis of the P^{31} data:

- (1) Using reasonable values for the other parameters, the potentials V_n and V_d were iterated over the range from 40 - 100 MeV discussed above.
- (2) The best fit potentials obtained in 1 were then used in a search in which only W_n and W_d were allowed to vary.
- (3) The best fit potential set obtained by using both visual and χ^2 criteria was chosen and the values of r_n and r_d were iterated using this potential set.

- (4) The values of the diffuseness parameters a_n and a_d , holding all other parameters constant, were then varied in an attempt to improve the fit further.
- (5) Finally V_n , V_d , W_n and W_d were varied over a selected range of values to check that they still represented "best-fits" to the data in view of the interaction between the various potential parameters in determining a best fit.

This search was initially confined to the data corresponding to the ground state transition in P^{31} . The angular distributions corresponding to the excited states of P^{31} were then fitted using the best fit potential set obtained for the ground state transition. In order to check that this potential set represented a best-fit to the excited states, the potentials V_n , V_d , W_n and W_d were varied over a selected region limited between 45 and 70 MeV for V_n and V_d and 6 - 8 MeV for W_n and 10 - 14 MeV for W_d . In general it was found that the best fit potential set found for the ground state of P^{31} also represented reasonable and/or best fits for all of the excited states analysed.

The potential well depth and shape parameters used in the calculation of the bound proton wave function are $r_{0p} = 1.4$ fm and $a_p = 0.7$ fm and were held constant throughout the present calculations. The potential depth V_p associated with the bound proton wave function is obtained by starting with the asymptotic solution and integrating inward numerically to the origin. An initial estimate of V_p is given by the relation

$$V_p R_{0p}^2 = 85 M_I^{2/3}.$$

The wave function at the origin is considered a function of V_p which is expanded in a second order Taylor's series and is solved for the potential

shift required to make the wave function zero at the origin. The potential depth is iterated in this manner until convergence of the wave function at the origin is obtained. The potential depth V_p obtained for the ground state of P^{31} in this calculation was 47 MeV.

This analysis was carried out for the results obtained at $E_d = 4$ and $E_d = 5$ MeV. However only the 5 MeV data will be presented here since the results obtained at $E_d = 4$ MeV were consistent with those obtained at $E_d = 5$ MeV. The "best-fits" to the experimental data are shown in figures (4-6) and (4-7). The spectroscopic factors for the best fit potentials obtained in the present analysis are shown in tables (4-8) and (4-9) along with those for two other reasonable potential sets which bracket the best fit potential. It is seen from the tables that the spectroscopic factors show a maximum variation of 15% as a function of the potential variations shown. Considering only the best fit parameters the spectroscopic factors obtained in the analysis of the data at $E_d = 4$ MeV show a typical variation of 15% from those obtained at $E_d = 5$ MeV except for the levels at 6.38 and 6.48 MeV which show variations of 18% and 38% respectively. In the calculation of the spectroscopic factor for the 6.48 MeV state at $E_d = 4$ MeV no correction for the contamination from the 1.96 MeV level of P^{29} was made which could amount to as much as 20% of the observed cross section.

It is seen from figures (4-6) and (4-7) that the angular distribution of the neutrons leading to the 3.133 and 5.25 MeV states can only be fitted by an $\ell_p = 0$ stripping curve which allows an unambiguous spin and parity assignment of $1/2^+$ to be made for these states. A discussion of the angular

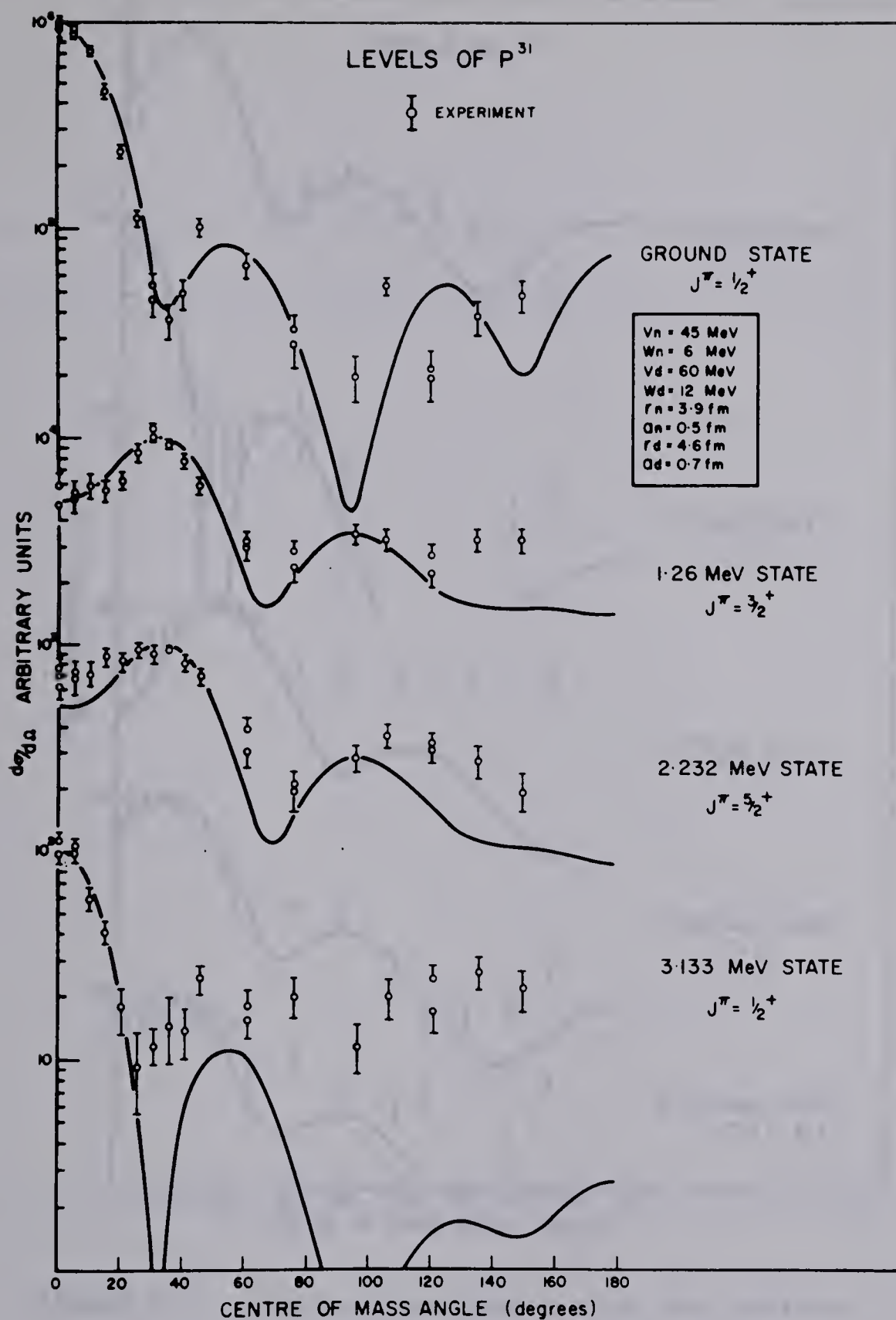


Figure 4-6. Angular distributions of the neutrons leading to the ground state and excited states at 1.26, 2.23, and 3.13 MeV for $E_d \approx 5$ MeV. The smooth curves were calculated using the DWB approximation with parameters as indicated.

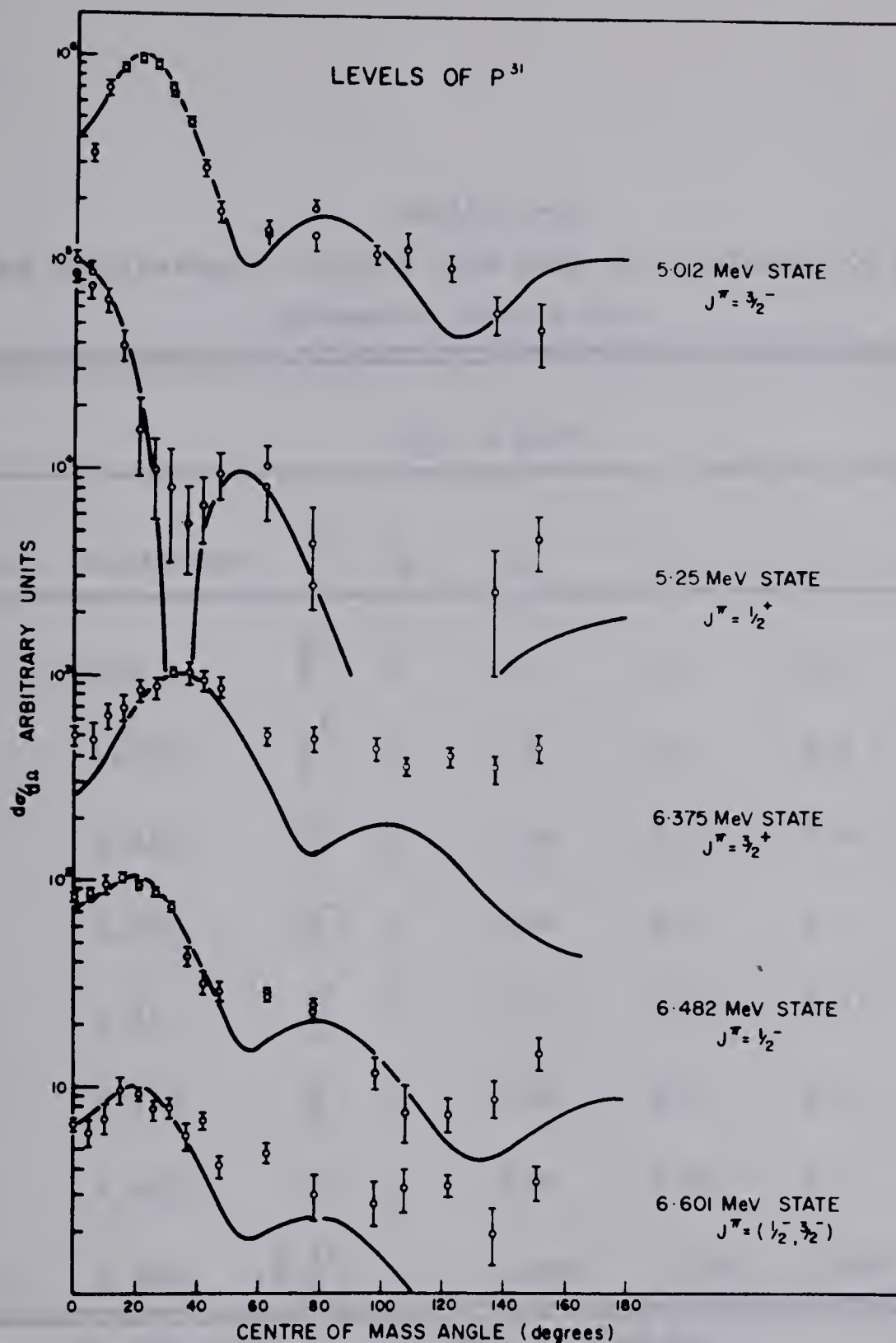


Figure 4-7. Angular distributions of the neutrons leading to the 5.01, 5.25, 6.38, 6.48 and 6.60 MeV states of P^{31} . The smooth curves were calculated using the DWB approximation with the same parameters as those shown in figure (4-6).

TABLE (4-8)

Relative Spectroscopic Factors from DWBA Calculations for Selected
Parameter Combinations

$E_d = 4 \text{ MeV}$						
Level	Excitation	J^π	ℓ_p	S_a^*	S_b	S_c
0	0.0	$\frac{1}{2}^+$	0	1.0	1.0	1.0
1	1.265	$\frac{3}{2}^+$	2	1.6	1.7	1.8
2	2.232	$\frac{5}{2}^+$	2	0.50	0.53	0.54
13	5.012	$\frac{3}{2}^-$	1	0.84	0.93	1.0
15	5.25	$\frac{1}{2}^+$	0	0.12	0.13	0.14
23	6.375	$\frac{3}{2}^+$	2	0.98	1.0	1.0
24	6.482	$\frac{1}{2}^-$	1	0.84	0.95	1.1
25	6.601	$(\frac{1}{2}, \frac{3}{2}^-)$	1	0.068	0.078	0.086

* S_a calculated using $V_n = 46 \text{ MeV}$, $V_d = 60 \text{ MeV}$

S_b calculated using $V_n = 47 \text{ MeV}$, $V_d = 58 \text{ MeV}$ (best fit potentials)

S_c calculated using $V_n = 49 \text{ MeV}$, $V_d = 56 \text{ MeV}$

$W_n = 6 \text{ MeV}$ and $W_d = 12 \text{ MeV}$ for all calculations.

TABLE (4-9)

Relative Spectroscopic Factors from DWBA Calculations for Selected
Parameter Combinations

$E_d = 5 \text{ MeV}$						
Level	Excitation	J^π	ℓ_p	S_a^*	S_b	S_c
0	0	$\frac{1}{2}^+$	0	(0.25	0.20	0.19) _{abs}
1	1.265	$\frac{3}{2}^+$	2	1.76	1.98	2.12
2	2.232	$\frac{5}{2}^+$	2	0.69	0.76	0.75
3	3.133	$\frac{1}{2}^+$	0	0.07	0.07	0.07
13	5.012	$\frac{3}{2}^-$	1	0.60	0.70	0.75
15	5.25	$\frac{1}{2}^+$	0	0.16	0.19	0.19
23	6.375	$\frac{3}{2}^+$	2		0.82	
24	6.482	$\frac{1}{2}^-$	1		0.59	
25	6.601	$(\frac{1}{2}^-, \frac{3}{2}^-)$	1	0.07	0.088	0.07

* S_a calculated using $V_n = 45 \text{ MeV}$, $V_d = 65 \text{ MeV}$

S_b calculated using $V_n = 45 \text{ MeV}$, $V_d = 60 \text{ MeV}$ (best fit)

S_c calculated using $V_n = 49 \text{ MeV}$, $V_d = 56 \text{ MeV}$

$W_n = 6 \text{ MeV}$ and $W_d = 12 \text{ MeV}$ for all calculations.

distributions leading to the 5.012, 6.38, 6.48, 6.60 and 7.14 MeV states will be given in the next section.

4.5 Negative Parity and Isobaric Analogue States in p^{31}

The angular distributions of the neutrons leading to the 5.012, 6.482, and 6.601 MeV states of p^{31} and the associated DWBA fits are shown in figure (4-8) for a deuteron bombarding energy of 5 MeV. Since the results obtained at $E_d = 4$ MeV are consistent with those obtained at $E_d = 5$ MeV only the 5.0 MeV data will be presented here. In all cases it is seen (figure (4-8)) that the $\ell_p = 1$ fit is favoured over the $\ell_p = 2$ fit establishing an odd parity assignment for these states.

The spin dependent structure found by Schiffer and Lee (Le 64) for $\ell_n = 1$ transitions in (d,p) reactions can be summarized as follows. The $J = 1/2$ states show a sharp minimum in the region between $\theta = 90^\circ$ and $\theta = 145^\circ$ but the $J = 3/2$ states do not show this minimum. Although at the present time this spin dependent structure is largely phenomenological in nature some progress has been made in the explanation of this phenomenon by Greider (Gr 64) on the basis of the diffraction model. It is interesting to note that current formulations of the distorted wave Born approximation for deuteron stripping have been unable to predict this effect. Inspection of the angular distributions given in figure (4-8) clearly shows the minimum mentioned above in the angular distribution of the neutrons leading to the 6.482 MeV state of p^{31} , while the angular distribution of the neutrons leading to the 5.012 MeV state does not show this minimum.

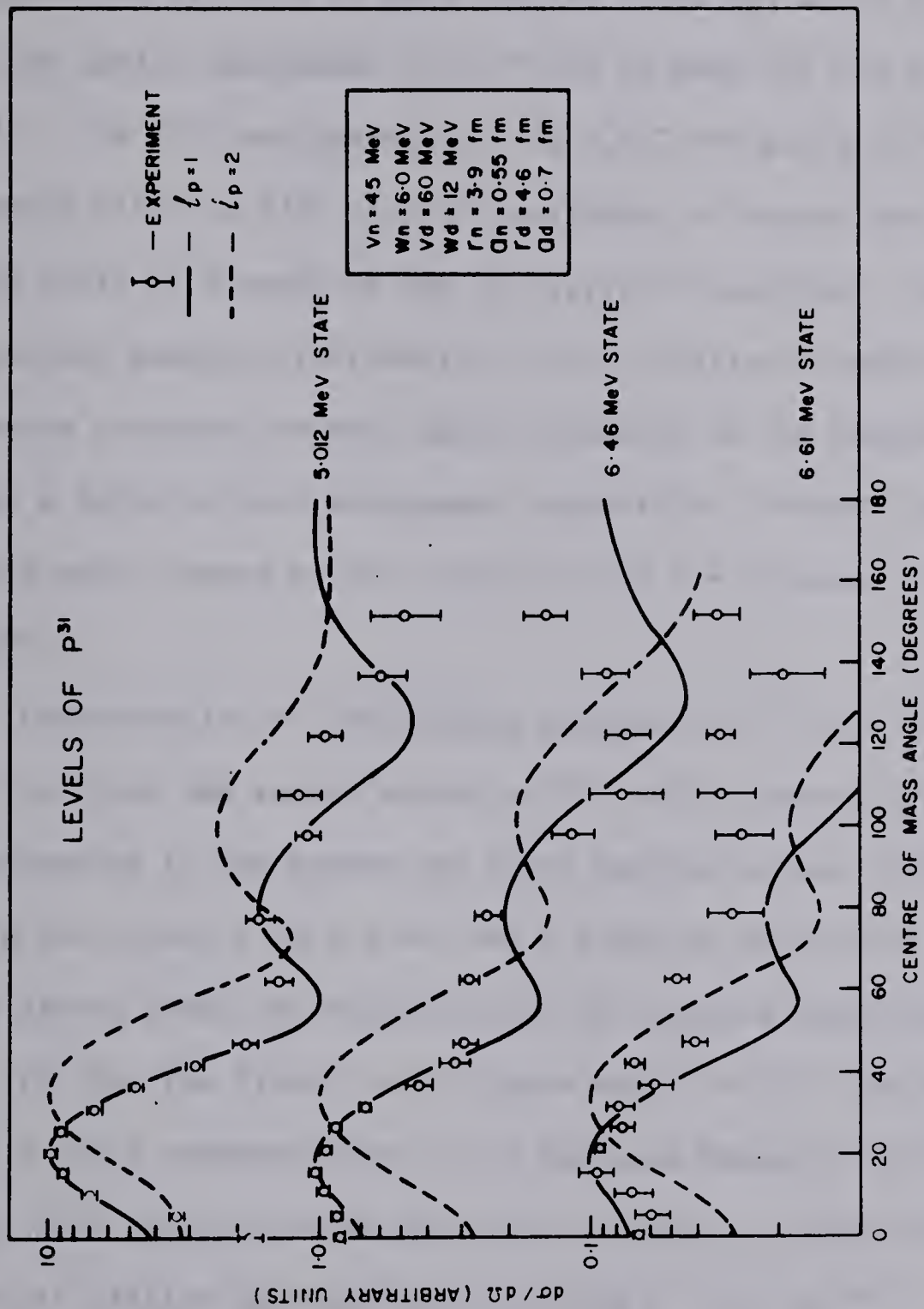


Figure 4-8. Angular distributions of the neutrons leading to the 5.01, 6.48 and 6.60 MeV states of P^{31} for $E_d = 5$ MeV. The smooth curves were calculated using the DWB approximation with parameters as indicated.

Assuming this spin dependent structure occurs for (d,n) reactions as indicated by recent experiments (See chapter 3), a spin and parity assignment of $1/2^-$ can be made for the 6.482 MeV state in P^{31} while a spin and parity assignment of $3/2^-$ can be made for the 5.012 MeV state in P^{31} . The $3/2^-$ assignment for the 5.012 MeV state in P^{31} is in disagreement with the $1/2^+$ or $3/2^+$ assignment of Harris and Seagondollar on the basis of a study of the $Si^{30}(p,\gamma)P^{31}$ reaction. Uncertainties in the neutron angular distribution of the relatively weakly excited 6.601 MeV state obscures the weak spin dependence of the angular distribution making a definite spin assignment impossible. However the spin and parity of this state formed by the capture of an $\ell = 1$ proton is limited to $1/2^-$ or $3/2^-$.

Consideration of the binding energies of P^{31} and Si^{31} indicates that the first and second states of P^{31} with isobaric spin $T = 3/2$, corresponding to the ground and first excited states of Si^{31} , should lie in the vicinity of 6.4 MeV and 7.2 MeV of excitation respectively. These states should be characterized by spin and parity assignments $J^\pi = 3/2^+$ for the first $T = 3/2$ state and $J^\pi = 1/2^+$ for the second $T = 3/2$ state corresponding to the analogue states of Si^{31} . Both states should have reaction cross sections comparable to those for the strongest states of similar spin and parity having $T = 1/2$ in P^{31} .

The states in P^{31} at 6.38 and 7.14 fulfill most of the conditions set out above. In particular, figure (4-9) shows that the angular distribution of the neutrons leading to the 6.38 MeV state of P^{31} can only be fitted by an $\ell_p = 2$ stripping curve, limiting the possible spin and parity assignments to $3/2^+$ or $5/2^+$. The state at 7.14 MeV, although not

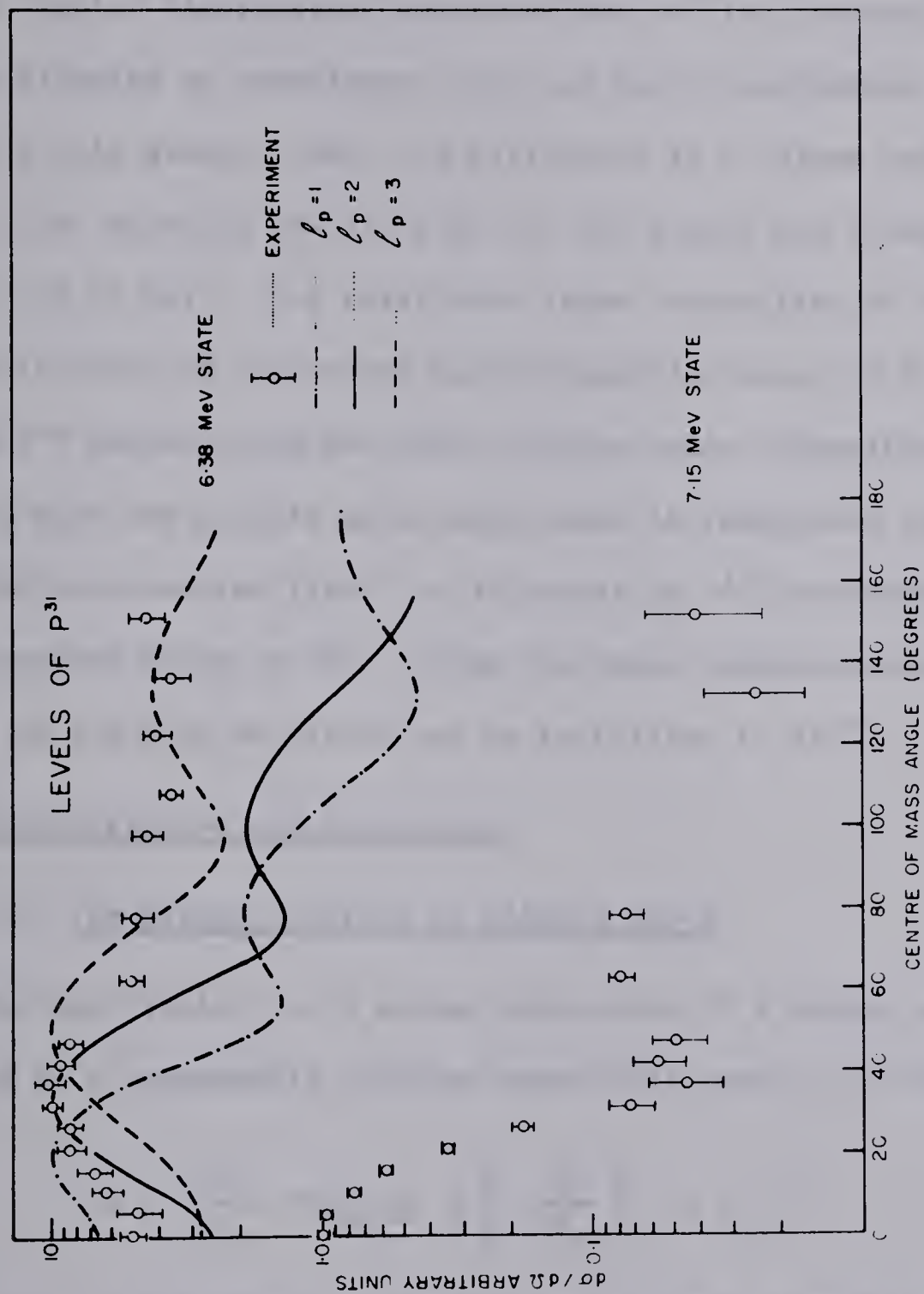


Figure 4-9. Angular distributions of the neutrons leading to the 6.38 and 7.14 MeV states of P^{31} . The smooth curves were calculated using the DWB approximation with optical angular momenta as indicated. The optical potential parameters are the same as those shown in figure (4-8).

amenable to analysis by the DWBA program (because of computational difficulties occurring for Q values near the deuteron binding energy) has an angular distribution characteristic of the transfer of the $\ell = 0$ proton allowing an unambiguous spin and parity assignment of $1/2^+$ to be made for this state. Also, the difference in Q values for these states is 0.76 MeV which is exactly that for the ground and first excited states of Si^{31} (0.76 MeV). The relatively large intensities of these states (the 7.14 and 6.38 MeV states have intensities equal to 90% and 76% of the P^{31} ground state and first excited state intensities respectively), coupled with the results given above make it reasonable to identify the 6.38 MeV state as the first $T = 3/2$ state of P^{31} corresponding to the first excited state of Si^{31} . From the above considerations the spin and parity of the 6.38 MeV state can be restricted to $3/2^+$.

4.6 Interpretation and Discussion

(i) The Strong Coupling or Nilsson Model

The Hamiltonian for a system consisting of a single particle strongly coupled to a permanently deformed spheroidal core is (Da 65a)

$$H = \frac{p^2}{2m} + V(\underline{r}, \underline{\ell}, \underline{s}) + \sum_K^3 \frac{\hbar^2}{2\mathcal{J}_K} \left| \mathcal{J}_K - j_K \right|^2 \quad (4-1)$$

where \mathcal{J}_K is the moment of inertia and I and J are the spins of the nucleus and of the odd particle respectively. If the Hamiltonian possesses an axis of symmetry ($\mathcal{J}_1 = \mathcal{J}_2 = \mathcal{J}$) then equation (4-1) can be written as (Da 65a)

$$H = H_p + H_R + H_c \quad (4-2a)$$

where

$$H_p = (p^2/2m) + V(\underline{r}, \underline{l}, \underline{s}) + (\frac{\hbar^2}{2\mathcal{J}}) \underline{j} \cdot \underline{j} \quad (4-2b)$$

$$H_R = (\hbar^2/2\mathcal{J}) [I(I+1) - 2K^2] \quad (4-2c)$$

$$\begin{aligned} H_c &= (-\hbar^2/\mathcal{J}) I_1 j_1 + I_2 j_2 \\ &= (-\frac{\hbar^2}{2\mathcal{J}}) (I_+ j_- + I_- j_+) \quad . \end{aligned} \quad (4-2d)$$

The term H_c is the rotation-particle coupling term given by Kerman (Ke 56) which is in fact a coriolis force $\underline{\omega} \cdot \underline{j}$ since H_p and H_R are not individually the particle and rotator Hamiltonians but mixtures of the two. In the approximation that H_c can be neglected H_p and H_R commute and can be solved independently of one another. The solution of this problem leads to the wave function (Ni 55)

$$\psi_{MK}^I = \left[\frac{2I+1}{16\pi^2} \right]^{1/2} \phi \left[D_{MK}^I(\theta_i) \chi_K + (-1)^{I-j_p} D_{M-K}^I(\theta_i) \chi_{-K} \right] \quad (4-3)$$

where $D_{MK}^I(\theta_i)$ is the rotator wave function, $\chi_K = \sum_j c_j \chi_K^j$ is the wave function of the particle in the field of the deformed core ($H_R \chi_K = E_p \chi_K$), ϕ represents the vibrational motion and K and M are the projections of I on the axis of symmetry and the z axis (axis of quantization) respectively. When the term H_c is included the diagonal matrix elements of the Hamiltonian can be expressed as

$$\begin{aligned} \langle IK | H | IK \rangle &= E_K^p + \frac{\hbar^2}{2} \{ I(I+1) + \delta_{K,1/2} a(-1)^{I+1/2} (I+1/2) \} \\ &- 4 \left[\frac{\hbar^2}{2\mathcal{J}} \right]^3 \left[\frac{3}{(\hbar\omega_\beta)^2} + \frac{1}{(\hbar\omega_\gamma)^2} \right] [I(I+1) + \delta_{K,1/2} a(-1)^{I+1/2} (I+1/2)]^2 \quad (4-4) \end{aligned}$$

where the decoupling parameter a is given by

$$a = - \sum_j (-1)^{j+1/2} (j+1/2) |c_j|^2 .$$

The third term of equation (4-4) represents the rotation-vibration interaction term in which $\hbar\omega_\beta$ and $\hbar\omega_\gamma$ are the vibrational quanta associated with the β and γ vibrations respectively. The off-diagonal terms of the Hamiltonian arising from H_c are

$$\begin{aligned} \langle IK' | H_c | IK \rangle = & - \delta_{K', K+1} \{ (I-K)(I+K+1) \}^{1/2} \\ & \times \frac{\hbar^2}{2J} \left[\sum_j c_j^K c_j^{K'} \{ (j-K)(j+K+1) \}^{1/2} \right] \text{ for } K' \geq K \neq 1/2 \end{aligned} \quad (4-5)$$

$$\langle IK' | H | IK \rangle = - \delta_{K, 1/2} (I+1/2) \frac{\hbar^2}{2J} \sum_j (-1)^{I-j} c_j^K c_j^{K'} (j+1/2)$$

$$\text{for } K = K' = 1/2$$

The coefficients c_j^K can be calculated from the tables of wave functions prepared by Nilsson (Ni 55).

In accord with the work of Broude et al (Br 58) and Ejiri (Ej 64) a negative deformation $\eta = -3$ was chosen in the present calculation. This choice is consistent with the experimentally determined magnetic moment $\mu = 1.13$ n.m. (Br 58) and with the level sequence of P^{31} and P^{29} (See figure (4-10)). Following Ejiri the β and γ vibration terms were chosen as $\hbar\omega_\beta = \hbar\omega_\gamma = 20$ MeV with $\frac{\hbar^2}{2J} = 0.400$ MeV. In the calculation of the energy levels the ground state of P^{31} was identified as the first member of a rotational band based on Nilsson orbit 9 and

the excited states were calculated taking into account the $K = 3/2$ and $K = 1/2$ Nilsson orbits 8 and 11 respectively. Using reasonable values for the energies E_K^P in equation (4-4), the energy levels of P^{31} were calculated by diagonalizing the matrices generated by equations (4-4) and (4-5). The results of these calculations are shown in figure (4-10). It is seen that reasonable agreement is obtained between theory and experiment for the five lowest excited states of P^{31} . A further discussion of the applicability of this model will be given in section (iii).

A comparison of the P^{29} and P^{31} level sequences given in figure (4-10) shows that the low lying positive parity states and the first three negative parity states are very similar. A comparison of the negative parity states in these two nuclei is particularly interesting since the occurrence of a $7/2^-$ state as the first negative parity level can only be interpreted in terms of the Nilsson model if the deformation is negative (See figure (2-11) and references (Br 57) (Mc 65)). Also it is seen that the negative parity states in P^{31} at 4.43, 5.01 and 6.48 MeV have excitation energies that are consistently about 1 MeV higher than the corresponding levels at 3.47, 4.34 and 5.53 MeV in P^{29} . This suggests that the deformation η for P^{31} is less than that for P^{29} as can be seen by inspection of the Nilsson diagram, figure (4-11).

The interpretation that the deformation of P^{31} is less than that for P^{29} is consistent with the criterion of Bohr and Mottelson (Bo 55) for the transition from rotational to vibrational motion, viz. rotational spectra are to be expected for even A nuclei if the first 2^+ excited

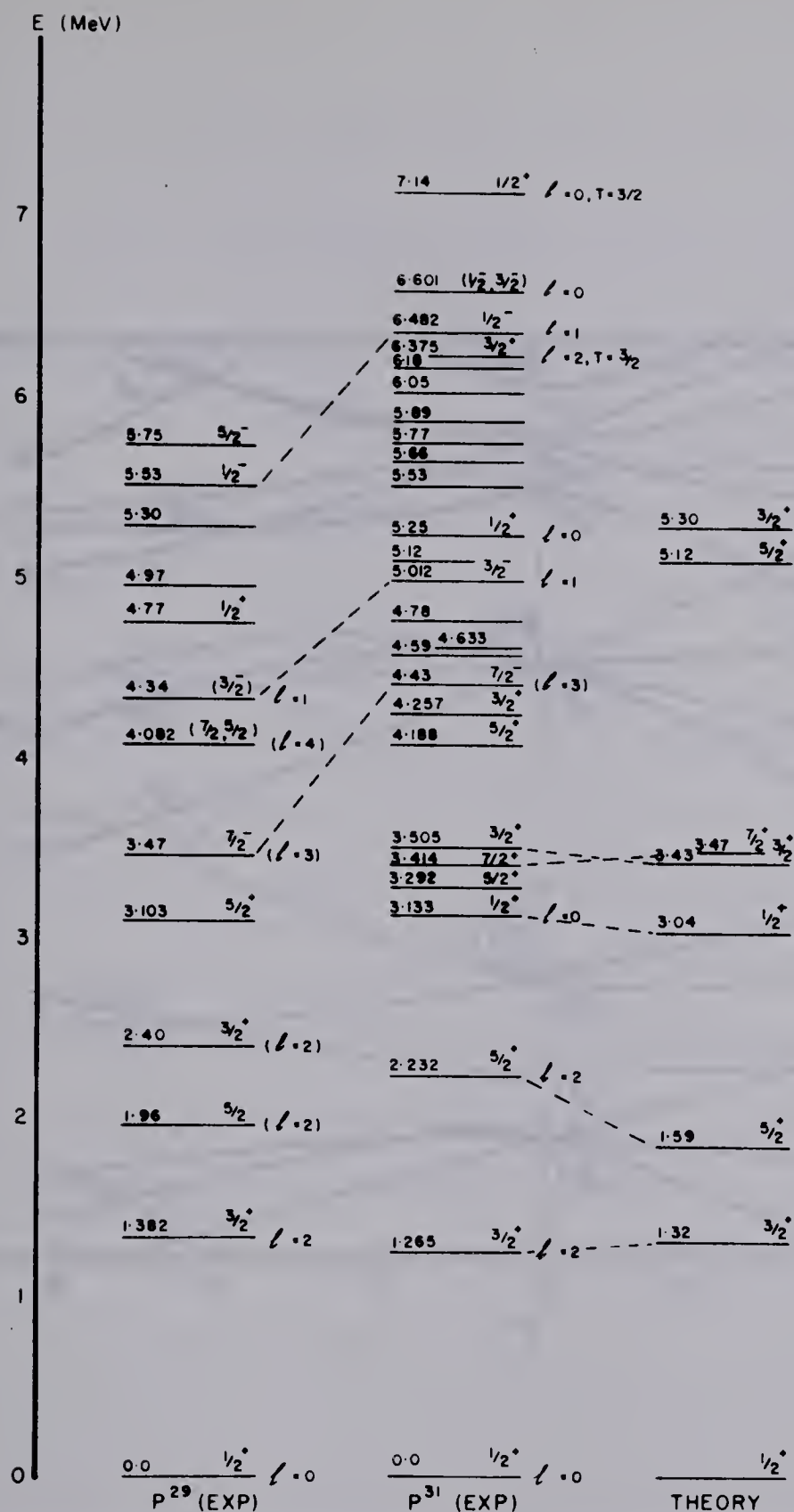


Figure 4-10 Energy level diagram of P^{31} and P^{29} showing the similarities in the structure of the two nuclei. The level diagram marked theory was calculated using the Nilsson model with $\hbar^2/(2\mathcal{I}) = 0.400$, $\hbar\omega_\beta = \hbar\omega_\gamma = 20$ MeV and $\eta = -3$. The data on the levels of P^{31} were taken from table (4-7). The data on the levels of P^{29} were obtained from references (En 62) and (Ej 64).

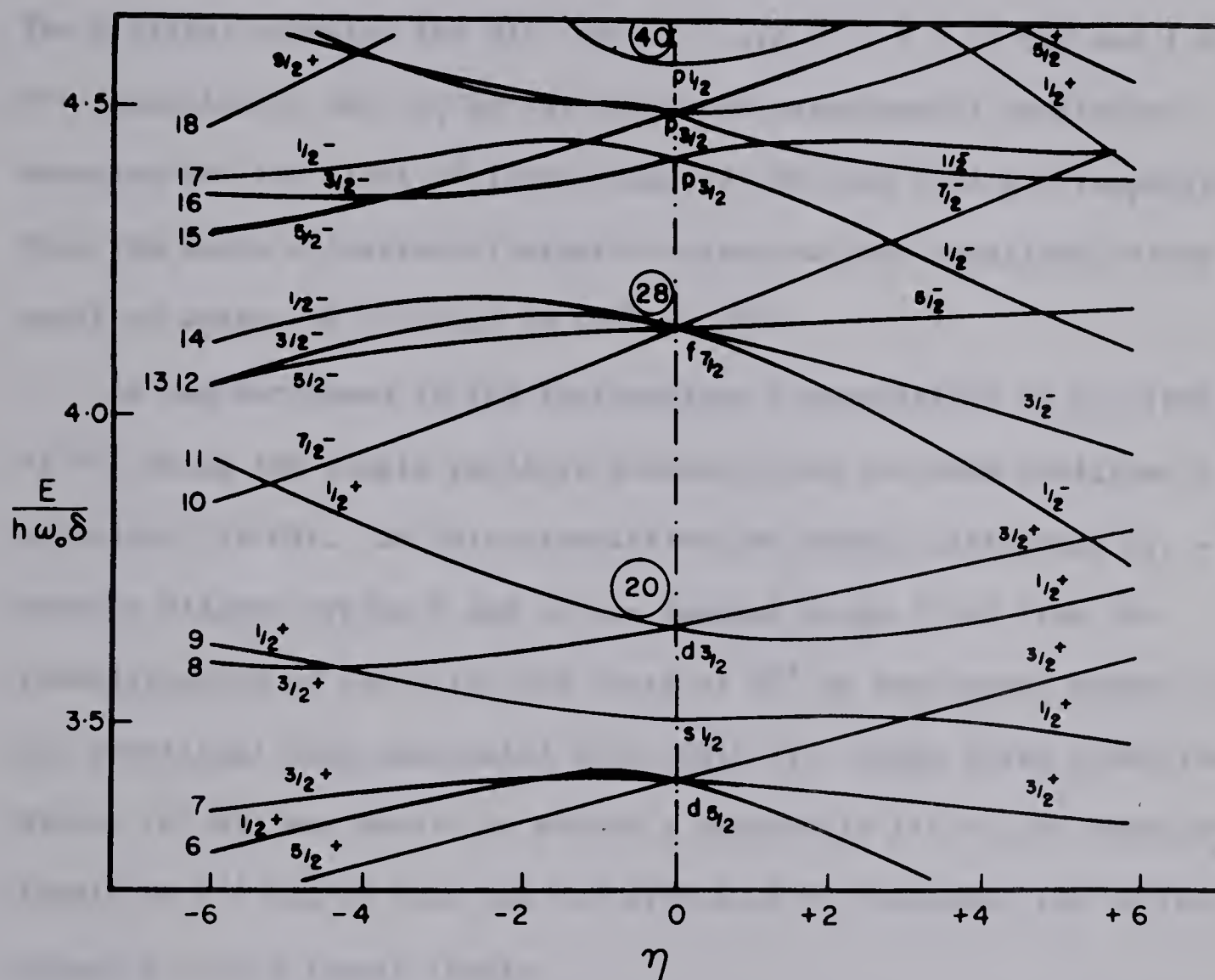


Figure 4-11. Single particle energy levels of the Nilsson model (Ni 55) as a function of the deformation η .

state has an excitation energy less than the critical value

$$E(2) = 32\hbar^2 / (MAR_0^2) = 3\hbar^2 / (0.23 \mathcal{I}_{\text{rigid}}) \quad .$$

The critical energies for Si^{28} and Si^{30} are $E(2) = 2.22$ MeV and 1.85 MeV respectively (Br 57, Ej 64) while the experimental excitation energies for the first 2^+ levels are 1.77 MeV and 2.23 MeV respectively. From the above criterion it might be expected that rotational effects would be weaker in P^{31} than in Si^{29} or P^{29} .

As was mentioned in the introduction a calculation of the levels of P^{31} using the single particle Nilsson model has been published recently by Bishop (Bi 65). In this calculation the energy difference $E_{11} - E_9$ between Nilsson orbits 9 and 11 was assumed to be 3 MeV from the identification of the 3.133 MeV state of P^{31} as the lowest member of the rotational band associated with orbit 11. Under these conditions Bishop (Bi 65) was unable to obtain a reasonable fit to the experimental levels of P^{31} and in fact was not even able to reproduce the correct sequence of the lowest levels.

An asymmetric core collective model calculation for both P^{29} and P^{31} has been made by Chi and Davidson (Ch 63). This calculation reproduces the energy levels for Si^{29} and P^{29} quite accurately up to 3.5 MeV of excitation but does not predict the negative parity level at 3.47 MeV in P^{29} . The first three levels of P^{31} are also accurately predicted. However this model does not predict the existence of a second $1/2^+$ level in the region of excitation up to 5 MeV. It does however predict a $7/2^+$

level in the region of 3 - 4 MeV of excitation as does the symmetric core Nilsson model calculation discussed above. Consequently there seems to be little advantage in introducing the extra complexity of the asymmetric core model at this time.

Since only fair agreement could be obtained with the single particle Nilsson model Dr. K. Ramavataram undertook a three particle calculation in which the single proton and two neutrons outside the Si^{28} core were assumed to occupy Nilsson orbits 8, 9 and 11. Properly antisymmetrized wave functions were constructed and the resulting Hamiltonian matrices diagonalized. At the time of this writing there are not yet sufficient results to allow a comparison with experiment to be made.

(ii) The Weak Coupling or Vibrational Model

The Hamiltonian for a system consisting of a single particle weakly coupled to a vibrating core can be written as (Ra 63), (Ej 64)

$$H = H_p + H_c + H_{int} \quad (4-6)$$

where H_p is the term representing the particle motion, H_c is the surface vibration term and H_{int} is the term representing the particle-surface interaction. Using the creation and annihilation operators for the surface vibrations b_μ^\dagger and b_μ , one can write H_c and H_{int} in the form

$$H_c = (N + \frac{5}{2})\hbar\omega \quad (4-7a)$$

$$H_{int} = -k \left[\frac{\hbar\omega}{2C} \right]^{1/2} \sum_\mu (b_\mu + (-1)^\mu b_{-\mu}^\dagger) Y_{2\mu}(\theta, \phi) \quad (4-7b)$$

where $N = \sum_{\mu} b_{\mu}^{\dagger} b_{\mu}$ is the number of spin two phonons, $\hbar\omega = \hbar(C/B)^{1/2}$ is the phonon excitation energy, C is the surface tension constant and $k = r \frac{\partial V}{\partial r}$ is the strength of the interaction which is usually treated as a constant. The quantity V is the shell model potential for the particle and r is its radial coordinate. The wave functions for the system can be written as

$$\psi_{IM} = \sum_{NRj} a_{NRj} |NRj; IM \rangle$$

where the spin R of the core state is coupled to the particle state j to give a total spin I with z component M . In this representation the Hamiltonian $H_0 = H_p + H_c$ is diagonal and represents the sum of the phonon and single particle energies. The off-diagonal terms in the Hamiltonian matrix arise from the term H_{int} in the Hamiltonian H . In these calculations the parameter Δ is defined as

$$\Delta = \left(\frac{1}{\hbar\omega}\right) [\langle 1d_{3/2} | H_p | 1d_{3/2} \rangle - \langle 2s_{1/2} | H_p | 2s_{1/2} \rangle]$$

which represents the energy difference between the $1d_{3/2}$ and $2s_{1/2}$ subshells, and the particle surface coupling constant q is given by

$$q = k / (2\pi\hbar\omega C)^{1/2}.$$

By diagonalizing the resulting Hamiltonian matrices the excitation energies and the wave functions for spin $I = 1/2, 3/2, 5/2$, and $7/2$ were obtained for various values of Δ and q . Phonon excitations up to $N = 3$ were allowed in these calculations.

The results of this calculation are shown in figure (4-12) for $\Delta = 1.2$, $q = 1.9$, and $\hbar\omega = 2.4$ MeV. It is seen that the weak coupling model gives a reasonable description of P^{31} up to 4 MeV of excitation.

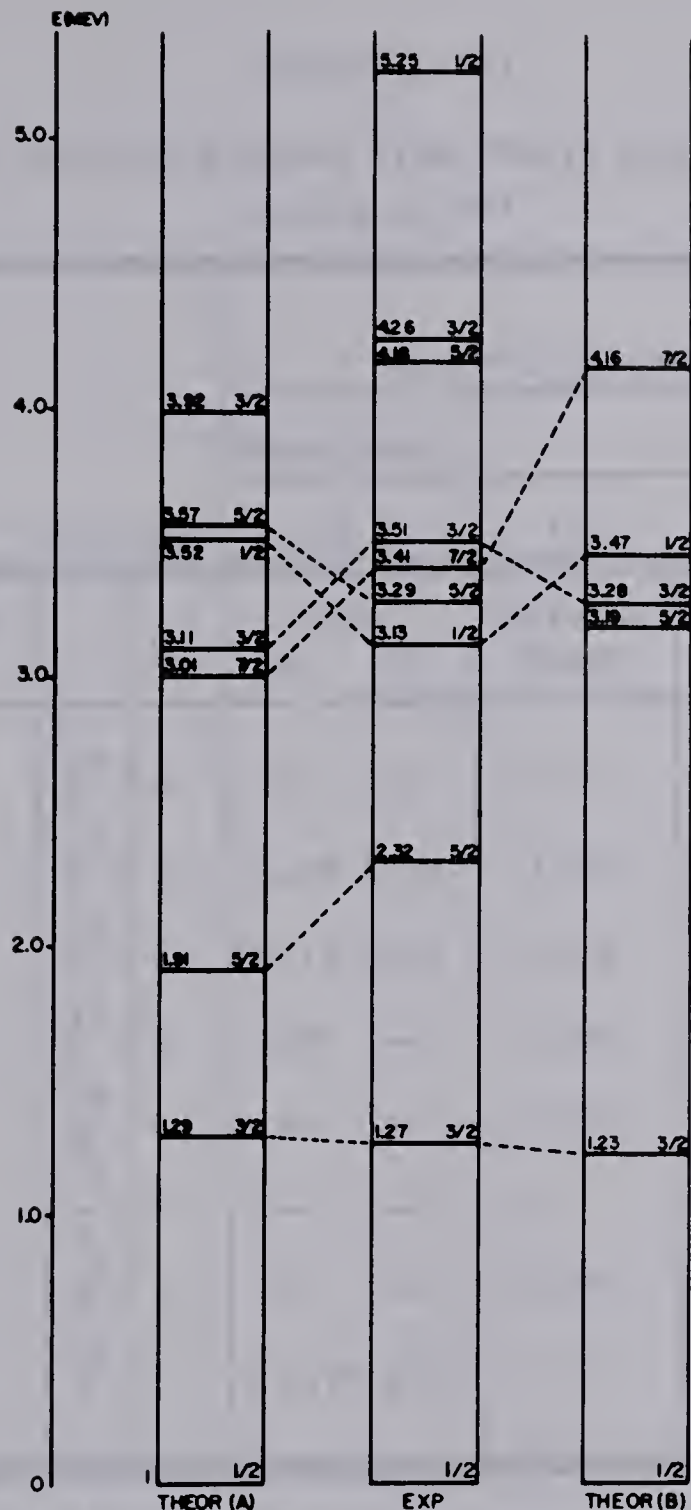
A similar vibrational model calculation taking into account core excitations up to 3 phonons was made by Thankappen (Th 62) yielding a level sequence very similar to that obtained in the calculation discussed above.

(iii) Discussion

The spectroscopic factors for the low lying states of P^{31} have been computed using the wave functions obtained in the Nilsson model and vibrational model calculations discussed in the preceding sections (Ra 65). A summary of the theoretical and experimental spectroscopic factors obtained above as well as those obtained by Glaudemans (Gl 64) for the shell model is given in table (4-10).

The spectroscopic factor for the first excited state relative to the ground state obtained from the DWBA analysis indicates that the ground state of P^{31} does not carry the full single particle strength for the $2s_{1/2}$ transition. This result is not in quantitative agreement with the predictions of either the vibrational model or the shell model. In particular the vibrational model predicts a vanishing spectroscopic factor for the $5/2^+$ level at 2.232 MeV of excitation while the experimental value of the spectroscopic factor is $S_{rel} = 0.76$ at $E_d = 5$ MeV. In the vibrational model this level arises from the coupling of vibrational states to the odd proton in the $2s_{1/2}$ orbit (Th 60) so that no single

ENERGY LEVELS OF P^{31}



(A) ENERGY LEVELS PREDICTED BY THE PHONON MODEL;
 $q = 1.9$, $\Delta = 1.2$; $\hbar\omega = 2.1$ MEV
 (B) SHELL MODEL PREDICTIONS, ASSUMING A Si^{28} CORE.
 ALL THE ABOVE LEVELS HAVE POSITIVE PARITY

Figure 4-12. Energy levels of P^{31} compared with the predictions of (a) The vibrational model. (b) The shell model.

TABLE (4-10)

Spectroscopic Factors Obtained from Theory and Experiment for the
Levels of p^{31}

(1) (2) (3) (4)				Relative Spectroscopic Factor			
				Experiment		Theory	
				(5)	(6)	(7)	(8)
Level	Excitation Energy	J	ℓ_p	DWBA (a) (b)	Nilsson Model	Vibrational Model	Shell Model
0	0	$\frac{1}{2}^+$	0	1.0 1.0	1.0	1.0	1.0
1	1.265	$\frac{3}{2}^+$	2	1.98 1.70	1.54	0.7	0.63
2	2.232	$\frac{5}{2}^+$	2	0.76 0.53	0.46	0	0
3	3.133	$\frac{1}{2}^+$	0	0.07 --	0.16	0.06	0.038
4	3.292	$\frac{5}{2}^+$	-	-- --	0.01	0	0
5	3.414	$\frac{7}{2}^+$	-	-- --	0	0	0
6	3.505	$\frac{3}{2}^+$	-	-- --	0.27	0.20	0.59
15	5.25	$\frac{1}{2}^+$	0	0.19 0.13	--	0.03	--

The information in columns (1) to (8) is derived from the following sources:

- (1), (2), and (3) from references (Er 62), (Ha 63), (Ha 64), (En 64)
 (4), (5), (6), and (7) from the present work
 (8) from (Gl 64)

Sub-column (a) of column (5) refers to the work at $E_d = 5$ MeV

Sub-column (b) of column (5) refers to the work at $E_d = 4$ MeV.

particle strength is available for stripping to this level. The shell model calculation of Glaudemans et al (Gl 64) does not predict a $5/2^+$ level in this region of excitation which indicates that a hole state may be important in the formation of this level. However the DWBA results are in fairly good agreement with the predictions of the Nilsson model, a result which is not altogether unexpected since in the Nilsson model the deformed potential well causes mixing of the $1d_{5/2}$, $2s_{1/2}$ and $1d_{3/2}$ orbits. The weak-coupling model calculation given above does not appear to have core states which properly take into account the excitations of the $d_{5/2}$ nucleons into the $s_{1/2}$ and $d_{3/2}$ orbits. The weak-coupling model could possibly be improved by assuming a Si^{30} core in which a proton could be excited from the $1d_{5/2}$ sub-shell into the $2s_{1/2}$ or $1d_{3/2}$ sub-shells. It is also clear from the work of Glaudemans et al (Gl 64) that configurations in which nucleons in the $d_{5/2}$ sub-shell are allowed to be excited into the $s_{1/2}$ and $d_{3/2}$ sub-shells must be included in a shell model calculation if a substantial improvement in the correspondence with experiment is to be obtained for P^{31} .

That "hole" states are important in the description of P^{31} has been pointed out by Clegg and Foley (Cl 62) who identified the 1.26 ($3/2^+$) MeV state of P^{31} as a hole state corresponding to Nilsson orbit 7 and the 3.29 ($5/2^+$) MeV state of P^{31} as a hole state corresponding to Nilsson orbit 5. The evidence for these assignments was based on a study of the $S^{32}(p,2p)P^{31}$ reaction in which the 1.26 and the 3.29 MeV states were strongly excited with cross-sections of 36 ± 8 mb and 34.5 ± 5 mb

respectively. The large cross section obtained for the 1.26 MeV state is incompatible with the large stripping width obtained in the present experiment. The spectroscopic factor for this level obtained at $E_d = 5$ MeV is $S_{abs} = 0.4 \pm 0.2$ ($S_{rel} = 2.0 \pm 0.5$) which indicates that the 1.26 MeV level carries a fairly large proportion of the $d_{3/2}$ single particle strength. This is not consistent with the interpretation that the 1.26 MeV state in P^{31} as a hole state. Although the 3.29 MeV state could not be analysed in the present experiment, its intensity is less than 1/20 of that of the 1.26 MeV state and could reasonably be interpreted as a hole state arising from the excitation of a proton from Nilsson orbit 5.

The negative parity states in P^{31} at 4.43(7/2⁻), 5.012(3/2⁻) and 6.482(1/2⁻) and the states in P^{29} at 3.47(7/2⁻), 4.34(3/2⁻) and 5.53(1/2⁻) can be identified with the $1f_{7/2-}$, $2p_{3/2-}$ and $2p_{1/2-}$ single particle states of the j-j coupling shell model. This model predicts a 5/2⁻ level lying between the 3/2⁻ and 1/2⁻ levels. A 5/2⁻ level is observed in P^{29} at 5.75 MeV of excitation which is consistent with this interpretation. At this time no $J^\pi = 5/2^-$ level has been reported in P^{31} . However on the basis of the present discussion a $J^\pi = 5/2^-$ level should exist in the region of excitation between 6 and 8 MeV.

The above discussion also applies to the vibrational model but in this case the surface vibration states couple with the single particle states. It is still reasonable to identify the 7/2⁻ and 3/2⁻ states as the $1f_{7/2-}$ and $2p_{3/2-}$ single particle states. However the odd parity

states at higher excitation (i.e. the $1/2^-$ level at 6.48 and the ($1/2^-$ or $3/2^-$) level at 6.601 MeV in P^{31}) may have mixed phonon and particle modes of excitation.

A similar discussion also applies in the case of the Nilsson model. In this case the $7/2^-$, $3/2^-$ and $1/2^-$ levels can be identified with Nilsson orbits 10, 13, and 14. A $5/2^-$ level corresponding to Nilsson orbit 12 is also expected in this region of excitation but because of band mixing it is not possible to estimate the ordering of these levels. Ejiri (Ej 64) identifies the levels of P^{29} at 3.47 ($7/2^-$), 4.34 ($3/2^-$) and 5.75 ($5/2^-$) with Nilsson orbits 16 and 12 originating in the $f_{7/2^-}$ and $p_{3/2^-}$ shell model states. A similar interpretation could also be made for the corresponding states in P^{31} .

In conclusion it can be said that the overall agreement between the results obtained in this experiment and the predictions of the Nilsson model indicates the applicability of the strong coupling collective model to a description of the P^{31} nucleus. It would be interesting to compare the results of the present analysis with the predictions of a three particle Nilsson model calculation or with the results of a vibrational model or shell model calculation which includes hole states obtained by exciting a $d_{5/2}$ proton into the $s_{1/2}$ or $d_{3/2}$ sub-shells. In this respect it appears that a much more extensive experimental investigation of the existence of hole states is warranted. It would also be worthwhile to investigate the stability of the spectroscopic factors obtained from the (d,n) reaction at higher bombarding energies where

interference from reaction mechanisms other than the direct interaction should be considerably reduced. Finally a somewhat more rigorous comparison of the negative parity levels of P^{29} and P^{31} with the predictions of the various nuclear models might further clarify the roles played by these models in the description of the nuclei in the d-s shell around $A = 28$.

APPENDIX I

THE STATISTICAL ANALYSIS OF EXPERIMENTAL DATA

I.1 Introduction

The advent of the modern pulse height analyser has facilitated the collection of enormous amounts of experimental data. This has forced the physicist to employ automatic methods for the reduction and analysis of this data. An important by-product of this automation has been the development of objective statistical methods for the analysis of the data.

This section describes five programs written by the author for the analysis of experimental data, the theory associated with these programs and a discussion of the applicability of the methods to the analysis of experimental data.

I.2 The Statistics of Nuclear Events

Most experiments in nuclear physics involve counting nuclear radiations as a function of the space-time coordinates. The probability that m nuclear events will be counted in a given interval $\delta\Omega$ of the coordinates is quite accurately given by the Poisson distribution (Ev 59). This probability distribution is a limiting case of the binomial distribution in which $n \rightarrow \infty$ and $p \rightarrow 0$ in such a way that the

product $np = a$ where a is a constant of finite magnitude, n is the total number of "trials" and p is the probability of a success in any individual trial. The results of this limiting process in the probability function

$$P(m) = \frac{a^m e^{-a}}{m!} \quad . \quad (I-1)$$

Thus the Poisson distribution represents the situation in which a very large number of "trials" are required to produce a small but finite number of events.

The expectation value and the variance of the distribution are easily shown to be (Ke 51):

$$E(m) = \sum_{m=0}^N mP(m) = a$$

$$\text{Var}(m) = \sum_{m=0}^N m^2 P(m) - a^2 = a.$$

Therefore the standard deviation of the Poisson distribution is $\sigma = (a)^{1/2}$. It is also seen that $\sum_{m=1}^{\infty} P(m) = 1$ as required if $P(m)$ is a probability distribution.

The problem the physicist encounters in the analysis of experimental data is the translation of the N experimental measurements into the physical parameters involved in the theory used to describe the nuclear processes.

In order that maximum value be obtained from the experimental data, optimum methods of estimating these parameters must be used. Couched in statistical language, this says that one wants to find the most probable or "maximum likelihood" values for the parameters.

I.3 The Likelihood Function and the Method of Maximum Likelihood

Consider an experiment in which N statistically independent measurements were made, each measurement with a probability distribution $P(\underline{a}; \underline{x})$ where $\underline{a} = a_1, a_2, a_3, \dots, a_m$, and $\underline{x} = x_1, x_2, \dots, x_p$. The quantities \underline{a} are parameters of the probability distribution (mean, standard deviation, etc.) and the quantities \underline{x} are the coordinates of the distribution (time, solid angle, or distance, etc.). If each measurement is statistically independent of the others, then the probability of obtaining exactly the result given by the N measurements is

$$L(\underline{a}; \underline{x}) = P(\underline{a}; \underline{x}) = P_1(\underline{a}; \underline{x}) P_2(\underline{a}; \underline{x}) \dots P_N(\underline{a}; \underline{x}) = \prod_{i=1}^N P_i(\underline{a}; \underline{x}_i) \quad (\text{I-2})$$

The quantity L is known as the likelihood function for the experiment.

In order to obtain information about the physical parameters in the theory there must be a functional relationship between these parameters and the physical measurements. Suppose that the N measured quantities μ_i with standard errors σ_i are related to s theoretical parameters α_λ by the function

$$\xi = \xi(\alpha_1, \alpha_2, \dots, \alpha_p; x_1, x_2, \dots, x_m)$$

For convenience suppose that the measurements μ_i have Gaussian probability distributions with standard deviations σ_i . Then the likelihood function has the form

$$L(\underline{\alpha}) = \prod_{i=1}^N \frac{1}{\sqrt{2\pi} \sigma_i} \exp \left(-\frac{(\mu_i - \xi_i)^2}{2\sigma_i^2} \right)$$

$$= \frac{1}{(2\pi)^{N/2} \sigma_1 \sigma_2 \dots \sigma_N} \exp \left(-\sum_{i=1}^N \frac{(\mu_i - \xi_i)^2}{2\sigma_i^2} \right) \quad (I-3)$$

for the parameters $\underline{\alpha}$.

Estimates of the parameters α_λ must be found that maximize the probability that they be as close as possible to their true values. This can be done by maximizing the likelihood function with respect to the parameters α_λ that are to be determined. This is equivalent to minimizing the exponent; therefore the maximum likelihood values of the parameters α_λ are given by

$$F(\underline{\alpha}, \underline{x}) = \frac{d}{d\alpha_\lambda} \ln(L(\underline{\alpha}))$$

$$= \sum_{i=1}^N \frac{(\mu_i - \xi_i)}{\sigma_i^2} \frac{\partial \xi_i}{\partial \alpha_\lambda} = 0 \quad (I-4a)$$

where $\lambda = 1, 2, \dots, P$.

The sum

$$\sum \frac{(\mu_i - \xi_i)^2}{2\sigma_i^2} = \frac{1}{2} \chi^2(\alpha_\lambda) \quad (\text{I-4b})$$

and the result is therefore called a least-squares fit.

It is shown by Janossy (Ja 65) and Keeping (Ke 51) that the form

$$F(\underline{\alpha}; \underline{x}) = \frac{d}{d\alpha_\lambda} \ln L(\underline{\alpha}; \underline{x}); \lambda = 1, 2, \dots, P \quad (\text{I-5})$$

is of general applicability for functions that have nearly Gaussian probability distributions (for example, the Poisson, Bernouli and chi-square distributions).^{†*}

[†]Keeping gives sufficient conditions for a distribution to be "nearly Gaussian." Under these conditions the maximum likelihood method is the most efficient method of estimation of the parameters.

*The maximum likelihood method is most generally derived from the condition that the standard error of the estimates of the parameters be a minimum. This result can be obtained by minimizing Fisher's inequality which states that

$$\text{var}(T) \geq \frac{1}{\int_{-\infty}^{\infty} \frac{\partial \ln L(T)}{\partial T} L(T) dx}$$

where T is a statistic being measured by the sample N .

I.4 The Maximum Likelihood Method for the Poisson Distribution

As previously stated, the counting experiments encountered in nuclear physics obey Poisson statistics. The probability of obtaining n counts in a given measurement is

$$P(n) = \frac{(\bar{n})^n e^{-\bar{n}}}{n!}$$

Therefore, the likelihood function for obtaining a given result for N measurements is

$$L = \prod_{i=1}^N P_i(n) = \prod_{i=1}^N \frac{e^{-\bar{n}_i} (\bar{n}_i)^{n_i}}{n_i!} \quad (\text{I-6})$$

If the expectation values \bar{n}_i are related to the theoretical parameters by the function $\bar{n}_i = \xi_i = \xi_i(\underline{\alpha}; \underline{x})$, then the likelihood function for the parameters α_λ becomes

$$L = \prod_{i=1}^N \frac{e^{-\xi_i} \xi_i^{\mu_i}}{\mu_i!} \quad (\text{I-7})$$

in analogy with equation 3.

The function $F(\underline{\alpha}; \underline{x})$ for obtaining the Maximum likelihood values of the parameters α_λ is therefore

$$\begin{aligned} F(\underline{\alpha}; \underline{x}) &= \frac{\partial}{\partial \alpha_\lambda} \ln L(\underline{\alpha}) = \frac{\partial}{\partial \alpha_\lambda} \ln \left[\prod_{i=1}^N \frac{e^{-\xi_i} \xi_i^{\mu_i}}{\mu_i!} \right] \\ &= \frac{\partial}{\partial \alpha_\lambda} [-\xi_i + \mu_i \ln \xi_i - \ln(\mu_i!)] = \sum_i \left(1 - \frac{\mu_i}{\xi_i} \right) \frac{\partial \xi_i}{\partial \alpha_\lambda} = 0 \end{aligned} \quad (\text{I-8})$$

$$\lambda = 1, 2, \dots, P$$

which generally forms a nonlinear system of equations in the parameters α_λ . In most cases these equations can only be solved by iterative numerical methods. Consequently one would like to find a method of linearizing the equations while maintaining reasonable accuracy. To obtain the desired linearization, $\partial\mu_i$ is defined by the equation $\mu_i = \xi_i + \partial\mu_i$.

Therefore

$$\frac{\mu_i}{\xi_i} = 1 + \frac{\partial\mu_i}{\xi_i}$$

Similarly

$$\frac{\xi_i}{\mu_i} = \frac{\xi_i}{\xi_i + \partial\mu_i} = \left(1 - \frac{\partial\mu_i}{\xi_i} + \dots\right)$$

Hence

$$1 - \frac{\mu_i}{\xi_i} = - \left(1 - \frac{\xi_i}{\mu_i}\right)$$

to first order.

This gives us a system of linear equations

$$\sum_i \left(1 - \frac{\xi_i}{\mu_i}\right) \frac{\partial \xi_i}{\partial \alpha_\lambda} = 0 \quad (I-9)$$

which are identical to the least squares equations above if $\sigma_i^2 = \mu_i$, which is true for the Poisson distribution.

Thus it is seen that the method of least squares can be used for estimating the physical parameters of a theory when the probability

distribution of the experimental measurements is Poisson subject to the condition that $(\partial \mu_i / \xi_i)^2 \ll 1$.

I.5 Formulation of the Least Squares Problem

The maximum likelihood equations derived in the last section have been shown to be identical to the well known least-squares method. In this section the least-squares method will be treated generally so that the case when ξ is a nonlinear function of the parameters α_λ can be treated as well as the case when ξ is a linear function of the parameters.

To show the connection between the linear and nonlinear cases and to familiarize the reader with the notation being used, the linear problem will be treated in detail even though it is well known.

(i) The Linear Case

Suppose the function ξ can be written as

$$\xi_i = \sum_{\gamma} \alpha_{\gamma} P_{i\gamma} \quad (\text{I-10})$$

and setting $\omega_i = 1/\sigma_i^2$ then the least squares equations can be written as

$$\frac{\partial}{\partial \alpha_{\lambda}} \chi^2 = \sum_i \omega_i (\mu_i - \sum_{\gamma} \alpha_{\gamma} P_{i\gamma}) P_{i\lambda} = 0 \quad (\text{I-11})$$

$$\text{or } \sum_i \omega_i \mu_i P_{i\lambda} = \sum_i \sum_{\gamma} \omega_i \alpha_{\gamma} P_{i\gamma} P_{i\lambda}. \quad (\text{I-12})$$

Equation 12 has the appearance of a matrix equation $X = C\alpha$. If we set

$$\chi_{\lambda} = \sum_i \omega_i \mu_i P_{i\lambda} \quad \text{where } \chi_{\lambda} \text{ is a column vector and} \quad (\text{I-13})$$

$$C_{\lambda\gamma} = C_{\gamma\lambda} = \sum_i \omega_i P_{i\gamma} P_{i\lambda} \quad \text{with } \alpha_{\gamma} = \alpha \quad (\text{I-14})$$

then the matrix properties can be directly verified. That is

$$X_{\lambda} = \sum_{\gamma} C_{\lambda\gamma} \alpha_{\gamma} \quad (\text{I-15})$$

Therefore $X = C\alpha$ with the parameters α given by

$$\alpha = C^{-1}X \quad (\text{I-16})$$

The variance and covariance of each parameter α_{λ} can be obtained most easily by imagining that the experiment is carried out a large number of times in exactly the same way. The generalized variance is

$$\sigma_{m\ell} = \langle (\alpha_m - \bar{\alpha}_m)(\alpha_{\ell} - \bar{\alpha}_{\ell}) \rangle \quad (\text{I-17})$$

From equations (I-13) and (I-15) $(\alpha_m - \bar{\alpha}_m)$ can be written as

$$(\alpha_m - \bar{\alpha}_m) = \sum_k (C^{-1})_{mk} (X_k - \bar{X}_k) = \sum_{kj} (C^{-1})_{mk} \omega_j P_{jk} (\mu_j - \bar{\mu}_j)$$

$$\text{Now, } \langle (\mu_j - \bar{\mu}_j)(\mu_i - \bar{\mu}_i) \rangle = \sigma_i^2 \delta_{ij}$$

since the μ_j 's are assumed to be statistically independent. Thus

$$\langle (\alpha_m - \bar{\alpha}_m)(\alpha_{\ell} - \bar{\alpha}_{\ell}) \rangle = \sum_{kjnl} (C^{-1})_{mk} \omega_j P_{jk} (C^{-1})_{\ell n} \omega_i P_{in} \sigma_i^2 \delta_{ij}$$

$$= \sum_{kn} (C^{-1})_{mk} (C^{-1})_{\ell n} C_{nk} = (C^{-1})_{m\ell}$$

Hence the variance is $\sigma(\alpha_m) = \langle (\alpha_m - \bar{\alpha}_m)^2 \rangle = C_{mm}^{-1}$ (I-18)

and the covariance is

$$\sigma(\alpha_m, \alpha_\ell) = \langle (\alpha_m - \bar{\alpha}_m)(\alpha_\ell - \bar{\alpha}_\ell) \rangle = C_{m\ell}^{-1} \quad (\text{I-19})$$

In section III it was seen that the least squares condition was the same as the maximum likelihood result if the likelihood function was a product of Gaussian distributions. The maximization of the likelihood function was also seen to be equivalent to the minimization of the expression

$$\chi^2 = \sum_i \omega_i (\mu_i - \xi_i)^2.$$

We will now investigate the relationship between the minimum value of χ^2 and the goodness of fit. Later this will be seen to be an important criterion in estimating the total error of the resultant parameters.

Following Mathews and Walker (Ma 64) we assume that the true values of parameters α are known. The function ξ then becomes

$$\xi_i^\circ = \xi(\alpha_1^\circ, \alpha_2^\circ, \dots, \alpha_p^\circ, \underline{x}).$$

Replacing ξ by ξ° in the likelihood function, eqn. (I-3), we obtain the normalized probability function

$$P(\mu_1, \mu_2, \dots, \mu_N) dx_1 dx_2 \dots dx_N = \prod_{i=1}^N \frac{1}{\sqrt{2\pi} \sigma_i} \exp - \frac{(\mu_i - \xi_i^\circ)^2}{2\sigma_i^2} dx_i \quad (\text{I-20})$$

Making the change of variable $q_i = (\chi_i - \xi_i^0)/\sigma_i$

then

$$Q(q_i)d\mathbf{q} = P(\mu_i)d\mathbf{\mu} = \left(\frac{1}{2\pi}\right)^{N/2} \exp\left(-\frac{1}{2} \sum_{i=1}^N q_i^2\right) d\mathbf{q} . \quad (\text{I-21})$$

Now, Q depends on q_i only through the relation

$$\chi^2 = \sum_{i=1}^N q_i^2$$

which has the same value everywhere on the N dimensional spherical surface in q space. (Note that since the μ_i are statistically independent the space is orthogonal.)

Therefore χ^2 must have the form $\chi + d\chi$

$$F(\chi^2)d\chi^2 = F(\chi^2)2\chi d\chi = \int_{\chi}^{\chi+d\chi} Q(q_i)d\mathbf{q} = 2A e^{\chi^2/2} \chi^{N-1} d\chi \quad (\text{I-22})$$

Spherical Shell

where the constant A is determined by the normalization criterion

$$\int_0^\infty F(\chi^2)d\chi^2 = A \int_0^\infty e^{z/2} z^{(N/2)-1} dz.$$

Thus

$$A = \frac{1}{[2^{N/2} \Gamma(N/2)]} . \quad (\text{I-23})$$

Hence

$$F(\chi^2)d\chi^2 = \frac{1}{2^{N/2} \Gamma(N/2)} e^{-\chi^2/2} (\chi^2)^{(N/2)-1} d\chi^2 \quad (\text{I-24})$$

which is the χ^2 distribution (Ke 51) with N degrees of freedom. This function is directly related to Pearson's γ distribution (Ke 51).

The probability that χ^2 exceeds the observed value χ_0^2 is

$$P_N(\chi^2 > \chi_0^2) = \int_{\chi_0^2}^{\infty} F(\chi^2) d\chi^2 \quad (I-25)$$

If the probability of χ^2 exceeding the value χ_0^2 is large, then the fit is good.

In the case where the values of ξ_1 are estimated from the distribution itself, the number of degrees of freedom is $n = N - p$ where p is the number of free parameters.

Keeping (Ke 51) shows that

$$S^2 = \chi^2 / (N-p) \quad (I-26)$$

is an unbiased estimate of σ^2 the variance of the fit. This result does not depend on the distribution being Gaussian.

By a similar argument to the one given above for the statistical error, Rose (Ro 53) shows that the mean square deviation of the least-squares result to the "true" value of the parameters is related to the variance of the fit. The calculation, which will not be reproduced here, leads to the result

$$\langle (\alpha_Y - \alpha_Y^0)^2 \rangle = \sum_{ij} \langle E_i E_j \rangle \sqrt{\omega_i} \sum_Y C_{\lambda Y}^{-1} P_{iY} \sqrt{\omega_j} \sum_{\lambda} C_{\lambda Y} P_{j\lambda} \quad (I-27)$$

where $E_k = \sum_{\lambda} \alpha_{\lambda}^0 \sqrt{\omega_k} P_{k\lambda} - \sqrt{\omega_k} \mu_k$ which is a normalized residual.

Since E_i and E_j are statistically independent

$$\langle E_i E_j \rangle = \langle E_i^2 \rangle \delta_{ij} = s^2 \delta_{ij} \quad (\text{I-28})$$

where s^2 is taken to be the variance of the fit. (See equation 26).

Hence

$$\langle (\alpha_{\gamma} - \alpha_{\gamma}^0)^2 \rangle = s C_{\gamma\gamma}^{-1} \quad (\text{I-29})$$

This result is called the "total error" in the programs to be discussed.

(ii) The Nonlinear Case

If the function ξ cannot be written as a linear function of the parameters α then it is apparent from the previous work that the elegant matrix formulation cannot be used directly since the system of equations that must be solved is nonlinear in the parameters. Various methods have been attempted in the solution of this problem, but the most efficient method is one attributed to Gauss.*

The general least-squares equations are (Eq. (I-4a))

$$\sum_i \omega_i (\mu_i - \xi_i) \frac{\partial \xi_i}{\partial \alpha_{\lambda}} = 0.$$

The Gauss method consists of expanding the function $\xi(\underline{\alpha}; \underline{x})$ in a Taylor series in the parameters α_{λ} . The expansion is

$$\xi_i = \xi_{i0} + \sum_{\gamma} \left. \frac{\partial \xi_i}{\partial \alpha_{\gamma}} \right|_0 \delta \alpha_{\gamma} + \frac{1}{2} \sum_{\lambda, \eta} \left. \frac{\partial^2 \xi_i}{\partial \alpha_{\lambda} \partial \alpha_{\eta}} \right|_0 \delta \alpha_{\lambda} \delta \alpha_{\eta} + \dots \quad (\text{I-30})$$

*This method is known variously as "Gauss' Method," "Seidel's Method," "Gauss-Seidal Method," and the "Gauss-Newton Method" among others.

where $\xi_{i0} = \xi(\alpha_{10}, \alpha_{20}, \dots, \alpha_{p0}; \underline{x})$

and $\alpha_{\lambda 0}$ is the initial estimate of α_{λ} about which the Taylor series is expanded. If the series is truncated to first order, then

$$\xi_i = \xi_{i0} + \sum_{\gamma} \left(\frac{\partial \xi_i}{\partial \alpha_{\gamma}} \bigg|_0 \right) \delta \alpha_{\gamma}$$

and the generalized least squares equations become

$$\sum_i \omega_i \left[\mu_i - \xi_{i0} - \sum_{\gamma} \left(\frac{\partial \xi_i}{\partial \alpha_{\gamma}} \bigg|_0 \right) \delta \alpha_{\gamma} \right] \left(\frac{\partial \xi_i}{\partial \alpha_{\lambda}} \bigg|_0 \right) = 0. \quad (\text{I-31})$$

Once again the equations can be put in matrix form if we write

$$\sum_i \omega_i (\mu_i - \xi_{i0}) \frac{\partial \xi_i}{\partial \alpha_{\lambda}} \bigg|_0 = \sum_i \sum_{\gamma} \omega_i \left(\frac{\partial \xi_i}{\partial \alpha_{\gamma}} \bigg|_0 \right) \left(\frac{\partial \xi_i}{\partial \alpha_{\lambda}} \bigg|_0 \right) \delta \alpha_{\gamma}.$$

This leads to the definitions

$$X = \sum_i \omega_i (\mu_i - \xi_{i0}) \left(\frac{\partial \xi_i}{\partial \alpha_{\lambda}} \bigg|_0 \right) \quad (\text{I-32})$$

and

$$C_{\gamma\lambda} = C_{\lambda\gamma} = \sum_i \omega_i \left(\frac{\partial \xi_i}{\partial \alpha_{\gamma}} \bigg|_0 \right) \left(\frac{\partial \xi_i}{\partial \alpha_{\lambda}} \bigg|_0 \right) \quad (\text{I-33})$$

with $\alpha_{\lambda} = \delta \alpha_{\lambda}$.

Consequently the same matrix formulation of the problem can be used for both the linear and nonlinear cases. By solving the matrix equation, we

get
$$\delta\alpha_\lambda = C_{\lambda\gamma}^{-1} X_\gamma$$

which leads to
$$\alpha_{1\lambda} = \alpha_{0\lambda} + \delta\alpha_\lambda .$$

This procedure can be iterated by replacing the $\alpha_{0\lambda}$ in the above equation by $\alpha_{1\lambda}$ and resolving the matrix equation until "convergence" is obtained, at which point the $\alpha_{q\lambda}$ are taken as the least-squares estimates of the α_λ .

The convergence requirements can be obtained in at least two ways. The simplest criterion for convergence is to demand that the gradient of χ^2 be less than a certain value ϵ . In practice this becomes

$$\left| \chi_{q-1}^2 - \chi_q^2 \right| < \epsilon_1 . \quad (\text{I-34})$$

The second convergence criterion, which can be used in conjunction with the first if desired, is that the current value $\delta\alpha_\lambda$ satisfy the inequality

$$\left| \frac{\partial \alpha_\lambda}{\partial p_\lambda} \right| < \epsilon_2 . \quad (\text{I-35})$$

This is seen to be a more stringent requirement and is often more desirable. However, both methods have been used successfully as will be seen in the discussion of the programs.

The variance and covariance of the parameters α_λ can be found by a parallel argument to the one used in the linear case as will now be shown. Assume that starting values for the α_λ have been chosen, which can always be done, so that the "correct" solution is obtained after one iteration. Since each iteration is independent of the last, the

number of iterations required to find a solution in no way affects the error analysis. The generalized variance can be written

$$\begin{aligned}
 \sigma(\alpha_m, \alpha_\ell) &= \langle (\alpha_m - \bar{\alpha}_m)(\alpha_\ell - \bar{\alpha}_\ell) \rangle \\
 &= \langle (\alpha'_m + \delta\alpha_m - \alpha'_m - \bar{\delta\alpha}_m)(\alpha'_\ell + \delta\alpha_\ell - \alpha'_\ell - \bar{\delta\alpha}_\ell) \rangle \\
 &= \langle (\delta\alpha_m - \bar{\delta\alpha}_m)(\delta\alpha_\ell - \bar{\delta\alpha}_\ell) \rangle. \tag{I-36}
 \end{aligned}$$

Thus on substituting $\delta\alpha_m$ for α_m in the error analysis for the linear case, equations (I-17) through (I-19), we obtain the same expression for the generalized variance, namely

$$\sigma(\alpha_m, \alpha_\ell) = \langle (\alpha_m - \bar{\alpha}_m)(\alpha_\ell - \bar{\alpha}_\ell) \rangle = C_{m\ell}^{-1}. \tag{I-37}$$

This analysis assumes that the same α'_m is sufficiently close to the true solution that one iteration is sufficient to produce convergence for each of the "trial" experiments. This cannot always be the case; however, for good statistics the above analysis should be sufficient. It is shown by Box (Bo 56) that the errors derived by the maximum likelihood principle are slightly different than those given in the present analysis for Gauss' method. It appears, though, that the difference is negligible.

It is evident that an argument similar to the one given by Rose (Ro 53) can be used to find the "total error" of the parameters found by Gauss' method.

It can easily be seen from equation (I-32) that the linear least-squares equations are obtained if the ξ_{i0} are set to zero. Therefore, if the function to be fitted is a linear function of the parameter α Gauss' method can be used by setting the initial estimates of the α_λ to zero. Thus it is seen that the linear problem can always be solved by application of Gauss' method. This is true even if the initial estimates of the parameters are not set to zero.

I.6 General Discussion of the Method of Least Squares

In the previous section the method of least squares has been developed and a discussion of the usefulness and validity of the method has been given. In this section some of the more practical aspects of using the least squares method will be discussed.

The method of maximum likelihood has been shown to be the best method of estimating parameters from experimental data for most of the distributions encountered in physics, though it should be pointed out that the maximum likelihood method is not always the best approach for every problem in measurement. (For a good discussion of this point see Janossy (Ja 65) chapter seven.) Moreover the likelihood equations are often very difficult to solve and approximate methods must be used. As was seen for the case of the Poisson distribution, the method of least squares provided the necessary approximation. In fact for any nearly-Gaussian distribution, the method of least squares will give a reasonable, if not an optimal, answer. However, the method of least squares is often assumed to be optimal and is used when the

method of maximum likelihood gives a more accurate answer by a simpler procedure. A good example of this is in the combination of experimental data from different experiments where the data obeys Poisson statistics (Cr 65). Another example is in the measurement of nuclear decay lifetimes.

Incorrect use of the weighting factors is a frequent cause of poor least squares estimates of parameters. The error most commonly made is when the weights are arbitrarily set to unity. Estimates obtained under these conditions are certainly not optimal and may be grossly inaccurate. Another example in which the method of least squares can give a poor result is the case where the fitted curve must pass through a given point or points (i.e. the origin). This is an example of the general case of the least squares problem with constraints. There is no general method of treating the least squares problem with constraints and no attempt will be made to discuss this problem here. However, one technique that is often satisfactory when a curve must pass through a point or points is to weight the experimental value (perhaps artificially introduced) very heavily at the required point or points. Another technique that is sometimes useful is the method of Lagrange multipliers. This technique must be used with care since the function that is fitted is not the function describing the distribution and erroneous results may occur.

Another situation that must be treated carefully is the case when the weights are functions of the parameters. Janossy (Ja 65) gives a

good discussion of this problem for different probability distributions. A good rule of thumb is to do a least squares fit holding the weights constant, then substitute the "best-fit" parameters into the weights and iterate the fit until the procedure converges. This procedure, however, may not give the maximum likelihood result.

The class of functions that can be fitted by the method of least squares is quite large. The only requirements are that accurate values of the derivatives with respect to the parameters be available and that there are no singularities in the function or its derivatives in the region of parameter space under consideration.

However, even if the above conditions are met, there can still be severe problems encountered in the numerical solution of the equations. This problem is most easily illustrated by considering the case of fitting for the coefficients of non-orthogonal polynomials. Hamming (Ha 62a) shows that for polynomials such as a power series in x or ordinary Legendre polynomials the determinant of the matrix of the normal equations rapidly approaches zero as the degree of the polynomial increases. In fact for a power series in x of seventh degree the determinant has the value 4.8×10^{-25} . Under these circumstances it is very difficult to get accurate estimates of the parameters. Unfortunately the fit is often very good even though the parameters may be grossly in error. This problem arises from the fact that the rows of the C matrix are almost linearly dependent.

Thus when a problem of fitting non-orthogonal polynomials is encountered it is very important to ascertain the degree of linear

dependence of the normal equations. If this is not possible or if it is required that a fit of high degree be obtained, the polynomials should be orthogonalized or be replaced by a set of polynomials that are orthogonal under summation. The above criteria can be summarized as follows: If the functions being fitted are nearly linearly dependent, then difficulty is likely to arise for more than five or six free parameters. If the functions are nearly orthogonal, then a problem with 20 to 30 free parameters should be tractable. In all cases though, care must be taken to determine the validity of the answers.

The final topic that will be discussed is the determination of goodness of fit. The chi-squared criterion was developed in section I.5 and it was shown there that the integral from χ_0^2 to ∞ was a measure of the goodness of fit. This criterion is not convenient for use and a simpler method of determining goodness of fit will be given.

A reasonable criterion may be obtained by considering the maximum likelihood estimate for the expectation value of χ^2 which is

$$E\left[\sum \omega_i (\mu_i - \xi_i)^2\right] = N \text{ as } N \rightarrow \infty$$

From this we see that

$$s^2 = \frac{\chi^2}{(N-P)} \rightarrow 1 \text{ as } N \rightarrow \infty. \quad (\text{I-37})$$

Therefore if the errors in the experimental measurements are purely statistical the value of s^2 should be close to unity. A value of

$s^2 \gg 1$ indicates either that the function being used to fit the data is incorrect or that there was something wrong with the experiment.

Conversely when $s^2 \ll 1$, or in other words when the fit is "too good," this does not imply that the data are very good or that the estimates of the parameters are very accurate, but that there are too many free parameters or that there is some systematic tendency in the data that cannot be accounted for on a purely statistical basis.

I.7 The Error of a Function of Stochastic Variables

A problem which frequently occurs in the analysis of experimental data is the determination of the error of a function when its arguments are stochastic variables. This problem often arises within the least squares problem itself but more frequently in the results calculated from the parameters obtained by a least squares fit.

The so called "calculus of errors" is often applied to this problem but in many cases it is incorrectly used since this procedure is not based on sound statistical theory. In this section a method of calculating the error of a function of stochastic variables will be derived and the connection with the more commonly used "calculus of errors" will be given.

For simplicity let us first assume that $y = f(x)$ where x is a single stochastic variable with mean value μ and variance $\mu_2 = \sigma^2$. That is

$$E(x) = \mu \quad \text{and} \quad E(x^2) - (E(x))^2 = \mu_2 = \sigma^2.$$

Now, let us expand y in a Taylor series about the mean, μ , giving

$$y = f(\mu) + \left. \frac{\partial f(x)}{\partial x} \right|_{\mu} (x-\mu) + \frac{1}{2} \left. \frac{\partial^2 f(x)}{\partial x^2} \right|_{\mu} (x-\mu)^2 + \frac{1}{6} \left. \frac{\partial^3 f(x)}{\partial x^3} \right|_{\mu} (x-\mu)^3 + \dots$$

(I-38)

Therefore the expectation value of y is

$$E(y) = f(\mu) + f^i(\mu)E(x-\mu) + \frac{1}{2} f^{ii}(\mu)E(x-\mu)^2 + \frac{1}{6} f^{iii}(\mu)E(x-\mu)^3 + \dots$$

(I-39)

where

$$f^\lambda(\mu) = \left. \frac{\partial^\lambda f(x)}{\partial x^\lambda} \right|_{\mu}.$$

Similarly y^2 can be expanded in a Taylor series about μ giving

$$\begin{aligned} y^2 = & f^2(\mu) + 2f(\mu)f^i(\mu)(x-\mu) + [f(\mu)f^{ii}(\mu) + (f^i(\mu))^2](x-\mu)^2 \\ & + \frac{1}{3} [f(\mu)f^{iii}(\mu) + 3f^i(\mu)f^{ii}(\mu)](x-\mu)^3 + \frac{1}{12} [f(\mu)f^{iv}(\mu) \\ & + 4f^i(\mu)f^{iii}(\mu) + 3(f^{ii}(\mu))^2](x-\mu)^4 + \dots \end{aligned} \quad (I-40)$$

It is seen that the expectation value of the linear term in each series is always equal to zero since $E(x-\mu) = E(x) - E(\mu) = 0$.

In fact if the distribution of x is approximately normal, then to a good approximation $E(x-\mu)^{2n+1} = 0$

$$\text{for } n = 0, 1, 2, 3, 4, \dots \quad (I-41)$$

and $E(x-\mu)^{2n} = 1 \cdot 3 \cdot 5 \dots (2n-1)^n \mu_2^n$.

Defining $E(x-\mu)^n = \mu_n$ we can write the expectation values of y and y^2 as

$$E(y) = f(\mu) + \frac{1}{2} f^{ii}(\mu) \mu_2 + \frac{1}{6} f^{iii}(\mu) \mu_3 + \frac{1}{24} f^{iv}(\mu) \mu_4 + \dots$$

and

$$\begin{aligned} E(y^2) = & f^2(\mu) + [f(\mu)f^{ii}(\mu) + (f^i(\mu))^2] \mu_2 + \frac{1}{3}[f(\mu)f^{iii}(\mu) \\ & + 3f^i(\mu)f^{ii}(\mu)] \mu_3 + \frac{1}{12}[f(\mu)f^{iv}(\mu) + 4f^i(\mu)f^{iii}(\mu) \\ & + 3(f^{ii}(\mu))^2] \mu_4 + \dots \end{aligned}$$

Hence the variance of y is $E(y^2) - (E(y))^2$ becomes

$$\begin{aligned} \text{Var}(y) = & f^2(\mu) \left[1 + \left(\frac{f^{ii}}{f} + \frac{(f^i)^2}{f^2} \right) \mu_2 + \frac{1}{3} \left(\frac{f^{iii}}{f} + 3 \frac{f^i f^{ii}}{f^2} \right) \mu_3 \right. \\ & \left. + \frac{1}{12} \frac{f^{iv}}{f} + 4 \frac{f^i f^{iii}}{f^2} + 3 \frac{(f^{ii})^2}{f^2} \mu_4 + \dots \right] \\ & - f^2(\mu) \left(1 + \left[\frac{f^{ii}}{f} \mu_2 + \frac{1}{3} \frac{f^{iii}}{f} \mu_3 + \frac{1}{12} \frac{f^{iv}}{f} \mu_4 + \dots \right] \right. \\ & \left. + \left[\frac{1}{2} \frac{f^{ii}}{f} \mu_2 + \frac{1}{6} \frac{f^{iii}}{f} \mu_3 + \frac{1}{24} \frac{f^{iv}}{f} \mu_4 + \dots \right]^2 \right) \\ = & (f^i)^2 \mu_2 + f^i f^{ii} \mu_3 + \left(\frac{1}{3} f^i f^{iii} + \frac{1}{4} (f^{ii})^2 \right) \mu_4. \end{aligned} \quad (\text{I-43})$$

If the distribution of x is normal, this reduces to

$$\text{Var}(y) = (f^i(\mu)^2) \mu_2 + \left(\frac{1}{3} f^i(\mu) f^{iii}(\mu) + \frac{1}{4} (f^{ii}(\mu))^2 \right) \mu_4 + \dots \quad (\text{I-44})$$

To first order equations (I-43) and (I-44) become

$$\text{Var}(y) = (f^i(\mu))^2 \mu_2 = (f^i(\mu))^2 \sigma^2 \quad (\text{I-45})$$

which is identical with the result given by the calculus of errors for a single stochastic variable.

It is seen that the above approximation is a good one if

$$\frac{f^\lambda}{f} \mu_\lambda \rightarrow 0 \quad \text{sufficiently rapidly as } n \rightarrow \infty.$$

The result for a single variable can be easily extended to the case where $y = f(x_1, x_2, x_3, \dots, x_n)$ if all the stochastic variables x_j are statistically independent. From the above considerations we can immediately write down the result

$$\text{Var}(y) = \sum_i \left(\frac{\partial f}{\partial x_i} \bigg|_{\mu_i} \right)^2 \sigma_i^2. \quad (\text{I-46})$$

This analysis shows that the commonly used "calculus of errors" is correct to first order if all of the variables are statistically independent.

The case where $y = f(x_1, x_2, x_3, \dots, x_n)$ and some or all of the variables x_j are statistically dependent can be handled in a similar way. Expanding y and y^2 in a Taylor series as before we obtain

$$y = f + \sum_i \frac{\partial f}{\partial x_i} \bigg|_{\mu_i} (x_i - \mu_i) + \frac{1}{2} \sum_{i,j} \frac{\partial^2 f}{\partial x_i \partial x_j} \bigg|_{\mu_i, \mu_j} (x_i - \mu_i)(x_j - \mu_j) + \dots$$

and

$$y^2 = f^2 + 2 \sum_i f \left. \frac{\partial f}{\partial x_i} \right|_{\mu_i} (x_i - \mu_i) \quad (\text{I-47})$$

$$+ \frac{1}{2} \sum_{i,j} \left. \frac{\partial f}{\partial x_j} \right|_{\mu_i} \left. \frac{\partial f}{\partial x_j} \right|_{\mu_i} + f \left. \frac{\partial^2 f}{\partial x_j \partial x_i} \right|_{\mu_i \mu_j} (x_i - \mu_i)(x_j - \mu_j) + \dots$$

Hence the expectation values of y and y^2 are

$$E(y) = f(\mu_1, \mu_2, \dots, \mu_n) + \frac{1}{2} \sum_{i,j} \left. \frac{\partial^2 f}{\partial x_i \partial x_j} \right|_{\mu_i, \mu_j} \sigma_{ij}^2 + \dots \quad (\text{I-48})$$

$$E(y^2) = f^2(\mu_1, \mu_2, \dots, \mu_n) + \frac{1}{2} \sum_{i,j} \left. \frac{\partial f}{\partial x_j} \right|_{\mu_i} \left. \frac{\partial f}{\partial x_i} \right|_{\mu_i}$$

$$+ f \left. \frac{\partial^2}{\partial x_i \partial x_i} \right|_{\mu_i \mu_i} \sigma_{ij}^2$$

where σ_{ij}^2 is the generalized variance (see equation I-17).

Thus it is easily seen that

$$\text{Var}(y) = \sum_i \sum_j \left. \frac{\partial f}{\partial x_i} \right|_{\mu_i} \left. \frac{\partial f}{\partial x_j} \right|_{\mu_j} \sigma_{ij}^2 \quad (\text{I-49})$$

to first order. The region of validity of this expression is the same as that for the function of a single stochastic variable.

(i) Introduction

This section gives documentation and instruction on the use of five programs written for the SDS 920 computer for the analysis of experimental data with particular application to neutron time-of-flight experiments. Most of the programs are written in a form which should allow their application to other problems with little modification. Extensive use of subroutines has been made to facilitate adaptation of the programs to allow the solution of problems not covered in their present formulation.

(ii) General Purpose Least Squares Program

This program is designed to fit, by the method of least squares, any continuous analytic function to a set of experimentally determined data points. The program is specifically written for a function of a single variable with up to 15 free parameters and 75 input-data sets. The program could be modified to fit m dimensional data without major modification to the mainline program or its subprograms.

Input Data

The input data are punched on up to 23 IBM 80 column cards where the number of cards depends upon the particular problem being solved. Table (I-1) indicates the information contained on each card and the format in which the data must appear. The cards MUST be arranged in the order given in the table. In addition to the input data the user must supply the function subroutine (Subroutine FCT) that generates the particular function to be fitted. A description of this subroutine and the requirements that must be met for its operation will be described under the heading Subroutine FCT.

TABLE (I-1)

Card Set	Symbol	Definition	Format
1		Title card. The first 54 columns beginning with column 1 are available for writing an alphameric title.	54H
2	N $N \leq 15$	The number of free parameters in the fit. Must be right justified in the field.	I4
3	GB	Initial values of the free parameters of the fit. For a linear fit blank cards may be inserted on the SDS 920 and these will be read as zeros. N/3 cards are required.	3E15.8 or 3F15.8
4	M $M \leq 75$	Number of data sets to be input. This is also equal to the number of values of x.	I4
5	X, Y, SD	Each card contains one data set which consists of: (a) the value of X. (b) the value of Y. (c) the standard deviation of Y in absolute units M cards are required.	3E15.8 or 3F15.8

Control Switches

Breakpoint 1 controls typing of the input data: x , y , SD .

BPT 1 SET: types x , y , SD on the console typewriter as the input data is being read.

BPT 1 RESET: does not type input data on read-in.

Breakpoint 2 controls typing of the inverted matrix during the output cycle.

BPT 2 SET: types inverted matrix (matrix C).

BPT 2 RESET: does not type inverted matrix.

Output

A typical output page is shown in figure (I-1). The initial parameters and the input data are typed in the order in which they were input and are given in the same units. The coefficients of the fit are printed in the order of their location in the array P (see Subroutine FCT) along with their statistical and total errors (see Section (I-5)). With the exception of the initialization cycle the value of χ -squared ($Chisq$) is printed after each iteration cycle has been completed, which allows the operator to check on the progress of the fit.

The inverted matrix is typed in string format by rows according to the format `/5E12.5`.

Comments on the Use of the Program

The program is able to fit a fairly wide variety of functions. In all cases, though, care must be taken in determining the reliability of the answers in view of the limitations of the Gauss method and the problem which may arise in the numerical solution of the matrix of the normal equations.

GENERAL LEAST SQUARES PROGRAM
 RELATIVE EFFICIENCY N DET FCT 2 JUNE 29/65 CURVE A
 INITIAL PARAMETERS

0.100000E 01 0.100000E 01 0.100000E 01

INPUT DATA

0.131000E 01	0.534000E 00	0.259999E-01
0.151000E 01	0.104600E 01	0.499999E-01
0.172000E 01	0.139400E 01	0.650000E-01
0.192000E 01	0.152100E 01	0.749999E-01
0.212000E 01	0.156300E 01	0.749999E-01
0.232000E 01	0.169800E 01	0.899999E-01
0.257000E 01	0.173000E 01	0.899999E-01
0.283000E 01	0.167900E 01	0.859999E-01
0.303000E 01	0.160500E 01	0.799999E-01
0.333000E 01	0.173400E 01	0.599999E-01
0.550000E 01	0.141400E 01	0.699999E-01

CHISQ = 0.264118E 02
 CHISQ = 0.758536E 01
 CHISQ = 0.950094E 00
 CHISQ = 0.637733E 00
 CHISQ = 0.513041E 00
 CHISQ = 0.465171E 00
 CHISQ = 0.448878E 00
 CHISQ = 0.443737E 00
 CHISQ = 0.442276E 00
 CHISQ = 0.441952E 00

COEFFICIENT	STATISTICAL ERROR	TOTAL ERROR
0.113015E 01	0.200343E-01	0.133187E-01
0.121013E 01	0.149426E-01	0.993379E-02
0.797421E 00	0.455057E-01	0.302519E-01

INVERTED MATRIX

0.40137E-03 0.12052E-03-0.14577E-03 0.12052E-03 0.22328E-03
 -0.60546E-03-0.14577E-03-0.60546E-03 0.20707E-02

EXIT
 LOADING COMPLETE

FIGURE I-1. Typical output page from General Purpose Least Squares Program.

The deviation of the initial estimates of the parameters from their "true" values that can be tolerated and still obtain convergence is highly dependent on the form of the function being fitted, the number of free parameters in the fit and the "scatter" of the input data. In some cases, fits have been obtained when the input parameters were wrong by an order of magnitude; in other cases convergence failed to occur even for parameters that were as close as 90% of the values that were finally shown to be correct.

Structure of the Program

The program consists of a Fortran mainline program and three Fortran subprograms.

Mainline: Handles all I/O and generates the matrix of the normal equations.

Subroutine FCT: Generates the tables of the value of the function and its derivatives with respect to the parameters for each value of x specified in the input data. This is the only part of the program that must be changed when new functions are required. Since in most cases the user will be required to write his own function subroutine, the structure and requirements of this subprogram will be dealt with in detail. At this point it should be pointed out that there is NO difference between a linear and a nonlinear function as far as this subroutine or the mainline program is concerned. Exactly the same procedures are used for both cases.

Table (I-2) lists the definitions and modes of the important variables. The general structure of the subroutine can be discerned by studying the structure of the "Function Subroutine to generate a Power Series Fit in X ." Note that the subroutine definition must always appear

TABLE (I-2)

Symbol	Definition	Mode
N	The number of free parameters in the fit. This number is not necessarily required by the sub-routine in the generation of the function tables.	Integer scalar
M	The number of data sets (number of values of x that are to be used. Sets the size of the X vector. This number is always required.	Integer scalar
GB	This vector contains the current values of the parameters being fitted. At the beginning the vector GB contains the initial or starting values of the free parameters.	Floating point vector
X	This vector contains the values of x that will be used in calculating the tables of the function and its derivatives. This table has been read in by the mainline program.	Floating point vector
F	This vector contains the value of the function for each value of x stored in the vector X .	Floating point vector
P	The two dimensional array P contains the derivatives of the function with respect to each free parameter calculated for each value of x in the vector X . Each row of the array corresponds to a parameter of the fit while a column corresponds to a given value of x .	Floating point array

in exactly the order given in the example. The dimension declarations must also have exactly the values shown in the example.

Subroutine CHISQ: Generates the residuals ($\text{Resid.} = \omega(\mu - \xi)$) required in the formation of the normal equations. It also calculates the quantity s^2 which is output as CHISQ.

Subroutine MINV: Inverts the matrix of the normal equations using Jordan's method.

(iii) Weighted Nonlinear Least Squares Program for Gaussian Analysis

This program was written primarily to aid in the analysis of neutron time-of-flight spectra. The program calculates the means standard deviations and areas of peaks which are assumed to have a Gaussian form. Various forms of a background function can be used to allow removal of the background from under a spectrum. The program can fit up to 100 channels of experimental data at a time and will store 512 channels of experimental data which can be called upon by control parameters.

Input Data

The input data and control information for this program can be read from various devices depending on which version of the program is being used. The program control information can be read from cards or paper tape while the data from the pulse height analyser can be read from paper tape or magnetic tape. Since the control information on paper tape is usually generated by the program "Neutron time-of-flight control Generator for Nonlinear Gaussian Analysis," only the card version of the program will be discussed here. A discussion of the possible data formats for

the pulse height analyser data will be given in conjunction with the discussion of Subroutine DATA.

Table (I-3) gives a list of the functions available in the program while table (I-4) indicates the information contained on each input card and the format in which the data must appear. A typical input data set is shown in figure (I-2) which gives the order and format of the control information. It should be emphasized that only ten free parameters and 100 channels of experimental data can be handled in any one fit. The ten free parameters include both the background and peak parameters exclusive of the END statements which are for control purposes only. No breakpoints or sense switches are used in the operation of the program. (In early versions of the program BPT 2 was used to control the program to obtain a linear or nonlinear fit. Recent versions do this automatically.) Table (I-5) lists the versions of the program that are currently available for data analysis.

Output

A typical output page is shown in figure (I-3). The initial estimates of the parameters required for the functions denoted by EX and PK are output immediately after the title card is printed. If the fit is nonlinear (that is, one of the parameters DB, DM or DS has been used) the values of the linear parameters obtained in an initial linear fit are printed immediately after s^2 (CHISQ) is printed. This linear fit is used to estimate starting values of the linear parameters required in the iterative nonlinear fitting procedure. If the fit is linear, then the


```
P31 2.232,1.256. GND
1
  300 700
A0
A1
END
PK22DM22
625.56          1.5
PK12DM12
645.297        1.5
PKG DMG
666.76         1.5
END
  610 685
```

FIGURE I-2. Example of control information for
Nonlinear Gaussian Analysis Program.


```

NONLINEAR GAUSSIAN ANALYSIS
RUN 1 FEB 12/65 BE9(D,N)B10 CALIBRATION
LOAD DATA
START LOAD - 1 STOP - 512
PK21MEAN - 0.326300E 03 SD - 0.200000E 01
PK17MEAN - 0.340550E 03 SD - 0.200000E 01
PK.7MEAN - 0.370729E 03 SD - 0.200000E 01
PKG MEAN - 0.387464E 03 SD - 0.200000E 01
START FIT - 306 STOP FIT - 405
CHISQ - 0.227711E 01
INITIAL PARAMETERS
A0 - 0.259527E 00
A1 - -0.142100E-02
PK21- 0.327463E 02
PK17- 0.213264E 02
PK.7- 0.832103E 02
PKG - 0.611167E 02
CHISQ - 0.218442E 01
CHISQ - 0.215070E 01
CHISQ - 0.214600E 01
CHISQ - 0.214475E 01
CHISQ - 0.214446E 01

BACKGROUND
COEFFICIENT STATISTICAL ERROR TOTAL ERROR
A0 - 0.183116E 00 0.781348E-01 0.114420E 00
A1 - -0.118755E-02 0.228923E-02 0.335234E-02

PEAK
COEFFICIENT STATISTICAL ERROR TOTAL ERROR
PK21- 0.305494E 02 0.283783E 01 0.415571E 01
AREA - 0.170420E 03 0.158309E 02 0.231827E 02
DS21- 0.222550E 01 0.131778E 00 0.192976E 00
PK17- 0.196275E 02 0.238619E 01 0.349433E 01
AREA - 0.111136E 03 0.135113E 02 0.197859E 02
DS17- 0.225892E 01 0.200142E 00 0.293087E 00
PK.7- 0.737548E 02 0.478429E 01 0.700609E 01
AREA - 0.423302E 03 0.274585E 02 0.402101E 02
DS.7- 0.228965E 01 0.980177E-01 0.143537E 00
PKG - 0.591343E 02 0.403987E 01 0.591597E 01
AREA - 0.309323E 03 0.211320E 02 0.309456E 02
DSG - 0.208681E 01 0.858231E-01 0.125679E 00

```

FIGURE I-3. Typical output page from the Nonlinear Gaussian Analysis Program.

TABLE (I-3)

Functions Available for Gaussian Analysis		
Symbol*	Function	Definition
A0	$A0 \circ 1$	Constant background function
A1	$A1 \circ x$	Linear background function
A2	$A2 \circ x^2$	Quadratic background function
EX	$EX \circ \exp(bx)$	Exponential background function
DB	$x \circ EX \circ \exp(bx)$	Determines b in the exponential function EX
PK	$\frac{PK}{\sqrt{2\pi} \sigma} \exp \left[-\frac{1}{2} \left(\frac{x-\bar{x}}{\sigma} \right)^2 \right]$	Gaussian function which can be used as a peak or a background function in a fit. PK is the area of the Gaussian function.
DM	$\frac{PK}{\sqrt{2\pi} \sigma} \left[\frac{x-\bar{x}}{\sigma^2} \right] \exp \left[-\frac{1}{2} \left(\frac{x-\bar{x}}{\sigma} \right)^2 \right]$	Calculates the mean \bar{x} of the Gaussian function PK.
DS	$\frac{PK}{\sqrt{2\pi} \sigma} \left[\frac{(x-\bar{x})^2}{\sigma^3} - \frac{1}{\sigma} \right]$	Calculates the standard deviation σ of the Gaussian curve PK.
	$x \exp \left[-\frac{1}{2} \left(\frac{x-\bar{x}}{\sigma} \right)^2 \right]$	

*Note that each operation symbol also represents a particular parameter in the function as well as the function itself.

TABLE (I-4)

Card Set	Symbol	Definition	Format
1		Title card. The first 48 columns beginning with column 1 are available for writing an alphameric title.	48H
2	1 or 2	A 1 in column 1 indicates that a set of experimental data is to be read following the reading of the next card (Set 2a). A 0 in column 1 indicates that no data is to be input and that set 2A is not to be read.	I4
2A	JI and JE	When card set 2 contains a 1 in column 1 then a card containing two integer numbers is read. These numbers are the channel begin and channel end locations of the experimental data which is to be read immediately following the reading of this card. The maximum number of channels that can be input is 512; that is $JE - JI + 1 \leq 512$. Channel zero is always ignored.	2I4
2B	KS	When the experimental data is to be read from cards it must be punched on $(JE - JI + 1) / 10$ cards which follow immediately after set 2A. In all cases the experimental data are read after reading card set 2A.	I5,9I7
3	Up to 9 of A0,A1,A2,Ex,DB,PK,DM,DS, and END	This control set is for the background function. All linear parameters must appear starting in column one with each <u>linear</u> parameter on a separate card. The non-linear parameters associated with a given linear parameter must appear on the same card as the corresponding linear parameter. The last control word must be an END statement. This can appear on a separate card, or on	3A4

Card Set	Symbol	Definition	Format
	b x σ	<p>the last function control card if room is available. Immediately following the card containing the symbol EX there must appear a card containing an initial estimate of the nonlinear parameter b. Similarly immediately after the card containing PK there must be a card containing initial estimates of the nonlinear parameters x and σ. These parameters are in units of channel number. (See figure (I-2)).</p>	2F12.6
4	Up to 9 of PK,DM, DS, and END	<p>This control set is for the peaks in the spectrum. The general form is the same as in set 3. Various peaks in the spectrum can be identified by two alphameric characters which follow immediately after the control symbol (i.e. PKF 1). All four characters are output to allow identification of the peak. The last control word must be an END statement which can appear on a separate card or on the last function control card if room is available.</p>	3A4
5	MS and JM	<p>This card contains the start fit location MS and the stop fit location JM. The number of channel fitted is $JM-MS+1$ where $JM-MS+1 < 100$.</p>	2I4

TABLE (I-4A)

A0

A1

A2

EX (DB)

XXXX Initial estimate of b. (F12.6)

°

°

°

END

PK (DM) (DS)

XXXX(AV) YYYY(SD) (2F12.6)

°

°

°

END

AV Peak mean in channels

SD Peak standard deviation in channels.

TABLE (I-5)

Control Input	Mode	DATA Input	Mode	Format*
Card	BCD	Card	BCD	
Card	BCD	Magnetic tape	BIN	
Card	BCD	Paper tape	BCD	LGP 30
Card	BCD	Paper tape	BCD	SDS
Card	BCD	Paper tape	BCD	ND
Paper tape	BCD	Magnetic tape	BIN	

*LGP 30 tape punched by TMC Pulse Height Analyser in LGP 30 format.

SDS tape punched by TMC PHA in SDS format.

ND tape punched by Nuclear Data PHA in SDS format. However, tape character format differs from that marked SDS format.

final results are printed after the printing of CHISQ. As shown in the figure the output parameters are identified by the symbols A0, A1 etc. and an estimate of the statistical and total errors of the parameters follow the printing of the value of the parameter itself (see section (I-5)). In the new versions of the program the peak height, denoted by ORD, is printed immediately following the printing of the peak area (PK). In the old versions of the program, the peak height (PK) was printed first with the area (AREA) following.

Comments on the Use of the Program

The program has been successfully used in the analysis of a large number of neutron time-of-flight spectra. In general it is advisable to fix as many of the free parameters as possible. This will not only reduce the errors on the parameters but will increase the chances of obtaining convergence of the fitting procedure. In particular, it is almost essential that the standard deviations of the peaks be fixed if a number of unresolved or semi-resolved peaks are to be fitted.

The usual fitting procedure is as follows:

1. A typical spectrum is analysed with reasonable estimates for the standard deviations leaving only the peak means as free parameters.
2. Then the spectrum is re-analysed with the means fixed but with the standard deviations left as free parameters.
3. Then all the spectra are fitted using the estimates for the standard deviations obtained in the above analysis.

Of course, if all peaks are well resolved and it is only necessary to remove a relatively small background from under the peaks both the means and standard deviations can be left as free parameters in the fit. It

should be mentioned though that as a peak approaches the background level (as in an angular distribution measurement at some particular angle) the standard deviation tends to become larger and erroneous peak intensities will result. Consequently considerable care must be taken in determining the validity of the answers obtained in the use of this program, as in all least squares fitting procedures.

Structure of the Program

The program consists of a Fortran mainline program and nine subprograms.

Mainline program: Handles most of the I/O and contains the basic logic of the program.

Subroutine DATA: This subroutine reads the experimental data from the pulse height analyser. The data is stored in memory in integer form. The only requirements that must be met in modifying this subroutine are that the calling sequence be DATA (I,JE,KS) and that the dimensions of the vector KS be set at (512), where KS is the vector that holds the experimental data.

Subroutine DECOD: This subroutine reads and decodes the control information for the fit, (See Input Data for an explanation of the codes.) and sets up the operation tables for generating the normal equations of the fit. These tables can be broken into two classes:

1. Program control vectors.
2. Initial parameter vectors.

The initial parameter vectors store the initial estimates of the parameters in a sequence which corresponds to the sequence of information in the control vectors to be described. Three control vectors, the name table NS, the sequence table IM and the relation table KM, are constructed by subroutine DECOD to control the generation of the normal equation and to supply information for output identification. Briefly, the name table contains the alphameric names of the functions (i.e. A0, etc.) to be

fitted while the sequence table contains the numeric code names of these functions in the same order. These tables are ordered such that all linear parameter names appear first followed by the nonlinear parameter names. The relation table contains information which relates the linear and nonlinear parameters belonging to the same function.

Subroutine FCT: Calculates the values of the functions required to generate the normal equations of the fit and stores these values in the array P.

Subroutine GEN: Calculates the matrix of the normal equations for both the linear and nonlinear fits. The routine has built into it implicitly the fact that the input data obeys Poisson statistics.

Subroutine MINV: Inverts the matrix of the normal equations using Jordan's method.

Subroutine REGEN: Regenerates or updates the parameter tables GB, SD and AV after each iteration.

Subroutine CHISQ: This routine calculates the residuals and s^2 which is output as CHISQ. The Poisson character of the experimental data is implicit in the subroutine.

Subroutine DMA: Rearranges the parameter tables so that they are in a form suitable for output.

Subroutine NOM: Decodes the alphanumeric operation codes (A0, etc.) in Subroutine DECOD and returns a numeric code corresponding to each alphanumeric operation code.

(iv) Neutron Time-of-Flight Control Generator for Nonlinear Gaussian Analysis

This program was written to facilitate the analysis of neutron time-of-flight angular distribution data. Since the peak positions corresponding to given neutron groups is a function of the laboratory angle, the input data for each spectrum is different. This program carries out the necessary kinematic calculations and computes the positions of the various peaks for each spectrum to be analysed. The output of the program is in a form that can be read by the Weighted Nonlinear Least Squares Program for Gaussian Analysis - paper tape version.

The program is divided into two sections.

1. The calibration line program.
2. Gaussian Analysis Input Data Generator.

Two versions of the program exist. One which calculates and uses a linear time calibration line and the other which calculates and uses a quadratic time calibration line. The two programs are identical except for the form of the time calibration line and, therefore, only the program using the quadratic calibration line will be discussed here.

Quadratic Calibration Line

This program uses the method of least squares to obtain a quadratic time calibration line for a time-of-flight spectrum.

Input Data

The input data requirements are given in table (I-6). All input data is punched on standard IBM cards and must appear in the order given in the table.

Output

A typical output page is shown in figure (I-4). The output consists of the title, the input data and the coefficient of the line with their respective errors.

Neutron Time-of-Flight Control Generator for Nonlinear Gaussian Analysis

This program uses the time calibration line and the mass, Q-value and excitation energy of the various neutron groups to calculate the peak positions of the neutron groups for the different laboratory angles of

LOADING COMPLETE

QUADRATIC CALIBRATION LINE FITTING PROGRAM
CALIBRATION RUN 13 JUNE 30/65

TIME	CHANNEL NO	ERROR
274.336000	381.620000	2.267000
269.223000	394.217000	0.800000
251.659000	432.060000	2.112000
246.677000	443.260000	0.360000
208.431000	526.500000	2.120000
203.491000	538.000000	2.130000
194.621000	557.620000	0.160000
173.822000	603.180000	2.240000
163.627000	625.560000	2.190000
154.427000	645.300000	0.200000
144.644000	666.760000	2.056000

CHISQ = 0.418991E 01 CHI = 0.204693E 01
THE CALIBRATION LINE $Y = A + B \cdot T + C \cdot T^2$
COEFFICIENT STATISTICAL ERROR TOTAL ERROR
A = 0.980617E 03 0.824682E 00 0.168806E 01
B = -0.215478E 01 0.842797E-02 2.172514E-01
C = -0.103690E-03 0.202011E-04 0.413503E-04

EXIT

LOADING COMPLETE

FIGURE I-4. Typical output page from the Quadratic Calibration Line Fitting Program.

TABLE (I-6)

Card Set	Symbol	Definition	Format
1		Title card. The first 48 columns beginning with column one are available for writing an alpha-meric title.	48H
2	M	The number of data sets to be input.	I4
3	T,Y,SDX	Each card contains one data set which consists of (a) the value of T is the time of flight in nanoseconds (b) the channel position Y of the peak which corresponds to time T (c) the standard deviation of Y in units of channel number.	3F12.6

neutron emission. The data input requirements are quite similar to those of the Gaussian analysis program.

Input Data

The input data is punched on standard IBM cards in the sequence shown in table (I-7), table (I-7A) and figure (I-5). The program can read the control information for 15 fits on any one spectrum. The number of different spectra that can be handled is 9999. All the control information used to generate the input data for other fits must be taken from one spectrum at a particular angle of neutron emission (ALPHA). The program then reproduces this data with the appropriate kinematic variations for all other spectra that are to be fitted by the Gaussian Analysis program.

Control Switches

Breakpoint 1 controls the reading of a calibration line for each angle.

BPT 1 Set: Read new time calibration line after each angle THETA.

BPT 1 Reset: Do not read new time calibration line after each angle THETA.

Output

The program outputs the title (set 1), the calibration line constants (A,B,C) and the angle of neutron emission (THETA). The control data for the Gaussian Analysis program is punched on paper tape.

Structure of the Program

The program consists of a Fortran mainline program and two Fortran subprograms.

Mainline: Two programs are used, one which calculates the time calibration line and a second which generates the Gaussian


```

JUNE 30/65 SI30(D,N)P31 CAL FOR EACH RUN
977.906 -2.1282 -.00015553
0.0
2.0147425 1.008986 5.0424, 6.309
1 5
P31 2.232 , 1.265, GND JUN 30 THETA =
1 300 700
A0
A1
END
PK22DM22 1.4 29.98329 5.062
2.232
PK12DM12 1.4 29.98329 5.062
1.265
PKG DMG 1.5 29.98329 5.062
0.0
END
610 30. 680 30.
105.
120.
981.648 -2.14754 -.00012608
150.
979.946 -2.14435 -.00014621
95.
977.539 -2.11777 -.000175459
135.
978.934 -2.1274 -.000177

```

FIGURE I-5. Example input data set for the Neutron Time-of-Flight Control Generator for Nonlinear Gaussian Analysis Program.

TABLE (I-7)

Card Set	Symbol	Definition	Format
1		Title card. The first 48 columns are available for writing an alphanumeric title.	48H
2	A,B,C	This card contains the coefficients of the quadratic calibration line. The coefficients are punched in alphabetic order across the card.	3F12.6
3	ALPHA	The angle of neutron emission of the spectrum used to generate the input data.	F8.3
4	AMU1, AMU3, E1, D	The mass of the bombarding particle (AMU the mass of the neutron (AMU the bombarding energy E1 and the length of the neutron flight path D are punched in the order given on one card.	4F12.6
5	MA,MF	The number of angles MA and the number of fits per angle MF.	2I4
6		This data set contains up to 15 complete control sets for the Gaussian analysis program. The input format is essentially the same as those used in the card versions of the Gaussian fitting program. All control sets must originate with the same spectrum. No provision has been made for mixing fits from different spectra. See table (I-7A) for details on the card formats used in this card set.	3A4 and 4F12.6
7	THETA	The angles of neutron emission in laboratory coordinates at which the MA spectra to be fitted were obtained.	F12.6

TABLE (I-7A)

Possible Order for Input Data Set 6 in Table (I-7)
Each line represents one card.

Title card (48H)

1 or 0 (I4)

XXXX(JI) YYYY(JE) (2I4) If previous card contains 1.

A0

A1 (3A4)

A2

EX (DB)

XXXX Initial estimate of b (F12.6)

°

°

°

END

PK (DM) (DS) (3A4)

XXXX(EXN) YYYY(SD) ZZZZ(MASS) VVVV(QO) (4F12.6)

°

°

°

END

XXXX(MS) YYYY(MASS) ZZZZ(JM) VVVV(MASS) (I4, F12.6, I4, F12.6)

°

°

°

°

Table (I-7A) cont'd.

JI	Channel begin location for data input
JE	Channel end location for data input
EXN	Excitation energy of the peak in MeV
SD	Standard deviation of the peak in channels
MASS	Mass of the target nucleus in AMU
QO	Q to the ground state for the reaction in MeV
MS	Start fit location in channels
JM	Stop fit location in channels

Analysis input data. Two versions of the program exist;
(1) a linear calibration line program, and (2) a
quadratic calibration line program.

Subroutine ASSEMBLE: This subroutine is very similar to
Subroutine DECOD. The subroutine decodes and stores
the Gaussian Analysis control information in such a
manner that it can be output on paper tape in a form
consistent with the Gaussian Analysis input requirements.

Subroutine ENEG*: Calculates the kinematic variation of
neutron energy as a function of the angle of emission.

(Subroutine MINV): Matrix inversion routine used in the
quadratic calibration line version of the program.

Comments on the Use of the Program

In general it has been found that when the peaks in the spectra are
well separated the linear program can be used with only one calibration
line. When many closely spaced or semi-resolved peaks are involved it
has been found that the quadratic program gives fewer divergent fits.
If it becomes necessary to fix the means of the peaks to obtain conver-
gence, then it is usually necessary to have a separate calibration line
for each spectrum.

Considerable care is necessary in the choice of the boundaries of
the fit to ensure that peaks arising from reactions with different masses
remain within the boundaries at all angles. A judicious choice of boundary
mass can often alleviate the difficulties that arise under these conditions.
A little care in setting up the input data can save a considerable amount
of "hand" fitting of the fits which would otherwise fail to converge. In
general it has been found that about 10% of the fits in a large automatic
operation fail to converge or give erroneous results.

*This subroutine was taken from the Relativistic Kinematics program
written by Mr. T. B. Grandy.

(v) Least Squares Mass and Q Identification

This program calculates the mass of the residual nucleus and the Q-value of the reaction by fitting the variation in the energy of the detected particle as a function of its angle of emission. The program can accept either the energy or the time-of-flight of the detected particle as input data along with its appropriate standard deviation. After the mass of the residual nucleus has been determined, the program allows the "correct" mass and ground state Q-value to be read, which is then used to calculate the excitation energy of the residual nucleus.

Input Data

The program has three modes of operation, each mode with differing input requirements. They are:

1. E3 read-in. The energy of the detected particle is used to determine the mass and Q.
2. The time-of-flight of the detected particle is used to determine the mass and Q.
3. The channel position of the peak is used along with an appropriate calibration line to determine the mass and Q. (The only subroutine currently in existence utilizes a time calibration line for the analysis of neutron time-of-flight spectra.)

The input data requirements are as follows:

1. E3 read-in, table (I-8)
2. Time read-in, table (I-9)
3. Channel number read-in for time-of-flight, table (I-10)

TABLE (I-8)

Input Requirements for E3 Read-in			
Card Set	Symbol	Definition	Format
1	XM1	The mass of the bombarding particle XM1 and the mass of the detected particle XM3 in AMU.	2F12.6
2	E1	The bombarding energy of MeV.	F12.6
3	NOM	Control character. A 1 in column 1 means read input data set 5. A 0 in column 1 means do not read data set 5.	I3
4	M	Number of data sets.	I3
5	THETA E3 SD	The angle of particle emission in degrees, the energy of the detected particle in MeV and the standard deviation of the energy of the detected particle in MeV. M cards are required.	3F12.6
6	XM4 Q0	The mass of the residual nucleus XM4 in MeV and the Q to the ground state.	2F12.6

TABLE (I-9)

Input Requirements for Time Read-in			
Card Set	Symbol	Definition	Format
1	D,DD	The flight path D in meters and the error in the flight path DD in meters.	2F12.6
2	XM1, XM3	The mass of the bombarding particle XM1 and the mass of the detected particle XM3 in AMU.	2F12.6
3	E1	The bombarding energy in MeV	F12.6
4	NOM	Control character. A 1 in column 1 means read input data set 6. A 0 in column 1 means do not read input data set 6.	I3
5	M	Number of data sets.	I3
6	THETA T SD	The angle of particle emission in degrees, the time-of-flight of the detected particle in nanoseconds and the standard deviation of the time-of-flight of the detected particle in nanoseconds.	3F12.6
7	XM4 Q0	The mass of the residual nucleus XM4 in MeV and the Q to the ground state.	2F12.6

TABLE (I-10)

Input Requirements for Channel Number Read-in for Time-of-Flight			
Card Set	Symbol	Definition	Format
1	D, DD	The flight path D in meters and the error in the flight path DD in meters.	2F12.6
2	XM1 and XM3	The mass of the bombarding particle XM1 and the mass of the detected particle XM3 in AMU.	2F12.6
3	E1	The bombarding energy in MeV.	F12.6
4	NOM	Control character. A 1 in column 1 means read input data set 7. A 0 in column 1 means do not read input data set 7.	I3
5	M	Number of data sets.	I3
6	A, DA, B, DB	The intercept A and error DA and the slope B and error DB of the linear time calibration line. If BPT4 set, a new calibration line is read before reading each card in card set 7. If BPT4 is reset, only one time calibration line is read.	4E12.5
7	THETA CH SD	The angle of particle emission in degrees, the channel position of the detected particle and the standard deviation of the peak position in channels.	3E12.5 or 3F12.5
8	XM4	The mass of the residual nucleus XM4 and the Q to the ground state in MeV.	3F12.6

Control Switches

All four breakpoint switches are used in the control of this program.

BPT 1 Set: Sets up program for E3 read-in.

BPT 1 Reset: Sets up program for T or CH read-in.

BPT 2 Set: Transfer control to routine that calculates the excitation energy of the residual nucleus. The breakpoint is tested after completion of the least squares fit for mass and Q . If BPT 2 remains set, the program will remain in excitation energy routine. To exit from this routine breakpoint 2 must be RESET.

BPT 2 Reset: Do not enter excitation energy routine. Control is transferred back to the least squares routine which asks for a new data set. If control is within the excitation energy routine, then control is transferred back to the least squares fitting part of the program when breakpoint 2 is RESET.

BPT 3 Set: Sets up program for CH read-in.

BPT 3 Reset: Sets up program for T read-in.

BPT 4 Set: Reads new calibration line with each data set.
(See table (I-10)).

BPT 4 Reset: Reads only one time calibration line before reading the angular distribution data. (See table (I-10)).

Output

A typical output page is shown in figure (I-6). All input parameters and the input data THETA, E3 and SD, etc. are output for identification purposes. An initial estimate of M_4 and Q are calculated and output as $M_4=0$ and $Q=0$. The values of s^2 and s after each iteration are output as EPSILON SQUARED and EPSILON. The quantities DAM and DAW are related to the mass and Q . Finally the BEST FIT M_4 and BEST FIT Q are printed with the corresponding statistical errors and total errors. The excitation energy routine reads and immediately prints the values of XM_4 and Q_0 , which

LOADING COMPLETE

LEAST SQUARES MASS AND Q IDENTIFICATION

D - 6.309000
M1 - 2.014742 M3 - 1.008986
E1 - 5.042400

INPUT DATA

0.000000	176.000000	0.673000
5.000000	176.200000	0.673000
10.000000	176.700000	0.673000
20.000000	177.200000	0.673000
30.000000	178.800000	0.673000
45.000000	180.100000	0.673000
60.000000	181.800000	0.673000

M4-0 - 18.98805

Q-0 - 1.76380

EPSILON SQUARED - 0.124140E 01 EPSILON - 0.111418E 01

DAM --0.100832E-02 DAW - 0.886011E 02

EPSILON SQUARED - 0.590446E 00 EPSILON - 0.768405E 00

DAM --0.189860E-05 DAW - 0.288072E 01

EPSILON SQUARED - 0.564439E 00 EPSILON - 0.751292E 00

DAM --0.361508E-07 DAW - 0.480952E-02

EPSILON SQUARED - 0.564439E 00 EPSILON - 0.751292E 00

BEST FIT M4 - 19.40036 SD - 2.43404 TOTAL ERROR - 1.82867

BEST FIT Q - 1.72621 SD - 0.36981 TOTAL ERROR - 0.27784

M4 - 19.004456 Q0 - 5.768000

MEAN EXCITATION - 4.038795 SD - 0.013010

THETA	EXCITATION	ERROR
0.000	4.004215	0.009910
5.000	4.016268	0.009887
10.000	4.044559	0.009831
20.000	4.043164	0.009776
30.000	4.099073	0.009602
45.000	4.057953	0.009464
60.000	4.004587	0.009288

FIGURE I-6. Typical output page from the Least Squares Mass and Q Identification program.

allows future identification of the nucleus. The mean excitation with its standard deviation is then printed, followed by a listing of the angle and the excitation energy at that angle with its standard deviation.

Comments on the Use of the Program

Very little difficulty should be encountered in the use of this program. Convergence usually occurs even when the initial estimates of M_4 and Q are wrong by a factor of two or three. When difficulties are encountered it is usually because one data point is off by a considerable amount, or a "reversal" in the order of energies or times occurs for angles near zero degrees. The first and last values of THETA read should be as far apart as possible since the program solves the Q equation for $M_4=0$ and $Q=0$ using the first and last values read. The error analysis used in this program (see section (I-7)) requires that the standard deviation of the quantity input is always much smaller than the absolute value of the quantity itself. (i.e. $|E_3| \ll \sigma_{E_3}$). The program fits the nonrelativistic Q equation (Ev 55).

$$\sqrt{E_3} = a \cos \theta + \sqrt{a^2 \cos^2 \theta + \omega}$$

where

$$a = \frac{\sqrt{M_1 M_3 E_1}}{M_3 + M_4}$$

$$\omega = \frac{M_4 Q + E_1 (M_4 - M_1)}{M_3 + M_4}$$

and solves the resulting best fit values of a and w for the mass and Q .

The time-of-flight of the detected particle is treated relativistically up to third order so that this program should be valid for bombarding energies and/or detected particle energies up to 10 or 11 MeV.

(vi) Angular Distribution Analysis*

The program does a least squares fit of ordinary Legendre polynomials to the input data supplied. The program fits up to 10 polynomials from P_1 to P_{20} .

Input Data

The control information and input data are punched on standard IBM cards. Table (I-11) gives a list of the input requirements. No control switches are used in this program.

Output

The program prints the title card and then proceeds to read the control information and input data. The program then prints s^2 and s under the headings EPSILON SQUARED and EPSILON. The printing of the variance of the fit is followed by the printing of the coefficients of the polynomials. This is in turn followed by the printing of the normalized coefficients. The input data is then printed along with the value calculated from the fitted polynomial. A typical output page is shown in figure (I-7).

Comments on the Use of the Program

Little difficulty should be encountered in the use of this program. However, for fits with 6 or more polynomials, care must be taken in determining

*The author would like to acknowledge the help of Dr. W. K. Dawson who translated this program from LGP-30 language into Fortran.

ANGULAR DISTRIBUTION ANALYSIS
ERR CRDS
TTEST OF P(1) TO P(6)

EPSILON SQUARED = 0.00000 EPSILON = 0.00000

UNNORMALIZED COEFFICIENTS		
COEFFICIENT	STATISTICAL ERROR	TOTAL ERROR
A 0= 0.63904E 03	0.62929E 04	0.00000E 00
A 1= 0.36254E 01	0.15498E 05	0.00000E 00
A 2= 0.20753E 03	0.17209E 05	0.00000E 00
A 3= 0.20063E 02	0.12687E 05	0.00000E 00
A 4= 0.14120E 03	0.64487E 04	0.00000E 00
A 5= 0.86221E 02	0.21055E 04	0.00000E 00
A 6= 0.10232E 03	0.34049E 03	0.00000E 00

NORMALIZED COEFFICIENTS		
COEFFICIENT	STATISTICAL ERROR	TOTAL ERROR
A 0= 0.10000E 01	0.00000E 00	0.00000E 00
A 1= 0.56731E-02	0.24252E 02	0.00000E 00
A 2= 0.32475E 00	0.27119E 02	0.00000E 00
A 3= 0.31394E-01	0.19856E 02	0.00000E 00
A 4= 0.22096E 00	0.10323E 02	0.00000E 00
A 5= 0.13492E 00	0.35526E 01	0.00000E 00
A 6= 0.16012E 00	0.16643E 01	0.00000E 00

THETA	OBSERVED Y	CALCULATED Y
0.00	1200.00	1200.00
15.00	1029.96	1029.96
30.00	724.19	724.19
45.00	585.00	585.00
60.00	606.14	606.14
75.00	604.36	604.36
90.00	556.25	556.25

FIGURE I-7. Typical output page from the Angular Distribution Analysis program.

TABLE (I-11)

Input Requirements for Angular Distribution Analysis			
Card Set	Symbol	Definition	Format
1		Title card. The first 39 columns beginning with column 1 are available for writing an alphameric title.	39H
2	NPOLY	The number of polynomials in the fit. The integer must be right justified in the field.	I2
3	KPOLY	This set consists of NPOLY cards. Each card contains the order of polynomial in the fit. P_0 is automatically included and should not be called. For example a fit consisting of P_0, P_2 and P_4 would be obtained with NPOLY = 2 and two cards in card set 3 containing a 02 and 04 in columns 1 and 2 respectively.	I2
4	NANG	The number of angles for which data will be given.	I2
5	DEGREE COUNT WEIGHT	Each data card contains the angle in degrees, the count, and the standard deviation of the count in this order.	3F12.6

the validity of the coefficients. Although good fits will usually be obtained, the sign and magnitude of any individual coefficient may be grossly in error. This problem is a result of the difficulty in inverting the matrix of the normal equations for the case of non-orthogonal polynomials. (See section (I-6)).

Structure of the Program

The program consists of a mainline program and the matrix inversion subroutine MINV. The program is a straightforward least squares fitting program which should be relatively easy to follow.

\$IBSYS

C GENERAL PURPOSE LEAST SQUARES FITTING PROGRAM

C MAIN LINE PROGRAM

DIMENSION X(75),Y(75),W(75),P(15,75),C(15,16),CSI(15),RESID(75)
1LR(15),LC(15),EPSQ(20),GB(15),F(75),DA(15)

EQUIVALENCE (CSI,DA)

TYPE 41

READ 59

TYPE 59

READ 43,N

TYPE 52

READ 51,(GB(J),J=1,N)

TYPE 44,(GB(J),J=1,N)

READ 43,M

TYPE 42

DO 2 J=1,M

READ 51,X(J),Y(J),SD

W(J)=1.0/(SD*SD)

IF(SENSE SWITCH 1)3,2

3 TYPE 46,X(J),Y(J),SD

2 CONTINUE

IT=0.0

NI=N+1

DF=M-N

IF(DF)17,17,18

17 DF=1.0

TYPE 47

18 CALL FCT(N,M,GB,X,F,P)

CALL CHISQ(IT,M,Y,W,F,RESID,EPSQ,DF)

C GENERATE CSI

110 DO 111 I=1,N

CSI(I)=0.0

DO 111 K=1,M

111 CSI(I)=RESID(K)*P(I,K)+CSI(I)

C GENERATE MATRIX OF THE NORMAL EQUATIONS

DO 102 I=1,N

DO 102 J=I,N

C(I,J)=0.0

DO 103 K=1,M

103 C(I,J)=W(K)*P(I,K)*P(J,K)+C(I,J)

102 C(J,I)=C(I,J)

DO 4 I=1,N

4 C(I,N+1)=CSI(I)

CALL MINV(N,NI,C,LR,LC)

C REGENERATE THE PARAMETER TABLE

DO 10 I=1,N

10 GB(I)=C(I,N+1)+GB(I)

CALL FCT(N,M,GB,X,F,P)

CALL CHISQ(IT,M,Y,W,F,RESID,EPSQ,DF)

IF(EPSQ(IT)-EPSQ(IT-1))5,29,6

6 IF(IT-3)110,110,29

5 DO 8 J=1,N

IF (ABS(C(J,N+1)/GB(J))-0.001)8,7,7

8 CONTINUE

IF(EPSQ(IT-1)-EPSQ(IT)-0.001)29,29,7

7 IF(IT-20)110,29,29

29 EPS=SQRT(EPSQ(IT))

DO 30 K=1,N

30 DA(K)=SQRT(ABS(C(K,K)))

TYPE 53


```

DO 61 I=1,N
TDA = DA(I)*EPS
61 TYPE 54,GB(I),DA(I),TDA
IF(SENSE SWITCH 2)63,62
63 TYPE 58
TYPE45,((C(I,J),J=1,N),I=1,N)
62 CALL EXIT
41 FORMAT(5X$GENERAL LEAST SQUARES PROGRAM$)
59 FORMAT($
43 FORMAT(I4)
51 FORMAT(3E15.8)
42 FORMAT(5X$INPUT DATAS$)
52 FORMAT(5X$INITIAL PARAMETERS$)
47 FORMAT(5X$PARAMETER EXCESS$)
53 FORMAT(5X$COEFFICIENT$6X$STATISTICAL FRROR$5X$TOTAL ERROR$)
54 FORMAT(5X,E14.6,5X,E14.6,5X,E14.6)
58 FORMAT(5X$INVERTED MATPIX$)
45 FORMAT(/5E12.5)
44 FORMAT(5X,5E13.6/5X,5E13.6/5X,5E13.6)
46 FORMAT(5X,3E15.6)
END
C SUBROUTINE CHISQ GENERATES THE RESIDUALS AND EPSQ
SUBROUTINE CHISQ(IT,M,Y,W,F,RESID,EPSQ,DF)
DIMENSION Y(75),W(75),F(75),RESID(75),EPSQ(20)
IT=IT+1
SUM=0.0
DO 10 K=1,M
RESID(K)=W(K)*(Y(K)-F(K))
10 SUM=RESID(K)**2/W(K)+SUM
EPSQ(IT)=SUM/DF
15 TYPE 49,EPSQ(IT)
49 FORMAT(5X$CHISQ =$E14.6)
RETURN
END

```


SIBSYS

```
C  FUNCTION SUBROUTINE  TO GENERATE A POWER SERIES FIT IN X
      SUBROUTINE FCT(N,M,GB,X,F,P)
      DIMENSION GB(15),X(75),F(75),P(15,75)
      DO 1 J=1,M
      P(1,J)=1.0
      DO 1 I=2,N
1     P(I,J)=P(I-1,J)*X(J)
      DO 2 K=1,M
      F(K)=0.0
      DO 2 I=1,N
2     F(K)=P(I,K)*GB(I)+F(K)
      RETURN
      END
```


SIBSYS

C RELATIVE EFFICIENCY FUNCTION 1 SUB FCT FOR GENERAL LEAST SQUARES

SUBROUTINE FCT(N,M,GB,X,F,P)

DIMENSION GB(15),X(75),F(75),P(15,75)

N=3

DO 10 J=1,M

SIGMA=4.83/SQRT(X(J))-0.578

FF=((X(J)-GB(2))/X(J))**GB(3)

P(1,J)=FF*SIGMA

F(J)=GB(1)*P(1,J)

P(2,J)=F(J)*GB(3)/(GB(2)-X(J))

P(3,J)=F(J)*ALOG((X(J)-GB(J))/X(J))

10 CONTINUE

RETURN

END

C RELATIVE EFFICIENCY FUNCTION 2 SUB FCT FOR GENERAL LEAST SQUARES

SUBROUTINE FCT(N,M,GB,X,F,P)

DIMENSION GB(15),X(75),F(75),P(15,75)

N=3

DO 10 J=1,M

SIGMA= 9.424778/(1.206*X(J)+(0.09415*X(J)+0.000130*X(J)**2-1.860)
1**2)+3.14159/(1.206*X(J)+(0.4223+0.130*X(J))**2)

FF=((X(J)-GB(2))/X(J))**GB(3)

P(1,J)=FF*SIGMA

F(J)=GB(1)*P(1,J)

P(2,J)=F(J)*GB(3)/(GB(2)-X(J))

P(3,J)=F(J)*ALOG((X(J)-GB(J))/X(J))

10 CONTINUE

RETURN

END

\$IRSYS

C WEIGHTED NONLINEAR LEAST SQUARES FITTING PROGRAM FOR GAUSSIAN ANALYSIS
C MAIN LINE PROGRAM

DIMENSION KS(512),IM(10),KM(10),NS(10),P(10,100),C(10,11),CSI(10),
1RESID(100),GB(10),AV(10),SD(10),DA(10),LR(10),LC(10),
2EPSQ(15)
EQUIVALENCE(CSI,DA),(AV(1),TDA),(AV(2),AORD),(AV(3),TDORD),
1(AV(4),DAORD)

20 TYPE 41

1 READ 59

TYPE 59

N=1

JM=1

K=1

L=0

IT=0

SENSE LIGHT 0

READ 43,J

IF(J)2,3,2

2 TYPE 42

READ 43,JI,JE

TYPE 44,JI,JE

PAUSE

72 CALL DATA (JI,JE,KS)

3 CALL DECOD(N,JM,L,K,NS,IM,KM,LC,AV,SD,LR)

NOB=N-1

SENSE LIGHT 1

CALL DECOD(N,JM,L,K,NS,IM,KM,LC,AV,SD,LR)

NI=N+1

READ 43,MS,JM

TYPE 45,MS,JM

M=JM-MS+1

DF=JM-MS-N+1

IF(DF)17,17,18

17 DF=1.0

TYPE 47

18 CALL FCT(L,JM,MS,IM,KM,P,GB,AV,SD)

C GENERATE CSI FOR LINEAR FIT

DO 80 J=1,L,1

80 GB(J)=0.0

100 DO 101 I=1,L,1

CSI(I)=0.0

DO 101 K=1,M,1

101 CSI(I)=CSI(I)+P(I,K)

MX=MS-JI+1

CALL GEN(L,MX,M,KS,P,C,CSI)

K=L+1

CALL MINV(L,K,C,LR,LC)

CALL REGEN(L,IM,KM,C,GB,AV,SD)

CALL CHISQ(IT,L,M,MX,KS,P,GB,RESID,EPSQ,DF)

C TEST FOR LINEAR OR NONLINEAR FIT

IF(L-N)4,29,29

C NONLINEAR FIT

4 TYPE 46

DO 8 J=1,L,1

8 TYPE 54,NS(J),GB(J)

CALL FCT(N,JM,MS,IM,KM,P,GB,AV,SD)

C GENERATE CSI FOR NONLINEAR FIT

110 DO 111 I=1,N,1

CSI(I)=0.0


```

DO 111 K=1,M,1
111 CSI(I)=RESID(K)*P(I,K)+CSI(I)
CALL GEN(N,MX,M,KS,P,C,CSI)
CALL MINV(N,NI,C,LR,LC)
CALL REGEN(N,IM,KM,C,GB,AV,SD)
CALL FCT(N,JM,MS,IM,KM,P,GB,AV,SD)
CALL CHISQ(IT,L,M,MX,KS,P,GB,RESID,EPSQ,DF)
IF(EPSQ(IT)-EPSQ(IT-1))5,29,6
6 IF(IT-3)110,110,29
5 IF(EPSQ(IT-1)-EPSQ(IT)-0.001)29,29,7
7 IF(IT-15)110,29,29
29 EPS=SQRT(EPSQ(IT))
DO 30 K=1,N,1
30 DA(K)=SQRT(ABS(C(K,K)))
CALL DMA(N,IM,KM,GB,AV,SD,NS,DA)
TYPE 51
TYPE 53
DO 61 I=1,NOB,1
TDA=DA(I)*EPS
61 TYPE 54,NS(I),GB(I),DA(I),TDA
TYPE 52
TYPE 53
DO 62 I=NOB+1,N,1
TDA=DA(I)*EPS
TYPE 54,NS(I),GB(I),DA(I),TDA
IF(KM(I))62,63,62
63 GAUS=2.50663*SD(I)
AORD=GB(I)/GAUS
DAORD=DA(I)/GAUS
TDORD=DAORD*EPS
TYPE 58,AORD,DAORD,TDORD
62 CONTINUE
GO TO 1
51 FORMAT(//10X$BACKGROUND$)
52 FORMAT(//10X,4HPEAK)
53 FORMAT(10X$COEFFICIENTS$14X$STATISTICAL ERROR$5X$TOTAL ERROR$)
54 FORMAT(10X,A4,2H= E14.6,5X,E14.6,6X,E14.6)
58 FORMAT(10X,$ ORD = $E14.6,4X,E14.6,6X,E14.6)
59 FORMAT(48H
41 FORMAT(5X$NONLINEAR GAUSSIAN ANALYSIS$)
42 FORMAT(10X,9HLOAD DATA)
43 FORMAT(2I4)
44 FORMAT(10X$START LOAD =$I4,5X$STOP =$I4)
45 FORMAT(10X$START FIT =$I4,5X$STOP FIT =$I4)
46 FORMAT(10X$INITIAL PARAMETERS$)
47 FORMAT(5X$PARAMETER EXCESS$)
CALL EXIT
END
13 ACCEPT TAPE 100,AV(K),SD(K)
12 ACCEPT TAPE 100,SD(K)
15 ACCEPT TAPE 1,NAME(1),NAME(2),NAME(3)
IF (SENSE SWITCH 1) 71,72
71 CALL DAT2 (JI,JE,KS)
GO TO 3

```


\$IBSYS

```
C  SUBROUTINE DECOD  FOR GAUSSIAN ANALYSIS      PAPER TAPE INPUT
C  GENERATES SYMBOL TABLE, SEQUENCE TABLE AND AND READS PARAMETERS
      SUBROUTINE DECOD(N,M,L,K,NS,IM,KM,KT,AV,SD,NAME)
      DIMENSION NS(10),IM(10),KM(10),KT(10),AV(10),SD(10),NAME(10),KX(6)
15  READ 1,NAME(1),NAME(2),NAME(3)
      DO 2 J=1,3,1
      I=NOM(J,NAME)
      IF(I-9)4,20,20
4    GO TO (5,6,6),J
5    IF(I)20,10,7
7    GO TO (11,11,11,12,13),I
12  READ 100,SD(K)
      TYPE 101,NAME(J),SD(K)
      GO TO 11
13  READ 100,AV(K),SD(K)
      TYPE 102,NAME(J),AV(K),SD(K)
11  NS(K)=NAME(J)
      IM(K)=I
      L=L+1
      K=K+1
      GO TO 9
6    IF(I)2,10,8
8    KT(M)=I
      KX(M)=K-1
      NAME(11-M)=NAME(J)
      M=M+1
9    N=N+1
2    CONTINUE
      GO TO 15
20  TYPE 103
      GO TO 15
10  IF(SENSE LIGHT 1)21,22
21  LL=L+1
      N=N-1
      IF(L-N)23,24,24
23  DO 17 J=LL,N,1
      NS(J)=NAME(11-J+L)
      IM(J)=KT(J-L)
17  KM(J)=J-KX(J-L)
24  DO 18 J=1,L,1
18  KM(J)=0
1    FORMAT(3A4)
100  FORMAT(2F12.6)
101  FORMAT(10X,A4,5HEB = ,E14.6)
102  FORMAT (10X,A4$MEAN =$E14.6,5X$SD =$E14.6)
103  FORMAT($ILLEGAL OP CODE$)
22  RETURN
      END
```


SIRSYS

```
SUBROUTINE FCT(N,M,MS,IM,KM,P,GB,AV,SD)
DIMENSION IM(10),KM(10),P(10,100),GB(10),AV(10),SD(10)
JM=M-MS+1
DO 11 I=1,N,1
  X=MS
  X1=(MS-M)/2
  DO 12 J=1,JM,1
    GO TO (1,2,3,4,5,6,7,8),IM(I)
1   P(I,J)=1.0
    GO TO 10
2   P(I,J)=X1
    GO TO 10
3   P(I,J)=X1*X1
    GO TO 10
4   P(I,J)=EXP(SD(I)*X1)
    GO TO 10
6   K=KM(I)
    P(I,J)=GB(I-K)*X1*P(I-K,J)
    GO TO 10
5   P(I,J)=EXP(-0.5*((X-AV(I))/SD(I))**2)/(2.50663*SD(I))
    GO TO 10
7   K=KM(I)
    XX=(X-AV(I-K))
    P(I,J)=GB(I-K)*XX/(SD(I-K)**2)*P(I-K,J)
    GO TO 10
8   K=KM(I)
    XX=X-AV(I-K)
    P(I,J)=(XX*XX/(SD(I-K)*SD(I-K)**2)-1.0/SD(I-K))*GB(I-K)*P(I-K,J)
10  X=X+1.0
12  X1=X1+1.0
11  CONTINUE
    RETURN
  END
```


\$IBSYS

C SUBROUTINE GEN GENERATES THE MATRIX OF THE NORMAL EQUATIONS

SUBROUTINE GEN(N,MS,M,KS,P,A,CSI)

DIMENSION KS(512),P(10,100),A(10,11),CSI(10)

DO 1 I=1,N,1

DO 1 J=I,N,1

A(I,J)=0.0

DO 3 K=1,M,1

CH=KS(K+MS-1)

IF(CH)2,2,3

2 CH=0.05

3 A(I,J)=A(I,J)+(P(I,K)*P(J,K))/CH

1 A(J,I)=A(I,J)

DO 4 I=1,N,1

4 A(I,N+1)=CSI(I)

RETURN

END

C SUBROUTINE REGEN REGENERATES THE ITERATED PARAMETER TABLES

SUBROUTINE REGEN(N,IM,KM,A,GB,AV,SD)

DIMENSION IM(10),KM(10),A(10,11),GB(10),AV(10),SD(10)

DO 10 I=1,N,1

GO TO (1,1,1,1,1,5,7,5),IM(I)

1 GB(I)=A(I,N+1)+GB(I)

GO TO 10

7 K=KM(I)

AV(I-K)=A(I,N+1)+AV(I-K)

GO TO 10

5 K=KM(I)

SD(I-K)=A(I,N+1)+SD(I-K)

10 CONTINUE

RETURN

END

C SUBROUTINE MINV MATRIX INVERSION BY JORDONS METHOD

```

SUBROUTINE MINV(N,M,A,LR,LC)
DIMENSION A(10,11),LR(10),LC(10)
3  KZ=1
   DO 16 K=1,N,1
   LR(K)=K
   LC(K)=K
   I=K
   IZ=K
   P=A(K,K)
   DO 5 J=K,N,1
   DO 5 JZ=K,N,1
   IF(ABS(P)-ABS(A(J,JZ)))4,5,5
4  P=A(J,JZ)
   I=J
   IZ=JZ
5  CONTINUE
   IF(I-K)6,6,23
6  IF(IZ-K)7,7,18
7  IF(A(K,K))12,8,12
8  TYPE 10
10  FORMAT(24H THE MATRIX IS SINGULAR.)
   GO TO 32
12  P=1.0/A(K,K)
   A(K,K)=1.0
   DO 13 J=1,M,1
13  A(K,J)=P*A(K,J)
   DO 16 I=1,N,1
   IF(K-I)14,16,14
14  B=A(I,K)
   A(I,K)=0.0
   DO 15 J=1,M,1
15  A(I,J)=A(I,J)-B*A(K,J)
16  CONTINUE
   KZ=0
   K=N
   DO 26 IA=1,N,1
   IF(LR(K)-K)17,21,17
17  IZ=LR(K)
C  CHANGE COLUMNS IZ AND K
18  DO 19 J=1,N,1
   TS=A(J,IZ)
   A(J,IZ)=A(J,K)
19  A(J,K)=TS
   IF(KZ)20,21,20
20  LC(K)=IZ
   GO TO 12
21  IF(LC(K)-K)22,26,22
22  I=LC(K)
C  CHANGE ROWS I AND K
23  DO 24 J=1,M,1
   TS=A(I,J)
   A(I,J)=A(K,J)
24  A(K,J)=TS
   IF(KZ)25,26,25
25  LR(K)=I
   GO TO 6
26  K=K-1
32  RETURN
END

```


\$IBSYS

```
C SUBROUTINE CHISQ GENERATES THE RESIDUALS AND EPSQ
  SUBROUTINE CHISQ(IT,L,M,MS,KS,P,GB,RESID,EPSQ,DF)
    DIMENSION KS(512),P(10,100),GB(10),RESID(100),EPSQ(15)
    IT=IT+1
    SUM=0.0
    DO 10 K=1,M,1
      YI=0.0
      DO 11 I=1,L,1
11      YI=P(I,K)*GB(I)+YI
      CH=KS(K+MS-1)
      IF(CH)12,12,13
12      CH=0.05
13      RESID(K)=1.0-YI/CH
10      SUM=RESID(K)**2*CH+SUM
      EPSQ(IT)=SUM/DF
15      TYPE 49, EPSQ(IT)
49      FORMAT(10X$CHISQ =$E14.6)
      RETURN
    END

C SUBROUTINE DMA PUTS DATA IN A FORM SUITABLE FOR OUTPUT
  SUBROUTINE DMA(N,IM,KM,GB,AV,SD,NS,DA)
    DIMENSION IM(10),KM(10),GB(10),AV(10),SD(10),NS(10),DA(10)
    EQUIVALENCE(AV(1),G1),(AV(2),S1),(AV(3),D1),(IM(1),N1),(IM(2),K1)
    DO 10 J=1,N,1
      GO TO (10,10,10,10,10,8,7,8),IM(J)
7      K=KM(J)
      GB(J)=AV(J-K)
      GO TO 10
8      K=KM(J)
      GB(J)=SD(J-K)
10     CONTINUE
      L=1
      DO 20 J=1,N,1
        IF(KM(J))11,20,11
11      K=J-KM(J)+L
        IF(K-J)13,14,14
13      N1=NS(J)
          K1=KM(J)
          G1=GB(J)
          D1=DA(J)
          S1=SD(J)
          DO 12 M=J,K+1,-1
            NS(M)=NS(M-1)
            KM(M)=KM(M-1)
            SD(M)=SD(M-1)
            DA(M)=DA(M-1)
12      GB(M)=GB(M-1)
          L=L+1
          NS(K)=N1
          KM(K)=K1
          GB(K)=G1
          DA(K)=D1
          SD(K)=S1
20     CONTINUE
14     RETURN
  END
```


\$IBSYS

FORT

* SUBROUTINE NOM TO IDENTIFY OPERATION SEQUENCE DESIRED

PZE 0,1

PZE NOM

BCI 2,NOM

BLK 0

ORG 0

NOM

HLT

LDB* EOIND

STB LOC,4

LDX EOADR

LDA 1,2

SUB P1

ADM LOC,4

LDB MASK,4

LDA* LOC,4

LDX M10,4

SKM IDEN+10,6

BRX *-1,4

CXA

ADD P9,4

BRR NOM,4

IDEN BCI 10, EN A0 A1 A2 EX PK DB DM DS

EOIND BOOL 74

EOADR BOOL 71

P9 DEC 9

P1 BOOL 24

M10 DEC -10

LOC PZE 0

MASK OCT 77770000

END

\$IBSYS

FORT

* SUBROUTINE TO READ SDS FORMAT KS TAPES KS(1) = (CH BEG)

PZE 0,1

PZE DATA

BCI 2,DATA

BLK 0

ORG 0

DATA HLT

LDA* EOIND

STA BEG,4

LDX EOADR

LDA* 1,2

STA END,4

SUB BEG,4

STA DEX,4

LDA 2,2

STA LOC,4

LDA BEG,4

MUL M12,4

RSH 1

BAC

SUB P4,4

CAX

STR TEP,4

RPTW 1,1

WIM JUNK,4

LDA JUNK,4

ETR MASK,4

SKE CRSDS,4

BRU *-4,4

WIM JUNK,4

BRX *-1,4

RNL LDX M5,4

WIM JUNK,4

LDA JUNK,4

ETR MASK,4

ADD TEP,4

MUL P10,4

RSH 1

STR TEP,4

BRX RNL+1,4

WIM JUNK,4

LDA JUNK,4

ETR MASK,4

ADD TEP,4

STA* LOC,4

MIN LOC,4

SKR DEX,4

BRU *+3,4

DISW

BRR DATA,4

LDX M6,4

WIM JUNK,4

BRX *-1,4

CLR

STA TEP,4

BRU RNL,4

BEG PZE 0

END PZE 0

DEX	PZE	0
LOC	PZE	0
TFP	PZE	0
JUNK	PZE	0
M5	DEC	-5
M6	DEC	-6
M12	DEC	-12
P4	DEC	4
P10	DEC	10
CRSDS	OCT	52
MASK	OCT	77
EOIND	BOOL	74
EOADR	BOOL	71
	END	
CR30	OCT	10
	RSH	1
	RSH	1
	SKE	CR30,4
	END	

\$IBSYS

FORT

*SUBROUTINE TO READ NUCLEAR DATA KS TAPES

PZE 0,1
PZE DAT2
BCI 2,DAT2
BLK 0
ORG 0

DAT2

HLT
CLR
STA TEP,4
LDA* EOIND
STA BEG,4
LDX EOADR
LDA* 1,2
STA END,4
SUB BEG,4
STA DEX,4
LDA 2,2
STA LOC,4
RPTW 1,1
WIM JUNK,4
LDA JUNK,4
ETR MASK,4
SKE TAB,4
BRU *-4,4
LDA BEG,4
SUB P1,4
SKE TEP,4
BRU *+2,4
RRU RNL,4
MUL M7,4
RSH 1

RNL

CBX
WIM JUNK,4
BRX *-1,4
LDX M5,4
WIM JUNK,4
LDA JUNK,4
ETR MASK,4
ADD TEP,4
MUL P10,4
RSH 1
STR TEP,4
BRX RNL+1,4
WIM JUNK,4
LDA JUNK,4
ETR MASK,4
ADD TEP,4
STA* LOC,4
MIN LOC,4
SKR DEX,4
RRU *+3,4
DISW
BRR DAT2,4
WIM JUNK,4
CLR
STA TEP,4
BRU RNL,4
PZE 0

END

BEG	PZE	0
EOADR	BOOL	71
EOIND	BOOL	74
JUNK	PZE	0
M7	DEC	-7
LOC	PZF	0
DFX	PZE	0
P10	DEC	10
TEP	PZE	0
M5	DEC	-5
MASK	OCT	77
TAB	OCT	72
P1	DEC	1
	END	

\$IBSYS

```
SUBROUTINE DATA ( JI, JE, KS )  
  DIMENSION KS(512)  
  READ 1, ( KS(J), J=1, JE-JI+1 )  
1  FORMAT (I5,9I7)  
  RETURN  
END
```


\$IBSYS

```
C  WEIGHTED NONLINEAR LEAST SQUARES FITTING PROGRAM FOR GAUSSIAN ANALYSIS
C  MAIN LINE PROGRAM
      DIMENSION KS(512),IM(10),KM(10),NS(10),P(10,100),C(10,11),CSI(10),
      1RESID(100),GB(10),AV(10),SD(10),DA(10),LR(10),LC(10),
      2EPSQ(15)
      EQUIVALENCE(CSI,DA),(AV(1),TDA),(AV(2),AORD),(AV(3),TDORD),
      1(AV(4),DAORD)
20  TYPE 41
1   ACCEPT TAPE 59,THETA
      TYPE 59,THETA
      N=1
      JM=1
      K=1
      L=0
      IT=0
      SENSE LIGHT 0
      ACCEPT TAPE 43,J
      IF(J)2,3,2
2   TYPE 42
      ACCEPT TAPE 43,JI,JE
      TYPE 44,JI,JE
      PAUSE
      CALL DATA(JI,JE,KS)
      PAUSE
3   CALL DECOD(N,JM,L,K,NS,IM,KM,LC,AV,SD,LR)
      NOB=N-1
      SENSE LIGHT 1
      CALL DECOD(N,JM,L,K,NS,IM,KM,LC,AV,SD,LR)
      NI=N+1
      ACCEPT TAPE 43,MS,JM
      TYPE 45,MS,JM
      M=JM-MS+1
      DF=JM-MS-N+1
      IF(DF)17,17,18
17  DF=1.0
      TYPE 47
18  CALL FCT(L,JM,MS,IM,KM,P,GB,AV,SD)
C  GENERATE CSI FOR LINEAR FIT
      DO 80 J=1,L,1
80   GB(J)=0.0
100  DO 101 I=1,L,1
      CSI(I)=0.0
      DO 101 K=1,M,1
101  CSI(I)=CSI(I)+P(I,K)
      MX=MS-JI+1
      CALL GEN(L,MX,M,KS,P,C,CSI)
      K=L+1
      CALL MINV(L,K,C,LR,LC)
      CALL REGEN(L,IM,KM,C,GB,AV,SD)
      CALL CHISQ(IT,L,M,MX,KS,P,GB,RESID,EPSQ,DF)
C  TEST FOR LINEAR OR NONLINEAR FIT
      IF(L-N)4,29,29
C  NONLINEAR FIT
4   TYPE 46
      DO 8 J=1,L,1
8   TYPE 54,NS(J),GB(J)
      CALL FCT(N,JM,MS,IM,KM,P,GB,AV,SD)
C  GENERATE CSI FOR NONLINEAR FIT
110 DO 111 I=1,N,1
```



```

      CSI(I)=0.0
      DO 111 K=1,M,1
111  CSI(I)=RESID(K)*P(I,K)+CSI(I)
      CALL GEN(N,MX,M,KS,P,C,CSI)
      CALL MINV(N,NI,C,LR,LC)
      CALL REGEN(N,IM,KM,C,GB,AV,SD)
      CALL FCT(N,JM,MS,IM,KM,P,GB,AV,SD)
      CALL CHISQ(IT,L,M,MX,KS,P,GB,RESID,EPSQ,DF)
      IF(EPSQ(IT)-EPSQ(IT-1))5,29,6
6     IF(IT-3)110,110,29
5     IF(EPSQ(IT-1)-EPSQ(IT)-0.001)29,29,7
7     IF(IT-15)110,29,29
29    EPS=SQRT(EPSQ(IT))
      DO 30 K=1,N,1
30    DA(K)=SQRT(ABS(C(K,K)))
      CALL DMA(N,IM,KM,GB,AV,SD,NS,DA)
      TYPE 51
      TYPE 53
      DO 61 I=1,NOB,1
      TDA=DA(I)*EPS
61    TYPE 54,NS(I),GB(I),DA(I),TDA
      TYPE 52
      TYPE 53
      DO 62 I=NOB+1,N,1
      TDA=DA(I)*EPS
      TYPE 54,NS(I),GB(I),DA(I),TDA
      IF(KM(I))62,63,62
63    GAUS=2.50663*SD(I)
      AORD=GB(I)/GAUS
      DAORD=DA(I)/GAUS
      TDORD=DAORD*EPS
      TYPE 58,AORD,DAORD,TDORD
62    CONTINUE
      GO TO 1
51    FORMAT(/10X$BACKGROUND$)
52    FORMAT(/10X,4HPEAK)
53    FORMAT(10X$COEFFICIENT$14X$STATISTICAL ERROR$5X$TOTAL ERROR$)
54    FORMAT(10X,A4,2H= F14.6,5X,F14.6,6X,F14.6)
58    FORMAT(10X,$ ORD = $E14.6,4X,F14.6,6X,F14.6)
59    FORMAT(48H
41    FORMAT(5X$NONLINEAR GAUSSIAN ANALYSIS$)
42    FORMAT(10X,9HLOAD DATA)
43    FORMAT(2I4)
44    FORMAT(10X$START LOAD =$I4,5X$STOP =$I4)
45    FORMAT(10X$START FIT =$I4,5X$STOP FIT =$I4)
46    FORMAT(10X$INITIAL PARAMETERS$)
47    FORMAT(5X$PARAMETER EXCESS$)
      CALL EXIT
      END

```

,F8.3)


```

$IBSYS
C QUADRATIC CALIBRATION FITTING PROGRAM
  DIMENSION A(3,4),LR(4),LC(4)
C QUADRATIC CALIBRATION LINE FOR TIME OF FLIGHT
  DIMENSION P(3,25),C(3,4),Y(25),CSI(3),W(25),T(25),LR(4),LC(4)
  TYPE 500
1  READ 600
  TYPE 600
  READ 400,M
600  FORMAT(48H
  DF=M-3
  IF(DF)2,2,3
2  TYPE 510
510  FORMAT($PARAMETER EXCESS$)
  DF=1.0
3  TYPE 513
  DO 4 J=1,M,1
  READ 401,T(J),Y(J),SDX
  W(J)=1.0/SDX**2
4  TYPE 501,T(J),Y(J),SDX
  DO 5 J=1,M,1
  P(1,J)=1.0
  P(2,J)=T(J)
5  P(3,J)=T(J)**2
  DO 6 I=1,3
  CSI(I)=0.0
  DO 6 K=1,M,1
6  CSI(I)=W(K)*Y(K)*P(I,K)+CSI(I)
  DO 7 I=1,3
  DO 7 J=I,3
  C(I,J)=0.0
  DO 103 K=1,M,1
103  C(I,J)=W(K)*P(I,K)*P(J,K)+C(I,J)
7  C(J,I)=C(I,J)
  DO 8 J=1,3
8  C(J,4)=CSI(J)
  CALL MINV(3,4,C,LR,LC)
  DA=SQRT(ABS(C(1,1)))
  DB=SQRT(ABS(C(2,2)))
  DC=SQRT(ABS(C(3,3)))
  SUM=0.0
  DO 9 K=1,M,1
  YI=C(1,4)+C(2,4)*T(K)+C(3,4)*T(K)**2
9  SUM=W(K)*(Y(K)-YI)**2+SUM
  EPSQ=SUM/DF
  EPS=SQRT(EPSQ)
  TYPE 502,EPSQ,EPS
  DDA=DA*EPS
  DDB=DB*EPS
  DDC=DC*EPS
  TYPE 503
  TYPE 505
  A=C(1,4)
  B=C(2,4)
  TYPE 506,A,DA,DDA,B,DB,DDB,C(3,4),DC,DDC
  CALL EXIT
500  FORMAT($QUADRATIC CALIBRATION LINE FITTING PROGRAM$)
400  FORMAT(2I4)
401  FORMAT(4F12.6)
501  FORMAT(10XF12.6,5X,F12.6,5X,F12.6)

```



```
513  FORMAT(12X$TIMES$13X$CHANNEL NOS$8X$ERRORS$)
502  FORMAT(10X$CHISQ =$E13.6,5X$CHI =$E13.6)
503  FORMAT(10X$THE CALIBRATION LINE  Y = A + B*T + C*T**2$)
505  FORMAT(10X$COEFFICIENT$6X$STATISTICAL ERROR$5X$TOTAL ERROR$)
506  FORMAT(10X$A =$E13.6,2X,E13.6,10X,E13.6/10X$B =$E13.6,2X,E13.6,
110X,E13.6/10X$C =$E13.6,2X,E13.6,10X,E13.6)
      END
```


\$IBSYS

CNEUTRON TIME OF FLIGHT CONTROL GENERATOR FOR NONLINEAR GAUSSIAN ANALYSIS

C QUADRATIC CALIBRATION LINE

DIMENSION TITLE(15,6),LD(15),JI(15),NS(3),NAME(15,12,3),MS(15),
1XMS(15),JM(15),XJM(15),LN(15),KM(15,12),QO(15,12),AV(15,12),
2SD(15,12),XMU2(15,12),JE(15)

EXF(AMU)=(1.0+AMU3/(AMU3+AMU))*E3-(1.0-AMU1/(AMU3+AMU))*E1-
12.0/(AMU3+AMU)*COS(ALPHA)*SQRT(AMU1*AMU3*E1*E3)

E3F(AMU)=0.5*AMU*(X-0.25*X**2+0.125*X*X**2)

YF(XM3)=(DC*(E3+XM3)/SQRT(E3**2+2.0*E3*XM3))**2*C+(DC*(E3+XM3)/
1SQRT(E3**2+2.0*E3*XM3))*B+A

SENSE LIGHT 0

TYPE 500

1 READ 600

TYPE 600

600 FORMAT(48H

100 READ 401,A,B,C

TYPE 506,A,B,C

READ 406,ALPHA

TYPE 507,ALPHA

12 READ 401,AMU1,AMU3,E1,D

AMU1=931.141*AMU1

AMU3=931.141*AMU3

DC=D/0.299793

READ 400,MA,MF

DO 13 J=1,MF,1

READ 404,TITLE(J,1),TITLE(J,2),TITLE(J,3),TITLE(J,4),TITLE(J,5),

1TITLE(J,6)

READ 400,LD(J)

IF(LD(J))14,15,14

14 READ 400,JI(J),JE(J)

15 CALL ASSEMBLE(J,K,L,NAME,KM,SD,AV,XMU2,QO,NS)

LN(J)=L

READ 403,MS(J),XMS(J),JM(J),XJM(J)

13 CONTINUE

DO 50 JK=1,MA,1

READ 401,THETA

IF(SENSE SWITCH 1)101,102

101 IF(SENSE LIGHT 5)103,102

103 READ 401,A,B,C

TYPE 506,A,B,C

102 SENSE LIGHT 5

DO 50 J=1,MF,1

PUNCH TAPE 404,(TITLE(J,K),K=1,6,1),THETA

PUNCH TAPE 400,LD(J)

IF(LD(J))51,52,51

51 PUNCH TAPE 400,JI(J),JE(J)

PAUSE

52 DO 53 I=1,LN(J),1

PUNCH TAPE 405,NAME(J,I,K),K=1,3,1

IF(KM(J,I))53,53,55

55 GO TO (53,53,53,21,22,53,53,53),KM(J,I)

21 PUNCH TAPE 401,SD(J,I)

GO TO 53

22 AMU2=931.141*XMU2(J,I)

QO=QO(J,I)

EXN=AV(J,I)

CALL ENEG(AMU1,AMU2,AMU3,E1,QO,EXN,THETA,E3)

AXE=YF(AMU3)

PUNCH TAPE 401,AXE,SD(J,I)


```

53  CONTINUE
    EXN=-(SQRT(B**2-4.0*(A-MS(J))*C)+B)/(2.0*C)
    X=D**2/((0.299793*EXN)**2-D**2)
    AMU2=931.141*XMS(J)
    E3=E3F(AMU3)
    EXN=-EXF(AMU2)
    QO=0.0
    CALL ENEG(AMU1,AMU2,AMU3,E1,QO,EXN,THETA,E3)
    MX=YF(AMU3)
    EXN=-(SQRT(B**2-4.0*(A-JM(J))*C)+B)/(2.0*C)
    X=D**2/((0.299793*EXN)**2-D**2)
    AMU2=931.141*XJM(J)
    E3=E3F(AMU3)
    EXN=-EXF(AMU2)
    CALL ENEG(AMU1,AMU2,AMU3,E1,QO,EXN,THETA,E3)
    JX=YF(AMU3)
    IF(99-JX+MX)57,58,58
57  MX=JX-99
58  IF(MX)59,59,60
59  MX=2
60  PUNCH TAPE 400,MX,JX
60  CONTINUE
    CALL EXIT
500  FORMAT($GAUSSIAN ANALYSIS INPUT DATA GENERATOR$)
400  FORMAT(2I4)
401  FORMAT(4F12.6)
403  FORMAT(I4,F12.6,I4,F12.6)
404  FORMAT(6A8,F8.3)
406  FORMAT(F8.3)
405  FORMAT(3A4)
506  FORMAT(10X$A =$F12.6,3X$B =$F12.6,3X$C =$F12.6)
507  FORMAT(10X$ALPHA =$F8.3)
    END

```


\$IBSYS

```
      SUBROUTINE ASSEMBLE(N,K,L,NAME,KM,SD,AV,XMU2,Q0,NS)
      DIMENSION NAME(15,12,3),KM(15,12),SD(15,12),AV(15,12),XMU2(15,12)
      1 Q0(15,12),NS(3)
      K=1
      L=1
15     READ 1,NS(1),NS(2),NS(3)
      DO 2 J=1,3,1
      I=NOM(J,NS)
      IF(I-9)4,20,20
4      GO TO (5,6,6),J
5      ASSIGN 11 TO JI
      IF(I)20,10,7
7      GO TO (11,11,11,12,13),I
12     READ 100,SD(N,K)
      GO TO 11
13     READ 100,AV(N,K),SD(N,K),XMU2(N,K),Q0(N,K)
11     KM(N,K)=I
      NAME(N,L,J)=NS(J)
      K=K+1
      GO TO 2
6      ASSIGN 8 TO JI
      IF(I)8,10,8
8      NAME(N,L,J)=NS(J)
2      CONTINUE
9      L=L+1
      GO TO 15
10     IF(SENSE LIGHT 1)21,22
22     SENSE LIGHT 1
      GO TO JI
21     IF(12-L)20,25,25
20     TYPE 104
      GO TO 15
23     TYPE 103
24     PAUSE
1      FORMAT(3A4)
100    FORMAT(4F12.6)
103    FORMAT($ERROR$)
104    FORMAT($ILLEGAL OP CODE$)
25     NAME(N,L,J)=NS(J)
      KM(N,K)=I
      RETURN
      END
```


\$IBSYS

```
SUBROUTINE ENEG(AMU1,AMU2,AMU3,E1,Q0,EXN,THET,E3)
RAD=.017453292
PI=3.14159265
Q=Q0-EXN
18 AMUI=AMU1+AMU2
W1=E1
ET=AMUI+W1
16 QQ=AMU3+Q
QQQ=AMU3+Q/2.
A1=2.*(AMU2*W1-Q*QQQ+AMUI*QQ)
P12=2.*AMU1*W1+W1*W1
V2=P12/(ET*ET)
V3=1.-V2
ET2B=ET*ET*V3
PF2=(A1*A1-4.*ET2B*AMU3*AMU3)/(4.*ET2B)
RHO=SQRT(P12)*(A1/(2.*SQRT(ET2B)))/(SQRT(PF2)*ET)
21 COSN=COS(THET*RAD)
19 AMARS=ET*ET-P12*COSN*COSN
Z1=A1*ET/(AMARS*2.)
Z=SQRT(P12)*COSN*SQRT(A1*A1-4.*AMU3*AMU3*AMARS)/(AMARS*2.)
E3=Z1+Z
23 E3=E3-AMU3
RETURN
END
```


\$IBSYS

CNEUTRON TIME OF FLIGHT CONTROL GENERATOR FOR NONLINEAR GAUSSIAN ANALYSIS

C LINEAR CALIBRATION FITTING PROGRAM

```
      DIMENSION P(2,25),C(2,3),Y(25),CSI(3),W(25),T(25), TITLE(15,6),
1     1LD(15),JI(15),JE(15),NS(3),NAME(15,12,3),MS(15),XMS(15),
2     2JM(15),XJM(15),          LN(15),KM(15,12),QO(15,12),AV(15,12),
3     3SD(15,12),XMU2(15,12)
      TYPE 500
1     READ 600
      TYPE 600
      READ 400,M
600   FORMAT(48H
      DF=M-2
      IF(DF)2,2,3
2     TYPE 510
510   FORMAT($PARAMETER EXCFSS$)
      DF=1.0
3     TYPE 513
      DO 4 J=1,M,1
      READ 401,T(J),Y(J),SDX
      W(J)=1.0/SDX**2
4     TYPE 501,T(J),Y(J),SDX
      DO 5 J=1,M,1
      P(1,J)=1.0
5     P(2,J)=T(J)
      DO 6 I=1,2,1
      CSI(I)=0.0
      DO 6 K=1,M,1
6     CSI(I)=W(K)*Y(K)*P(I,K)+CSI(I)
      DO 7 I=1,2,1
      DO 7 J=I,2,1
      C(I,J)=0.0
      DO 103 K=1,M,1
103   C(I,J)=W(K)*P(I,K)*P(J,K)+C(I,J)
7     C(J,I)=C(I,J)
      DELTA=C(1,1)*C(2,2)-C(1,2)**2
      IF(DELTA)202,200,202
200   TYPE 512
      PAUSE
      GO TO 1
202   TS=C(1,1)
      C(1,1)=C(2,2)/DELTA
      C(2,2)=TS/DELTA
      C(1,2)=-C(1,2)/DELTA
      C(2,1)=C(1,2)
      DO 8 I=1,2,1
      C(I,3)=0.0
      DO 8 J=1,2,1
8     C(I,3)=CSI(J)*C(I,J)+C(I,3)
      DA=SQRT(ABS(C(1,1)))
      DB=SQRT(ABS(C(2,2)))
      SUM=0.0
      DO 9 K=1,M,1
      YI=C(1,3)+C(2,3)*T(K)
9     SUM=W(K)*(Y(K)-YI)**2+SUM
      EPSQ=SUM/DF
      EPS=SQRT(EPSQ)
      TYPE 502,EPSQ,EPS
512   FORMAT($MATRIX IS SINGULAR$)
      DDA=DA*EPS
```



```

DDB=DB*EPS
TYPE 503
TYPE 505
A=C(1,3)
B=C(2,3)
TYPE 506,A,DA,DDA,B,DB,DDB
CALL EXIT
500  FORMAT($GAUSSIAN ANALYSIS INPUT DATA GENERATORS$)
400  FORMAT(2I4)
401  FORMAT(4F12.6)
501  FORMAT(10XF12.6,5X,F12.6,5X,F12.6)
513  FORMAT(10X$TIMES$13X$CHANNEL NOS$7X$ERRORS$)
502  FORMAT(10X$CHISQ =$E13.6,5X$CHI =$E13.6)
503  FORMAT(10X$THE CALIBRATION LINE  Y = A + B*TS)
505  FORMAT(10X$COEFFICIENT$6X$STATISTICAL ERROR$5X$TOTAL ERRORS$)
403  FORMAT(I4,F12.6,I4,F12.6)
406  FORMAT(F8.3)
507  FORMAT(10X$ALPHA =$F8.3)
506  FORMAT(10X$A =$F12.6,2X,F12.6,10X,F12.6/10X$B =$F12.6,2X,F12.6,
110X,F12.6)
END

```


\$IBSYS

CNEUTRON TIME OF FLIGHT CONTROL GENERATOR FOR NONLINEAR GAUSSIAN ANALYSIS

C LINEAR CALIBRATION LINE

```

  DIMENSION P(2,25),C(2,3),Y(25),CSI(3),W(25),T(25), TITLE(15,6),
  1LD(15),JI(15),JE(15),NS(3),NAME(15,12,3),MS(15),XMS(15),
  2JM(15),XJM(15), LN(15),KM(15,12),QO(15,12),AV(15,12),
  3SD(15,12),XMU2(15,12)
  EXF(AMU)=(1.0+AMU3/(AMU3+AMU))*F2-(1.0-AMU1/(AMU3+AMU))*E1-
  12.0/(AMU3+AMU)*COS(ALPHA)*SQRT(AMU1*AMU2*E1*F3)
  F3F(AMU)=0.5*AMU*(X-0.25*X**2+0.125*X*X**2)
  YF(XM3)=(DC*(F3+XM3)/SQRT(E3**2+2.0*F3*XM3))*B+A
  SENSE LIGHT 0
100 READ 401,A,B
  READ 406,ALPHA
12 READ 401,AMU1,AMU3,F1,D
  AMU1=931.141*AMU1
  AMU3=931.141*AMU3
  DC=D/0.299793
  READ 400,MA,MF
  DO 13 J=1,MF,1
  READ 404,TITLE(J,1),TITLE(J,2),TITLE(J,3),TITLE(J,4),TITLE(J,5),
  1TITLE(J,6)
  READ 400,LD(J)
  IF(LD(J))14,15,14
14 READ 400,JI(J),JE(J)
15 CALL ASSEMBLE(J,K,L,NAME,KM,SD,AV,XMU2,QO,NS)
  LN(J)=L
  READ 403,MS(J),XMS(J),JM(J),XJM(J)
13 CONTINUE
  DO 50 JK=1,MA,1
  READ 401,THETA
  IF(SENSE SWITCH 1)101,102
101 IF(SENSE LIGHT 5)103,102
103 READ 401,A,B
  TYPE 506,A,B
102 SENSE LIGHT 5
  DO 50 J=1,MF,1
  PUNCH TAPE 404,(TITLE(J,K),K=1,6,1),THETA
  PUNCH TAPE 400,LD(J)
  IF(LD(J))51,52,51
51 PUNCH TAPE 400,JI(J),JE(J)
  PAUSE
52 DO 53 I=1,LN(J),1
  PUNCH TAPE 405,NAME(J,I,K),K=1,3,1
  IF(KM(J,I))53,53,55
55 GO TO (53,53,53,21,22,F2,F2,F2),KM(J,I)
21 PUNCH TAPE 401,SD(J,I)
  GO TO 53
22 AMU2=931.141*XMU2(J,I)
  QO=QO(J,I)
  EXN=AV(J,I)
  CALL ENEG(AMU1,AMU2,AMU3,E1,QO,FXN,THETA,E3)
  AXE=YF(AMU3)
  PUNCH TAPE 401,AXE,SD(J,I)
53 CONTINUE
  FXN=(MS(J)-A)/R
  X=D**2/((0.299793*FXN)**2-D**2)
  AMU2=931.141*XMS(J)
  F3=F3F(AMU3)
  EXN=-EXF(AMU2)
```



```

Q0=0.0
CALL ENEG(AMU1,AMU2,AMU3,E1,Q0,EXN,THETA,E3)
MX=YF(AMU3)
EXN=(JM(J)-A)/B
X=D**2/((0.299793*EXN)**2-D**2)
AMU2=931.141*XJM(J)
E3=E3F(AMU3)
EXN=-EXF(AMU2)
CALL ENEG(AMU1,AMU2,AMU3,F1,Q0,FXN,THETA,E3)
JX=YF(AMU3)
IF(99-JX+MX)57,58,58
57  MX=JX-99
58  IF(MX)59,59,60
59  MX=2
60  PUNCH TAPE 400,MX,JX
50  CONTINUE
CALL EXIT
500  FORMAT($GAUSSIAN ANALYSIS INPUT DATA GENERATORS)
506  FORMAT(10X$A =$F12.6,3X$B =$F12.6)
400  FORMAT(2I4)
401  FORMAT(4F12.6)
501  FORMAT(10XF12.6,5X,F12.6,5X,F12.6)
513  FORMAT(10X$TIME$13X$CHANNEL NO$7X$ERRORS)
502  FORMAT(10X$CHISQ =$F13.6,5X$CHI =$E13.6)
503  FORMAT(10X$THE CALIBRATION LINE Y = A + B*$T$)
505  FORMAT(10X$COEFFICIENT$6X$STATISTICAL FRROR$5X$TOTAL ERRORS)
403  FORMAT(I4,F12.6,I4,F12.6)
404  FORMAT(6A8,F8.3)
405  FORMAT(3A4)
406  FORMAT(F8.3)
507  FORMAT(10X$ALPHA =$F8.3)
END

```


\$IBSYS

```
SUBROUTINE ASSFMBLE(N,K,L,NAME,KM,SD,AV,XMU2,QO,NS)
  DIMENSION NAME(15,12,3),KM(15,12),SD(15,12),AV(15,12),XMU2(15,12)
  1QO(15,12),NS(3)
  K=1
  L=1
15  READ 1,NS(1),NS(2),NS(3)
  DO 2 J=1,3,1
    I=NOM(J,NS)
    IF(I-9)4,20,20
4    GO TO (5,6,6),J
5    ASSIGN 11 TO JI
    IF(I)20,10,7
7    GO TO (11,11,11,12,13),I
12   READ 100,SD(N,K)
    GO TO 11
13   READ 100,AV(N,K),SD(N,K),XMU2(N,K),QO(N,K)
11   KM(N,K)=I
    NAME(N,L,J)=NS(J)
    K=K+1
    GO TO 2
6    ASSIGN 8 TO JI
    IF(I)8,10,8
8    NAME(N,L,J)=NS(J)
2    CONTINUE
9    L=L+1
    GO TO 15
10   IF(SENSE LIGHT 1)21,22
22   SENSE LIGHT 1
    GO TO JI
21   IF(12-L)20,25,25
20   TYPE 104
    GO TO 15
23   TYPE 103
24   PAUSE
1    FORMAT(3A4)
100  FORMAT(4F12.6)
103  FORMAT($ERROR$)
104  FORMAT($ILLEGAL OP CODE$)
25   NAME(N,L,J)=NS(J)
    KM(N,K)=I
    RETURN
  END
```


\$IBSYS

```
SUBROUTINE ENEG(AMU1,AMU2,AMU3,E1,Q0,EXN,THET,E3)
RAD=.017453292
PI=3.14159265
Q=Q0-EXN
18 AMUI=AMU1+AMU2
W1=E1
ET=AMUI+W1
16 QQ=AMU3+Q
QQQ=AMU3+Q/2.
A1=2.*(AMU2*W1-Q*QQQ+AMUI*QQ)
P12=2.*AMU1*W1+W1*W1
V2=P12/(ET*ET)
V3=1.-V2
ET2B=ET*ET*V3
PF2=(A1*A1-4.*ET2B*AMU3*AMU3)/(4.*ET2B)
RHO=SQRT(P12)*(A1/(2.*SQRT(ET2B)))/(SQRT(PF2)*ET)
21 COSN=COS(THET*RAD)
19 AMARS=ET*ET-P12*COSN*COSN
Z1=A1*ET/(AMARS*2.)
Z=SQRT(P12)*COSN*SQRT(A1*A1-4.*AMU3*AMU3*AMARS)/(AMARS*2.)
E3=Z1+Z
23 E3=E3-AMU3
RETURN
END
```



```

$IBSYS
  DIMENSION KS(512),IM(10),KM(10),NS(10),P(10,100),C(10,11),CSI(10),
1RESID(100),GB(10),AV(10),SD(10),DA(10),LR(10),LC(10)
  ACCEPT TAPE 59,THETA
  IF(SENSE SWITCH 1) 161,162
161 WRITE OUTPUT TAPE 7, 59,THETA
  GO TO 160
162 TYPE 59,THETA
160 N=1
  JM=1
  K=1
  L=0
  ACCEPT TAPE 43,J
  IF(J)2,3,2
2  ACCEPT TAPE 43,JI,JE
  IF(SENSE SWITCH 1) 171,170
171 WRITE OUTPUT TAPE 7, 44,JI,JE
  GO TO 3
170 TYPE 44,JI,JE
3  CALL DECOD(N,JM,L,K,NS,IM,KM,LC,AV,SD,LR)
  NOB=N-1
  SENSE LIGHT 1
  CALL DECOD(N,JM,L,K,NS,IM,KM,LC,AV,SD,LR)
  ACCEPT TAPE 43,MS,JM
  IF(SENSE SWITCH 1) 181,180
181 WRITE OUTPUT TAPE 7, 45,MS,JM
  GO TO 185
180 TYPE 45,MS,JM
43  FORMAT(2I4)
44  FORMAT(10X$START LOAD =$I4,5X$STOP =$I4)
45  FORMAT(10X$START FIT =$I4,5X$STOP FIT =$I4)
54  FORMAT(10X,A4,2H= F14.6,5X,E14.6,6X,F14.6)
59  FORMAT(48H
185 CALL EXIT
  END

```

,F8.3)

\$IBSYS

```
C LEAST SQUARES MASS AND Q IDENTIFICATION WITH MEAN EXCITATION AND ERRORS
  DIMENSION P(2,25),C(2,3),CSI(2),W(25),THETA(25),Y(25),F(25),WQ(25),
  1CO(25),SRE3(25),AV(25),AZ(25),RESID(25),EPSQ(10)
  QF(1)=A1*E3+A2-A3*SQRT(A0*E3)*CO(1)
  SENSE LIGHT 0
  IF(SENSE SWITCH 1)16,61
16  ASSIGN 90 TO J1
  ASSIGN 81 TO J2
  TYPE 31
10  NK=1
  READ 401,XM1,XM3
  TYPE 301,XM1,XM3
  9  READ 401,E1
  TYPE 309,E1
20  A0=XM1*XM3*E1
  SRA0=SQRT(A0)
  7  READ 402,NOM
  IF(NOM)8,1000,8
  8  READ 402,M
  GO TO J1
90  TYPE 3
  DO 23 J=1,M,1
  READ 403,THETA(J),E3,SD
  TYPE 303,THETA(J),E3,SD
  W(J)=(4.0*E3)/(SD**2)
  Y(J)=SQRT(E3)
23  CO(J)=COS(1.74532925E-2*THETA(J))
29  TS=2.0*SRA0*(Y(1)*CO(1)-Y(M)*CO(M))
  XM4=TS/(Y(1)**2-E3)-XM3
  I=M
  DF=M-2
  IF(DF)35,35,24
35  DF=1.0
  TYPE 36
24  A1=XM3/XM4+1.0
  A2=(XM1/XM4-1.0)*E1
  A3=2.0/XM4
26  Q=QF(1)
  GO TO J2
28  A4=XM3+XM4
  AM=1.0/A4
  AW=(XM4*Q+(XM4-XM1)*E1)*A4
  SUM=0.0
  DO 34J=1,M,1
34  AV(J)=SRA0*CO(J)
32  DO 30 J=1,M,1
  AZ(J)=SQRT(AV(J)**2+AW)
  SRE3(J)=(AV(J)+AZ(J))*AM
  RESID(J)=(Y(J)-SRE3(J))*W(J)
30  SUM=RESID(J)**2/W(J)+SUM
  EPSQ(NK)=SUM/DF
  EPS=SQRT(EPSQ(NK))
  TYPE 308,EPSQ(NK),EPS
  IF(NK-1)40,40,33
33  IF(EPSQ(NK)-EPSQ(NK-1))45,50,46
46  IF(NK-2)40,40,50
45  IF(EPSQ(NK-1)-EPSQ(NK)-0.0001)50,50,47
47  IF(NK-10)40,50,50
40  DO 41 J=1,M,1
```



```

      P(1,J)=AV(J)+AZ(J)
41    P(2,J)=AM/(2.0*AZ(J))
100   DO 104 I=1,2,1
      CSI(I)=0.0
      DO 104 K=1,M,1
104   CSI(I)=RESID(K)*P(I,K)+CSI(I)
      DO 102 I=1,2,1
      DO 102 J=1,2,1
      C(I,J)=0.0
      DO 103 K=1,M,1
103   C(I,J)=W(K)*P(I,K)*P(J,K)+C(I,J)
102   C(J,I)=C(I,J)
      DELTA=C(1,1)*C(2,2)-C(1,2)*C(2,1)
      IF(DELTA)202,200,202
200   TYPE 107
      GO TO 7
202   TS=C(1,1)
      C(1,1)=C(2,2)/DELTA
      C(2,2)=TS/DELTA
      C(1,2)=-C(1,2)/DELTA
      C(2,1)=C(1,2)
      DO 203 I=1,2,1
      C(I,3)=0.0
      DO 203 J=1,2,1
203   C(I,3)=CSI(J)*C(I,J)+C(I,3)
      TYPE 310,C(1,3),C(2,3)
      AM=AM+C(1,3)
      AW=AW+C(2,3)
      NK=NK+1
      SUM=0.0
      GO TO 32
50    SDM4=SQRT(ABS(C(1,1)))
      SDQ=SQRT(ABS(C(2,2)))
      XM4=(1.0-AM*XM3)/AM
      Q=(AM*AW+(XM1-XM4)*E1)/XM4
      DM4=(1.0/(AM*AM)+XM3)*SDM4
      DQ=(AM*SDQ+AW*SDM4+E1*DM4)*DM4/(XM4*XM4)
      TDM4=DM4*EPS
      TDQ=DQ*EPS
      TYPE 311,XM4,DM4,TDM4
      TYPE 312,Q,DQ,TDQ
      NK=1
      PAUSE
      IF(SENSE SWITCH 2)70,7
C ENTRY POINT FOR TIME READIN
61    ASSIGN 5 TO J1
      ASSIGN 81 TO J2
      TYPE 31
      READ 401,D,DD
      TYPE 305,D
      GO TO 10
5     XMEV=0.5*931.141*XM3
      D2=D**2
      TYPE 3
      IF(SENSE SWITCH 3)63,60
60    DO 62 I=1,M,1
      READ 403,THETA(I),T,SD
      TYPE 303,THETA(I),T,SD
      X=D2/((0.299793*T)**2-D2)
      Y(I)=SQRT(XMEV*(X-0.25*X**2+0.125*X**3))

```



```

      W(I)=(0.299793**2*T**4)/(XMEV*D2*SD**2)
62    CO(I)=COS(1.74532925E-2*THETA(I))
      E3=Y(M)**2
      GO TO 29
63    CALL CAL(D,DD,D2,XMEV,Y,W,CO,E3,THETA,M)
      GO TO 29
81    TYPE 313,XM4
      TYPE 314,Q
      GO TO 28
C    ENTRY POINT FOR EXCITATION ENERGY
70    READ 401,XM4,Q0
      TYPE 315,XM4,Q0
      ASSIGN 71 TO J2
      GO TO 24
71    SUM=0.0
      SUMN=0.0
      SM2=0.0
      DO 72 J=1,M,1
        E3=Y(J)**2
        TS=(2.0*E3*A1+A3*SRA0*CO(J))
        WQ(J)=W(J)/(TS**2)
        Q=QF(J)
        F(J)=Q
        XM2=Q**2
        SUMN=WQ(J)+SUMN
        SUM=WQ(J)*F(J)+SUM
72    SM2=WQ(J)*XM2+SM2
        Q=SUM/SUMN
        AM2=SM2/SUMN
        DQ=AM2-Q**2
        FSN=M-1
        DQ=SQRT(DQ/FSN)
        EXN=Q0-Q
        TYPE 316,EXN,DQ
        TYPE 317
        DO 80 I=1,M,1
          Q=Q0-F(I)
          DQ=1.0/SQRT(W(I))
80    TYPE 318,THETA(I),Q,DQ
      ASSIGN 81 TO J2
      PAUSE
      IF(SENSE SWITCH 2)70,7
1000 CALL EXIT
31    FORMAT(5X$LEAST SQUARES MASS AND Q IDENTIFICATIONS$)
404  FORMAT(A3)
401  FORMAT(2F12.6)
301  FORMAT(10X,5HM1 = ,F12.6,5X,5HM3 = ,F12.6)
305  FORMAT(10X,4HD = ,F12.6)
309  FORMAT(10X,5HE1 = ,F12.6)
402  FORMAT(I3)
3    FORMAT(10X$INPUT DATA$)
403  FORMAT(3(F12.6))
303  FORMAT(10X,3(F12.6,3X))
36   FORMAT(5X$NO OF FITTED PARAMETERS EQUALS NO OF DATA POINTS$)
308  FORMAT(10X$EPSILON SQUARED =$E13.6,5X$EPSILON =$E13.6)
107  FORMAT(5X$MATRIX IS SINGULAR$)
310  FORMAT(/10X$DAM =$E13.6,5X$DAW =$E13.6)
311  FORMAT(/10X$BEST FIT M4 =$F10.5,5X$SD =$F10.5,5X$TOTAL ERROR =$
1F10.5)
312  FORMAT(10X$BEST FIT  Q =$F10.5,5X$SD =$F10.5,5X$TOTAL ERROR =$

```



```
1F10.5)  
313  FORMAT(//10X,7HM4-0 = ,F10.5)  
314  FORMAT(10X,7H Q-0 = ,F10.5)  
315  FORMAT(10X,5HM4 = ,F10.6,5X,5HQ0 = ,F10.6)  
316  FORMAT(10X,18HMEAN EXCITATION = ,F9.6,5X,5HSD = ,F9.6)  
317  FORMAT(/10X$THETA$10X$EXCITATION$10X$ERROR$)  
318  FORMAT(10X,F8.3,7X,F9.6,11X,F9.6)  
END
```


\$IBSYS

```
SUBROUTINE CAL(D,DD,D2,XMEV,Y,W,CO,E3,THETA,M)
DIMENSION Y(1),W(1),CO(1),THETA(1)
60 DO 62 I=1,M
  IF(SENSE SWITCH 4)63,64
64 IF(SENSE LIGHT 2)65,63
63 READ 403,A,DA,B,DB
  SENSE LIGHT 2
  TYPE 303,A,DA,B,DB
65 READ 403,THETA(I),CH,SD
  TYPE 303,THETA(I),CH,SD
  T=(CH-A)/B
  SD=(DCH+DA)/ABS(B)+((A-CH)*DB)/B**2
  X=D2/((0.299793*T)**2-D2)
  Y(I)=SQRT(XMEV*(X-0.25*X**2+0.125*X**3))
  W(I)=(0.299793**2*T**4)/(XMEV*(D2*SD**2+(T*DD)**2))
62 CO(I)=COS(1.74532925E-2*THETA(I))
  E3=Y(M)**2
403 FORMAT(4E12.5)
303 FORMAT(10X,4(F12.6,3X))
RETURN
END
```



```

$IRSYS
* ANGULAR DISTRIBUTION ANALYSIS
  DIMENSION KPOLY(11),DEGREE(37),COUNT(37),WEIGHT(37),RADIAN(37),
  1POLY(11,37),RHS(11),TRIX(11,12),UNSTAT(11),UNTOT(11),
  2STAT(11),TOT(11),REL(11),BO(11),LC(11),LR(11),P(20)
500  TYPE 103
      READ 102
      TYPE 102
      LINE=0
21   READ 100, NPOLY
      NPOLY=NPOLY+1
      KPOLY(1)=0
      READ 100, (KPOLY(I), I=2,NPOLY)
      READ 100, NANG
      READ 101, (DEGREE(I),COUNT(I),WEIGHT(I), I=1,NANG)
      DO 25 I=1, NANG
        RADIAN(I)=DEGREE(I)*0.0174532925
        WEIGHT(I)=1.0/WEIGHT(I)**2
25   POLY(1,I)=1.0
      MAX=KPOLY(1)
      DO 950 I=2, NPOLY
        IF (KPOLY(I)-MAX) 950,950,951
951   MAX=KPOLY(I)
950   CONTINUE
      DO 900 N=1,NANG
        X=COS(RADIAN(N))
        P(1)=X
        P(2)=1.5*X**2-0.5
        DO 901 J=3, MAX
901   P(J)=((2*J-1)*X*P(J-1)-(J-1)*P(J-2))/J
        DO 902 K=2, NPOLY
902   POLY(K,N)=P(KPOLY(K))
900   CONTINUE
      NPOLY1=NPOLY+1
      DO 30 I=1,NPOLY
        RHS(I)=0.0
        DO 29 J=1,NANG
29   RHS(I)=WEIGHT(J)*COUNT(J)*POLY(I,J)+RHS(I)
        TRIX(I,NPOLY1)=RHS(I)
30   CONTINUE
      DO 31 I=1,NPOLY
        DO 31 J=1,I
          TRIX(I,J)=0.0
        DO 28 K=1, NANG
28   TRIX(I,J)=WEIGHT(K)*POLY(I,K)*POLY(J,K)+TRIX(I,J)
          TRIX(J,I)=TRIX(I,J)
31   CONTINUE
      CALL MINV(NPOLY,NPOLY1,TRIX,LR,LC)
      A0=TRIX(1,NPOLY1)
      DO 32 K=1, NPOLY
        UNSTAT(K)=SQRT(ABS(TRIX(K,K)))
        REL(K)=(UNSTAT(K)/TRIX(K,NPOLY1))**2
        BO(K)=TRIX(K,NPOLY1)/A0
32   STAT(K)=ABS(SQRT(REL(1))+REL(K))*BO(K)
      STAT(1)=0.0
      IF (NANG-NPOLY) 40,40,35
40   EPSQ=0.0
      EPS=0.0
      GO TO 41
35   SUM=0.0

```



```

SUMN=0.0
DO 36 I=1, NANG
36 SUM=WEIGHT(I)*(COUNT(I)**2)+SUM
DO 37 I=1, NPOLY
37 SUMN=TRIX(I,NPOLY1)*RHS(I)+SUMN
SUM=SUM-SUMN
IF (SUM) 40,38,38
38 EPSQ=SUM/(NANG-NPOLY)
EPS=SQRT(EPSQ)
41 DO 42 I=1, NPOLY
UNTOT(I)=UNSTAT(I)*EPS
42 TOT(I)=STAT(I)*EPS
TYPE 104, (EPSQ,EPS)
TYPE 105
TYPE 106
TYPE 107, (KPOLY(I),TRIX(I,NPOLY1),UNSTAT(I),UNTOT(I),I=1,NPOLY)
TYPE 108
TYPE 106
TYPE 107, (KPOLY(I),BO(I),STAT(I),TOT(I), I=1, NPOLY)
LINE=2*(NPOLY+4)+9+NANG+LINE
IF (LINE-56) 70,70,60
70 TYPE 109
DO 71 I=1, NANG
Y=0.0
DO 72 J=1, NPOLY
72 Y=TRIX(J,NPOLY1)*POLY(J,I)+Y
TYPE 110, (DEGREE(I),COUNT(I),Y)
71 CONTINUE
80 DO 81 I=LINE,66
81 TYPE 111
GO TO 500
60 LINE=LINE-NANG-3
DO 75 I=LINE,66
75 TYPE 111
LINE=NANG+3
GO TO 70
100 FORMAT(I2)
101 FORMAT (F12.6,F12.6,F12.6)
102 FORMAT ($ )
103 FORMAT ($ ANGULAR DISTRIBUTION ANALYSIS$)
104 FORMAT (//,$EPSILON SQUARED =$,F10.5,$ EPSILON =$,F9.5)
105 FORMAT(//,15X,$UNNORMALIZED COEFFICIENTS$)
106 FORMAT(3X,$COEFFICIENT STATISTICAL ERROR TOTAL ERRORS$)
107 FORMAT(1HA,I2,1H=,E13.5,5X,E13.5,7X,E13.5)
108 FORMAT(//,16X,$NORMALIZED COEFFICIENTS$)
109 FORMAT(//,1X,$THETA$,5X,$OBSERVED Y$,5X,$CALCULATED Y$)
110 FORMAT(F7.2,2X,F10.2,6X,F10.2)
111 FORMAT ( )
CALL EXIT
END

```


APPENDIX II

Absolute differential cross sections (mb/sr) for $\text{Si}^{30}(\text{d},\text{n})\text{P}^{31}$
at $E_d = 5 \text{ MeV}$.

ANGULAR DISTRIBUTION OF THE 0.0000 STATE OF				
P 31 FROM $\text{Si}^{30}(\text{D},\text{N})\text{P}^{31}$ JUNE 30/65				
RLN NC	ANGLE C CF M	CORRECTED AREA	ERROR	
2	30.939	0.49766391	0.08207419	
3	0.000	10.80136327	0.41010021	
4	15.486	4.90478377	0.22445750	
5	46.328	1.11956121	0.11003203	
6	61.626	0.72522352	0.08944369	
7	121.626	0.21552935	0.05208049	
8	150.938	0.03238550	0.08161339	
9	76.814	0.31197308	0.06440901	
10	30.939	0.58429717	0.09246733	
11	20.642	2.52937888	0.13202278	
12	5.164	10.00750369	0.40765179	
13	0.000	10.58105264	0.41038024	
14	25.794	1.22355697	0.11255792	
15	36.077	0.40675992	0.06824073	
16	96.870	0.22681793	0.05364241	
17	136.327	0.41887399	0.07515032	
18	76.814	0.36643810	0.12863321	
19	41.207	0.53792416	0.08058302	
20	5.164	9.72084629	0.44218483	
21	10.326	7.84625940	0.37613191	
22	61.626	0.75541992	0.10104224	
23	106.813	0.60278626	0.04665885	
24	0.000	9.98625408	0.46080886	
25	121.626	0.23869601	0.03417164	

ANGULAR DISTRIBUTION OF THE 1.26500 STATE OF				
P 31 FROM $\text{Si}^{30}(\text{D},\text{N})\text{P}^{31}$ JUNE 30/65				
RLN NC	ANGLE C CF M	CORRECTED AREA	ERROR	
2	31.005	1.90042360	0.13215674	
3	0.000	0.90563426	0.13077351	
4	15.520	1.05208779	0.10964973	
5	46.422	1.10367963	0.09952241	
6	61.741	0.56395892	0.07507385	
7	121.741	0.41868619	0.06207195	
8	151.005	0.61582531	0.08007312	
9	76.942	0.53616214	0.07015254	
10	31.005	1.92142978	0.14576338	
11	20.688	1.37199939	0.09550466	
12	5.175	1.00951232	0.14459968	
13	0.000	1.10728483	0.14170949	
14	25.850	1.60914040	0.12448564	
15	36.153	1.75006542	0.10778449	
16	97.003	0.65540826	0.06813534	
17	136.421	0.60848723	0.07985538	
18	76.942	0.45431106	0.12240422	
19	41.292	1.46336895	0.10720573	
20	5.175	0.95306053	0.14993777	
21	10.349	1.11223911	0.14694506	
22	61.741	0.60362528	0.08564776	
23	106.942	0.62356371	0.07397105	
24	0.000	0.89321597	0.15757268	
25	121.741	0.51787324	0.04230537	

ANGULAR DISTRIBUTION OF THE 2.23200 STATE OF P 31 FROM SI30(D,N) P31 JUNE 30/65				
RLN NC	ANGLE C CF M	CORRECTED AREA	ERRCR	
2	31.067	1.55035995	0.11922182	
3	0.000	1.08892019	0.13538621	
4	15.552	1.33341891	0.11620457	
5	46.509	1.05894906	0.09696668	
6	61.848	0.46673824	0.06913691	
7	121.847	0.50913558	0.06276986	
8	151.066	0.30156590	0.06355664	
9	77.061	0.32271721	0.05388373	
10	31.067	1.36922579	0.11832803	
11	20.730	1.24649245	0.08776555	
12	5.186	1.09139977	0.14323138	
13	0.000	1.16871364	0.14075264	
14	25.902	1.44404333	0.11440894	
15	36.224	1.43549551	0.09375274	
16	97.125	0.43856544	0.05759847	
17	136.508	0.42702492	0.06866411	
18	77.061	0.29565413	0.10755156	
19	41.372	1.24926958	0.09849637	
20	5.186	1.03423189	0.15320394	
21	10.371	1.10751558	0.14511059	
22	61.848	0.59307459	0.08418878	
23	107.061	0.56098559	0.06838609	
24	0.000	0.96071509	0.16041897	
25	121.847	0.48161351	0.03915990	

ANGULAR DISTRIBUTION OF THE 3.13300 STATE OF P 31 FROM SI30(D,N) P31 JUNE 30/65				
RLN NC	ANGLE C CF M	CORRECTED AREA	ERRCR	
2	31.136	0.00000000	0.00000000	
3	0.000	1.14032488	0.10187756	
4	15.588	0.47538056	0.06481073	
5	46.607	0.28601827	0.04940799	
6	61.968	0.18116840	0.03921844	
7	121.967	0.28553014	0.04848449	
8	151.135	0.25610438	0.05915030	
9	77.195	0.23374463	0.05475317	
10	31.136	0.13648971	0.03109222	
11	20.777	0.20698317	0.05648682	
12	5.198	1.22534136	0.10399147	
13	0.000	1.09496047	0.11526738	
14	25.960	0.10924799	0.04751137	
15	36.303	0.17067777	0.06165652	
16	97.263	0.13540791	0.03871002	
17	136.606	0.30885612	0.05890245	
18	77.195	0.00000000	0.00000000	
19	41.460	0.16111544	0.04741328	
20	5.198	1.11620855	0.10376523	
21	10.395	0.67972366	0.08751734	
22	61.968	0.21319331	0.05333908	
23	107.194	0.23334784	0.05352248	
24	0.000	1.27900227	0.10064720	
25	121.967	0.20174265	0.03429800	

ANGULAR DISTRIBUTION OF THE 4.18800 STATE OF
P 31 FROM SI30(D,N) P31 JUNE 30/65

RLN NC	ANGLE C CF M	CORRECTED AREA	ERROR
2	31.237	0.40387112	0.10000996
3	0.000	0.13696286	0.14112008
4	15.641	0.26253641	0.09588347
5	46.750	0.46417085	0.11167991
6	62.143	0.32415180	0.05781816
7	122.143	0.46093146	0.09760799
8	151.237	0.48907059	0.09066997
9	77.391	0.22607601	0.07237383
10	31.237	0.39557008	0.08939852
11	20.846	0.19542845	0.07224668
12	5.216	0.27969667	0.13563583
13	0.000	0.10358244	0.14674503
14	26.046	0.41194181	0.07304993
15	36.419	0.38578244	0.08152239
16	97.465	0.38806825	0.07064535
17	136.749	0.54897026	0.06318259
18	77.391	0.17623797	0.11750301
19	41.591	0.50151426	0.10298032
20	5.216	0.22860668	0.13548754
21	10.430	0.14511417	0.11609923
22	62.143	0.39985924	0.08795875
23	107.390	0.35526761	0.06225395
24	0.000	0.34762900	0.15882710
25	122.143	0.42354660	0.06456775

ANGULAR DISTRIBUTION OF THE 4.25700 STATE OF
P 31 FROM SI30(D,N) P31 JUNE 30/65

RLN NC	ANGLE C CF M	CORRECTED AREA	ERROR
2	31.245	0.39286847	0.09932954
3	0.000	0.61416544	0.16499322
4	15.644	0.48009580	0.10358218
5	46.761	0.20837532	0.09312793
6	62.157	0.27793262	0.05741909
7	122.156	0.29084803	0.08818083
8	151.244	0.39636072	0.09014809
9	77.405	0.32350253	0.07194963
10	31.245	0.29572704	0.08453810
11	20.852	0.50633780	0.08452123
12	5.217	0.68182011	0.14744410
13	0.000	0.52293171	0.16723846
14	26.052	0.51995311	0.07261444
15	36.428	0.43853545	0.08524979
16	97.481	0.24546038	0.06140493
17	136.760	0.37141991	0.05826537
18	77.405	0.00000000	0.00000000
19	41.601	0.41726137	0.09800480
20	5.217	0.62225488	0.15567191
21	10.432	0.61354022	0.14011834
22	62.157	0.19208427	0.07423539
23	107.405	0.25163457	0.05743450
24	0.000	0.53704635	0.17056496
25	122.156	0.27555686	0.05895926

ANGULAR DISTRIBUTION OF THE 4.43000 STATE OF
P 31 FROM SI30(D,N) P31 JUNE 30/65

RLN NC	ANGLE C CF M	CORRECTED AREA	ERROR
2	31.265	0.80901377	0.11006065
3	0.000	1.06542472	0.19878687
4	15.655	0.71594321	0.11818443
5	46.789	1.12045966	0.14431303
6	62.191	1.19785895	0.08331652
7	122.190	0.61256666	0.09575734
8	151.264	0.36442385	0.08005637
9	77.444	0.66780433	0.08424183
10	31.265	0.77662948	0.09992912
11	20.865	0.69261725	0.09146540
12	5.220	1.07960860	0.17814507
13	0.000	1.12055892	0.22351036
14	26.069	0.83368684	0.07996807
15	36.451	1.19716037	0.10938561
16	97.520	0.64758512	0.07792285
17	136.788	0.47668530	0.05312468
18	77.444	0.37128034	0.13264196
19	41.626	1.24337623	0.12610715
20	5.220	1.14047748	0.19862239
21	10.439	0.76084299	0.15394590
22	62.191	1.33995852	0.12514022
23	107.443	0.65247302	0.06983459
24	0.000	0.78752978	0.19283116
25	122.190	0.65949797	0.06850769

ANGULAR DISTRIBUTION OF THE 4.63000 STATE OF
P 31 FROM SI30(D,N) P31 JUNE 30/65

RLN NC	ANGLE C CF M	CORRECTED AREA	ERROR
2	31.289	0.41050145	0.09175411
3	0.000	0.86151365	0.21455468
4	15.667	0.37078262	0.11169338
5	46.823	0.19240643	0.10263456
6	62.233	0.45141403	0.06828169
7	122.232	0.12822689	0.09831470
8	151.288	0.07003360	0.11380611
9	77.490	0.41687081	0.08258766
10	31.289	0.39085721	0.08557309
11	20.882	0.47968547	0.08953864
12	5.225	0.72158108	0.18659134
13	0.000	0.63165494	0.22713872
14	26.089	0.52564473	0.07407271
15	36.479	0.44733914	0.08218009
16	97.568	0.23758243	0.07215302
17	136.822	0.16076681	0.06518992
18	77.490	0.62060702	0.15199547
19	41.657	0.36946154	0.09447656
20	5.225	0.73298572	0.20259174
21	10.448	0.58304970	0.16666908
22	62.233	0.28656178	0.08432176
23	107.490	0.25659547	0.06846150
24	0.000	0.82926992	0.22591792
25	122.232	0.22524470	0.07229732

ANGULAR DISTRIBUTION OF THE 4.78000 STATE OF
P 31 FROM SI30(D,N) P31 JUNE 30/65

RLN NC	ANGLE C CF M	CORRECTED AREA	ERROR
2	31.308	0.34551485	0.09429124
3	0.000	0.31672420	0.17989472
4	15.677	0.31415839	0.10214756
5	46.850	0.26545519	0.10115945
6	62.266	0.24771351	0.05463384
7	122.265	0.43497277	0.09299469
8	151.307	0.29433759	0.09093076
9	77.527	0.27413749	0.06857589
10	31.308	0.10428619	0.07621484
11	20.895	0.35637630	0.08414941
12	5.228	0.35135390	0.15574564
13	0.000	0.29276204	0.20738993
14	26.105	0.31553630	0.06882896
15	36.500	0.33561014	0.08900735
16	97.606	0.28895661	0.06705048
17	136.849	0.57554725	0.06460461
18	77.527	0.13698999	0.13699517
19	41.681	0.26697034	0.09306542
20	5.228	0.36295710	0.16755035
21	10.454	0.16798216	0.13673790
22	62.266	0.28667310	0.08313210
23	107.527	0.51098466	0.70103382
24	0.000	0.26281594	0.20217998
25	122.265	0.48163136	0.06651392

ANGULAR DISTRIBUTION OF THE 5.01200 STATE OF
P 31 FROM SI30(D,N) P31 JUNE 30/65

RLN NC	ANGLE C CF M	CORRECTED AREA	ERROR
2	31.339	6.15352428	0.18965801
3	0.000	1.63831981	0.20301484
4	15.693	7.93235947	0.23514136
5	46.894	1.59002841	0.14908604
6	62.320	1.29385917	0.16066549
7	122.319	0.87080703	0.12051431
8	151.339	0.44269207	0.13200385
9	77.587	1.24568555	0.15136295
10	31.339	6.28627458	0.32990618
11	20.916	8.74623099	0.35267473
12	5.233	3.01043955	0.22384716
13	0.000	1.66792577	0.26648233
14	26.132	8.13350870	0.31644417
15	36.536	4.33082501	0.22839373
16	97.668	1.00954837	0.09480490
17	136.893	0.53185134	0.10139620
18	77.587	1.69345427	0.22681505
19	41.722	2.60150899	0.15976008
20	5.233	3.02291639	0.16191471
21	10.465	6.34913476	0.31777677
22	62.320	1.26815170	0.16295091
23	107.587	1.09368386	0.17423212
24	0.000	1.61907647	0.22948601
25	122.319	0.86920408	0.10289767

ANGULAR DISTRIBUTION OF THE 5.12000 STATE OF
P 31 FROM SI30(D,N) P31 JUNE 30/65

RL NC	ANGLE C CF M	CORRECTED AREA	ERROR
2	31.354	0.53512272	0.12155203
3	0.000	0.33238600	0.26064009
4	15.701	0.88399679	0.15199199
5	46.915	0.18750243	0.12637308
6	62.346	0.43099377	0.17488439
7	122.345	0.13159987	0.11104368
8	151.354	0.19434003	0.15632449
9	77.617	0.49844196	0.14959115
10	31.354	0.55054403	0.30632567
11	20.926	0.96727685	0.27870241
12	5.236	0.84465251	0.25465912
13	0.000	0.43205474	0.32209937
14	26.145	0.79362299	0.28156662
15	36.554	0.43003283	0.21895739
16	97.699	0.29698547	0.10987143
17	136.915	0.04606823	0.11726516
18	77.617	0.38191927	0.25740034
19	41.741	0.21906616	0.16431045
20	5.236	0.80525245	0.19277165
21	10.470	1.89449909	0.18564805
22	62.346	0.12472887	0.18508460
23	107.616	0.48457716	0.19715613
24	0.000	0.44134744	0.28123899
25	122.345	0.22157357	0.10998735

ANGULAR DISTRIBUTION OF THE 5.25000 STATE OF
P 31 FROM SI30(D,N) P31 JUNE 30/65

RL NC	ANGLE C CF M	CORRECTED AREA	ERROR
2	31.373	0.39336210	0.20233404
3	0.000	4.81207638	0.46441693
4	15.711	1.89462140	0.27391530
5	46.942	0.45885133	0.10876206
6	62.379	0.50210407	0.11256870
7	122.379	0.03665335	0.05701725
8	151.373	0.22614797	0.06284321
9	77.654	0.13138527	0.09854494
10	31.373	0.18982540	0.15309358
11	20.939	0.75227757	0.25211451
12	5.239	4.15629392	0.42398804
13	0.000	4.18228622	0.40086663
14	26.161	0.47462987	0.18526616
15	36.576	0.26244020	0.11966279
16	97.737	0.00000000	0.00000000
17	136.942	0.12449029	0.07055121
18	77.654	0.21337840	0.11490959
19	41.766	0.32443583	0.10431933
20	5.239	3.65391806	0.35499535
21	10.477	3.12473097	0.32882908
22	62.379	0.39748788	0.10340077
23	107.653	0.03413943	0.05689971
24	0.000	4.07787633	0.34099969
25	122.379	0.00000000	0.00000000

ANGULAR DISTRIBUTION OF THE 5.53000 STATE OF
P 31 FROM SI30(C,N) P31 JUNE 30/65

RUN NC	ANGLE C CF M	CORRECTED AREA	ERROR
2	31.418	0.99110904	0.29892660
3	0.000	1.02391491	0.28636784
4	15.734	0.94639932	0.22948353
5	47.005	0.49759725	0.12937809
6	62.456	0.34447215	0.10573636
7	122.455	0.31537866	0.07589848
8	151.417	0.42796739	0.07413854
9	77.739	0.22436412	0.12020833
10	31.418	0.71469903	0.22342144
11	20.970	0.98759783	0.27115618
12	5.247	0.72510824	0.25903750
13	0.000	1.00967581	0.25632554
14	26.198	0.81427251	0.22524589
15	36.626	1.14893849	0.30052546
16	97.825	0.22429784	0.07872052
17	137.004	0.34621868	0.08150425
18	77.739	0.42844940	0.13218256
19	41.823	0.00000000	0.00000000
20	5.247	0.89436324	0.23294885
21	10.492	0.91230306	0.23181881
22	62.456	0.31763289	0.10074575
23	107.739	0.33414511	0.07960023
24	0.000	0.95530800	0.22491993
25	122.455	0.33911803	0.06910768

ANGULAR DISTRIBUTION OF THE 5.66000 STATE OF
P 31 FROM SI30(C,N) P31 JUNE 30/65

RUN NC	ANGLE C CF M	CORRECTED AREA	ERROR
2	31.440	0.20506727	0.21227060
3	0.000	0.38261397	0.25748313
4	15.745	0.13653348	0.18324645
5	47.036	0.00000000	0.00000000
6	62.494	0.03868795	0.10832682
7	122.493	0.13456454	0.06729176
8	151.439	0.08169689	0.05719085
9	77.782	0.02813369	0.10698752
10	31.440	0.00000000	0.00000000
11	20.985	0.13927286	0.21624242
12	5.251	0.09858952	0.23004362
13	0.000	0.37928289	0.23056560
14	26.217	0.00000000	0.00000000
15	36.652	0.11122947	0.11864819
16	97.869	0.19869396	0.08182929
17	137.035	0.03556057	0.06465609
18	77.782	0.24553336	0.13070114
19	41.851	0.01670401	0.10022416
20	5.251	0.25898650	0.20792952
21	10.500	0.16437265	0.19653705
22	62.494	0.00000000	0.00000000
23	107.781	0.27583872	0.07883864
24	0.000	0.11462540	0.19597471
25	122.493	0.18210819	0.06382380

ANGULAR DISTRIBUTION OF THE 5.89000 STATE OF
P 31 FROM S130(D,N) P31 JUNE 30/65

RLN NC	ANGLE C CF M	CORRECTED AREA	ERROR
2	31.481	0.04574521	0.04222824
3	0.000	0.00000000	0.00000000
4	15.767	0.00000000	0.00000000
5	47.095	0.26141197	0.12125651
6	62.566	0.09099660	0.09858280
7	122.565	0.40588701	0.07422565
8	151.481	0.99342757	0.07703224
9	77.862	0.26442273	0.14389075
10	31.481	0.12941191	0.12582122
11	21.013	0.00000000	0.00000000
12	5.258	0.06424321	0.14276360
13	0.000	0.00000000	0.00000000
14	26.252	0.26445084	0.18476509
15	36.699	0.28655873	0.17412607
16	97.952	0.33717468	0.08050026
17	137.094	0.37909335	0.09979645
18	77.862	0.33422483	0.12050247
19	41.904	0.17073257	0.13078063
20	5.258	0.00000000	0.00000000
21	10.514	0.00000000	0.00000000
22	62.566	0.06753464	0.15382977
23	107.862	0.46555296	0.09704887
24	0.000	0.00000000	0.00000000
25	122.565	0.33459560	0.06755510

ANGULAR DISTRIBUTION OF THE 6.05000 STATE OF
P 31 FROM S130(D,N) P31 JUNE 30/65

RLN NC	ANGLE C CF M	CORRECTED AREA	ERROR
2	31.512	0.18025800	0.10747254
3	0.000	0.13764740	0.09291957
4	15.783	0.12105716	0.11760299
5	47.139	0.17553008	0.08591109
6	62.620	0.32545922	0.08608513
7	122.619	0.59593709	0.07753832
8	151.512	0.49752896	0.10036303
9	77.922	0.31493582	0.12292317
10	31.512	0.14873389	0.08853935
11	21.035	0.20468352	0.11293975
12	5.264	0.07028184	0.10191010
13	0.000	0.10377484	0.11451299
14	26.278	0.17126961	0.12845894
15	36.735	0.21086852	0.12152806
16	98.014	0.51178210	0.09484448
17	137.138	0.43176902	0.10303203
18	77.922	0.31475486	0.11517699
19	41.944	0.12530143	0.09308589
20	5.264	0.15797102	0.11585180
21	10.525	0.10661661	0.09974145
22	62.620	0.21100480	0.12957388
23	107.922	0.48791924	0.09610815
24	0.000	0.27399388	0.12811858
25	122.619	0.47177324	0.06852126

ANGULAR DISTRIBUTION OF THE 6.24000 STATE OF
P 31 FROM SI30(D,N) P31 JUNE 30/65

RLN NC	ANGLE C CF M	CORRECTED AREA	ERROR
2	31.552	0.07837274	0.11244973
3	0.000	0.28055274	0.14198593
4	15.803	0.31601946	0.12235866
5	47.195	0.81204152	0.08112450
6	62.689	0.12528688	0.10686732
7	122.688	0.24943611	0.06526538
8	151.552	0.15162138	0.07980668
9	77.999	0.25003844	0.10987933
10	31.552	0.34462106	0.11490172
11	21.062	0.23579480	0.11791033
12	5.271	0.34173197	0.12429218
13	0.000	0.34798270	0.13008025
14	26.312	0.30858263	0.11924705
15	36.781	0.13353718	0.08785889
16	98.093	0.05997549	0.05997690
17	137.195	0.02321233	0.05508031
18	77.999	0.20067308	0.16660244
19	41.996	0.11267455	0.07042639
20	5.271	0.18620699	0.12414571
21	10.539	0.22636120	0.12501661
22	62.689	0.24066380	0.10576030
23	107.999	0.06845920	0.08367363
24	0.000	0.24466766	0.13982206
25	122.688	0.13582521	0.05282439

ANGULAR DISTRIBUTION OF THE 6.37500 STATE OF
P 31 FROM SI30(D,N) P31 JUNE 30/65

RLN NC	ANGLE C CF M	CORRECTED AREA	ERROR
2	31.582	1.46176086	0.13860298
3	0.000	0.59436302	0.12030721
4	15.819	0.94675882	0.13451560
5	47.238	1.24663342	0.11313612
6	62.741	0.72237826	0.09503628
7	122.741	0.61505640	0.08417331
8	151.582	0.64893396	0.10756980
9	78.058	0.51444465	0.09769453
10	31.582	1.37630922	0.14141587
11	21.082	1.21293481	0.14759293
12	5.276	0.72632751	0.13309353
13	0.000	0.86460384	0.13209812
14	26.337	1.24410088	0.14236708
15	36.815	1.45222741	0.15668439
16	98.153	0.62542933	0.08200716
17	137.237	0.51372768	0.07849963
18	78.058	0.93447529	0.15025093
19	42.034	1.33009366	0.15697059
20	5.276	0.63701007	0.12612370
21	10.550	0.89784904	0.11366589
22	62.741	0.72927446	0.09760975
23	108.057	0.52175881	0.09836208
24	0.000	0.66984700	0.11404732
25	122.741	0.54536543	0.07215096

ANGULAR DISTRIBUTION OF THE 6.482 STATE OF
P 31 FROM SI30(D,N)P31 JUNE 30/65

RUN NO	ANGLE (C OF M)	CORRECTED AREA	ERROR
2	31.608	2.73	0.172
3	0.000	2.98	0.190
4	15.832	3.75	0.215
5	47.274	1.05	0.116
6	62.785	0.995	0.113
7	122.785	0.296	0.076
8	151.607	0.533	0.108
9	78.107	0.840	0.120
10	31.608	2.42	0.185
11	21.100	3.41	0.219
12	5.280	3.00	0.207
13	0.000	3.12	0.201
14	26.359	3.17	0.208
15	36.844	1.55	0.180
16	98.204	0.421	0.085
17	137.273	0.315	0.074
18	78.107	0.900	0.160
19	42.067	1.16	0.166
20	5.280	3.12	0.200
21	10.558	3.49	0.180
22	62.785	1.03	0.115
23	108.106	0.274	0.094
24	0.000	3.04	0.179
25	122.785	0.221	0.067

ANGULAR DISTRIBUTION OF THE 6.6C100 STATE OF
P 31 FROM SI30(D,N)P31 JUNE 30/65

RUN NO	ANGLE C OF M	CORRECTED AREA	ERROR
2	31.637	1.04532675	0.17221029
3	0.000	0.84843459	0.07237921
4	15.847	1.25194271	0.17489188
5	47.316	0.52545996	0.05734500
6	62.837	0.76929717	0.09365719
7	122.836	0.45278578	0.09137956
8	151.637	0.44613493	0.07971555
9	78.164	0.45607544	0.09274546
10	31.637	0.99353173	0.10497902
11	21.120	1.19053993	0.05775332
12	5.285	0.74603354	0.10717770
13	0.000	0.80392705	0.09554463
14	26.384	0.99010980	0.08533248
15	36.878	0.75099039	0.10253515
16	98.263	0.36167542	0.08860366
17	137.315	0.25060873	0.07833081
18	78.164	0.29275819	0.22235610
19	42.105	0.89333175	0.06871998
20	5.285	0.79205190	0.15048860
21	10.569	0.91041154	0.14750008
22	62.837	0.49446473	0.07477540
23	108.164	0.42058511	0.09767207
24	0.000	0.90103643	0.09843184
25	122.836	0.39504053	0.05389143

ANGULAR DISTRIBUTION OF THE 7.14100 STATE OF P 31 FROM SI30(D,N) P31 JUNE 30/65			
RUN NC	ANGLE C CF M	CORRECTED AREA	ERROR
2	31.796	0.53610655	C.16376823
3	0.000	9.10074121	C.29271825
4	15.930	5.27590689	0.17955252
5	47.540	0.44266798	0.10810430
6	63.111	C.68092606	C.08482879
7	123.111	1.66220871	C.48177741
8	151.795	0.37228335	0.16962385
9	78.471	0.56833167	0.14304603
10	31.796	C.77395564	C.18371387
11	21.228	3.12963262	C.15107137
12	5.313	8.83271229	C.38880640
13	0.000	9.10152312	0.29539229
14	26.518	1.61599456	C.10273644
15	37.060	0.42793498	C.13271994
16	98.579	0.75900082	0.21850479
17	137.540	0.22192470	0.12913167
18	78.471	0.79520715	0.14667057
19	42.309	0.51638713	C.11664791
20	5.313	8.60066908	0.24503227
21	10.624	6.98650112	0.35418535
22	63.111	C.74014817	C.11530667
23	108.470	1.74500479	0.24309185
24	0.000	8.78194855	0.33528877
25	123.111	1.45860290	0.04054310

ANGULAR DISTRIBUTION OF THE 7.73000 STATE OF P 31 FROM SI30(D,N) P31 JUNE 30/65			
RUN NC	ANGLE C CF M	CORRECTED AREA	ERROR
2	32.036	C.18010329	C.13426997
3	0.000	0.64674529	0.16659514
4	16.054	0.54592775	0.05836727
5	47.880	C.15098543	0.07910296
6	63.528	0.09606313	0.13301477
7	123.527	0.11698488	0.07201982
8	152.036	0.29738715	0.05077627
9	78.935	C.12126593	C.07433758
10	32.036	0.15722668	C.05688608
11	21.393	0.38346207	0.06949718
12	5.355	0.49718066	0.11782668
13	0.000	0.49608285	C.11993120
14	26.721	0.17446163	C.08388947
15	37.336	0.00000000	0.00000000
16	99.059	0.12690834	0.10645366
17	137.879	0.24982322	C.10100164
18	78.935	0.00000000	0.00000000
19	42.618	0.00000000	0.00000000
20	5.355	0.00000000	0.00000000
21	10.707	0.59939513	C.07709050
22	63.528	0.00000000	0.00000000
23	108.935	0.15378814	0.07692896
24	0.000	0.00000000	0.00000000
25	123.527	C.07785759	0.05133101

ANGULAR DISTRIBUTION OF THE 7.91000 STATE OF
P 31 FROM SI30(D,N) P31 JUNE 30/65

RLN NC	ANGLE C OF M	CORRECTED AREA	ERROR
2	32.131	1.58766657	0.37287878
3	0.000	2.92401953	0.34082571
4	16.103	3.03378596	0.28166671
5	48.015	0.94644422	0.11292799
6	63.693	0.69084135	0.11687154
7	123.692	0.20767185	0.08625724
8	152.131	0.27780576	0.10080491
9	79.119	0.12061244	0.39927343
10	32.131	0.00000000	0.00000000
11	21.458	0.00000000	0.00000000
12	5.371	3.05494601	0.23138506
13	0.000	3.40703363	0.26964212
14	26.801	0.00000000	0.00000000
15	37.445	0.89305537	0.10601176
16	99.249	0.32074498	0.08931097
17	138.014	0.16578343	0.12717844
18	79.119	0.00000000	0.00000000
19	42.740	0.64642937	0.11747498
20	5.371	2.98793575	0.26749522
21	10.740	2.85971622	0.34116029
22	63.693	0.73739420	0.08131568
23	109.119	0.22602612	0.08019421
24	0.000	3.06444567	0.22717998
25	123.692	0.00000000	0.00000000

ANGULAR DISTRIBUTION OF THE 8.26000 STATE OF
P 31 FROM SI30(D,N) P31 JUNE 30/65

RLN NC	ANGLE C OF M	CORRECTED AREA	ERROR
2	32.362	0.43993564	0.06877814
3	0.000	1.16928607	0.10226933
4	16.223	0.85090231	0.09095583
5	48.342	0.36820160	0.07335297
6	64.094	0.00000000	0.00000000
7	124.093	0.24696864	0.09880533
8	152.362	0.00000000	0.00000000
9	79.567	0.00000000	0.00000000
10	32.362	0.47394056	0.09056014
11	21.616	0.68821882	0.08102820
12	5.412	1.02798174	0.09983614
13	0.000	1.08126236	0.12885958
14	26.997	0.75595194	0.09105175
15	37.710	0.43963197	0.07609664
16	99.710	0.37392167	0.08927962
17	138.341	0.00000000	0.00000000
18	79.567	0.00000000	0.00000000
19	43.038	0.00000000	0.00000000
20	5.412	0.94523447	0.10316724
21	10.820	0.94834777	0.10902802
22	64.094	0.25324169	0.07340948
23	109.567	0.10935503	0.09378734
24	0.000	0.95704154	0.12770116
25	124.093	0.23698647	0.06993788

Relative differential cross sections for $\text{Si}^{30}(\text{d},\text{n})\text{P}^{31}$ at
 $E_d = 4 \text{ MeV}$.

1 ANGULAR DISTRIBUTION OF THE 0.00000 STATE OF
P 31 FROM $\text{Si}^{30}(\text{D},\text{N})\text{P}^{31}$

RUN NO	ANGLE[C OF M]	CORRECTED AREA	ERROR
2	0.000	0.32529950	0.02374693
3	30.881	0.03247137	0.00415727
4	0.000	0.28813951	0.02029249
5	15.456	0.16774868	0.01285367
6	30.881	0.03922499	0.00462008
7	61.526	0.04514728	0.00448450
8	121.525	0.02084207	0.00349168
9	150.881	0.03231006	0.00357157
10	76.702	0.03034592	0.00348607
11	46.246	0.04608986	0.00510258
12	36.011	0.02847028	0.00385117
13	25.745	0.04712090	0.00616868
14	10.306	0.24001289	0.01813385
15	101.735	0.01137799	0.00191834
16	20.603	0.10142820	0.00869708
17	5.154	0.19378204	0.01465691
18	30.881	0.03291838	0.00391845

1 ANGULAR DISTRIBUTION OF THE 1.26500 STATE OF
P 31 FROM $\text{Si}^{30}(\text{D},\text{N})\text{P}^{31}$

RUN NO	ANGLE[C OF M]	CORRECTED AREA	ERROR
2	0.000	0.02831718	0.00475020
3	30.951	0.05417144	0.00533303
4	0.000	0.02714030	0.00391829
5	15.492	0.03669366	0.00443343
6	30.951	0.05278008	0.00536506
7	61.647	0.05678405	0.00487913
8	121.647	0.03194650	0.00256799
9	150.951	0.03851924	0.00370193
10	76.837	0.05230400	0.00467510
11	46.345	0.06691184	0.00610348
12	36.091	0.06727379	0.00598976
13	25.804	0.04539707	0.00539275
14	10.330	0.03355232	0.00471256
15	101.873	0.02840730	0.00275421
16	20.651	0.04276535	0.00462363
17	5.166	0.03381319	0.00433528
18	30.951	0.05555349	0.00505953

ANGULAR DISTRIBUTION OF THE 2.23200 STATE OF
P 31 FROM SI30(D,N)P31

RUN NO	ANGLE[C OF M]	CORRECTED AREA	ERROR
2	0.000	0.00851411	0.00351780
3	31.018	0.02596795	0.00351577
4	0.000	0.00880460	0.00274584
5	15.527	0.01657263	0.00292367
6	31.018	0.03332430	0.00389877
7	61.763	0.03764567	0.00362940
8	121.762	0.03058880	0.00388241
9	151.017	0.04582088	0.00398279
10	76.966	0.02549808	0.00294403
11	46.439	0.04331857	0.00447272
12	36.167	0.03454718	0.00380659
13	25.860	0.02043017	0.00363604
14	10.353	0.01330383	0.00305468
15	102.004	0.02234930	0.00238326
16	20.696	0.02389796	0.00321974
17	5.177	0.01659260	0.00304882
18	31.018	0.03081983	0.00337484

ANGULAR DISTRIBUTION OF THE 5.01200 STATE OF
P 31 FROM SI30(D,N)P31

RUN NO	ANGLE[C OF M]	CORRECTED AREA	ERROR
2	0.000	0.00000000	0.00000000
3	31.336	0.38880847	0.03366040
4	0.000	0.11070961	0.00738542
5	15.692	0.33593755	0.01922689
6	31.336	0.36032466	0.02035551
7	62.314	0.06762203	0.00645053
8	122.314	0.04377173	0.00319849
9	151.336	0.03759236	0.00307646
10	77.581	0.05259208	0.00634663
11	46.890	0.15933209	0.01050653
12	36.533	0.30039044	0.01768835
13	26.129	0.41692206	0.02249866
14	10.464	0.22515056	0.01294425
15	102.632	0.04614113	0.00341653
16	20.914	0.38959221	0.02199992
17	5.233	0.26518637	0.01410717
18	31.336	0.35694689	0.02184612

1 ANGULAR DISTRIBUTION OF THE 6.37500 STATE OF
P 31 FROM SI30(D,N)P31

RUN NO	ANGLE[C OF M]	CORRECTED AREA	ERROR
2	0.000	0.03084366	0.00446762
3	31.666	0.06794952	0.00528325
4	0.000	0.02700762	0.00473391
5	15.862	0.03905657	0.00437112
6	31.666	0.05396342	0.00495331
7	62.887	0.04117119	0.01156271
8	122.886	0.00000000	0.00000000
9	151.666	0.00000000	0.00000000
10	78.220	0.03158522	0.00413791
11	47.357	0.07125427	0.00517331
12	36.911	0.06900513	0.00453592
13	26.408	0.04793573	0.00399562
14	10.579	0.02227552	0.00424754
15	103.283	0.00000000	0.00000000
16	21.140	0.04414935	0.00367115
17	5.290	0.02727246	0.00308090
18	31.666	0.05558341	0.00415463

ANGULAR DISTRIBUTION OF THE 5.25000 STATE OF
P 31 FROM SI30(D,N)P31

RUN NO	ANGLE[C OF M]	CORRECTED AREA	ERROR
2	0.000	0.00000000	0.00000000
3	31.380	0.00000000	0.00000000
4	0.000	0.09048383	0.01338658
5	15.714	0.05317166	0.01355929
6	31.380	0.02025145	0.00775645
7	62.390	0.03997822	0.00598751
8	122.389	0.01204198	0.00458367
9	151.379	0.01766698	0.00427279
10	77.666	0.03815734	0.00568481
11	46.951	0.02519843	0.00797098
12	36.583	0.02826038	0.00986441
13	26.166	0.05228114	0.01455728
14	10.479	0.00000000	0.00000000
15	102.718	0.02411716	0.00653887
16	20.944	0.08654126	0.01872834
17	5.240	0.11744034	0.01384689
18	31.380	0.03069933	0.01181855

1 ANGULAR DISTRIBUTION OF THE 6.48200 STATE OF
P 31 FROM SI30(D,N)P31

RUN NO	ANGLE[C OF M]	CORRECTED AREA	ERROR
2	0.000	0.15699359	0.00861239
3	31.704	0.16460964	0.00786500
4	0.000	0.13886017	0.00723372
5	15.882	0.18422606	0.00828059
6	31.704	0.15145600	0.00744505
7	62.952	0.04865266	0.00302724
8	122.951	0.00000000	0.00000000
9	151.703	0.00000000	0.00000000
10	78.293	0.04301030	0.00426718
11	47.410	0.07927181	0.00518596
12	36.955	0.12920524	0.00584035
13	26.440	0.17022721	0.00677708
14	10.592	0.15691912	0.00757704
15	103.357	0.00000000	0.00000000
16	21.165	0.18200114	0.00710711
17	5.297	0.15750583	0.00626793
18	31.704	0.13735007	0.00603764

1 ANGULAR DISTRIBUTION OF THE 6.60100 STATE OF
P 31 FROM SI30(D,N)P31

RUN NO	ANGLE[C OF M]	CORRECTED AREA	ERROR
2	0.000	0.02678719	0.00532179
3	31.749	0.03296893	0.00446840
4	0.000	0.01994940	0.00419432
5	15.905	0.03171043	0.00417081
6	31.749	0.03261544	0.00425276
7	63.030	0.00000000	0.00000000
8	123.030	0.00000000	0.00000000
9	151.748	0.00000000	0.00000000
10	78.380	0.03838521	0.00449061
11	47.474	0.02611125	0.00414632
12	37.006	0.02835754	0.00326903
13	26.478	0.03630842	0.00327844
14	10.607	0.02790758	0.00395559
15	103.446	0.00000000	0.00000000
16	21.196	0.03414624	0.00317801
17	5.305	0.02535411	0.00302790
18	31.749	0.02607841	0.00314835

Relative differential cross sections for $\text{Si}^{28}(\text{d},\text{n})\text{P}^{29}$
at $E_d = 6 \text{ MeV}$.

2

ANGULAR DISTRIBUTION OF THE 0.00000 STATE OF
P 29 FROM SI 28(D,N) P 29 JULY 3/65

RUN NO	ANGLE[C OF M]	CORRECTED AREA	ERROR
1	0.000	0.40657229	0.02615780
2	31.379	0.01133225	0.00159116
3	62.389	0.01626440	0.00069254
4	122.389	0.00198637	0.00037060
5	46.951	0.02303237	0.00108131
6	0.000	0.41712370	0.02547375
7	15.714	0.19762450	0.01622055
8	26.166	0.03709700	0.00294612
9	41.773	0.01846472	0.00114030
10	136.950	0.00322363	0.00049112
11	52.113	0.02504752	0.00126892
12	31.379	0.01163808	0.00125211
13	10.479	0.27648656	0.01536711
14	36.582	0.00926907	0.00080118
15	77.665	0.00244630	0.00042349
16	151.379	0.00623056	0.00051671
17	107.664	0.00242970	0.00043327
18	57.260	0.01963838	0.00091737
19	31.379	0.00974786	0.00132160
20	20.944	0.08356482	0.00476518
21	5.240	0.32957539	0.01704605
22	5.240	0.30175990	0.01443242
23	0.000	0.35824190	0.02007744

2

ANGULAR DISTRIBUTION OF THE 1.38200 STATE OF
P 29 FROM SI 28(D,N) P 29 JULY 3/65

RUN NO	ANGLE[C OF M]	CORRECTED AREA	ERROR
1	0.000	0.00747141	0.00137748
2	31.566	0.02874433	0.00136569
3	62.713	0.00705675	0.00056379
4	122.712	0.00629335	0.00046425
5	47.215	0.01797823	0.00114299
6	0.000	0.01004703	0.00113889
7	15.811	0.01706147	0.00103119
8	26.324	0.02791279	0.00131132
9	42.013	0.02233841	0.00105514
10	137.214	0.00650877	0.00050488
11	52.400	0.01010373	0.00096887
12	31.566	0.02670572	0.00174850
13	10.544	0.01110958	0.00151356
14	36.797	0.02679272	0.00148161
15	78.026	0.00764699	0.00065204
16	151.565	0.00678165	0.00063921
17	108.025	0.00579508	0.00058976
18	57.566	0.00750476	0.00071239
19	31.566	0.02861269	0.00204340
20	21.071	0.02109833	0.00114705
21	5.273	0.00859333	0.00142637
22	5.273	0.00705703	0.00251239
23	0.000	0.00539999	0.00241962

ANGULAR DISTRIBUTION OF THE 1.96227 STATE OF
P 29 FROM SI 28(D,N) P 29 JULY 3/65

RUN NO	ANGLE[C OF M]	CORRECTED AREA	ERROR
1	0.000	0.00364606	0.00069233
2	31.671	0.0172766	0.00286492
3	62.894	0.07562695	0.0035128
4	122.893	0.00252789	0.00237195
5	47.363	0.0978483	0.00263926
6	0.000	0.07269278	0.00249457
7	15.865	0.00637113	0.00255921
8	26.412	0.00933193	0.00251559
9	42.148	0.0103749	0.00273914
10	137.362	0.00404739	0.00254170
11	52.560	0.00762247	0.00251683
12	31.671	0.00892898	0.00253449
13	10.580	0.00360796	0.00254787
14	36.916	0.00965390	0.00266054
15	78.228	0.00404402	0.00248617
16	151.670	0.00000000	0.00000000
17	108.228	0.00212406	0.00247438
18	57.737	0.00603174	0.00262279
19	31.671	0.00883482	0.00262014
20	21.143	0.00687079	0.00264946
21	5.291	0.00341833	0.00277160
22	5.291	0.00231332	0.00250122
23	0.000	0.00288773	0.00251421

ANGULAR DISTRIBUTION OF THE 2.40000 STATE OF
P 29 FROM SI 28(D,N) P 29 JULY 3/65

RUN NO	ANGLE[C OF M]	CORRECTED AREA	ERROR
1	0.000	0.00000000	0.00000000
2	31.766	0.00535833	0.00220784
3	63.060	0.01547818	0.00290163
4	123.059	0.00273655	0.00374233
5	47.498	0.00892718	0.00121660
6	0.000	0.00339706	0.00172168
7	15.914	0.00507689	0.00219952
8	26.493	0.00682566	0.00244292
9	42.271	0.00835181	0.00143734
10	137.497	0.00219335	0.002039751
11	52.706	0.00966923	0.00195123
12	31.766	0.00641428	0.00202020
13	10.613	0.00279360	0.00171819
14	37.026	0.00756124	0.00177042
15	78.413	0.00000000	0.00000000
16	151.765	0.00221261	0.00245751
17	108.412	0.00013147	0.00288783
18	57.894	0.00926105	0.00150033
19	31.766	0.00682235	0.00204308
20	21.208	0.00465811	0.00225028
21	5.308	0.00256401	0.00182702
22	5.308	0.00214630	0.00150255
23	0.000	0.00245471	0.00153437

2

ANGULAR DISTRIBUTION OF THE 3.12300 STATE OF
P 29 FROM SI 28(D,N) P 29 JULY 3/65

RUN NO	ANGLE[C OF M]	CORRECTED AREA	ERROR
1	0.000	0.00000000	0.00000000
2	31.962	0.00525449	0.00119078
3	63.396	0.00259582	0.00068262
4	123.395	0.00147422	0.00054674
5	47.772	0.00553722	0.00096017
6	0.000	0.00581626	0.00152986
7	16.015	0.00667970	0.00108232
8	26.657	0.00567787	0.00108529
9	42.520	0.00377612	0.00082252
10	137.772	0.00431239	0.00100011
11	53.004	0.00334645	0.000234266
12	31.960	0.00625013	0.00086838
13	10.681	0.00457065	0.00134649
14	37.249	0.00552115	0.00096062
15	78.788	0.00284724	0.00093210
16	151.959	0.00462981	0.000418902
17	108.788	0.00568223	0.00122071
18	58.212	0.00171371	0.00099466
19	31.960	0.00754644	0.00094897
20	21.341	0.00678926	0.00093971
21	5.342	0.00347304	0.00165409
22	5.342	0.00477084	0.00150307
23	0.000	0.00571377	0.00158388

2

ANGULAR DISTRIBUTION OF THE 3.47000 STATE OF
P 29 FROM SI 28(D,N) P 29 JULY 3/65

RUN NO	ANGLE[C OF M]	CORRECTED AREA	ERROR
1	0.000	0.03571694	0.00211245
2	32.091	0.02547076	0.00180742
3	63.623	0.01730023	0.00104221
4	123.622	0.00839179	0.00066639
5	47.953	0.02463601	0.00142369
6	0.000	0.03160266	0.00200975
7	16.082	0.02644648	0.00143551
8	26.767	0.02571631	0.00157560
9	42.688	0.03011032	0.00234709
10	137.957	0.00696342	0.00081918
11	53.204	0.01858826	0.00163951
12	32.091	0.02699411	0.00127577
13	10.726	0.03512445	0.00185405
14	37.399	0.02682470	0.00139005
15	79.041	0.01083519	0.00117058
16	152.090	0.00408329	0.00078317
17	109.041	0.00646927	0.00079753
18	58.427	0.01811875	0.00132052
19	32.091	0.02662719	0.00131398
20	21.430	0.02834332	0.00129951
21	5.364	0.03768496	0.00223617
22	5.364	0.03511975	0.00197105
23	0.000	0.03697080	0.00205711

REFERENCES

- Al 60 W. D. Allen, "Flat Response Counters," ch. 3 A. Fast Neutron Physics, ed. by J. B. Marion and J. L. Fowler (Interscience Publishers, Inc., New York, 1960)
- Al 61 T. K. Alexander and F. S. Goulding, Nucl. Instr. and Meth. 13 (1961) 244.
- Al 63 T. K. Alexander and G.C. Neilson, Proceedings of the Conference on Instrument Technique in Nuclear Pulse Analysis, held at Monterey, Calif., April, 1963.
- Al 64 J. L. Alty, L. L. Green, G. C. Jones and J.F. Sharpey-Schafer, Physics Letters 13 (1964) 55.
- Au 63 N. Austern, Selected Topics in Nuclear Theory, edited by F. Janouch (International Atomic Energy Agency, 1963) p. 17.
- Au 64 N. Austern, R. M. Drisko, E. C. Halbert and G. R. Satchler, Phys. Rev. 133 (1964) B3.
- Ba 57 S. J. Bame, E. Haddad, J. E. Perry and K. K. Smith, Rev. Sci. Instr. 28 (1957) 997.
- Ba 62 E. E. Baart, L. L. Green and J. C. Willmott, Proc. Phys. Soc. (London) 79 (1962) 237.
- Be 61 T. A. Belote, E. Kashy and I. R. Risser, Phys. Rev. 122 (1961) 920.
- Be 61a P. R. Bevington, W. W. Roland and H. W. Lewis, Phys. Rev. 121 (1961) 871.
- Bi 65 G. R. Bishop, A. Bottino and R. M. Lombard, Physics Letters 15 (1965) 323.
- Bo 55 A. Bohr and B. R. Mottelson, Mat. Fys. Medd. Don. Vid. Selsk. 30 No. 1 (1955).
- Bo 56 G. E. P. Box and G. A. Couti, Proc. I.E.E. 103 (1956) 100, Part B, Supp. #1.
- Br 57 D. A. Bromley, H. E. Grove and A. E. Litherland, Can. J. Phys. 35 (1957) 1057.
- Br 57a D. A. Bromley, H. E. Grove, E. B. Paul, A. E. Litherland and E. Almqvist, Can. J. Phys. 35 (1957) 1042
- Br 58 C. Broude, L. L. Green and J. C. Willmott, Proc. Phys. Soc. (London) 72 (1958) 1097, Parts I, II, III.

- Br 64 K. L. Brown, K. Belbeoch and P. Bounin, Rev. Sci. Instr. 35 (1964) 481.
- Br 65 K. L. Brown, Rev. Sci. Instr. 36 (1965) 271.
- Ca 51 M. Camac, Rev. Sci. Instr. 22 (1951) 197.
- Ca 57 J. M. Calvert, A. A. Jaffe and E. E. Maslin, Proc. Phys. Soc. A70 (1957) 78.
- Ch 63 B. E. Chi and J. P. Davidson, Phys. Rev. 131 (1963) 366.
- Cl 62 A. B. Clegg and K. J. Foley, Phil. Mag. 7 (1962) 247, Series 8.
- Co 58 E. D. Courant and H. S. Snyder, Ann. of Phys. 3 (1958) 7.
- Co 64 L. Colli, P. Forti and E. Gadioli, Nucl. Phys. 54 (1964) 253.
- Cr 51 W. G. Cross, Rev. Sci. Instr., 22 (1951) 717.
- Cr 65 F. S. Crawford, Jr., Nucl. Instr. and Meth. 33 (1965) 332.
- Cu 65 B. Cujec, W. G. Davies, W. K. Dawson, T. B. Grandy, G. C. Neilson, and K. Ramavataram, Physics Letters 15 (1965) 266.
- Da 65 W. G. Davies, W. K. Dawson, G. C. Neilson, Physics Letters (in press)
- Da 65a J. P. Davidson, Rev. Mod. Phys. 37 (1965) 105.
- Ej 64 H. Ejiri, Nucl. Phys. 52 (1964) 578.
- En 62 P. M. Endt and C. Van der Leun, Nucl. Phys. 34 (1962) 1.
- Ev 55 R. P. Evans, The Atomic Nucleus (McGraw-Hill, 1959).
- Fo 60 T. K. Fowler and W. M. Good, Nucl. Instr. and Meth. 7 (1960) 245.
- Ge 52 J. Geerk and C. Heintz, Z. Phys. 133 (1952) 513, English translation AEC-tr-1890.
- Gl 64 P. W. M. Glaudemans, G. Wiechers and P. J. Brussaard, Nucl. Phys. 56 (1964) 529, 548.
- Go 59 H. Goldstein, Classical Mechanics (Addison Wesley, Reading, Mass. 1959).
- Go 60 H. E. Gove, Proc. Intern. Conf. on Nuclear Structure, ed. by D. A. Bromley and E. W. Vogt (University of Toronto Press, Toronto, 1960) 438.
- Go 61 M. D. Goldberg, J. D. Anderson, J. P. Stoering and C. Wong, Phys. Rev. 122 (1961) 1510.
- Gr 64 K. R. Greider, Phys. Rev. 136 (1964) B420.
- Ha 52 A. Hald, Statistical Theory with Engineering Applications (Wiley, N.Y. 1952) 118.
- Ha 62 G. I. Harris and L. W. Seagondollar, Phys. Rev. 128 (1962) 338.

- Ha 62a R. W. Hamming, Numerical Methods for Scientists and Engineers (McGraw-Hill, 1962).
- Ha 63 G. I. Harris and L. W. Seagondollar, Phys. Rev. 131 (1963) 787.
- Ha 63a R. P. Haddock, Rev. Sci. Instr. 34 (1963) 745.
- Ha 63b K. Halbach, Matrix Representation of Gaussian Optics, University of California Lawrence Radiation Laboratory Report UCRL - 10709.
- Ha 64 G. I. Harris, H. J. Hennecke and F. W. Prosser, Physics Letters, 9 (1964) 324.
- Ho 61 R. E. Holland, Nucl. Instr. and Meth. 12 (1961) 103.
- Ja 65 L. Jánossy, Theory and Practice of the Evaluation of Measurements (Oxford U. Press 1965).
- Ke 51 J. F. Kenney and E. S. Keeping, Mathematics of Statistics (Part II) (D. Van Nostrand 1951).
- Ke 56 A. K. Kerman, Mat. Fys. Medd. Dan. Vid. Selsk. 30 No. 15 (1956).
- Ku 60 J. A. Kuehner, E. Almqvist and D. A. Bromley, Nucl. Phys. 21 (1960) 555.
- La 62 L. Lapidus, Digital Computation for Chemical Engineers (McGraw-Hill 1962).
- Le 64 L. L. Lee and J. P. Schiffer, Phys. Rev. 136 (1964) B405.
- Li 58 A. E. Litherland, H. McManus, E. B. Paul, D. A. Bromley, H. E. Gove, Can. J. Phys. 36 (1958) 378.
- Ma 60 M. H. Macfarlane and J. B. French, Rev. Mod. Phys. 32 (1960) 567.
- Ma 62 R. N. Maddison, Proc. Phys. Soc. 79 (1962) 264.
- Ma 64 J. Mathews and R. L. Walker, Mathematical Methods of Physics (Benjamin 1964).
- Mc 63 M. H. Macfarlane, Direct Interactions and Nuclear Reaction Mechanisms, edited by C. Vili (Gordon and Breach, New York, U.S.A., 1963) 3.
- Mc 65 J. G. McLarnon, M.Sc. Thesis, University of Alberta (1965). Unpublished.
- Mo 52 R. C. Mobley, Phys. Rev. 88 (1952) 360.
- Mo 60 R. H. Moore and R. K. Zeigler, Los Alamos Scientific Laboratory Report LA-2367.
- Mo 63 R. C. Mobley, Rev. Sci. Instr. 34 (1963) 256.
- Ne 59 G. C. Neilson, W. K. Dawson and F. A. Johnson, Rev. Sci. Instr. 30 (1959) 963.
- Ne 60 G. C. Neilson, W. K. Dawson, F. A. Johnson and J. T. Sample, Suffield Technical Paper No. 176, Defence Research Board of Canada, Department of National Defence (1960).

- Ne 63 G. C. Neilson, J. T. Sample and J. B. Warren, Ch. V.Q., Fast Neutron Physics, edited by J. B. Marion and J. L. Fowler (Interscience Publishers, New York, 1963).
- Ni 55 S.G. Nilsson, Mat. Fys. Medd. Dan. Vid. Selsk 29 (1955) 16.
- Pa 57 E. B. Paul, Phil. Mag. 15 (1957) 311.
- Pa 58 E. B. Paul and J. Montague, Nucl. Phys. 8 (1958) 61.
- Pa 59 S. P. Pandya, Prog. Theor. Phys 21 (1959) 431.
- Pe 61 S. Penner, Rev. Sci. Instr. 32 (1961) 150.
- Ra 63 K. Ramavataram, Phys. Rev. 132 (1963) 2255.
- Ra 65 K. Ramavataram, private communication.
- Ri 62 P. J. Riley, Ph.D. Thesis, University of Alberta (1962) Unpublished.
- Ri 64 H. A. Van Rinsvelt and P. M. Endt, Physics Letters 9 (1964) 266.
- Ro 53 M. E. Rose, Phys. Rev. 91 (1953) 610.
- Sa 64 G. R. Satchler, Nucl. Phys. 55 (1964) 1.
- Sm 62 W. R. Smith and E. V. Ivash, Phys. Rev. 128 (1962) 1175
- Sm 63 W. R. Smith and E. V. Ivash, Phys. Rev. 131 (1963) 304.
- Sm 65 W. R. Smith, Phys. Rev. 137 (1965) B913.
- St 55 P. A. Sturrock, Static and Dynamic Electron Optics (Cambridge University Press, Cambridge, U.K., 1955).
- Sy 59 J. L. Synge and B. A. Griffith, Principles of Mechanics (McGraw-Hill, New York, 1959).
- Th 60 V. K. Thankappen and S. P. Pandya, Nucl. Phys. 19 (1960) 303.
- Th 62 V. K. Thankappen, Physics Letters 2 (1962) 122.
- Vo 59 J. Vorona, J. W. Olness, W. Haeberli and H. W. Lewis, Phys. Rev. 116 (1959) 1563.
- Wa 57 R. B. Walton, J. D. Clement and F. Boreli, Phys. Rev. 107 (1957) 1065.
- Wi 63 D. L. Wieber, Nucl. Instr. and Meth. 24 (1963) 269.
- Wi 64 B. H. Wildenthal, R. W. Krone and F. W. Prosser, Jr., Phys. Rev. 135 (1964) B680.
- Ya 61 B. Yaramis, Phys. Rev. 124 (1961) 836.

B29849